Ghent University

Faculty of Sciences – Department of Geography

TUNNEL OVALISATION MONITORING: 3D DATA ACQUISITION WITH LASER SCANNING AND POINT CLOUD PROCESSING

MONITORING VAN OVALISATIE VAN TUNNELS: 3D DATA ACQUISITIE MET LASERSCANNING EN DE VERWERKING VAN PUNTENWOLKEN

Timothy Nuttens

Promoter: Prof. dr. ir. Alain De Wulf

Dissertation submitted in accordance with the requirements for the degree of Doctor of Science: Geomatics and Surveying

TUNNEL OVALISATION MONITORING: 3D DATA ACQUISITION WITH LASER SCANNING AND POINT CLOUD PROCESSING

MONITORING VAN OVALISATIE VAN TUNNELS: 3D DATA ACQUISITIE MET LASERSCANNING EN DE VERWERKING VAN PUNTENWOLKEN

Timothy Nuttens

May, 16th 2014
Published by: Ghent University
Department of Geography (WE12)
Krijgslaan 281, S8
B-9000 Gent, Belgium

Supervisor

PROF. DR. IR. ALAIN DE WULF	Ghent University (Belgium) Department of Geography

Reading Committee

PROF. DR. ENG. JOSE LUIS LERMA GARCIA	Polytechnical University of Valencia (UPV) (Spain) Department of Cartographic Engineering, Geodesy and Photogrammetry
PROF. DR. ROLAND BILLEN	University of Liège (Belgium) Department of Geography
PROF. DR. IR. HANS DE BACKER	Ghent University (Belgium) Department of Civil Engineering
PROF. DR. IR. PHILIPPE VAN BOGAERT	Ghent University (Belgium) Department of Civil Engineering
PROF. DR. ING. GRETA DERUYTER	Ghent University (Belgium) Department of Industrial Technology and Construction Department of Geography

Examination Committee

PROF. DR. BEN DERUDDER (chairman)	Ghent University (Belgium) Department of Geography
PROF. DR. IR. ALAIN DE WULF (promoter)	Ghent University (Belgium) Department of Geography
PROF. DR. PHILIPPE DE MAEYER	Ghent University (Belgium) Department of Geography
PROF. DR. RUDI GOOSSENS	Ghent University (Belgium) Department of Geography

VOORWOORD

Beste lezer

Beste collega's, familie, vrienden of eventuele fans (?)

Na meer dan zes jaar bedenktijd zou je verwachten dat ik goed weet wat geschreven in het voorwoord van mijn doctoraatsproefschrift. Niet dus... Het blijkt zowaar bijna moeilijker te zijn dan het schrijven van een geschikte inleiding die de interesse voldoende zal opwekken of die allesomvattende-en-meerwaarde-aantonende conclusies die jullie verderop kunnen (en hopelijk ook zullen) lezen. Een voorwoord is echter dé unieke kans om eens achterom te kijken en iedereen te bedanken die op een of andere manier heeft bijgedragen aan dit moment. Het waren immers boeiende, spannende, leuke en verrijkende jaren aan de vakgroep Geografie.

Eerst en vooral wil ik de mensen uit de 3D Data Acquisitie onderzoeksgroep bedanken, vooral mijn promotor, Prof. dr. ir. Alain De Wulf, en Prof. dr. Rudi Goossens, voor de onderzoeksmogelijkheden, de binnenlandse en buitenlandse meetcampagnes en conferenties en de begeleiding doorheen de voorbije jaren. Uiteraard ook een dikke merci aan Coen ("merci" (Fr.) = "bedankt!"), Marijn, Leen, Frederik, Annelies en Nasem en andere collega's binnen de onderzoeksgroep. Binnen de vakgroep Geografie bedank ik graag ook Prof. dr. Philippe De Maeyer - niet alleen als vakgroepvoorzitter maar ook als 'behoeder van het AAP' -, de andere professoren van de vakgroep, de vele collega's die gekomen, gegaan of gebleven zijn en iedereen die me (al dan niet vrijwillig) vergezeld heeft tijdens de tunnelmetingen. Ik zal met plezier terugdenken aan onze babbels tijdens de lunchpauze, jullie continue steun, de plezante assistentenweekendjes, het squash-kotje als uitlaatklep en de vele taartjes-van-de-week!

Ook buiten de vakgroep kreeg ik veel feedback en medewerking tijdens de tunnelmetingen en het verwerken van de resultaten. Daarom wil ik zeker en vast Prof. dr. ir. Philippe Van Bogaert, Prof. dr. ir. Hans De Backer, ir. Ken Schotte, de vakgroep Civiele Techniek, Prof. dr. ing. Greet Deruyter, Prof. dr. Denis Constales en Jacky Chow bedanken. Ook bedankt aan alle leden van de lees- en examencommissie, co-auteurs, reviewers en alle anderen die papers en artikels hebben nagelezen voor hun feedback en leerrijke gesprekken.

Er was de voorbije jaren uiteraard ook meer dan onderzoek alleen. Les geven, oefeningen uitleggen, thesissen begeleiden en het kampgevoel op de Kemmelberg of in Vassivière vormen zeker en vast mooie herinneringen, met dank aan de aanwezige en enthousiaste studenten landmeetkunde en geomatica. Een extra vermelding gaat uit naar de thesis- of andere studenten die (on)rechtstreeks hebben bijgedragen aan dit onderzoek en die daarvoor vaak ook ettelijke uren in de tunnel hebben gemeten.

Naast de werkuren heb ik kunnen ontspannen, lachen, zeveren, feesten, reizen, eten en nog zoveel meer met een fantastische vriendengroep. Merci Lander, Bart, Jonas, Koen DB, Koen P, Marijke, Elke, Annelies, Eline, Dries, Thomas en alle partners… "LMK2003" is een superbende! Ook Katrien, Seb en Matthias: bedankt voor alle ontspannende uren samen. Ik kijk al uit naar de komende jaren!

Ik ben trots een landmeter te zijn en dat diploma heb ik uiteraard deels te danken aan de kansen en de steun die ik thuis heb gekregen. Mama en papa, dikke merci! En aan mijn zus, grootouders en de rest van de (schoon-)familie: bedankt voor jullie volharden tijdens de nieuwjaarswensen. Eindelijk ligt het er, dat lang verwachte doctoraat!

En de kaft ziet er nog goed uit ook, merci Stephanie.

Om af te sluiten zijn er nog twee (jonge)dames die ik absoluut niet mag vergeten:

Helga, je was de afgelopen jaren zoveel meer dan een collega. Je was een fantastische steun en toeverlaat, een vertrouwenspersoon en iemand waarbij ik altijd even mijn hart kon luchten. Bedankt voor alle praktische hulp, de vele complimentjes en het luisteren tijdens de voorbije jaren.

Liefste Katrien, dit boekje is ook van en voor jou. Jij bent diegene die me elke dag gelukkig maakt en die me dat duwtje in de rug geeft wanneer het nodig is. Het evenwicht tussen de S8 en thuis, tussen het doctoreren en de momenten voor ons 2 en tussen werk en ontspanning was soms ver te zoeken, maar bedankt voor het geduld, het vertrouwen en de onvoorwaardelijke steun. En wees gerust, ik hou het bij één doctoraat!

Bedankt voor alles!
Timo
Mei 2014

PREFACE

Dear reader

Dear colleagues, family, friends

After more than six years, I still have little clue about what to write in the preface of my PhD dissertation. It seems that writing this preface will even be harder than writing the introduction or the conclusions, which are respectively supposed to trigger your interest for what follows or supposed to convince you of the important added-value of this work. Nonetheless, this preface is the opportunity to look back on the past years and to thank everybody. It were exciting, interesting, fun and enriching years at the Department of Geography and therefore I would like to thank everybody who has contributed to those experiences.

First of all, I would like to thank the colleagues from my research group (3D Data Acquisition): especially my promoter, Prof. dr. ir. Alain De Wulf, and Prof. dr. Rudi Goossens for the support, for the research opportunities they have given me, for the field campaigns in Belgium and certainly also for the campaigns and conferences abroad. Of course, my gratitude also goes out to my close colleague Coen, to Marijn, Leen, Frederik, Nasem and to the other colleagues who joined of our research group during the past years. Further on, following persons certainly deserve to be thanked as well: our head of department, Prof. dr. Philippe De Maeyer, and the other professors from the Department of Geography. To the many colleagues who were or still are part of our department and especially to those of you who have (voluntarily?) joined me during the tunnel measurements: thanks a lot!

Prof. dr. ir. Philippe Van Bogaert, Prof. dr. ir. Hans De Backer, ir. Ken Schotte, the other staff from the Department of Civil Engineering, Prof. dr. ing. Greet Deruyter, Prof. dr. Denis Constales and Jacky Chow: thank you for the collaboration during the tunnel measurements and for your feedback during the processing and discussion of the results. Thanks to the members of the reading and examination committee, the co-authors and reviewers of my publications and all the others who have contributed in any way, for their support and helpful feedback.

The past six and a half years were much more than just research. Teaching, guiding exercises, guiding master theses and ‘camping’ on the Kemmelberg or in Vassivière were another big part of the wonderful memories. Thanks to the students for those memories and especially to those who have contributed to the tunnel measurements or the processing of the data.

To the “LMK2003 + Thomas” gang, Katrien & Seb, Matthias and other fantastic people I can call my friends: thanks for continuously supporting me, laughing with my jokes and listening to my more or less interesting conversations. May many more follow!

An important reason why I could become a surveyor and why I've reached this point is the love and support I got from my parents. I cannot thank them enough for that. Also to my sister, my grand-parents and other family members: thank you for your support and interest in my research. You will have to be more creative for the next New Year's wishes!

Thanks a lot to Stephanie for the layout of the cover of this book.

And finally, two ladies I absolutely cannot forget to thank:

Helga, thanks for being much more than 'just a colleague' during my years at the department. You were always there to listen when I needed some support or when I needed to get something of my chest!

Dear Katrien, this work, this little book, has certainly also written your name on it. You're the one that makes me happy every single day and you're the one who gives me that little loving push when I need it. Especially during the last months, it was sometimes difficult to balance work and our personal time, but I could not have done this without you. Thanks for your patience and your unconditionally love and support.

Thanks for everything!
Timo
May 2014

SAMENVATTING

Een grondige risicoanalyse van grote infrastructuurwerken (zoals bijvoorbeeld tunnels) behelst niet alleen het nagaan van de invloed van dit infrastructuurwerk op zijn omgeving, maar ook het onderzoek naar de sterkte en de duurzaamheid van het bouwwerk zelf. Een belangrijk onderdeel van een dergelijke risicoanalyse is het monitoren van het bouwwerk tijdens de constructiefase om eventuele vervormingen al in een vroeg stadium te kunnen detecteren. Het onderzoek voorgesteld in dit proefschrift levert een bijdrage aan deze monitoring, meer specifiek door het gebruik van laserscanning voor een gedetailleerde en zeer nauwkeurige meting van ronde tunnels tijdens hun constructie.

De centrale vraagstelling doorheen dit onderzoek is hoe nieuwe 3D-meettechnieken kunnen bijdragen tot het monitoren van de ovalisatie van tunnels. Deze brede probleemstelling wordt opgesplitst in meerdere specifieke onderzoeksvragen.

Een eerste vraag is welke methodologie kan toegepast worden om laserscanners te gebruiken voor de ovalisatiemonitoring van ronde tunnels tijdens constructie en wat de haalbare nauwkeurigheid is met deze ontwikkelde methodologie. Er wordt ook nagegaan of deze haalbare nauwkeurigheid afhankelijk is van het gebruikte type laserscanner. De methodologie voor de verwerking van de via laserscanning opgemeten puntenwolken focust op het zo duidelijk mogelijk definiëren van elke stap in het verwerkingsproces en op het bekomen van eindresultaten die ondubbelzinnig kunnen gelezen en geïnterpreteerd worden. Het onderzoek naar de haalbare nauwkeurigheden richt zich niet enkel op het halen van de projectvereisten (0,5 mm nauwkeurigheid), maar evenzeer op het verbeteren van de haalbare nauwkeurigheden van monitoringmethodes met laserscanning in vergelijking met methodes die tot nog toe in de wetenschappelijke literatuur worden vermeld.

Daarnaast worden de mogelijkheden onderzocht voor de integratie van de resultaten van zowel laserscanmetingen als rekmetingen, gekoppeld aan de vraag of het gebruik van laserscanning een significante meerwaarde betekent bij deformatiemetingen van tunnels. In de 'Liefkenshoekspoorverbinding' wordt een deel van de tunnels onder de Schelde tweemaal daags beïnvloed door de getijdencyclus van de Schelde. De bijdrage van laserscanmetingen tot het begrijpen van dergelijke complexe deformatieverschijnselen wordt onderzocht.

Ten slotte worden ook mogelijke denkpistes voor verbeteringen of uitbreidingen aan de ontwikkelde methodologie opgenomen in dit onderzoek.

De noodzakelijke metingen voor dit onderzoek werden uitgevoerd tijdens en na de bouw van in totaal vier tunnels in de projecten 'Diabolo' en 'Liefkenshoekspoorverbinding'. In het 'Diabolo' project (2007-2012) werd een dubbele treintunnel geboord over een lengte van 1 km (één tunnelkoker in elke richting) onder de luchthaven van Zaventem (Brussels Airport) om de toegankelijkheid van de luchthaven via het spoor te verbeteren. Beide tunnelkokers

werden geboord met een 'Tunnelboormachine' (TBM) en zijn opgebouwd uit een reeks aaneensluitende ringen met een diameter van 7,3 meter die elk bestaan uit zeven cirkelvormige betonnen segmenten en één kleinere sluitsteen voor het opspannen van de ringstructuur. Het 'Diabolo' project was het eerste infrastructuurproject in België waar in een systematische monitoring met laserscanning werd voorzien. Die systematische monitoring bestond niet alleen uit laserscanmetingen op verschillende locaties verspreid over de lengte van de tunnel, maar ook uit rekmetingen op dezelfde tunnelringen. Deze rekmetingen werden uitgevoerd door de Vakgroep Civiele Techniek (UGent). Een gelijkaardig monitoringprogramma werd uitgevoerd tijdens het project 'Liefkenshoekspoorverbinding' (2010-2014), één van de grootste infrastructuurprojecten ooit in België. Dit project verbindt de linkeroever van de Schelde en het havengebied op de rechteroever via een spoorverbinding voor vrachtvervoer, bestaande uit onder andere een nieuw geboorde tunnel met een lengte van 6 km onder de Schelde en het Kanaaldok.

In het eerste hoofdstuk van dit proefschrift worden zowel de onderzoeksvragen (cfr. supra) als beide tunnelprojecten ('Diabolo' en 'Liefkenshoekspoorverbinding') verder gedetailleerd. Hoofdstuk twee behandelt het meetprincipe van laserscanning, de verschillende types laserscanners en mogelijke meetfouten die kunnen optreden. Daarna wordt telkens een (deel van een) specifieke onderzoeksvraag besproken, te beginnen met de ontwikkelde methodologie voor het uitvoeren van de tunnelmetingen en het verwerken van de puntenwolken (hoofdstuk 3), de verschillende haalbare nauwkeurigheden (hoofdstuk 4) en de integratie van de laserscanmetingen en de rekmetingen (hoofdstukken 5 en 6). Hoofdstuk 7 bespreekt een automatisch filteringalgoritme dat werd ontwikkeld ter vervanging van de manuele filtering van de gemeten puntenwolken en dat aldus de methodologie optimaliseert. Op het einde van dit proefschrift volgt een discussie waarin een overzicht van de resultaten wordt gegeven en de bijdrage van dit onderzoek tot het onderzoeksveld van de ovalisatiemonitoring wordt besproken (hoofdstuk 8). Mogelijke toekomstige denkpistes, gebaseerd en verder bouwend op de waardevolle beschikbare datasets, worden behandeld in hoofdstuk 9. Ten slotte wordt dit proefschrift afgesloten met een aantal algemene conclusies (hoofdstuk 10).

Het ontwikkelen en toepassen van een methodologie voor het gebruik van laserscanning voor ovalisatiemonitoring gebeurde succesvol tijdens het 'Diabolo' project. Een verdere optimalisatie werd uitgevoerd tijdens het project 'Liefkenshoekspoorverbinding'. In deze methodologie worden de metingen van verschillende tijdstippen met elkaar vergeleken op basis van een manuele filteringprocedure, een berekende best passende cilinder, een *mesh* van de betonnen tunnelwand en een doorsnede door een gemarkeerd referentiepunt. Deze vergelijkingen van de metingen worden dan gebruikt ter evaluatie van de ovalisatie van de tunnelringen. Gebruik makend van bovenstaande methodologie werden verschillende types laserscanners getest en werden verschillende *smoothing* gradaties van de berekende doorsneden vergeleken. Uiteindelijk werd in dit onderzoek geopteerd voor de combinatie van de Leica HDS6100 fase-laserscanner met een *smoothing* interval van [x-0,5 gon; x+0,5

gon] van de doorsnede, wat overeenkomt met 5,7 cm op het tunneloppervlak. Dit onderzoek toonde aan dat deze methodologie kan resulteren in een haalbare standaardafwijking van 0,48 mm. Dergelijke resultaten voldoen aan de opgelegde vereisten van beide tunnelmonitoringprojecten en overtreffen bovendien de resultaten die in recente wetenschappelijke literatuur worden beschreven. Als er rekening wordt gehouden met een 95%-betrouwbaarheidsinterval, kunnen afwijkingen tussen twee vergeleken doorsneden groter dan 1,36 mm ($2\sigma\sqrt{2}$) worden geïnterpreteerd als significant. De ontwikkelde methodologie steunt echter op een relatief tijdrovende manuele filteringprocedure voor de puntenwolken. In de eindfase van voorliggend onderzoek werd deze manuele procedure dan ook vervangen door een geautomatiseerde filtering en cilinder *fitting* procedure, gebaseerd op het Levenberg-Marquardt algoritme. Deze geautomatiseerde aanpak reduceert de verwerkingstijd voor de filtering van puntenwolken en het berekenen van doorsneden van zo'n één à twee uur tot enkele tientallen seconden en verlaagt de haalbare standaardafwijkingen tot 0,27 à 0,30 mm.

De gelijktijdig uitgevoerde rekmetingen geven een duidelijk en nauwkeurig beeld van de realtime belasting van en druk uitgeoefend op de individuele betonnen segmenten waaruit de tunnelstructuur is opgebouwd. De combinatie van twee gelijktijdig gebruikte meettechnieken (laserscanning en rekmetingen) in dit onderzoek verschaft meer informatie over de veranderingen in de vorm van de tunnelringen en een gedetailleerdere kwantificatie van deze deformaties. In dit onderzoek wordt aangetoond dat de resultaten van beide technieken gecombineerd kunnen worden en dat ze elkaars conclusies over de geovaliseerde vorm van de tunnelringen bevestigen. Daarenboven toont dit onderzoek duidelijk aan dat een combinatie van rekmetingen en laserscanning, aangevuld met waterpassing in het geval van het project 'Liefkenshoekspoorverbinding', waardevolle inzichten kan bieden in het monitoren van meer complexe deformatiepatronen van tunnelconstructies. Meerdere meetreeksen met een waterpasinstrument hebben immers uitgewezen dat de tunnelringen onder de Schelde een variatie in hoogte tot 10 mm vertonen tussen hoog- en laagtij. Deze hoogtevariaties kunnen voornamelijk veroorzaakt worden door twee verschijnselen: een verandering van de vorm van de tunnelringen tijdens elke getijdencyclus (samendrukken van de tunnelring bij hoogtij en terug uitzetten bij laagtij) of een verticale beweging van een groter deel van de tunnel in zijn totaliteit. Afhankelijk van de mogelijke oorzaak, houdt deze vervorming bepaalde risico's in voor de sterkte en duurzaamheid van de tunnelstructuur en dit vraagt dan ook om specifieke maatregelen. De combinatie van gelijktijdig uitgevoerde waterpas-, rek- en laserscanningmetingen tijdens een getijdencyclus toont aan dat het niet de vorm van de tunnelringen zelf is die verandert tijdens een getijdencyclus. Dat leidt mogelijks tot de conclusie dat het deel van de tunnel onder de Schelde in zijn geheel een verticale beweging ondergaat, afhankelijk van het waterniveau in de Schelde. Deze conclusie heeft een belangrijke invloed op de risicoanalyse, op de duurzaamheid van de tunnelconstructie en de verder te nemen risicobeperkende maatregelen.

De bevindingen in dit doctoraatsonderzoek kunnen leiden tot een aantal mogelijke pistes voor toekomstig onderzoek. Daarbij lijken voornamelijk ontwikkelingen die zich focussen op de informatie die uit de gedetailleerde en nauwkeurige puntenwolken kan gehaald worden interessant. Naast de ovalisatiemonitoring gebaseerd op doorsneden (zoals de methodologie ontwikkeld in dit onderzoek), kan een monitoring op basis van de eigenlijke positieveranderingen van de individuele tunnelsegmenten tijdens de eerste maanden na constructie leiden tot nieuwe inzichten in het deformatiepatroon en tot verbeteringen aan de deformatiemodellen. De eerste stappen in die richting werden reeds geanalyseerd door het monitoren van de positieveranderingen van individuele segmenten op basis van de berekende 2D-doorsneden. Een belangrijke meerwaarde voor toekomstig onderzoek zit echter in het feit dat deze monitoring van individuele segmenten kan uitgebreid worden naar een 3D-benadering op basis van de beschikbare puntenwolken.

Samenvattend biedt dit onderzoek een antwoord op de vraag hoe laserscanning als vernieuwende meettechniek toegepast kan worden bij ovalisatiemetingen in tunnels. Er werd een methodologie ontwikkeld voor het uitvoeren van de metingen en het verwerken van de puntenwolken, met standaardafwijkingen tot 0,27 mm afhankelijk van het gebruikte type laserscanner en de toegepaste gradatie van *smoothing*. Bovendien wordt aangetoond hoe het gebruik van laserscanning voor monitoring niet alleen leidt tot nieuwe inzichten in complexe deformatiepatronen, maar ook hoe de gedetailleerde, nauwkeurige 3D-puntenwolken in de toekomst kunnen gebruikt worden voor andere vormen van tunnelmonitoring, bijvoorbeeld op basis van de individuele segmenten. Met deze vooruitgang in het gebruik van laserscanning voor deformatiemetingen levert dit proefschrift een relevante bijdrage tot een nauwkeurige en up-to-date risicoanalyse van tunnels, waarbij de methodologie en conclusies uit dit onderzoek ook als basis kunnen dienen voor de deformatiemonitoring van grote infrastructuurwerken in het algemeen.

ABSTRACT

A comprehensive risk assessment of large infrastructural projects, such as tunnel constructions, should not only focus on the impact of the structure on its surroundings, but also on the strength and durability of the structure itself. Monitoring the structure during the construction phase is one of the most important parts of such a risk assessment, in order to detect deformations in an early stage. The research presented in this dissertation contributes to that monitoring process by using laser scanning for highly accurate and detailed measurements of circular tunnels under construction.

The main research question in this dissertation is how the use of innovative 3D measurement techniques can contribute to tunnel ovalisation monitoring. To provide an answer to this key research question, several -more specific- topics are examined, such as which methodology should be used when applying laser scanning to monitor newly built circular tunnels and what accuracy could be achieved using this methodology, depending on the type of laser scanner. The laser scanning processing methodology presented in this dissertation attempts to result in unambiguously interpretable deliverables by clearly defining every step of the processing. The achievable accuracies should not only meet the project's requirement (0.5 mm accuracy), but should also focus on exceeding the accuracies currently described in literature dealing with laser scanning monitoring methodologies. Furthermore, the possibilities for an integration of laser scanning and strain gauge measurements are explored, linked to the question if the use of laser scanning results in a significant added-value for the deformation monitoring of tunnel constructions. More specifically, this added-value can be assessed by using laser scanning measurements to unravel the complex deformation pattern of the newly built tunnels under the River Scheldt that are influenced by the twice-daily tide cycle. Finally, this dissertation explores possible short or medium term improvements and expansions to the methodology.

The necessary measurements for this research were performed during two tunnel projects in Belgium. In the 'Diabolo' project (2007-2012) a 1 km long twin tube tunnel was drilled below 'Brussels National Airport' (Zaventem) to improve the northern accessibility of the airport. The two tunnel tubes were drilled with a Tunnel Boring Machine (TBM) and were constructed of consecutive tunnel rings with a diameter of 7.3 m, consisting of seven circular concrete segments and one smaller keystone. This was the first project in Belgium in which a systematic monitoring with laser scanning on several locations of a tunnel structure was performed. The monitoring of the tunnel structure did not only consist of laser scanning measurements on several points in the tunnels, but also of strain gauge measurements on the same locations executed by the Department of Civil Engineering (UGent). A similar monitoring project was performed in the 'Liefkenshoek Rail Link' project (2010-2014), one of the largest infrastructural projects in Belgium. This project established a freight train connection between the left and right bank of the River Scheldt in the Port of Antwerp. Part

of this connection consists of a bored twin tube tunnel of 6 km, crossing the River Scheldt and the Canal Dock.

Chapter 1 further details the above mentioned research questions and provides more background information on the 'Diabolo' and 'Liefkenshoek Rail Link' projects. The measurement principle of laser scanning, the different types of laser scanners and the possible measurement errors are explained in chapter 2. The following chapters each focus on one or more of the specific research questions, starting with the general measurement and processing methodology (chapter 3), the assessment of the different achievable accuracies (chapter 4) and the integration of laser scanning and strain gauge measurements (chapters 5 and 6). During the final phase of this research, an automated point cloud filtering algorithm (chapter 7) was developed to replace the manual filtering applied in the original methodology. In chapter 8, a discussion section deals with a general overview of the results and their contribution to the research field of ovalisation monitoring. Possible further research possibilities based on the available data are explained in chapter 9 and a general conclusion is given in chapter 10.

The developed methodology to use laser scanning for ovalisation monitoring was successfully implemented during the 'Diabolo' project and was further optimised during the 'Liefkenshoek Rail Link' project. Based on a manual point cloud filtering step, a best-fit cylinder, a mesh of the concrete tunnel section's surface and a cross-section through a marked reference point, the measurements from different epochs could be compared and the ovalised shape of the monitored tunnel rings could be assessed. Different types of laser scanners and different smoothing levels of the cross-sections were evaluated. The applied combination of a phase-based laser scanner (Leica HDS6100) with a [x-0.5 grad; x+0.5 grad] smoothing interval of the cross-section resulted in an achievable standard deviation of 0.48 mm. Such a smoothing interval matches with 5.7 cm on the tunnel's surface. These results meet the project requirements and surpass the methodologies currently described in literature. Considering a 95% confidence interval, deviations larger than 1.36 mm ($2\sigma\sqrt{2}$) are considered as significant deviations between cross-sections from consecutive epochs. However, this methodology contains a time consuming processing step for the manual filtering of the point clouds. The implementation of a Levenberg-Marquardt based automated point cloud filtering and cylinder fitting algorithm reduces this processing time to just a couple of tens of seconds (compared to 1 to 2 hours with the manual procedure) and it even increases the achievable accuracy up to a standard deviation of 0.27 - 0.30 mm.

The simultaneously performed strain gauge measurements provide us with a thorough view on the real-time loads acting on the individual precast concrete segments of the tunnel rings. Both measurement techniques (strain gauges and laser scanning) result in more information about the deformations in the shape of the monitored tunnel sections and a more detailed quantification of these deformations. The matching of both types of results reveals that the conclusions about the 'egg' or 'pumpkin' shape of the monitored tunnel

rings are confirmed by both techniques. But more importantly, this research has clearly shown that a combination of the results of both measurement techniques complemented with additional levelling measurements, can offer valuable insights in complex deformation problems of tunnel structures. Between the River Scheldt's low and high tide, a part of the 'Liefkenshoek Rail Link' bored tunnels shows a height variation up to 10 mm in the tunnel rings below the river, measured with levelling. This height variation could result from two major causes: a deformation of the ovalised shape of the tunnel rings during each tide cycle, or a vertical movement of a large part of the tunnel. Each of these causes implies its own risks on the strength and durability of the tunnel structure. The combination of levelling measurements with simultaneous strain gauge and laser scanning measurements revealed that no deformation of the shape of the tunnel rings occurs, but that the part of the tunnel situated under the River Scheldt undergoes a vertical displacement. This conclusion significantly influences the risk assessment for the durability of the structure.

Future developments in this research field seem to be particularly promising when focusing on the information retrievable from the highly detailed and accurate laser scanning point clouds. Besides the cross-section based monitoring of tunnel sections, as investigated in the developed methodology, monitoring the position of the individual segments during the first months after their construction can lead to new insights in the deformation patterns and can improve the deformation prediction models. First steps in this direction have already been initiated by monitoring individual segments based on the available 2D cross-sections. However, this monitoring aspect could be extended to a full 3D approach based on the available laser scanning data.

Summarised, this research provides an answer to the question how laser scanning, as a typical example of innovative 3D measurement techniques, can be used to contribute to tunnel ovalisation monitoring. A measurement and point cloud processing methodology has been developed resulting in achievable standard deviations up to 0.27 mm, depending on the used type of laser scanner and applied smoothing level. Moreover, it has been demonstrated that monitoring with laser scanning offers new insights in the deformation pattern of tunnels, besides the more established monitoring techniques. It is also proven that the detailed and accurate 3D point clouds can be used for an even more advanced segment wise monitoring. Based on these improvements in deformation monitoring with laser scanning, this research aims to support important steps forward in an accurate and up-to-date risk assessment of not only tunnel structures, but also large infrastructural projects in general.

TABLE OF CONTENTS

LIST OF FIGURES

LIST OF TABLES

CHAPTER 1
GENERAL INTRODUCTION

1. GENERAL INTRODUCTION

This general introduction gives an overview of the research on tunnel deformation monitoring presented in this dissertation. First of all, the wider context of the research is presented. This is done by discussing not only the need for monitoring large infrastructural constructions, but also the use of 3D measurement techniques for these applications. The second section focuses on laser scanning for deformation monitoring of newly constructed circular tunnels. Because the research and data collection is mainly project-based, the third section describes the two projects that lie at the base of this research, namely the 'Diabolo' project (Zaventem, Brussels, Belgium) and the 'Liefkenshoek Rail Link' project (Antwerp, Belgium). Then, the detailed research questions to which this work attempts to deliver a profound answer and significant contribution are explained. The introduction section ends with an overview of the content of the following chapters.

1.1. Research context

1.1.1. 3D data acquisition for monitoring

A still growing range of applications and projects asks for highly accurate and highly detailed 3D information. Therefore, high-end 3D measurement techniques such as laser scanning and 3D photo modelling are more and more being applied. These measurement techniques are being used for the fast 3D recording of objects, for example for recording archaeological sites and objects (Figure 1-1), rock slides, architectural heritage, forensics and crime scene investigation,… (e.g.: Barber, Mills, & Bryan, 2003; Kersten, Mechelke, Lindstaedt, & Sternberg, 2008; Lerma Garcia, Van Genechten, Heine, & Santana Quintero, 2008; Lichti, Gordon, & Tipdecho, 2005; Zogg & Ingensand, 2008). Besides, they are also being used for deformation monitoring of civil technical constructions.

Construction sites often have a large impact on their surroundings due to ground settlements during the building phase or even during the following years. Also, the risks on site during the construction phase have to be minimised and the safety of the workers has to be guaranteed. Therefore, a thorough risk assessment during construction and during the structure's further life cycle is of the utmost importance. Monitoring the stability of a civil technical structure is a challenging task and has already been addressed for a long time in literature. Such a risk assessment needs to be based on accurate and complete 3D data, up-to-date information and tools to quickly and unambiguously interpret the results (Caballero, Esteban, & Izquierdo, 2007; Lerma Garcia et al., 2008). However, the type and scale of the structure and the required accuracy influence the measurement techniques and measurement instruments that can be used. Moreover, other restrictions such as the available time on site and the location's accessibility also play an important role in the choice of the measurement technique and the measurement instruments.

Figure 1-1: Laser scanner used for the 3D recording of Sint-Baafs Abbey (Ghent, Belgium)

Not only the impact of the structure's deformations on its surroundings has to be followed up, the deformations can also impact the strength and durability of the structure itself. Therefore, an important part of a risk assessment should be situated during the construction phase of the structure to detect deformations in an early stage. This is also the part where this research focuses on: detecting deformations of large civil technical structures, from the moment of construction until stabilisation or several months after construction. More specifically, this research addresses the deformation monitoring of newly built railway tunnels in Belgium.

1.1.2. Monitoring techniques

Often, measurement time restrictions or the complexity of the object (or scene) result in the inadequacy of traditional surveying techniques and classical photogrammetry. Terrestrial laser scanning or 3D photo modelling based on Structure-from-Motion (SfM) and Multi-View Stereo (MVS) are the most recent alternatives for the still growing demand for very accurate and dense 3D geometrical data. In this research, the focus lies on terrestrial laser scanning applications; therefore other 3D measurement techniques such as aerial laser scanning or 3D photo modelling will not be discussed in detail.

Surveying engineering research has been continuously searching for techniques and methodologies that can be used for the detection of (sub-)centimetre deformations of structures, for example kinematic GNSS measurements (Global Navigation Satellite System) for bridges (Roberts, Brown, & Ogundipe, 2010); total station measurements for hydro-electrical dams (Alba, Fregonese, Prandi, Scaioni, & Valgoi, 2006); 2D or 3D laser scanning for monitoring bridges or harbour locks (Mizoguchi et al., 2013), tunnel monitoring (Argüelles-

Fraga, Ordonez, Garcia-Cortes, & Roca-Pardinas, 2013; Delaloye, Hutchinson, & Diederichs, 2011; Fekete, Diederichs, & Lato, 2010; Lindenbergh, Pfeifer, & Rabbani, 2005; Yoon, Sagong, Lee, & Lee, 2009), measuring beam deflections (Gordon & Lichti, 2007) or monitoring cultural heritage monuments (Beraldin et al., 2000; Ninkov, Bulatovic, Susic, & Vasic, 2010; Stal, De Wulf, et al., 2012). Classical surveying measurements with a total station offer a high to very high accuracy, but are limited in the number of points that can be measured in a certain time on site (Alba et al., 2006). Frequently, it is too dangerous to measure for a couple of hours with a total station on a location because of traffic, operational construction sites or plants,… (Livieratos, 1992). Besides, it is often not even possible to get close enough to the objects to measure all necessary details (Beraldin et al., 2000; Biosca & Lerma, 2008; Girardeau-Montaut, Roux, Marc, & Thibault, 2005; Zeibak & Filin, 2007). To measure a denser point grid on the structure, stereo photogrammetry could be an alternative. However, the measurement conditions on site often do not meet the requirements for photogrammetric recordings, such as a sufficient overlap between the images of a stereo couple, acceptable lighting conditions to guarantee high quality images or enough contrast on the object's surface.

In a lot of these projects, in which the circumstances make the use of total station or classical photogrammetry difficult or impossible, high resolution laser scanning could be a feasible alternative to collect the spatial information fast and with high accuracy (Alba, Roncoroni, & Scaioni, 2008; Rüther et al., 2009; Tao, Chapman, & Chaplin, 2001). Chapter 2 details more the technical specifications, the advantages and possible errors of using laser scanning. But already, it can be stated that the geometrical accuracy of laser scanning (mm-level), even over large distances (several hundreds of metres), and the large amount of points that can be measured in a very short time frame (up to 1 million points per second) are the most important advantages that have caused laser scanning to become more and more popular in a wide variety of applications (Boehler & Marbs, 2003; Lichti, Stewart, Tsakiri, & Snow, 2000; Rioux, 1994). However, the price of the equipment and the still relatively limited automated processing algorithms for the very large 3D point clouds remain important barriers for a practical implementation of laser scanning in a lot of projects (González, Lucena, Fuertes, Rueda, & Segura, 2012; Hesse & Stramm, 2004; Iyer, Jayanti, Lou, Kalyanaraman, & Ramani, 2005; Rahayem, Werghi, & Kjellander, 2012; Sternberg & Kersten, 2007; Walsh, Borello, Guldur, & Hajjar, 2013). Furthermore, a possible integration of laser scanning with high resolution images not only allows acquiring geometrically accurate 3D data, but also allows applying high resolution texture mapping on the laser scanning point clouds or other deliverables (Haala & Alshawabkeh, 2006; Yastikli, 2007). Besides laser scanning, the most recent advances in 3D photo modelling also offer a valuable alternative for the highly detailed 3D recording of objects and structures. In this technique, based on Structure-from-Motion and Multi-View Stereo, an extensive series of high resolution images of the object is simultaneously processed to obtain a full 3D geometric model with high resolution texture instead of processing individual stereo couples only partially covering the object. Notwithstanding the fact that a thorough accuracy and

performance assessment of 3D photo modelling for deformation measurements of structures is still lacking, the use of this technique in other fields such as archaeology, physical geography or crime scene investigation already gives very promising results (Favalli, Fornaciai, Isola, Tarquini, & Nannipieri, 2012; Stal, De Wulf, et al., 2012; Stal, Tack, De Maeyer, De Wulf, & Goossens, 2013).

1.1.3. Tunnel monitoring

When monitoring a tunnel structure, there is an important distinction to be made between monitoring the impact of the tunnel structure on the ground level of the surroundings and monitoring the deformations of the tunnel structure itself. However, deformations of the tunnel structure are likely to also have an influence on the ground surface. On the one hand, monitoring the surroundings covers the measurement, detection and evaluation of ground deformations or settlements of buildings above the tunnel construction's area. These monitoring measurements can be performed from the ground surface or from within the tunnel. On the other hand, monitoring the tunnel structure itself (tunnel convergence) deals with the changes in shape of the tunnel structure and can only be measured from within the tunnel (Kavvadas, 2003). This tunnel convergence monitoring forms the focus of the presented research.

Tunnel structure monitoring goes further than calculating the expected deformation pattern by using the already existing mathematical engineering models. Because of the real tunnel lining behaviour and possible non-uniform *in situ* stresses, peaks or unexpected stresses, observations during the construction phase and close monitoring of the structure are indispensable. These measurements then allow assessing the risk profile of the structure on different points in time, complementing the model analyses or even giving new deformation insights which can then be used to improve the model predictions (Mahdevari & Torabi, 2012; Špačková, Šejnoha, & Straub, 2013).

For measuring the tunnel shape different techniques can be used or combined, whether installed on the tunnel surface or operated from within the tunnel. However, most of them have in common that only a limited number of individual points on the tunnel surface or small areas can be measured, so other areas of the tunnel surface then have to be interpolated. As also stated by (Huang, Wang, Huang, & Jeng, 2010), this is not enough to obtain a detailed profile of the tunnel structure. For sufficiently detailed information, hundreds of points of a tunnel profile are needed. The existing monitoring techniques can be distinguished based on the measurement of the absolute position of the measured points or on the measurement of relative positions compared to an initial state of the reference points (Kavvadas, 2003).

Tunnel convergence between individual reference points can be measured with tape extensometers (contact method) or with a total station (non-contact method). Using metal tape extensometers to measure distances between reference points fixed to the tunnel surface can result in an accuracy of around 0.2 to 0.5 mm, for distances of about 10 to 15 m

(Clarke, 1996; Kavvadas, 2003; Kontogianni & Stiros, 2005). This technique allows monitoring deformations by comparing distances between two fixed points along the line of measurement. However, methodologies have been developed to combine these tape extensometer measurements with peripheral accessories available on site to determine absolute displacements of the fixed points, without using additional total station measurements (Moosavi & Khazaei, 2003). To measure deformations of the tunnel surface in three dimensions, a total station can be used for measuring prism reflectors fixed to the tunnel surface. In most cases, prism reflectors are installed every few metres (e.g. every 15-20 m) and on every location several reflectors are installed spread over the tunnel surface (Figure 1-2).

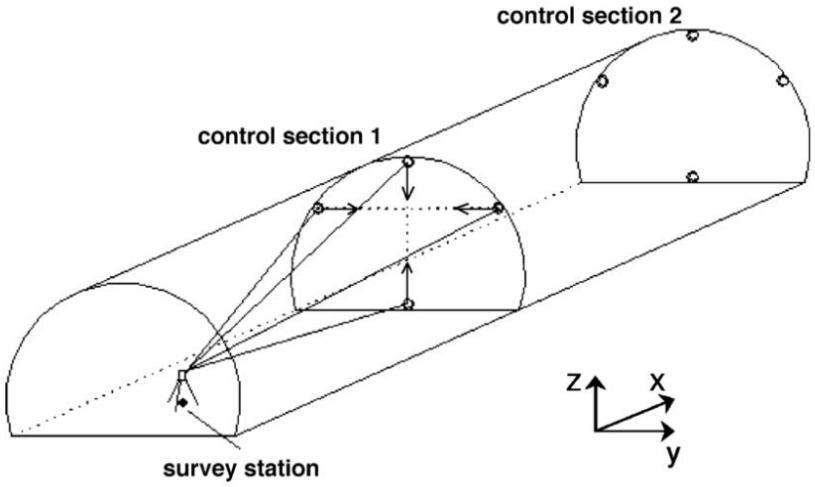

Figure 1-2: Tunnel deformation monitoring with total station by measuring fixed reflectors on the tunnel surface (Kontogianni & Stiros, 2005)

When using reflectorless total stations, which can measure directly on the tunnel surface, the installation of fixed prisms is no longer necessary. Notwithstanding the fact that the time consuming installation of fixed prisms is no longer necessary, the use of the reflectorless measurement principle makes it impossible to measure the same set of points during consecutive monitoring measurements as these points are not materialised (Clarke, 1996).

To obtain absolute coordinates for the measured points, stable reference positions outside the tunnel are foreseen. Based on materialised total station setup positions, successively moved forward, the 3D absolute coordinates of every prism or measured point can be obtained on various points in time. Depending on the length of the tunnel, the specifications of the total station and the use of multiple positions of the measurement instrument in the tunnel, achievable accuracies vary around 2-3 mm for measured lengths and 5 arcsec for angle measurements over distances of about 100 m. The materialised positions for the total station along the tunnel profile, however, cannot be considered as stable reference points. Because of the deformations of the tunnel structure, these total station setup positions are also influenced by these deformations (Kavvadas, 2003). By using a total station, the data

collection and even data processing can be performed in the field, but only a limited number of points can be measured in a fixed time frame (Clarke, 1996). When using motorised high precision total stations in combination with automatic target recognition, the tunnel convergence can continuously be measured and results can be transferred to a computer, giving an alarm when predefined thresholds are reached (Henriques & Casaca, 2006). Using conventional techniques such as total station measurements to obtain the necessary number of points for a detailed profile of the tunnel is very time consuming and not feasible during the construction works on site (Huang et al., 2010).

A first alternative to cover more points on the tunnel surface is the use of so-called 'Tunnel Profile Scanners' or profilometers (Figure 1-3). These instruments are based on the photogrammetric principle of recording stereographic images with two cameras mounted on a fixed frame. By covering the tunnel's surface or a part of it by two overlapping images, 3D information of that part of the surface can be derived, with an achievable accuracy of around 5 mm for each coordinate. Hereby, a total station is used to determine the coordinates of the two camera positions (Kavvadas, 2003). However, because sufficient overlap between the stereographic images and minimum lighting conditions are needed, this technique can often not be applied in tunnel monitoring projects.

Laser scanning is another technique which allows covering a larger part of the tunnel structure with a dense point grid, either from a static setup or from a mobile platform (Qingwu & Wanlin, 2012; Yoon et al., 2009). Because laser scanning is an active measurement technique, restrictions for lighting conditions are not to be considered. Earlier experiments and developed algorithms to process laser scanning data and to detect tunnel deformations result in detectable deformations of about 2 to 5 mm (Yoon et al., 2009). Moreover, laser scanning results in a dense and detailed point cloud of a larger part of the tunnel than just a single profile (Figure 1-4). Because of this large amount of information of the tunnel structure, the measured point cloud can also be used for further processing such as 2D or 3D individual segment monitoring, checking the piping infrastructure or installed railway infrastructure, … Furthermore, because the whole data set is recorded and stored, even later on in the monitoring process, earlier measurements can be reassessed if questions or problems occur.

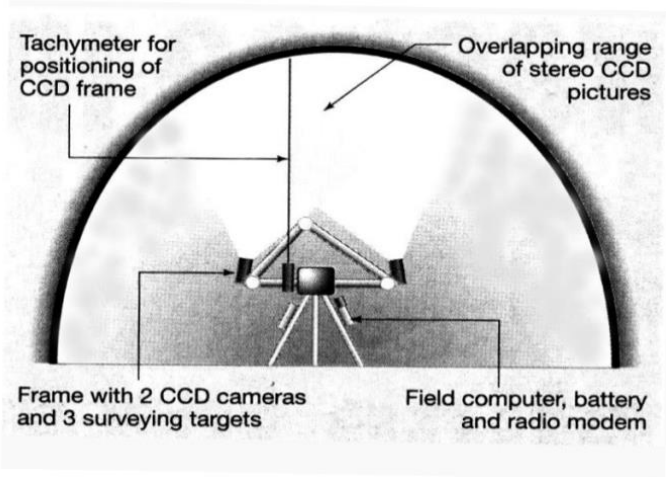

Figure 1-3: Example of a 'Tunnel Profile Scanner', consisting of 2 CCD cameras on a portable frame (Kavvadas, 2003)

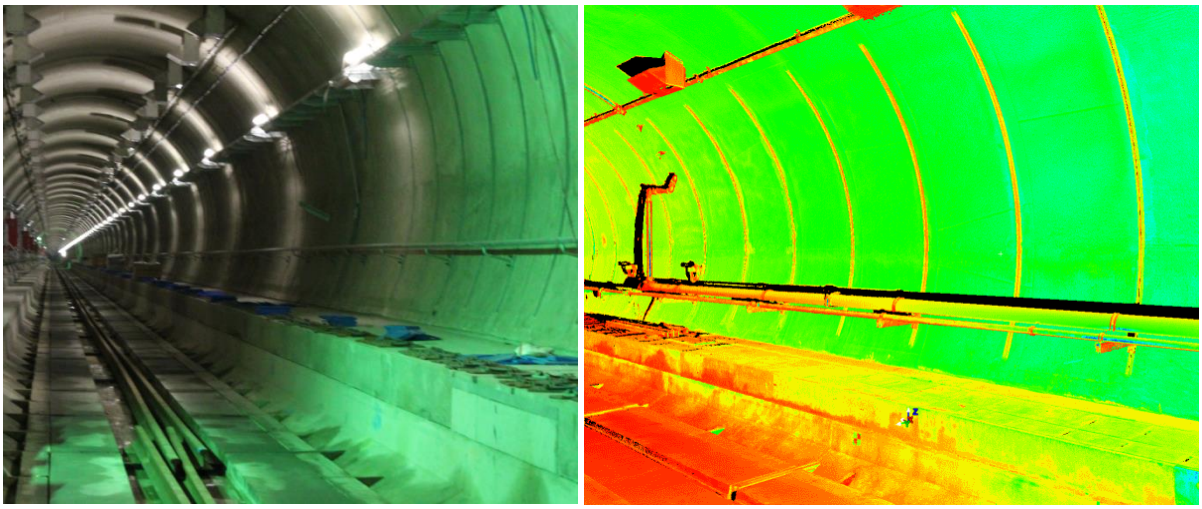

Figure 1-4: Image (left) and point cloud (right) of a tunnel surface, rail bed and installed piping

The above mentioned techniques mainly measure the changes in shape of the tunnel structure. This information is mostly interpreted in combination with measured deformations of such a concrete segment itself, for which strain gauge recordings can be used. By equipping the segments with strain gauges, both on the steel weaponing and on the outside concrete surface, detailed insights into the stress distribution in each segment can be obtained. Figure 1-5 shows an example of a circular tunnel ring equipped with different strain gauges on the individual segments (Bakker, de Boer, Admiraal, & van Jaarsveld, 1999; Schotte, De Backer, Nuttens, De Wulf, & Van Bogaert, 2011).

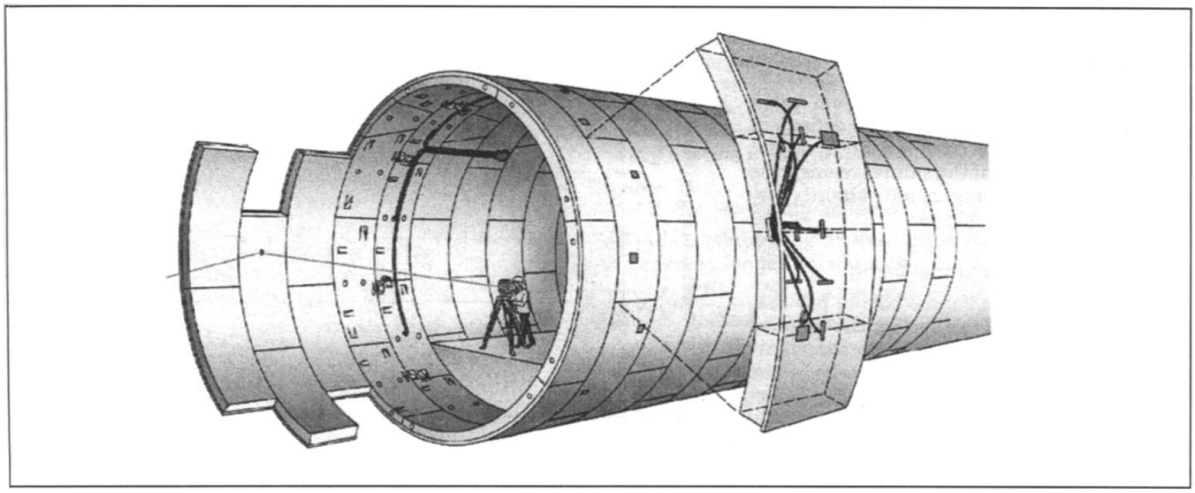

Figure 1-5: Example of a tunnel ring equipped with strain gauge elements (Bakker et al., 1999)

1.2. Research focus

Based on recent advances in 3D measurement techniques and the need for detailed 3D information in monitoring applications, existing research already partly deals with the use of laser scanning for circular tunnel monitoring projects. Based on laser scanning measurements from a mobile or static scanning platform, the measured tunnel structure can be compared with a design shape, in some cases simplified by a fitted flat surface even when the structure includes curved parts. Examples indicate detectable damage, cracks or deformations of 2 mm or larger (Yoon et al., 2009). When comparing measurements or specific cross-sections of a structure between different epochs, different methods can be used to place these measurements or cross-sections in a common coordinate system. One method implies the use of extra total station measurements to determine the coordinates of reference markers so that each measurement can be placed in the common absolute coordinate system (Hesse & Stramm, 2004). Alternatively, specific control features on site can also be used to define a common datum for the different measurements, without total station measurements for an absolute reference (Han, Guo, & Jiang, 2013a, 2013b). Using an absolute coordinate system, however, includes extra measurement equipment and measurement time. Using control features to define a common reference system does not take into account the possible changes in location of the control features caused by the deformation of the tunnel structure. Moreover, the described methodologies in literature lack an unambiguous definition of the longitudinal tunnel axis, which is important for the calculation of radius values (Grün & Akca, 2005; Han et al., 2013a, 2013b; van Gosliga, Lindenbergh, & Pfeifer, 2006).

The methodology developed in this dissertation therefore searches an answer to the definition of a common coordinate system with minimum influences of the tunnel deformation and no extra measurement techniques besides laser scanning. The main part of this research deals with developing a new methodology to use laser scanning for accurate

deformation monitoring, addressing gaps in current research and improving the achievable millimetre accuracy as found in monitoring projects discussed in literature. Additionally, the developed methodology is further optimised by automating the point cloud processing steps. Besides the above mentioned focus, the two recent tunnel monitoring projects in Belgium on which this research is based, the 'Diabolo' and 'Liefkenshoek Rail Link' project, are the first in Belgium in which a systematic monitoring with laser scanning is incorporated in the construction phase. Together with laser scanning, simultaneous strain gauge measurements are performed on most of the same monitored tunnel sections. Both measurement techniques cover different aspects of the deformation pattern of the tunnel's structure. In literature, very few simultaneous strain gauge measurements and laser scanning measurements of actual tunnel lining behaviour are available. Therefore, the question remains how well both data sets agree and how they can be integrated for better insights in the occurring deformation pattern. Therefore, the systematic monitoring with simultaneous laser scanning and strain gauge measurements from the moment of assembly of the tunnel rings until several months after assembly gives a unique data set to assess both measurement techniques and to assess the contributions of their integration to the monitoring of tunnels. The detailed research questions, elaborated in this dissertation, are specified in section 1.4.

One of the main advantages of laser scanning measurements is the almost complete and very detailed recording of a large part of a tunnel structure, without limiting the measurements to specific points or dimensions of the structure. That means that in a first stage of the processing a lot of points will often not be used to elaborate the specific required deliverables. In the first instance, the research focus goes out to cross-sections of the tunnel on a specific location derived from the measured point cloud. The high resolution point set is then available for further processing, allowing deformation monitoring on other tunnel sections or more specific research questions such as which more detailed information can be retrieved from the laser scanning point clouds to contribute to the monitoring of tunnel structures. Attention in that matter could especially go out to the identification of the individual tunnel segments and joints of the monitored sections and the 3D positions of the segments in relation to each other and the possible changes in position caused by the deformation of the tunnel structure.

1.3. Tunnel monitoring projects

1.3.1. 'Diabolo' project (2007-2012)

The tunnel monitoring projects, on which this research is based, are the first in Belgium in which a systematic monitoring with laser scanning was performed. In the first project, the 'Diabolo' project (2007-2012), a twin tube tunnel of 1 km long was drilled at a depth of 16.5 m below 'Brussels National Airport' in Zaventem (Figure 1-6, Figure 1-7). The 'Diabolo' project was set up to improve the northern accessibility of 'Brussels National Airport' starting from 2012. The airport was not easily reachable by train from the north (Antwerp

and The Netherlands). As part of this new railway connection, the newly bored tunnel complex allows trains to significantly reduce their travelling time from the north to the airport railway station, by avoiding the bottleneck in Brussels. More figures about the 'Diabolo' project can be found in chapter 4.

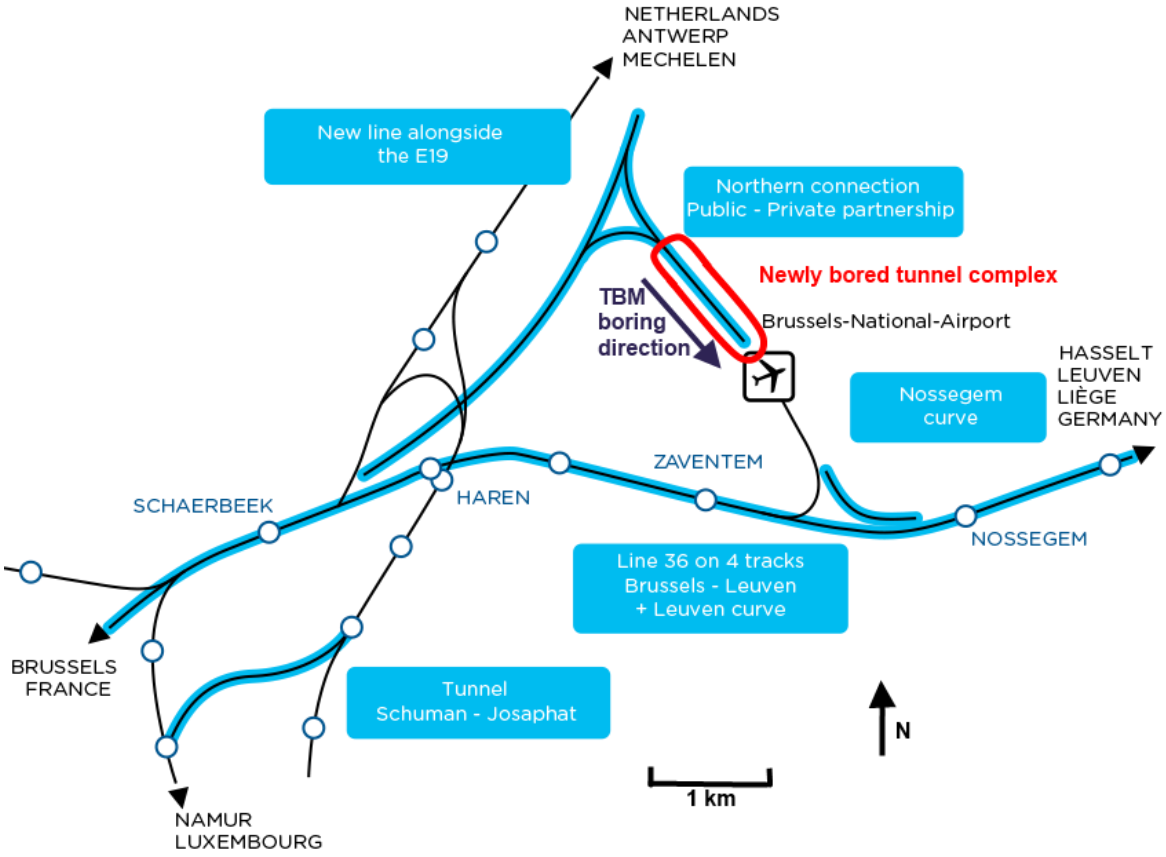

Figure 1-6: Overview of the 'Diabolo' project (based on (Infrabel, n.d.))

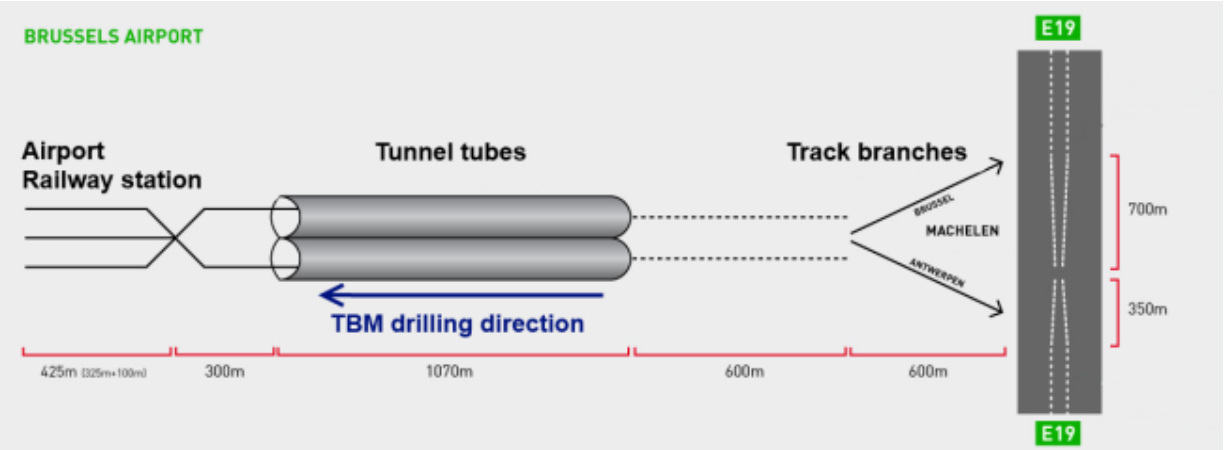

Figure 1-7: Longitudinal cross-section of the 'Diabolo' project (based on (Infrabel, 2009))

The tunnel is drilled using the mixshield method with a Tunnel Boring Machine (TBM), which pushes itself against the last built tunnel ring to move forward to continue boring. The TBM

consists of the boring head of the TBM (under high pressure), which is followed by a series of trailers carrying all the necessary equipment such as piping, electrical cables, a lunch room for the staff, the machine control room and a safety room (Figure 1-8). The segments of the tunnel rings are supplied in the TBM by smaller transportation trains.

The boring of the first tunnel started at the north side and the end point was located under the airport. Generally, in tunnelling projects, when reaching the end point, the TBM is turned to bore the other tunnel tube in reverse direction. However, no such large work site was allowed on the airport site, so the TBM had to be lifted from a relatively small excavation shaft and transported back to the departure location. From that location, the boring of the second tunnel started in the same direction as the first tunnel tube. The cross-passages foreseen between the tunnel tubes are constructed by freezing the soil and subsequent excavation with sprayed concrete (Van Bogaert, 2009). The level of the ground water on this site is about 2 m higher than the crown of the tubes and rises towards the end of the tunnel.

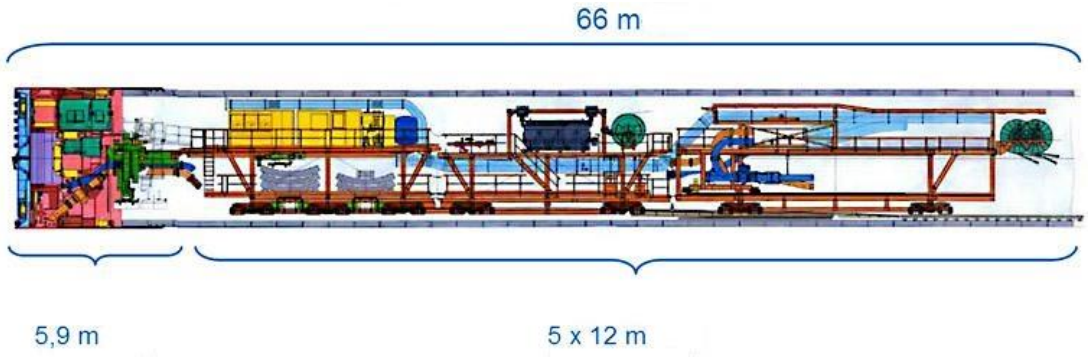

Figure 1-8: Schematic overview of a Tunnel Boring Machine (TBM) with the boring head (left) and trailers (Infrabel, 2009)

The circular concrete tunnel rings (tunnel sections) have an inner diameter of 7.300 m and the eight tunnel segments of which each ring is constructed (seven segments and one keystone) have a radial thickness of 0.350 m. Figure 1-9 shows an image of the situation at the front of the TBM during the assembly of a tunnel ring. On the last installed tunnel ring, the individual segments are visible, together with the smaller keystone at the upper side of the tunnel ring. Each tunnel ring is 1.5 m wide, measured along the longitudinal axis of the tunnel.

During construction, six tunnel sections in each tunnel tube were closely monitored because large settlements of the airport infrastructure or neighbouring hangars had to be avoided or at least detected in an early stage. To do so, close monitoring of the tunnel structure during the construction phase was ordered based on twelve monitored sections spread over the total length of both tunnels, but with one monitored tunnel section in each tube specifically under the airport (Schotte, De Backer, Nuttens, De Wulf, & Van Bogaert, 2010). The part of the bored tunnels under the airport is critical, because the tunnels cross an airport runway, aircraft taxi lanes and several of the other airport buildings and piers at a depth of only 16.5 m without shutting down any airport activity. Figure 1-10 indicates the location of the

monitored tunnel sections in Tunnel 1 of the 'Diabolo' project, together with the location of the main airport runway, the evacuation shaft and the two cross-passages between Tunnel 1 and 2. For Tunnel 2, the scheme would be very similar, although the monitored tunnel rings can differ a couple of ring numbers.

Figure 1-9: Assembly of a tunnel ring - different segments of the tunnel ring with the smaller keystone at the top

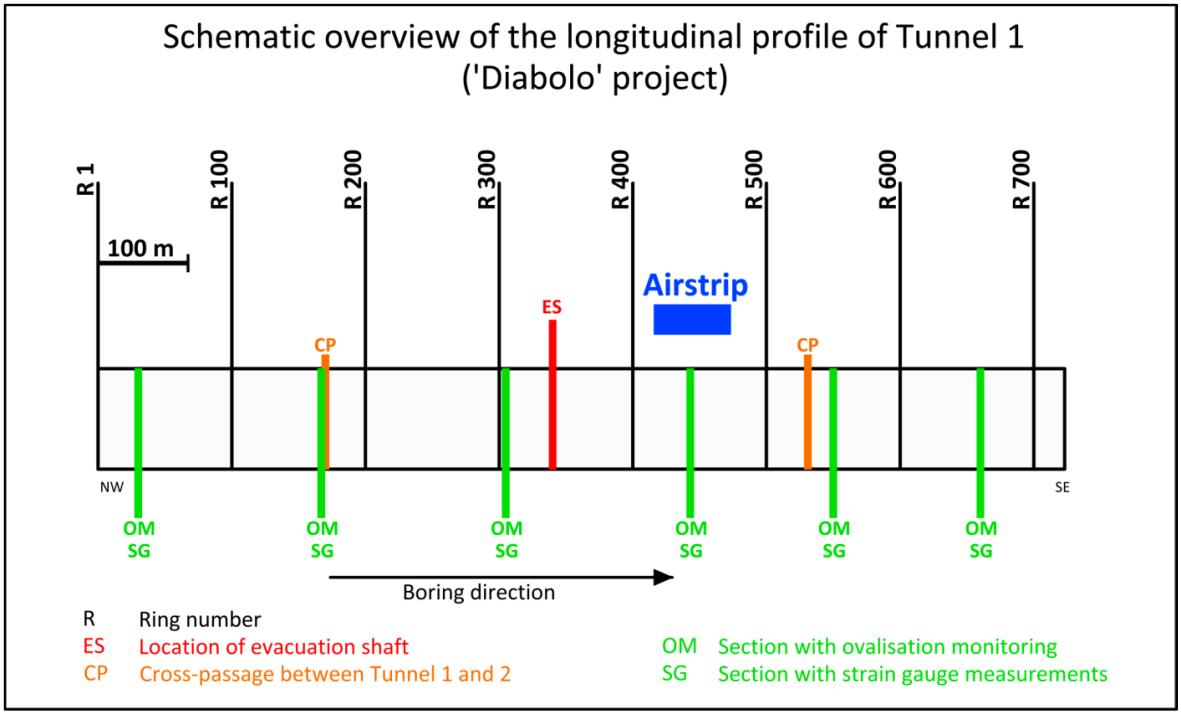

Figure 1-10: Overview of the locations of the monitored tunnel sections in Tunnel 1 ('Diabolo')

The monitoring of the deformation of the tunnel sections is based on static terrestrial laser scanning with a measurement immediately after assembly of the tunnel ring ('reference measurement') in the limited free space in the head of the TBM, followed by a series of measurements during the first three months after assembly (see section 3.4.1 for a detailed explanation about the measurement setups). During the first month after assembly of a tunnel section, measurements were scheduled every week ('control measurements 1 to 4'). 'Control measurements 5 and 6' were scheduled respectively two months and three months after the assembly of the tunnel section. Some of these scheduled measurements could not be performed, due to circumstances on site such as construction works that did not allow entering the tunnel. In total, around 85 monitoring reports were elaborated during this project. Most of these reports summarise the results of the performed reference and control measurements, other reports consider supplementary measurements such as a seven day period with daily monitoring measurements. Moreover, on all of the monitored tunnel sections, strain gauge measurements were performed by the Department of Civil Engineering (UGent, Faculty of Architecture and Engineering) to measure the strains of the individual concrete segments.

During this tunnel monitoring project, a measurement and data processing methodology was developed and tested, taking into account the different project restraints such as the limited allowable downtime of the TBM during the reference measurements and a required accuracy of 0.5 mm. The successful use of laser scanning for the deformation monitoring of the tunnels in the 'Diabolo' project was followed by a similar monitoring campaign for the 'Liefkenshoek Rail Link' project.

1.3.2. 'Liefkenshoek Rail Link' project (2010-2014)

The 'Liefkenshoek Rail Link' project (2010-2014) was one of the biggest infrastructural projects ever in Belgium and it was designed to establish a new railway connection between the left and right bank of the River Scheldt for freight traffic in the Port of Antwerp. By using this new railway connection, freight trains are able to reach both river banks without having to leave the port area and without occupying the rail connections used by passenger trains. The new railway connection has a total length of approximately 16 km, of which 6 km consists of two new side-by-side tunnel tubes. The newly constructed tunnel complex crosses two water ways (River Scheldt and Canal Dock/Port Canal). Another part of the railway connection also runs below the Waasland Canal through the existing but never used Beveren tunnel (Figure 6-1). For the drilling of both tunnel tubes two mixshield TBM's (called "Schanulleke" and "Wiske") were used. In January 2010, the first TBM started drilling one tunnel tube and the second TBM started drilling in March 2010. The two TBM's reached their end point after 6 km in respectively August and May 2011 (Figure 1-11). The first TBM started earlier and ended later because during its drilling works, the workers also prepared the construction of the cross-passages and the evacuation shafts.

Figure 1-11: Tunnel Boring Machine 1 ("Wiske") reaches its destination point at the arrival shaft

The ground composition along the tunnel's route has a variable nature (Figure 3-1). The soil stratification has a general downward slope from the west to the east. The left bank of the River Scheldt (west) consists of sandy layers until a depth of 4 to 6 m. Under these layers, a quaternary soil made out of soft clay, vases and peats is present. This clay layer does not occur on the right bank of the river (east). Below, there is a layer of the tertiary era of maximum 6 m, containing silt and a mixture of fine sand and clay. This layer lies on top of a 6 m thick tertiary sand stratum, containing silt and clay particles and further below there is a 9 to 14 m thick layer of tertiary fine sands but containing clay as well as glauconite. These sandy layers have a smaller thickness on the left river bank. At larger depth, the soil consists of Boom clay, which is a soil type saturated with water and acting as an impermeable soil layer. The tunnel's trajectory mostly runs through the tertiary sands, but at its deepest point (below the River Scheldt) it also runs partly through the Boom clay layer. The TBM's passing below the River Scheldt and the Canal Dock needed special attention and extra preparation works. For example, accessing the boring chamber or replacing parts of the cutting wheel was impossible while crossing under the River Scheldt. In the Canal Dock, other restrictions influenced the drilling works. When passing the Canal Dock, there was only about 3 m of sand between the upper side of the tunnel and the bottom of the channel. To increase the safety, the Canal Dock should have been filled with an extra layer of sand of about 7 m, but that was impossible for the ships traffic. A solution was found by replacing the 3 m sand layer by a concrete slab of about 2 m thick, which on its turn was again covered by a 2 m thick sand bed. After the boring of the tunnel, the sand bed was removed to recover the whole channel depth for ship traffic (Van Bogaert, 2009). Besides, because the water level in

the River Scheldt undergoes twice-daily tidal variations, these water level variations also influenced the allowable drilling pressure during construction phase and the stability of the structure after construction.

The characteristics of the tunnel structure are similar to the ones of the 'Diabolo' project, although there are some differences in dimensions. The tunnels also have an inside diameter of 7.300 m, but the concrete tunnel segments have a thickness of 0.400 m. The width of each tunnel section is 1.800 m. As with the 'Diabolo' project, each tunnel section consists of seven concrete segments and one smaller keystone (TUC Rail, 2010). In each tunnel tube ('Tunnel North' and 'Tunnel South'), fourteen tunnel sections were selected to be monitored, including a specific tunnel section in each tube under the River Scheldt. Figure 1-12 represents an overview of the locations of the monitored tunnel rings in Tunnel North of the 'Liefkenshoek Rail Link' project. This figure clearly shows the spread of the monitored tunnel rings over the total length of the tunnel and shows the specific monitored tunnel rings under the River Scheldt and the Canal Dock. Such a schematic overview for Tunnel South would look very similar, although there would be small differences in ring numbers. For each monitored tunnel section, seven measurements were scheduled, starting from immediately after assembly of the tunnel ring and continuing with four measurements during the first month after assembly, and measurements two and three months after assembly. During the whole monitoring period (2010-2013) more than 190 reports were finalised, including the monitoring reports for all scheduled measurements, a monitoring report on the impact of the drilling of one tunnel tube on the adjacent tunnel structure and a report on an integrated monitoring campaign during a tidal cycle of the River Scheldt.

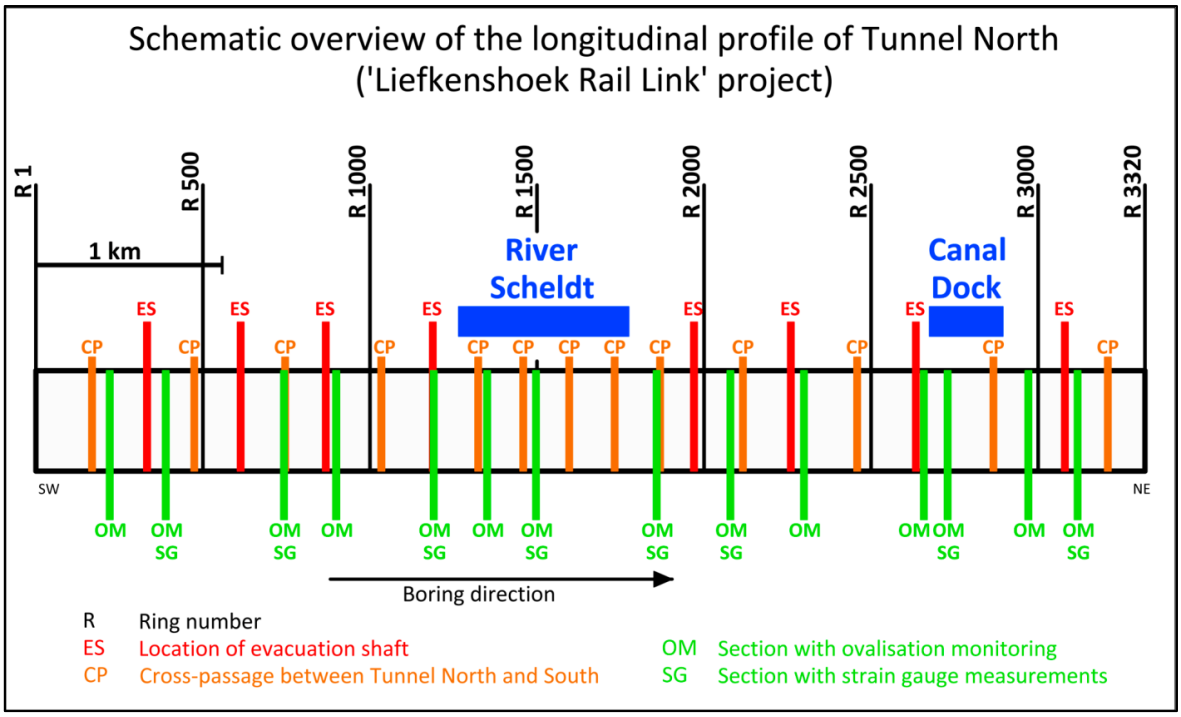

Figure 1-12: Overview of the locations of the monitored tunnel sections in Tunnel North ('Liefkenshoek Rail Link')

1.4. Research questions

The research summarised in this dissertation arose from one general research question, which covers the disquisition presented in the following chapters:

How can the use of innovative 3D measurement techniques contribute to tunnel ovalisation monitoring?

This general research question was the starting point for a number of more detailed research questions, described below. Each of these research questions deals with a part of the problem statement mentioned above. Notwithstanding the fact that the performed research answers the proposed research questions, along the way other questions arose. A preliminary answer to those new or more detailed questions could be given or initiated. However, a lot of opportunities to enhance the research in this field remain.

The more detailed research topics that are analysed in this research are:

Which methodology can be used to apply laser scanning for monitoring newly built circular tunnels?

The first and most important research topic was to develop and evaluate a methodology to perform the monitoring measurements with laser scanning in the 'Diabolo' project (2007-2012), anticipating on the restrictions on site and the required accuracy. The research consisted of selecting the most suited laser scanning instrument and other necessary measurement equipment and developing a methodology for the measurements on site, the processing of the data and the elaboration of detailed and clearly interpretable results of the measurements and deformations. This part of the research is meant to offer a highly accurate solution for reliable and consistent laser scanning measurements immediately after assembly of the tunnel rings in the front of the Tunnel Boring Machine (TBM) and during the following months. Not only do we need a repeatable and user controlled processing workflow resulting in unambiguously interpretable deliverables, we also need a profound solution for a stable reference system between consecutive measurements. Based on the experience from the 'Diabolo' project, this developed methodology was optimised and further developed in the 'Liefkenshoek Rail Link' project (2010-2014), including further automation of the point cloud processing.

Further on in this research, additional improvements to the methodology are proposed. The point cloud filtering and cylinder fitting steps in the methodology have been automated, resulting not only in a much shorter processing time, but also in even smaller achievable standard deviations.

What is the achievable accuracy of the developed methodology and how does it depend on the type of laser scanner?

A founded methodology to perform tunnel monitoring measurements with laser scanning is one thing, but -as part of research in surveying- an important question remains: the achievable accuracy. The achievable accuracy of the developed methodology has to be assessed, depending on the various types of laser scanning instruments. Therefore, different types of laser scanning instruments have been tested during this research, to compare and evaluate the differences in experimentally based achievable standard deviations and in performance on site. Moreover, the processing parameters, such as the smoothing of the cross-section's radius values, have been adjusted and compared to find the optimum between accuracy and visual interpretation of the results and to improve the monitoring accuracy compared with already existing methodologies.

Can these measurements be combined with the strain gauge measurements that are simultaneously performed during the tunnel monitoring projects?

Simultaneously with the laser scanning measurements, researchers from the Department of Civil Engineering of Ghent University performed strain gauge measurements on the same monitored tunnel sections. These strain gauge recordings give insight in the deformations of the tunnel structure, but on a different scale than the laser scanning measurements. As these results are available of the same tunnel sections from the same time frame, the question arises if these results lead to the same conclusions about the tunnel deformations and how these results can be combined and compared.

Does the use of laser scanning result in a significant added-value for the deformation monitoring of tunnel constructions?

Theoretically, laser scanning offers important advantages compared to more classical 3D measurement techniques such as total station and classical photogrammetry. Can it be concluded that, based on the application of laser scanning in both tunnel monitoring projects, these advantages also count for *in situ* tunnel measurements?

One case study that can be used to address this issue is the simultaneous use of laser scanning, strain gauge and levelling measurements in the 'Liefkenshoek Rail Link' tunnel during a tide cycle of the River Scheldt. These measurements provide the ideal data set to evaluate the added-value of the combination of new and more established monitoring techniques for deformation monitoring research. Besides, this research question also focuses on assessing the advantages of laser scanning for the 3D deformation pattern knowledge. The high resolution point cloud and high achievable accuracy allow further monitoring of the 3D displacements of individual tunnel segments and of the changes in the joints between the segments.

Does the short or medium term future still hold significant improvements for the proposed methodology?

During the research, it became clear that the developed methodology delivers very accurate and valuable results. Nevertheless, the developments in the field of 3D data acquisition advance very rapidly, so the question can already be posed which new or future developments could be implemented in tunnel monitoring research to further enhance the use of laser scanning in these applications. Besides the developments in the field of 3D laser scanning instruments and further improvements in the developed methodology, techniques such as 3D photo modelling based on Structure-from-Motion and Multi-View Stereo offer other possible innovative methodological improvements.

Above mentioned detailed research questions form the main part of the following study. However, the answers on these questions are not strictly independent. The research questions will be touched and partially answered over all following chapters.

1.5. Structure of the dissertation

The prior sections already provided the necessary background on the research topic and on the two tunnel monitoring projects during which the measurement data were collected. More detailed information and figures about the tunnel monitoring projects are given in the following chapters. Also the above mentioned research focus and the research questions will be elaborated in the following chapters.

Before the developed methodology is further detailed, the next chapter (chapter 2) first gives the necessary theoretical background on laser scanning. The laser scanning measurement principle, as well as the different types of laser scanners and possible measurement errors will be explained.

Further on, chapter 3 details the developed methodology for the measurements on site, the processing of the laser scanning data and the visualisation of the results to assess the deformation of the tunnel structure in the 'Diabolo' and 'Liefkenshoek Rail Link' project. The data from the 'Diabolo' project was used to develop a first version of the methodology. The 'Liefkenshoek Rail Link' measurements were then used to further optimise this methodology.

Chapter 4 details on two essential parts of the methodology, namely the determination of the achievable standard deviations, derived from *in situ* measurements in the measurement conditions of a tunnel construction site, and the testing and evaluation of different smoothing levels of the cross-sections.

One of the research questions also deals with the combination of laser scanning results with simultaneous strain gauge measurements. This research topic is covered in chapter 5, where more explanation about the strain gauge measurements is given. The development and the implementation of the methodology for the strain gauge measurements and for the

processing of the strain recordings (as also discussed in chapter 6) is performed by the Department of Civil Engineering (Prof. dr. ir. Hans De Backer & ir. Ken Schotte). The ovalisation monitoring detailed in this chapter, is performed and written in the framework of the presented dissertation.

A further investigation of the combination and of the possible integration of laser scanning and strain gauge measurements is described in chapter 6. This chapter elaborates the integration of both measurement techniques, in combination with traditional levelling measurements, to assess the tidal impacts of the River Scheldt on the tunnel structure of the 'Liefkenshoek Rail Link' project. The combination of the results of the different measurement techniques for this problem resulted in more profound and very essential insights in the deformation pattern of the tunnel tubes, caused by the variations in water level during the twice-daily tide changes of the River Scheldt.

Chapter 3 to 6 are based on the developed laser scanning methodology which includes a manual filtering procedure for the laser scanning point clouds. Further on in the research, however, the developed methodology has been improved by implementing an automated point cloud filtering and Levenberg-Marquardt cylinder fitting algorithm as discussed in chapter 7. This new implementation, elaborated in close collaboration with Cornelis Stal (Ghent University, Department of Geography, 3D Data Acquisition research group) resulted in even lower achievable standard deviations and a much shorter processing time. Cornelis Stal initiated the idea of the use of the Levenberg-Marquardt algorithm and programmed the implementation. The necessary adaptation of the algorithm to apply it for tunnel monitoring measurements was performed in close collaboration. The testing of the algorithm, the evaluation of the results and the comparison with the earlier developed methodology were performed by the author.

In chapter 8, the developed ovalisation monitoring methodology with laser scanning and the achieved results are discussed, together with the contribution of the research presented in this work to the general scientific research community. Based on the performed research and the gained experience, initiations of further research topics and formulations of possible further research questions are summarised in chapter 9. These topics cover more specific research questions, such as further accuracy assessments and calibration of laser scanning instruments and the monitoring of the changes in position of the different individual segments. In the general conclusion, a summary of the earlier stated research questions and the answers to these questions are given. Moreover, general thoughts on tunnel ovalisation monitoring and the use of laser scanning for this type of applications are shared with the reader.

1.6. References

Alba, M., Fregonese, L., Prandi, F., Scaioni, M., & Valgoi, P. (2006). Structural monitoring of a large dam by terrestrial laser scanning. In H.-G. Maas & D. Schneider (Eds.), *ISPRS Commission V Symposium "Image Engineering and Vision Metrology"* (Vol. XXXVI–5). Dresden, Germany.

Alba, M., Roncoroni, F., & Scaioni, M. (2008). Investigations about the accuracy of target measurement for deformation monitoring. In *XXIst ISPRS Congress - Technical Commission V* (Vol. XXXVII–B5, pp. 1053–1060). Beijing, China: The International Archives of the Photogrammetry, Remote Sensing and Spatial Information Sciences.

Argüelles-Fraga, R., Ordonez, C., Garcia-Cortes, S., & Roca-Pardinas, J. (2013). Measurement planning for circular cross-section tunnels using terrestrial laser scanning. *Automation in Construction*, 31, 1–9. doi:10.1016/j.autcon.2012.11.023

Bakker, K. J., de Boer, F., Admiraal, J. B. M., & van Jaarsveld, E. P. (1999). Monitoring Pilot Projects Using Bored Tunnelling: the Second Heinenoord Tunnel and the Botlek Rail Tunnel. *Tunnelling and Underground Space Technology, 14*(2), 121–129.

Barber, D., Mills, J., & Bryan, P. (2003). Towards a standard specification for terrestrial laser scanning of cultural heritage. In *CIPA International Archives for Documentation of Cultural Heritage*.

Beraldin, J.-A., Blais, F., Boulanger, P., Cournoyer, L., Domey, J., El-Hakim, S. F., Godin, G., Rioux, M., & Taylor, J. (2000). Real world modelling through high resolution digital 3D imaging of objects and structures. *ISPRS Journal of Photogrammetry & Remote Sensing, 55*, 230–250.

Biosca, J. M., & Lerma, J. L. (2008). Unsupervised robust planar segmentation of terrestrial laser scanner point clouds based on fuzzy clustering methods. *ISPRS Journal of Photogrammetry & Remote Sensing, 63*, 84–98. doi:10.1016/j.isprsjprs.2007.07.010

Boehler, W., & Marbs, A. (2003). *Investigating Laser Scanner Accuracy*. i3Mainz, Institute for Spatial Information and Surveying Technology, FH Mainz, University of Applied Sciences, Mainz, Germany.

Caballero, D., Esteban, J., & Izquierdo, D. B. (2007). ORCHESTRA: a Unified an Open Architecture for Risk Management Applications. *Geophysical Research Abstracts, 9*.

Clarke, T. A. (1996). A review of tunnel profiling methods. Optical Metrology Centre.

Delaloye, D., Hutchinson, J., & Diederichs, M. (2011). Accuracy issues associated with Lidar scanning for tunnel deformation monitoring. In *2011 Pan-Am CGS Geotechnical Conference*. Toronto, Ontario, Canada.

Favalli, M., Fornaciai, A., Isola, I., Tarquini, S., & Nannipieri, L. (2012). Multiview 3D reconstruction in geosciences. *Computers & Geosciences, 44*, 168–176. doi:10.1016/j.cageo.2011.09.012

Fekete, S., Diederichs, M., & Lato, M. (2010). Geotechnical and operational applications for 3-dimensional laser scanning in drill and blast tunnels. *Tunnelling and Underground Space Technology, 25*(5), 614–628. doi:10.1016/j.tust.2010.04.008

Girardeau-Montaut, D., Roux, M., Marc, R., & Thibault, G. (2005). Change detection on point cloud data acquired with a ground laser scanner. In *ISPRS WG III/3-4, V/3 Workshop "Laser scanning 2005"* (Vol. 36–3/W19, pp. 30–35). Enschede, The Netherlands.

González, M. J., Lucena, M., Fuertes, J. M., Rueda, A. J., & Segura, R. (2012). Automatic detection of unstructured elements in 3D scanned scenes. *Automation in Construction, 26*, 11–20. doi:10.1016/j.autcon.2012.05.005

Gordon, S. J., & Lichti, D. D. (2007). Modeling Terrestrial Laser Scanner Data for Precise Structural Deformation Measurement. *ASCE Journal of Surveying Engineering, May 2007*, 72–80. doi:10.1061/(ASCE)0733-9453(2007)133:2(72)

Grün, A., & Akca, D. (2005). Least squares 3D surface and curve matching. *ISPRS Journal of Photogrammetry & Remote Sensing, 59*, 151–174. doi:10.1016/j.isprsjprs.2005.02.006

Haala, N., & Alshawabkeh, Y. (2006). Combining Laser scanning and Photogrammetry - A Hybrid Approach for Heritage Documentation. In *CIPA 2006*. Cyprus.

Han, J.-Y., Guo, J., & Jiang, Y.-S. (2013a). Monitoring tunnel deformations by means of multi-epoch dispersed 3D LiDAR point clouds: An improved approach. *Tunnelling and Underground Space Technology, 38*, 385–389. doi:10.1016/j.tust.2013.07.022

Han, J.-Y., Guo, J., & Jiang, Y.-S. (2013b). Monitoring tunnel profile by means of multi-epoch dispersed 3-D LiDAR point clouds. *Tunnelling and Underground Space Technology, 33*(186-192), 186. doi:10.1016/j.tust.2012.08.008

Henriques, M. J., & Casaca, J. (2006). Uncertainty in tacheometric measurement of convergences in tunnels. In *3rd IAG / 12th FIG Symposium*. Baden, Switzerland: FIG.

Hesse, C., & Stramm, H. (2004). Deformation measurements with laser scanners. Possibilities and challenges. In *International Symposium on Modern Technologies, Education and Professional Practice in Geodesy and Related Fields* (pp. 228–240). Sofia, Bulgaria.

Huang, K.-P., Wang, T.-T., Huang, T.-H., & Jeng, F.-S. (2010). Profile deformation of a circular tunnel induced by ambient stress changes. *Tunnelling and Underground Space Technology, 25*(3), 266–278. doi:10.1016/j.tust.2009.12.006

Infrabel. (n.d.). The Diabolo Project. Retrieved December 27, 2013, from http://www.infrabel.be/en/about-infrabel/mobility-projects/airport-railway-projects?display=normal

Infrabel. (2009). Langsdoorsnede Diabolo. *Diabolo-boorschild graaft 13 meter per dag. Danté boort eerste tunnelkoker onder start- en landingsbaan luchthaven*.

Iyer, N., Jayanti, S., Lou, K., Kalyanaraman, Y., & Ramani, K. (2005). Three-dimensional shape searching: state-of-the-art review and future trends. *Computer-Aided Design, 37*, 509–530. doi:10.1016/j.cad.2004.07.002

Kavvadas, M. J. (2003). Monitoring and modelling ground deformations during tunnelling. In *11th FIG Symposium on Deformation Measurements*. Santorini, Greece: FIG.

Kersten, T. P., Mechelke, K., Lindstaedt, M., & Sternberg, H. (2008). Geometric Accuracy Investigations of the Latest Terrestrial Laser Scanning Systems. In *Integrating Generations - FIG Working Week 2008*. Stockholm, Sweden: FIG.

Kontogianni, V. A., & Stiros, S. C. (2005). Induced deformation during tunnel excavation: Evidence from geodetic monitoring. *Engineering Geology, 79*(1-2), 115–126. doi:10.1016/j.enggeo.2004.10.012

Lerma Garcia, J. L., Van Genechten, B., Heine, E., & Santana Quintero, M. (2008). *3D Risk Mapping, Theory and Practice on Terrestrial Laser Scanning. Training Material Based on Practical Applications*. Universidad Poltiecnica de Valencia, Spain.

Lichti, D. D., Gordon, S. J., & Tipdecho, T. (2005). Error Models and Propagation in Directly Georeferenced Terrestrial Laser Scanner Networks. *ASCE Journal of Surveying Engineering, November*, 135–142. doi:10.1061/(ASCE)0733-9453(2005)131:4(135)

Lichti, D. D., Stewart, M. P., Tsakiri, M., & Snow, A. J. (2000). Calibration and testing of a terrestrial laser scanner. In *International Archives of Photogrammetry and Remote Sensing (Vol. XXXII–B5)*. Amsterdam, The Netherlands.

Lindenbergh, R., Pfeifer, N., & Rabbani, T. (2005). Accuracy analysis of the Leica HDS3000 and feasibility of tunnel deformation monitoring. In *ISPRS WG III/3-4, V/3 Workshop "Laser scanning 2005"* (Vol. 36–3/W19, pp. 24–29). Enschede, The Netherlands.

Livieratos, E. (1992). Empiric, topographic or photogrammetric recording? Answers to properly phrased questions. In *Proceedings of "Terrestrial Photogrammetry and Geogrpahic Information Systems for the Documentation of the National Cultural Heritage."* Thessaloniki, Greece.

Mahdevari, S., & Torabi, S. R. (2012). Prediction of tunnel convergence using Artificial Neural Networks. *Tunnelling and Underground Space Technology, 28*, 218–228. doi:10.1016/j.tust.2011.11.002

Mizoguchi, T., Koda, Y., Iwaki, I., Wakabayashi, H., Kobayashi, Y., Shirai, K., Hara, Y., Lee, H.-S. (2013). Quantitative scaling evaluation of concrete structures based on terrestrial laser scanning. *Automation in Construction, 35*, 263–274. doi:10.1016/j.autcon.2013.05.022

Moosavi, M., & Khazaei, S. (2003). Absolute deformation profile measurement in tunnels using relative convergence measurements. In *Proceedings 11th FIG Symposium on Deformation Measurements*. Santorini, Greece.

Ninkov, T., Bulatovic, V., Susic, Z., & Vasic, D. (2010). Application of Laser Scanning Technology for Civil Engineering Projects in Serbia. In *The XXIV FIG International Congress 2010 "Facing the Challenges - Building the Capacity."* Sydney, Australia: FIG.

Qingwu, H., & Wanlin, Y. (2012). Tempo-space Deformation Detection of Subway Tunnel based on Sequence Temporal 3D Point Cloud. *Disaster Advances, 5*(4).

Rahayem, M., Werghi, N., & Kjellander, J. (2012). Best ellipse and cylinder parameters estimation from laser profile scan sections. *Optics and Lasers in Engineering, 50*(9), 1242–1259. doi:10.1016/j.optlaseng.2012.03.014

Rioux, M. (1994). Digital 3-D imaging: theory and applications. In *SPIE Proceedings, Videometrics III, International Symposium on Photonic and Sensors for Controls for Commercial Applications* (pp. 2–15). Boston, USA.

Roberts, G. W., Brown, C. J., & Ogundipe, O. (2010). Monitoring Bridges by GNSS. In *The XXIV FIG International Congress 2010 "Facing the Challenges - Building the Capacity."* Sydney, Australia: FIG.

Rüther, H., Chazan, M., Schroeder, R., Neeser, R., Held, C., Walker, S. J., Matmon, A., & Horwitz, L. K. (2009). Laser scanning for conservation and research of African cultural heritage sites: the case study of Wonderwerk Cave, South Africa. *Journal of Archaeological Science, 36,* 1847–1856. doi:10.1016/j.jas.2009.04.012

Schotte, K., De Backer, H., Nuttens, T., De Wulf, A., & Van Bogaert, P. (2010). Strain Gauge Measurements during the assembly of the Diabolo Tunnel. In *34th International Symposium on Bridge & Structural Engineering - IABSE Conference* (p. 8). Venice, Italy.

Schotte, K., De Backer, H., Nuttens, T., De Wulf, A., & Van Bogaert, P. (2011). Monitoring strains in the Liefkenshoek railway tunnel. In *Proceedings ITA-AITES World Tunnel Congress 2011* (pp. 254–255).

Špačková, O., Šejnoha, J., & Straub, D. (2013). Probabilistic assessment of tunnel construction performance based on data. *Tunnelling and Underground Space Technology, 37*, 62–78. doi:10.1016/j.tust.2013.02.006

Stal, C., De Wulf, A., De Coene, K., De Maeyer, P., Nuttens, T., & Ongena, T. (2012). Digital Representation of Historical Globes: Methods to Make 3D and Pseudo-3D Models of Sixteenth Century Mercator Globes. *The Cartographic Journal, 49*(2), 107–117. doi:10.1179/1743277412Y.0000000002

Stal, C., Tack, F., De Maeyer, P., De Wulf, A., & Goossens, R. (2013). Airborne photogrammetry and LIDAR for DSM extraction and 3D change detection over an urban area: a comparative study. *International Journal of Remote Sensing, 34*(4), 1087–1110.

Sternberg, H., & Kersten, T. P. (2007). Comparison of terrestrial laser scanning systems in industrial as-built-documentation applications. In Gruen & Kahmen (Eds.), *Optical 3-D Measurement Techniques VIII* (Vol. Vol. I, pp. 389–397). Zurich, Switzerland: Vol I.

Tao, C. V., Chapman, M. A., & Chaplin, B. A. (2001). Automated processing of mobile mapping image sequences. *ISPRS Journal of Photogrammetry & Remote Sensing, 55*, 330–346.

TUC Rail. (2010). Antwerp: The tunnel borers for the Liefkenshoek rail tunnel. TUC Rail - Belgian Rail Engineering.

Van Bogaert, P. (2009). Recent and future railway tunnels in Belgium. In *Proc. ITA World Tunnel Conference "Safe Tunnelling for the City and the Environment"* (pp. 689–690). Budapest: Hungarian Tunnelling Association, ISBN 9789630672399.

Van Gosliga, R., Lindenbergh, R., & Pfeifer, N. (2006). Deformation analysis of a bored tunnel by means of terrestrial laser scanning. In H.-G. Maas & D. Schneider (Eds.), *ISPRS Commission V Symposium "Image Engineering and Vision Metrology"* (Vol. Volume XXX). Dresden, Germany: IAPRS Volume XXXVI, Part 5.

Walsh, S. B., Borello, D. J., Guldur, B., & Hajjar, J. F. (2013). Data Processing of Point Clouds for Object Detection for Structural Engineering Applications. *Computer-Aided Civil and Infrastructure Engineering, 00*, 1–14. doi:10.1111/mice.12016

Yastikli, N. (2007). Documentation of cultural heritage using digital photogrammetry and laser scanning. *Journal of Cultural Heritage, 8*, 423–427. doi:10.1016/J.culher.2007.06.003

Yoon, J.-S., Sagong, M., Lee, J. S., & Lee, K. (2009). Feature extraction of a concrete tunnel liner from 3D laser scanning data. *NDT&E International, 42*, 97–105. doi:10.1016/j.ndteint.2008.10.001

Zeibak, R., & Filin, S. (2007). Change detection via terrestrial laser scanning. *In ISPRS WG III/3 III/4 V/3 VIII/11 "Laser Scanning 2007 and SilviLaser 2007"* (Internatio.). Espoo, Finland: IAPRS Volume XXXVI, Part 3/W52.

Zogg, H.-M., & Ingensand, H. (2008). Terrestrial laser scanning for deformation monitoring - load tests on the Felsenau Viaduct (CH). In *XXIst ISPRS Congress - Technical Commission V* (Vol. XXXVII–B5). Beijing, China: The International Archives of the Photogrammetry, Remote Sensing and Spatial Information Sciences.

CHAPTER 2
LASER SCANNING

2. LASER SCANNING

Since the mid 90's, laser scanning is being used in more and more applications. This chapter explains the general principles of the measurement technique, together with the different types of laser scanners and the measurement errors that can occur. Notwithstanding the intention to give a thorough overview of these aspects, the focus will lie on those elements that have an important influence on tunnel deformation measurements.

2.1. General principles

A laser scanner is a non-contact active surveying instrument that uses an emitted beam of laser light (Light Amplification by Simulated Emission of Radiation) to measure the distance between the instrument and an object (Rönnholm, Honkavaara, Litkey, Hyyppä, & Hyyppä, 2007). This laser beam is a narrow beam with low divergence and with a specific wavelength, which corresponds with a specific colour. Most laser scanners operate with a wavelength between near infrared (1064 nm) and green (532 nm) (Figure 2-1).

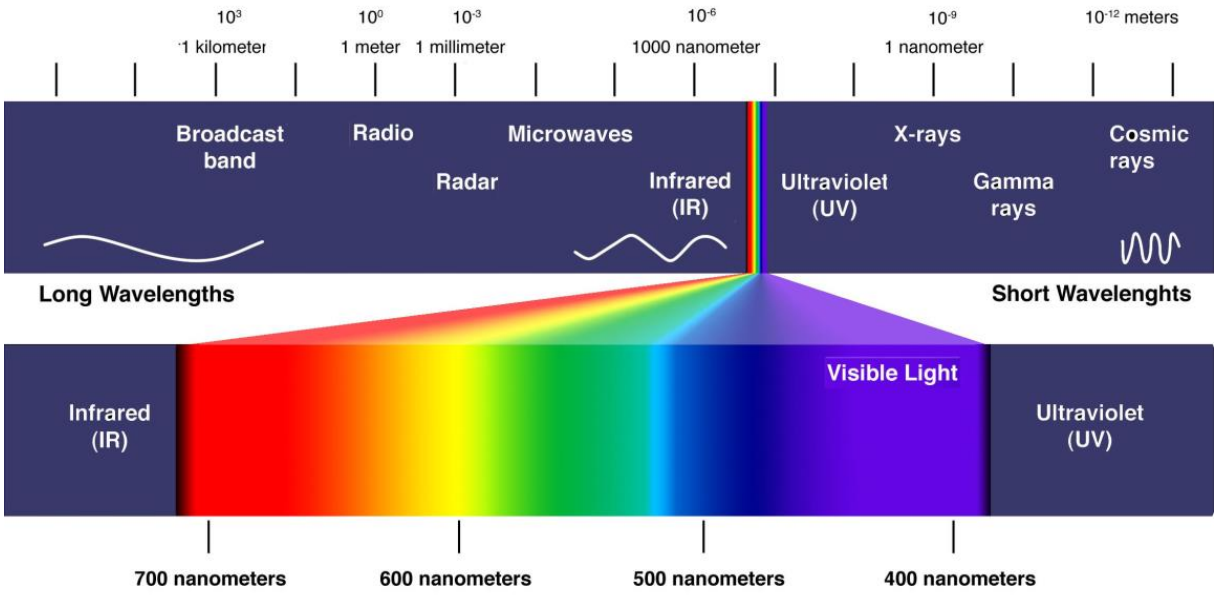

Figure 2-1: The electromagnetic spectrum (http://www.globalspec.com, 2013)

Laser scanning is considered as an automated measurement technique, because in a short period of time a large number of points are measured, resulting in a so-called 'point cloud' (Baltsavias, 1999; Lichti et al., 2000). A distinction can be made between aerial laser scanning (often referred to as 'LiDAR' – Light Detection And Ranging) and terrestrial laser scanning (TLS) (Pfeifer & Briese, 2007b). Terrestrial laser scanning results in a 3D representation of the measured object or space around the laser scanner. With a total station, the operator can only measure a limited number of selected points, whereas a laser scanner can, based on rotations of the range finder or a rotating mirror system, fully automatically measure the

field of view with a specified horizontal and vertical point density (Pfeifer & Briese, 2007b). The measured distance, combined with the registered horizontal and vertical angle of the instrument results in 3D coordinates for every measured point (Abellán, Vilaplana, Calvet, García-Sellés, & Asensio, 2011; Pfeifer & Briese, 2007b; Wehr & Lohr, 1999). Like a total station, a laser scanner is a line of sight instrument, which means that only the points in the line of sight of the instrument can be measured. Therefore, to cover a larger area or object, multiple setups are often necessary. However, specific features such as corners of an object are not directly measured and it is impossible to measure the same individual points multiple times with a laser scanner (Boehler & Marbs, 2003; Lichti et al., 2000). Possibly, laser scanning measurements can be complemented with a reflection intensity value or with RGB-values from a built-in digital camera (Haala & Alshawabkeh, 2006).

Next to the achievable accuracy of a laser scanning instrument and the maximum or useful range at which points can still be measured (see section 2.2), also the maximum field of view of the instrument is important. The field of view of a laser scanner represents the maximum angle range, both around the horizontal and vertical axes, in which the laser beam can be directed. Currently, most laser scanner types offer a 360° horizontal field of view, which means that the scanning head can make a full circle rotation around the vertical axis. For the vertical field of view, most laser scanners can reach a range of 270° to 320° (Figure 2-2).

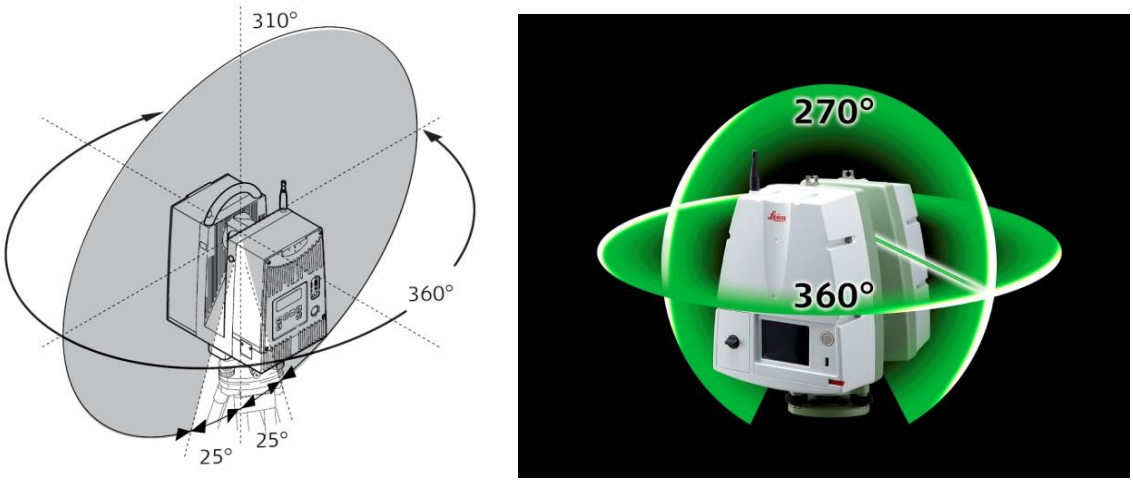

Figure 2-2: Field of view of the Leica HDS6100 laser scanner (left) and Leica C10 laser scanner (right) (Leica Geosystems, n.d., 2009b)

To combine different scanning setups into one point cloud, different registration methods are possible. The highest registration accuracy can be obtained by using artificial targets (planes, spheres, black-and-white markers, etc.) which are placed around the object or scene to be measured. Based on common targets between different point clouds, these point clouds can be registered using a so-called 'target-to-target registration'. Additionally, by measuring these targets with GNSS or total station, the point clouds can be placed in an absolute coordinate system. When the overlap between different point clouds is up to 30 or 40%, no artificial targets are necessary to register the point clouds, because then a 'cloud-to-

cloud registration' based on best-fit algorithms can be applied. However, a cloud-to-cloud registration generally results in a lower registration accuracy. If the project does not require different setups to be registered or if the site is not suited to place common targets, each individual setup can still be placed in a common reference system based on measuring the artificial targets with total station or GNSS for every individual setup (Jacobs, 2005).

In the measurement methodology further presented in this research, a target-to-target registration was used to register the different scanning setups in the measurements immediately after placement of the tunnel rings (reference measurements). Therefore, artificial black-and-white targets were printed on water-resistant polyester and attached on the tunnel surface (Figure 2-3). The used software (Leica Cyclone) was able to automatically calculate the centre point of each of the targets. For the control measurements, only one scanning setup was used, so no registration was necessary.

Figure 2-3: A scanning position during a reference measurement: example of two black-and-white targets

2.2. Different types of laser scanners

Terrestrial laser scanners can be divided into different types, based on the measurement principle of the distance measurement between the laser scanner and the object. The three most important types that can be identified are: triangulation laser scanners, pulse-based laser scanners and phase-based laser scanners. Each type of laser scanner has its specific characteristics, making it more suitable for different applications.

2.2.1. Triangulation laser scanners

Triangulation laser scanners are suited for high precision measurements over very short distances, limited to a few metres. Their measurement principle is based on widening the laser beam to form a plane or pattern and to record the image of the laser pattern on the object with a built-in camera (Figure 2-4). The laser print on the object, the laser emitter and the camera form a triangle. In this triangle, the distance between the camera and the laser emitter is known, together with the angle of the laser emitter. By measuring the location of the laser print on the object in the field of the camera sensor, the angle in the camera corner of the triangle can also be determined (Boehler & Marbs, 2003; Mayer, 1999). The distance to the object is determined via angle measurements instead of directly via the emitted laser beam. The accuracy that can be achieved with this technique is of the level of tens of micrometre, but the accuracy decreases with the square of the distance between the measured object and the laser scanner (Boehler & Marbs, 2003). Approximately 250 000 points can be measured per scan, because the method does not measure one point at a time, but a series of points along the laser curves on the object (Pfeifer & Briese, 2007b). Because the limited range of this technique, it is not suitable for the tunnel deformation measurements in this research. Therefore, this measurement principle will not be further detailed.

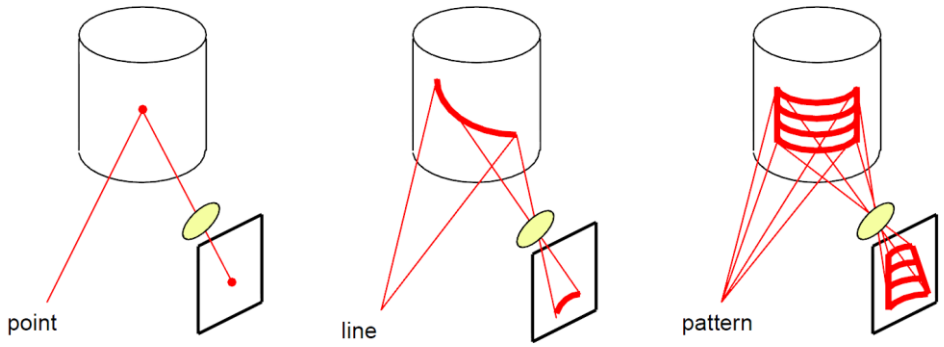

Figure 2-4: Triangulation scanner: laser print on the object (Schueremans & Van Genechten, 2008)

2.2.2. Pulse-based laser scanners

Pulse-based laser scanners (also called 'Time-of-Flight' or 'Pulse round trip' laser scanners) are based on the emission of a short (a few nanoseconds) but powerful laser pulse. The backscatter of the laser beam is recorded by the scanner and the travelling time of the laser pulse from the laser scanner to the object and back is calculated (Pfeifer & Briese, 2007b) (Figure 2-5). The accurate measuring of the travelling time of the laser beam is performed by a high-speed counter, controlled by a stable oscillator. The timing device starts counting when a certain threshold of the emitted laser beam is reached and stops when the threshold for the reflected beam is crossed again (Shan & Toth, 2009) (Figure 2-6).

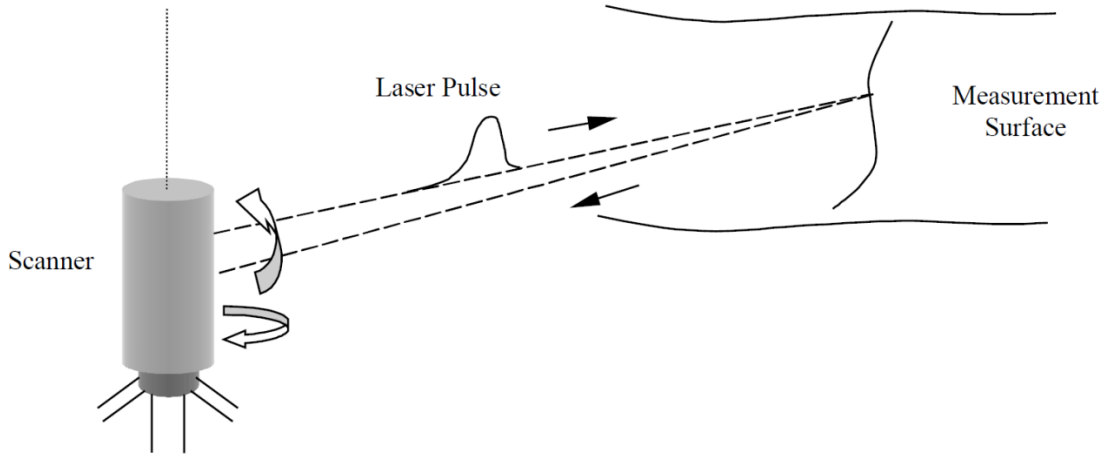

Figure 2-5: Measurement principle of a pulse-based laser scanner (Time-of-Flight) (Lichti et al., 2000)

The distance between the laser scanner and the object can then be calculated using the following formula:

$$r = c_g * \Delta t/2$$ (Pfeifer & Briese, 2007b)

With r = the distance between the laser scanner and the object

Δt = the time interval between emission of the laser pulse and registration of the backscatter

c_g = the speed of light (299 792 458 m/s)

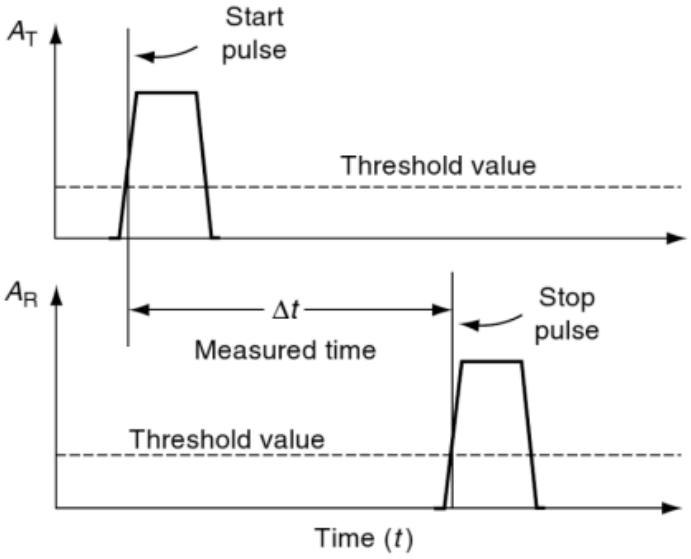

Figure 2-6: Pulse-based laser scanner: time counter principle (Shan & Toth, 2009)

Together with the 3D coordinates of each measured point, the strength of the backscatter is recorded as the intensity value. As can be seen in Figure 1-4, this intensity value can be visualised in a colour value, ranging from green to red (Pfeifer & Briese, 2007b).

Most laser scanners of the pulse-based type can only emit one pulse at a time, restricting the maximum achievable scanning speed to about 50 000 points per second (e.g. Leica C10) (Leica Geosystems, 2011). Because the measurement principle is based on a strong laser pulse, the range of this type of laser scanners within the required signal to noise ratio (SNR) for accurate measurements can be very large, up to 1 km or more (e.g. Leica HDS8810 has a range of up to 2 km) (Leica Geosystems, 2013a). The accuracy of the distance measurements largely depends on the accuracy of the time measurement and detection of the backscatter, typically resulting in cm-level accuracy (Pfeifer & Briese, 2007b). However, the latest technical developments on the market present pulse-based laser scanners with a scanning speed up to 1 million points per second, using specifically designed algorithms such as the 'WFD – Waveform Digitizing' (Leica Geosystems) or 'Lightning™ Technology' (Trimble) (Leica Geosystems, 2013b; Trimble, 2013).

2.2.3. Phase-based laser scanners

Higher accuracy (mm-level) and a higher scanning speed (up to 1 million points per second) can be obtained by using phase-based laser scanners (Pfeifer & Briese, 2007b). This type of laser scanner emits a continuous laser beam and uses the phase difference between the emitted signal and the reflected backscatter to determine the distance between scanner and object based on the following formula:

$$r = \Delta\varphi/(2*\pi)*\lambda/2 + \lambda/2*n$$ (Pfeifer & Briese, 2007b)

With
- r = the distance between the laser scanner and the object
- $\Delta\varphi$ = the phase difference between the emitted and reflected laser signal (in radians)
- λ = the wavelength of the signal (generally expressed in metre)
- n = the unknown number of full wavelengths between the laser scanner and the object

In general, more than one signal is used, each having a different wavelength. The longest wavelength defines the number of full wavelengths and the shortest wavelength determines the precision that can be obtained for the distance measurement. Because of the lower power of the emitted laser signal, the achievable range of this type of laser scanners is limited. Typically, distances of up to 80-100 m can be measured, depending on the reflectivity of the object (% albedo) (e.g. Leica HDS6100 has a range of 79 m; Trimble TX5 has a range of up to 120 m) (Leica Geosystems, 2009a; Trimble, 2012) (Figure 2-7).

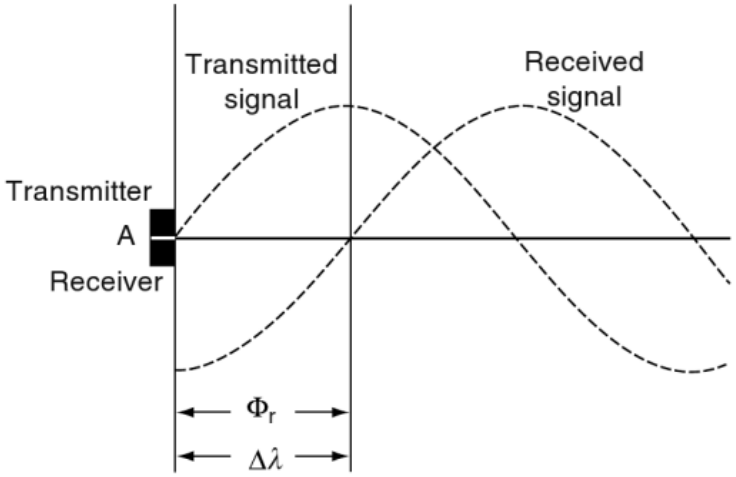

Figure 2-7: Phase-based laser scanner: measurement of phase difference between emitted and reflected laser beam (Shan & Toth, 2009)

2.3. Error sources in laser scanning

When discussing the term "accuracy", the focus lies on how close the measurements are located to the real point locations in space. The term "precision" on the other hand, refers mainly to the noise level of the data. When comparing scans from different epochs, a low noise is specifically desired, on the condition that the scans from different epochs have a comparable accuracy. If the purpose however, is to compare the measured data with a reference geometry, a highly accurate point cloud is specifically desired (Jacobs, 2005).

The possible errors in laser scanning can be divided into different categories, depending on the source. (Delaloye et al., 2011) for example, distinguish three large sources of errors: errors in the range measurement and errors in the vertical and horizontal angle measurements. These three errors form the total error E, which can be described by the following formula:

$$E = \sqrt{(\Delta X^2+\Delta Y^2+\Delta Z^2)} \qquad \text{(Delaloye et al., 2011)}$$

With ΔX = the horizontal error
ΔY = the range error
ΔZ = the vertical angle error

Besides these three instrument dependent errors, possible other errors are the phenomenon of spurious points, errors in the laser scanner operating procedures or in the processing of the data (Delaloye et al., 2011). The manufacturer's specifications of a laser scanner indicate the achievable accuracies, but experience shows that the actual accuracy differs from instrument to instrument. Moreover, manufacturer's specifications are often difficult to compare and the measurement conditions on site have a large influence on the

final accuracy that can be obtained (Boehler & Marbs, 2003; Jacobs, 2004; Lichti et al., 2000). In the case of this research for example, the dusty and hard conditions of a tunnel under construction make that an *in situ* accuracy assessment is indispensable.

Over the last years, different methodologies have been investigated to test a laser scanner for angular, range or other errors, to quantify these errors and to apply a correction model (Boehler & Marbs, 2003; Chow, Lichti, & Teskey, 2012; Delaloye et al., 2011). (Boehler & Marbs, 2003) suggest the measurement of short horizontal and vertical distances between reference objects and the comparison of these distances with measurements from more accurate surveying techniques such as high precision total stations. (Gielsdorf, Rietdorf, & Gruendig, 2004) use planar targets to develop a calibration and error modelling methodology using modelling parameters such as the vertical index and horizontal axis error, horizontal collimation error, additive rangefinder constant and eccentricity. Modelling angular systematic errors has been performed by (Amiri Parian & Grün, 2005) using 2D image point observations extracted from the scanner data, based on the common characteristics between a laser scanner and a panoramic camera. The self-calibration method described in (Chow et al., 2012), based on a large amount of reference markers evenly spread in a room and measured from different scanning positions, was tested on the Leica HDS6100 laser scanner from the Department of Geography (UGent), in close collaboration with the main author of the methodology (J. Chow), but not yet implemented in the developed methodology. By applying a bundle adjustment on the different scanning positions and calculating the residuals on the measured coordinates of the reference markers, a set of correction parameters can be determined to minimise or eliminate systematic instrument errors. Especially for measurements near the zenith of the laser scanner, this kind of calibration can significantly contribute to the improvement of the achievable accuracy. More details about this test are described in section 9.1.

2.3.1. Range error

The error on the distance measurement can be caused by a systematic error of the laser scanner as well as by the surface of the object being measured. Detecting range errors can be based on comparing measured distances with known reference distances in the range direction or comparing range differences between reference targets. These known reference distances or range differences between reference targets have to be measured with a more accurate surveying technique to assess the possible range errors of the laser scanner (Boehler & Marbs, 2003). A systematic error on the distance measurements is not easy to detect because it depends on, among other things, the reflectivity of the object's surface. If points located in different directions from the laser scanner are measured, the systematic error will have an influence on the distance measurement. However, if distance differences in the same direction are compared, the systematic error will be eliminated and thus not be detectable.

The accidental error on the range measurements, indicated by the noise, can be more easily detected by scanning a flat surface. The amount in which the measured points are scattered around this flat surface is a measure for the noise level of the scanning instrument. As earlier explained, lower noise levels are important when comparing point clouds of an object recorded on different points in time, although a lower noise level does not necessarily mean that the scanned point cloud is more accurate (Boehler & Marbs, 2003; Delaloye et al., 2011; Jacobs, 2005).

Besides the reflectivity of the object's surface, other aspects that influence the range error are the angle of incidence and the resolution of the scan. The reflectivity of the surface, defined as the percentage of the laser beam's power that is reflected by the surface, depends on the object's colour, roughness, conductivity etc. Also, the spectral characteristics of the laser beam used by the scanner play a role (Boehler & Marbs, 2003; Jacobs, 2004; Lichti, Gordon, Stewart, Franke, & Tsakiri, 2002). An angle of incidence of the laser beam perpendicular on the object results in the largest achievable accuracy of the range measurement. The more the object's surface becomes oblique to the scanner, the less accurate the measurements will be (Delaloye et al., 2011).

2.3.2. Angular error

Angular errors are caused by the scanning instrument itself. The errors on the rotating mirror inside the laser scanner influence the vertical accuracy, whereas the rotation of the laser scanner around its vertical axis influences the horizontal accuracy. These errors can be caused by, for example, faults in the assembly of the instrument and they can deteriorate during its use. However, these errors are difficult to detect because the positions of individual test points are difficult to compare (Boehler & Marbs, 2003; Delaloye et al., 2011).

2.3.3. Other errors

The range and angular errors can be considered to have an influence on the points that are supposed to be measured. Besides, a number of other errors cause points that do not represent a real part of the recorded object or scene to be measured. Due to atmospheric conditions, radiation interference, highly reflective surfaces, edge effects, etc. spurious points can appear in the measured point cloud (Boehler & Marbs, 2003; Delaloye et al., 2011).

Dust, raindrops or snowflakes often scatter the laser beam which increases the noise on the return signal or creates unwanted points. Also interfering sun rays can be detected by the scanner, resulting in spurious points. Unwanted points can also be caused by the backscatter of the laser beam which is being returned from another location than it was originally reflected, due to reflections on wet surfaces, mirrors or glass surfaces. The edge effect results in a wrongly measured distance between the laser scanner and the correct point of the object, because the footprint of the laser beam on the object is partly reflected on one side of the edge and the other part of the beam is reflected on another location on the object (Boehler & Marbs, 2003; Delaloye et al., 2011).

2.3.4. Beam divergence and spot size

The beam divergence and resulting spot size on the object's surface also play an essential role. Although most manufacturers mention the beam diameter and the divergence factor of their laser scanning instrument, it is difficult to interpret what these values mean for the daily practice of the laser scanners. Generally, two definitions of the spot size (the diameter of the laser beam when it hits the object) are used: the Gaussian method and the full-width-half-height method (FWHH) (Figure 2-8).

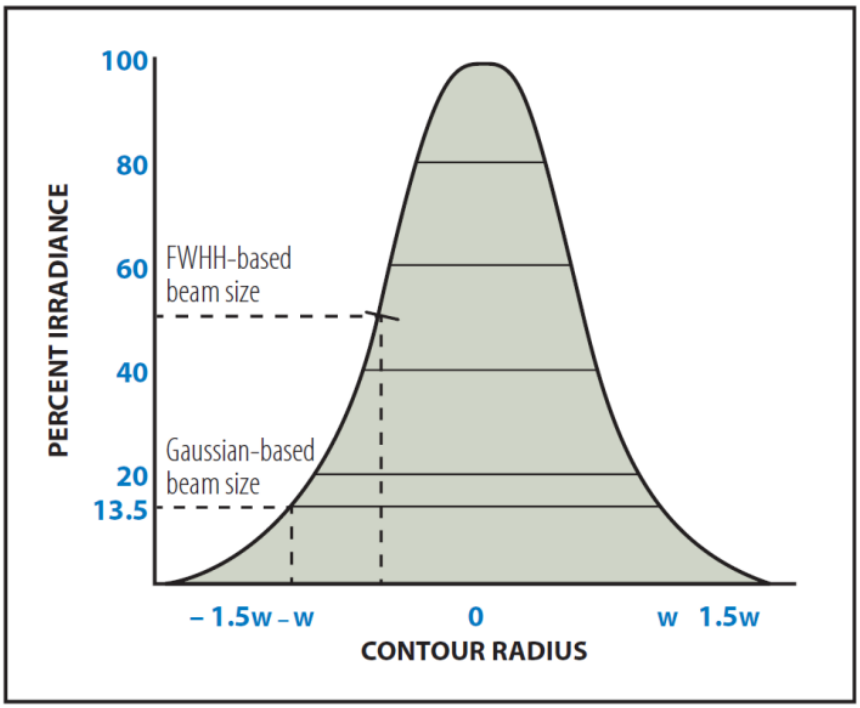

Figure 2-8: Diameter of a laser beam: Gaussian method and FWHH method (Jacobs, 2006)

In the Gaussian method, the laser beam is assumed to have a Gaussian clock shape and the spot size is then defined as the beam diameter for which the following condition is fulfilled:

$$I = 1/e^2 * I_{max}$$ (Jacobs, 2006)

With e = a mathematical constant (approximately 2.7183)
I = intensity of the laser beam
I_{max} = the maximum intensity of the laser beam

In this equation, $1/e^2$ approximately equals 13.5%. A beam diameter specification of 5 mm can then be interpreted as the fact that at this 5 mm diameter, the beam intensity is only 13.5% of the maximum beam intensity, located at the centre of the beam. The actual beam diameter extends this 5 mm diameter, but the remaining beam intensity beyond this diameter is too weak to be used for a distance measurement.

For laser beams following a Gaussian clock shape and for laser beams that do not follow a Gaussian profile, the FWHH method can also be used. Here, the spot size is defined as the

diameter of the laser beam at half the maximum intensity. This definition always results in a smaller value for the spot size for the FWHH method than for the Gaussian method (Jacobs, 2006).

The beam divergence factor (usually mentioned in mrad) indicates how the diameter of the laser beam changes as a function of the distance from the laser scanner. For most laser scanner types, the beam diameter becomes larger with a growing distance to the scanner. The further the object lays from the laser scanner, the larger the beam's diameter and the lower the accuracy of the measurement will be. However, some types of laser scanners emit a laser beam that first converges to a smaller diameter, and then diverges again to a larger diameter. In this case, collimated beams are generated by inserting a fixed beam expander, acting like a reverse telescope. Figure 2-9 represents what happens when using a beam expander: the emitted laser beam first converges until the minimum beam width is reached (beam waist w_0) and then the beam diverges again. Z_R is the so-called 'Rayleigh length', the distance along the beam's direction from the beam waist (w_0) until the place where the cross-section area is doubled:

$$z_R = \frac{\pi {w_0}^2}{\lambda}$$ (Damask, 2005)

With λ = the wavelength of the laser beam

An advantage of the collimated beam technique is that in the useful range of the laser scanner, the diameter of the laser beam can be kept relatively small. Moreover, by using a variable beam expander, the operator can select the appropriate spot size at a certain distance. However, this movable part causes extra unknown errors and points measured closer than or further away from the minimum spot size distance can then have a difficultly quantifiable larger spot size than with a conventional system (Delaloye et al., 2011; Jacobs, 2006).

A smaller spot size has several advantages, certainly in combination with a high point density (see section 2.3.5). This combination leads to less problems with edge effects, abrupt differences in reflectivity of the object's surface or surface curvature effects and allows penetrating more easily through vegetation or obstacles (Jacobs, 2006).

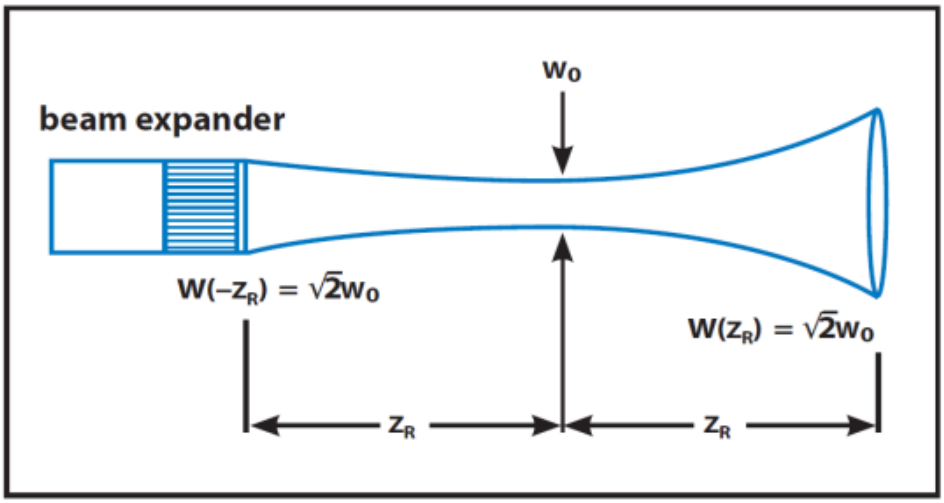

Figure 2-9: Application of a beam expander to limit the beam divergence (Jacobs, 2006)

2.3.5. Resolution

Depending on the source, the term "resolution" can have different meanings. First, resolution can describe the density of the point cloud or the scan density, comparable with the resolution of a camera (number of pixels per square inch). This scan density or resolution refers to the spacing between adjacent points and can be different for the horizontal and vertical direction.

Another meaning is the ability to detect small objects or details in the point cloud. In this case, the spot size on the object also has its influence on the resolution of the laser scanning measurements, together with the angular increment (Boehler & Marbs, 2003; Jacobs, 2005).

In a third sense, the term "resolution" can be used to describe the minimum measurement increment that can be distinguished by the laser scanner, both for the range and angular measurement. "Resolution" in this context represents how many decimal places or increments of a measurement can be determined by the measurement instrument. Important to notice is that a higher resolution in this context does not mean that the scanner can achieve a higher accuracy. It only says something about the number of increments that can be read (Jacobs, 2005).

2.4. References

Abellán, A., Vilaplana, J. M., Calvet, J., García-Sellés, D., & Asensio, E. (2011). Rockfall monitoring by Terrestrial Laser Scanning – case study of the basaltic rock face at Castellfollit de la Roca (Catalonia, Spain). *Natural Hazards and Earth System Science, 11*(3), 829–841. doi:10.5194/nhess-11-829-2011

Amiri Parian, J., & Grün, A. (2005). Integrated laser scanner and intensity image calibration and accuracy assessment. *The International Archives of the Photogrammetry, Remote Sensing and Spatial Information Sciences, XXXVI*(Part 3/W19), 18–23.

Baltsavias, E. P. (1999). A comparison between photogrammetry and laser scanning. *ISPRS Journal of Photogrammetry & Remote Sensing, 54*, 83–94.

Boehler, W., & Marbs, A. (2003). *Investigating Laser Scanner Accuracy*. i3Mainz, Institute for Spatial Information and Surveying Technology, FH Mainz, University of Applied Sciences, Mainz, Germany.

Chow, J. C. K., Lichti, D. D., & Teskey, W. F. (2012). Accuracy assessment of the FARO Focus3D and Leica HDS6100 panoramic-type terrestrial laser scanners through point-based and plane-based user self-calibration. In *FIG Working Week 2012 - Knowing to manage the territory, protect the environment, evaluate the cultural heritage* (p. 15). Rome, Italy.

Damask, J. N. (2005). *Polarization Optics in Telecommunications*. Springer Science+Business Media.

Delaloye, D., Hutchinson, J., & Diederichs, M. (2011). Accuracy issues associated with Lidar scanning for tunnel deformation monitoring. In *2011 Pan-Am CGS Geotechnical Conference*. Toronto, Ontario, Canada.

Gielsdorf, F., Rietdorf, A., & Gruendig, L. (2004). A Concept for the calibration of terrestrial laser scanners. In FIG (Ed.), *Proceedings of the FIG Working Week 2004*. Athens, Greece.

Haala, N., & Alshawabkeh, Y. (2006). Combining Laser scanning and Photogrammetry - A Hybrid Approach for Heritage Documentation. In *CIPA 2006*. Cyprus.

http://www.globalspec.com. (2013). Electromagnetic spectrum.

Jacobs, G. (2004). High Definition Surveying - 3D Laser Scanning: Understanding the “Useful Range” of Laser Scanners. *Professional Surveyor, 24*(11).

Jacobs, G. (2005). High Definition Surveying - 3D Laser Scanning: Understanding Laser Scanning Terminology. *Professional Surveyor, 25*(2).

Jacobs, G. (2006). 3DScanning. Understanding Spot Size for Laser Scanning. *Professional Surveyor Magazine*.

Leica Geosystems. (n.d.). Leica C10 Field of View. Leica Geosystems AG.

Leica Geosystems. (2009a). Leica HDS6100 Datasheet. Heerbrugg, Switzerland: Leica Geosystems AG. Retrieved from www.leica-geosystems.com/hds

Leica Geosystems. (2009b). Leica HDS6100 User Manual Version 2.0 English. Heerbrugg, Switzerland: Leica Geosystems AG. Retrieved from www.leica-geosystems.com

Leica Geosystems. (2011). Leica ScanStation C10 Datasheet. Heerbrugg, Switzerland: Leica Geosystems AG. Retrieved from www.leica-geosystems.com/hds

Leica Geosystems. (2013a). Leica HDS8810 Datasheet. Heerbrugg, Switzerland: Leica Geosystems AG. Retrieved from www.leica-geosystems.com

Leica Geosystems. (2013b). Leica ScanStation P20 Datasheet. Heerbrugg, Switzerland: Leica Geosystems AG. Retrieved from www.leica-geosystems.com/hds

Lichti, D. D., Gordon, S. J., Stewart, M. P., Franke, J., & Tsakiri, M. (2002). Comparison of Digital Photogrammetry and Laser Scanning. In *Proceedings of the CIPA WG6 International Workshop on scanning for cultural heritage recording*.

Lichti, D. D., Stewart, M. P., Tsakiri, M., & Snow, A. J. (2000). Calibration and testing of a terrestrial laser scanner. In *International Archives of Photogrammetry and Remote Sensing (Vol. XXXII–B5).* Amsterdam, The Netherlands.

Mayer, R. (1999). *Scientific Canadian : invention and innovation from Canada's National Research Council*. Vancouver, Canada: Raincoast Books.

Pfeifer, N., & Briese, C. (2007b). Laser scanning - Principles and applications. *GeoSiberia 2007*.

Rönnholm, P., Honkavaara, E., Litkey, P., Hyyppä, H., & Hyyppä, J. (2007). Integration of laser scanning and photogrammetry. In *ISPRS WG III/3 III/4 V/3 VIII/11 "Laser Scanning 2007 and SilviLaser 2007"* (Internatio.). Espoo, Finland: IAPRS Volume XXXVI, Part 3/W52.

Schueremans, L., & Van Genechten, B. (2008). The use of 3D-laser scanning in assessing the safety of masonry vaults - A case study on the church of Saint-Jacobs. *Optics and Lasers in Engineering, 47*, 329–335. doi:10.1016/J;optlaseng.2008.06.009

Shan, J., & Toth, C. K. (Eds.). (2009). *Topographic Laser Ranging and Scanning*. CRC Press, Taylor & Francis Group.

Trimble. (2012). Trimble TX5 scanner Datasheet. Trimble Navigation Limited. Retrieved from www.trimble.com

Trimble. (2013). Trimble TX8 Laser scanner Datasheet. Trimble Navigation Limited. Retrieved from www.trimble.com

Wehr, A., & Lohr, U. (1999). Airborne laser scanning—an introduction and overview. *ISPRS Journal of Photogrammetry and Remote Sensing, 54*(2-3), 68–82. doi:10.1016/S0924-2716(99)00011-8

CHAPTER 3
METHODOLOGY FOR THE OVALISATION MONITORING OF NEWLY BUILT CIRCULAR TRAIN TUNNELS BASED ON LASER SCANNING: LIEFKENSHOEK RAIL LINK (BELGIUM)

3. METHODOLOGY FOR THE OVALISATION MONITORING OF NEWLY BUILT CIRCULAR TRAIN TUNNELS BASED ON LASER SCANNING: LIEFKENSHOEK RAIL LINK (BELGIUM)

Modified from Nuttens, T., Stal, C., De Backer, H., Schotte, K., Van Bogaert, P., & De Wulf A. (2014). Methodology for the ovalization monitoring of newly built circular train tunnels based on laser scanning: Liefkenshoek Rail Link (Belgium). Automation in Construction, Vol. 43, p. 1-9, doi: 10.1016/j.autcon. 2014.02.017 (Published)

3.1. Abstract

The ovalisation monitoring methodology based on laser scanning, developed during two recent tunnelling projects in Belgium, elaborates a clear processing workflow and easily interpretable deliverables with sub-millimetre accuracy. The extensive and systematic monitoring coverage during the first three months after construction of a circular tunnel structure delivers an important contribution to the understanding of the tunnels' behaviour between the construction phase and the final stabilised shape. The observed differences of the average radius values generally show a decrease in the first week after ring erection and a stabilisation of the tunnel structure during the following weeks. The results of such a systematic monitoring program allow the contractors or engineers involved to validate the deformation models and to compare with the actual behaviour of large diameter shield tunnelling in soft soil. This is highly valuable, because very few measurements are available at this early stage of a tunnel construction to evaluate the performance and accuracy of such deformation models.

3.2. Introduction

Monitoring the stability of a civil technical structure is a challenging task, already being addressed for a long time in literature (Büyüköztürk, 1998). The use of total stations for monitoring constructions is still being applied in a wide range of applications (Bizjak & Petkovsek, 2004; Stiros & Psimoulis, 2012), but these measurements deliver only a small set of points that can be monitored in the limited time frame available for the measurements. Research is continuously focusing on techniques that can be used for the detection of centimetre or sub-centimetre deformations of constructions. Examples are: kinematic GNSS measurements for bridge deflections (Roberts et al., 2010), laser scanning in 2D or 3D mode for the monitoring of bridges or harbour locks (Lindenbergh & Pfeifer, 2005; Teza, Galgaro, & Moro, 2009), tunnel monitoring (Argüelles-Fraga et al., 2013; Delaloye et al., 2011; Fekete et al., 2010; Yoon et al., 2009), measuring beam deflections (Gordon & Lichti, 2007) or monitoring cultural heritage monuments (Beraldin et al., 2000; Ninkov et al., 2010; Stal, De Wulf, et al., 2012). In recent years, terrestrial laser scanning (TLS) is more and more being applied for the acquisition of accurate and dense 3D data sets, because a high scanning

speed and high accuracy offer laser scanners significant advantages compared to more traditional techniques. However, the necessary ad hoc processing of the laser scanning data and the price of the equipment remain important barriers for a practical and straightforward implementation of laser scanning in a lot of projects (Hesse & Stramm, 2004; Monserrat & Crosetto, 2008). Photogrammetry is another widely applied technique, but this requires sufficient lighting conditions and texture on the object's surface (Clarke, 1996; Schueremans & Van Genechten, 2008), requirements that cannot be guaranteed in tunnel construction projects. Laser scanning needs no specific lighting conditions and can deliver millions of accurate 3D coordinates in a limited time frame, making this a preferred measurement technique for the recent Belgian 'Diabolo' and 'Liefkenshoek Rail Link' tunnelling projects.

Recent developments presented in literature describe different tunnel deformation analysis techniques based on laser scanning. As described in (Yoon et al., 2009), static or mobile scanning systems are used to compare the measured construction to a fitted surface, even when the structure includes some curved parts. Detected damage, cracks or deformations with this technique are limited to 2 mm diameter objects or larger (Yoon et al., 2009). Other techniques based on the comparison of tunnel cross-sections suggest different possibilities to place cross-sections of different epochs in a common coordinate system. In (Hesse & Stramm, 2004), extra total station measurements are used to determine the coordinates of a number of reference targets and also in (Han et al., 2013a, 2013b), *in situ* control features are used to define a common datum between measurements at different epochs. However, these methodologies not only involve additional time consuming measurements, they also do not cope with a displacement of the reference features themselves caused by a deformation of the tunnel structure between different epochs. Moreover, no clear definition of the tunnel axis is given in these methodologies and the cross-sections are based on the point cloud of the measurements, by interpolating the point cloud to obtain a regular point grid on the cross-section or using a buffer size left and right of the cross-section location, resulting in achievable accuracies of millimetre level (Han et al., 2013a, 2013b; van Gosliga et al., 2006). The methodology developed in this dissertation includes not only a definition of the tunnel axis based on a best-fit cylinder, but also a meshing step in the workflow to determine the cross-section based on a triangulated surface instead of the original point cloud, taking the findings in (Delaloye et al., 2011) in mind that it is important to compare surface-based cross-sections instead of point-based cross-sections. Additionally, the cross-section evaluation is done using thousands of points, which is necessary to get a fully detailed picture of the profile (Huang et al., 2010), and the methodology presented in this chapter results in a much higher accuracy (sub-millimetre level). Thanks to this highly detailed picture of the cross-sections, the segment joints are detectable. Complying with the need for segmental deformation analysis as expressed in (Molins & Arnau, 2011; Teachavorasinskun & Chub-uppakarn, 2010), this makes further analysis of the individual segments possible, also during the settlement of the tunnels in the first weeks after construction. The presented methodology covers the measurements on site, a clear processing of the data and the elaboration of easily interpretable reports and plots

afterwards. Moreover, the developed methodology also includes a measurement setup in the head of the Tunnel Boring Machine (TBM) just after the construction of a tunnel ring which allows limiting the downtime of the drilling works. These measurements are very valuable, because few systematic measurements in such an early stage of tunnel construction are available to evaluate the performance or accuracy of deformation models.

This research focuses on the application of terrestrial laser scanning for ovalisation measurements of newly bored concrete tunnels from the moment of ring assembly until three months after construction. The extensive and systematic monitoring coverage during this time frame delivers an important contribution to the understanding of the tunnels' behaviour between construction and its stabilised shape. The two tunnel monitoring projects on which this research is based are the first projects in Belgium in which laser scanning was used to systematically monitor the ovalisation of multiple tunnel sections under construction. In the 'Diabolo' project (Zaventem - Brussels, Belgium), the use of laser scanning for this type of monitoring was tested and implemented (Nuttens et al., 2010). In the following 'Liefkenshoek Rail Link' project (Antwerp, Belgium), the workflows were optimised and the processing of the data sets further elaborated. In addition to laser scanning, strain gauge measurements were also performed on some of the same sections in order not only to measure the strains of the individual concrete segments, but also to investigate the link between the strain measurement results and the results of the laser scanning measurements (see chapter 5 and 6). The simultaneous data of both laser scanning and strain gauge measurements enables combining the conclusions from both methods and thus improving the knowledge of tunnel behaviour in *in situ* conditions.

Section 3.3 describes in detail the recent 'Liefkenshoek Rail Link' tunnel monitoring project in Belgium. Section 3.4 explains the measurement equipment, measurement workflows and processing methodology. The results of the monitoring measurements are presented in section 3.5, followed by a discussion section and final conclusions.

3.3. Tunnel monitoring project: 'Liefkenshoek Rail Link' (Belgium)

The 'Liefkenshoek Rail Link' project establishes a new railway connection for freight traffic between the left and right bank of the River Scheldt in the Port of Antwerp. This new connection has a total length of approximately 16 km, of which 6 km is constructed with two new side-by-side tunnels by two shield-driven TBM's using the mixshield method (Van Bogaert, 2009). This new bored tunnel complex crosses two waterways (River Scheldt and Canal Dock/Port Canal). Under the Waesland Canal, an already existing tunnel is integrated in the railway connection. An overview of the profile of the railway connection can be seen in Figure 3-1.

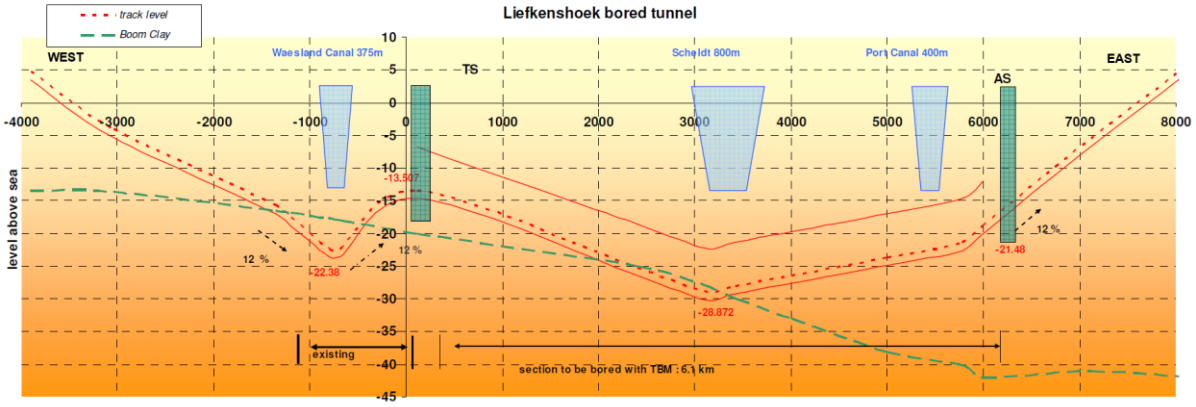

Figure 3-1: Longitudinal profile of the bored tunnel in the 'Liefkenshoek Rail Link' project (According to (Van Bogaert, 2009))

Along the tunnel's route, the soil stratification has a general downward slope from the west to the east, indicated by the Boom clay layer boundary in Figure 3-1. The left (west) bank of the River Scheldt consists of sandy layers until a depth of 4 to 6 m. Under these layers, a quaternary soil made out of soft clay is present. This clay layer does not occur on the right bank of the river. Further below, there are layers of the tertiary era containing silt and a mixture of fine sand and clay. At larger depth, the soil consists of Boom clay (indicated in Figure 3-1 with green dashed line), acting as an impermeable soil layer. The tunnel's trajectory mostly runs through the tertiary sands, but at its deepest point (below the River Scheldt) it also runs through the Boom clay layer. The TBM's passage below the River Scheldt and the Canal Dock needs special attention and extra preparation works which do not allow accessing the boring chamber or replacing parts of the cutting wheel while crossing those waterways.

The two newly bored tunnels have an inside diameter of 7.300 m and the concrete tunnel segments have a thickness of 0.400 m. The longitudinal size of each tunnel section is 1.800 m and each tunnel section is made out of seven concrete segments and one smaller closing stone (TUC Rail, 2010). In each tunnel tube ('Tunnel North' and 'Tunnel South'), fourteen tunnel sections were selected to be monitored, including a specific tunnel section in each tube under the River Scheldt and the Canal Dock.

In this tunnel project, seven moments in time were defined on which the selected tunnel sections had to be measured: the 'reference measurement' immediately following construction of the tunnel section; a measurement every week during the first month after placement ('control measurement 1 to 4') and measurements two and three months after placement ('control measurement 5 and 6'). The cross-sections are compared with the design shape and, if applicable, also with the reference measurement and the previous control measurement of that tunnel section. These comparisons are summarised in tables and visualised on different plots, which also indicate the areas where possible significant deformations appear.

The ovalisation monitoring with laser scanning measures the changes in position of the segments of the tunnel section. The deformations of the segments themselves however, fall outside the measurement range of the laser scanning instruments due to the very small dimensions of these deformations. Therefore, simultaneously with the laser scanning monitoring program, strain gauge measurements were performed to measure the real-time behaviour of the tunnel segments under the different loading conditions in this early stage of the tunnel construction. These general results of the strain gauge measurements comply with the monitoring conclusions based on the laser scanning measurements. Further details on the strain gauge methodology can be read in chapter 5.

In addition to the foreseen series of ovalisation measurements in the 'Liefkenshoek Rail Link' project, the impact of the drilling of Tunnel North on a neighbouring section in Tunnel South was also monitored based on the developed methodology. More specifically, a tunnel section under the Canal Dock in Tunnel South (tunnel section S_x) was measured while the TBM was approaching the neighbouring section in Tunnel North (tunnel section N_x) until several days after the TBM had passed the neighbouring ring.

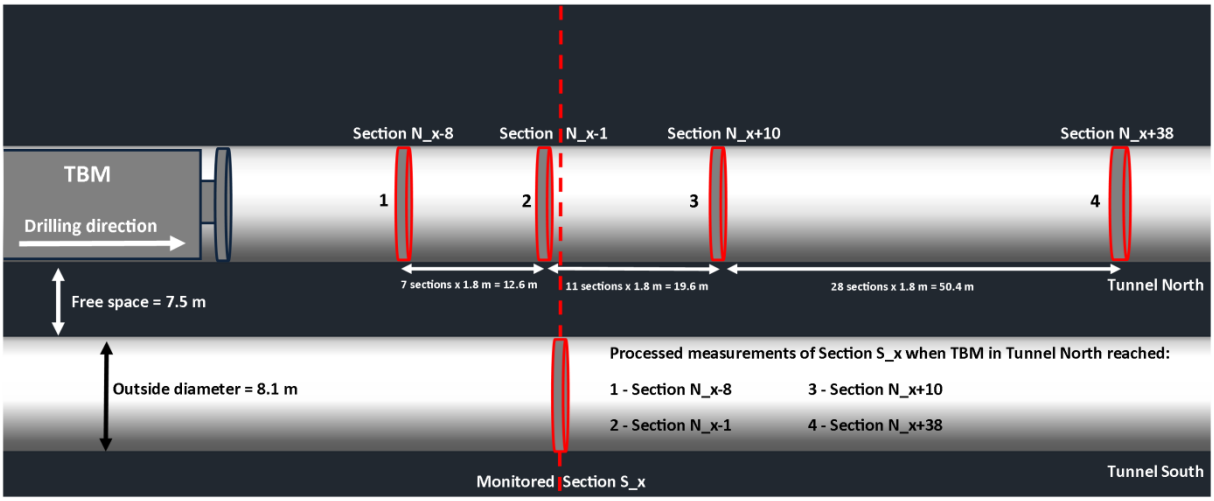

Figure 3-2: Top view scheme of the monitoring of the ovalisation of Tunnel South during the drilling of Tunnel North

The first measurement was performed when the TBM in Tunnel North reached tunnel section N_x-8, so eight sections before N_x (Figure 3-2). This measurement is considered as reference, as no impact of the TBM drilling on the section S_x is to be expected at that distance. During the following six days, the tunnel section was measured approximately every hour. The first of these following measurements to be processed, was when the TBM reached the tunnel section N_x very closely, more specifically after construction of tunnel ring N_x-1. After this critical moment, the measurements when the TBM was at ring N_X+10 and ring N_x+38 (approximately 2 days after construction of ring N_x) are processed.

3.4. Measurement and processing methodology

3.4.1. Different scanning setups for reference and control measurements

During the reference measurements, several restrictions have to be overcome. Because no vibrations or movements of the TBM are allowed during the measurements, the drilling works have to be stopped during each reference measurement. Of course, the downtime of the TBM during the measurements has to be minimised, so the time pressure for the preparation of the scanning positions and the measurements was significant. On average, about two hours are needed to perform the preparation and installation of the scanning positions, the scanning itself and the strain gauge installations which influence the progress of the laser scanning work. Moreover, the free space in the head of the TBM is very limited, which impedes the field of view of the laser scanner and the works of the measurement crew. Due to this limited free space and the characteristics of the TBM's construction, a complete tunnel section cannot be measured from one scanning position.

Figure 3-3: Laser scanner mounted on a bracket at one side of a tunnel section

To cover the whole tunnel section during a reference measurement and to limit the incidence angles of the laser beam (Argüelles-Fraga et al., 2013), three scanning positions are needed, taking into account the field of view specifications of the used Leica HDS6100 laser scanner. Two scanning positions are mounted on a bracket on the tunnel surface, one on the left side and one on the right side (Figure 3-3). The laser scanner is placed on a tribrach on this bracket and from each scanning position the full field of view is measured without placing the laser scanner in a specific direction. The third scanning position is in the centre of the bottom of the tunnel section, where the laser scanner is mounted on a tripod.

To enable the registration of the measurements from these three scanning positions into a single point cloud, sixteen Leica black-and-white targets are attached on the tunnel section surface. These targets are printed on waterproof polyester and attached to the concrete surface with special highly adhesive glue to guarantee the further use of these targets during the following measurements. These sixteen targets are equally spread over the tunnel surface. Both at the bottom and at the top of the tunnel section, four targets are attached to the concrete and also at the left and right side, four targets are attached so that there are at least six to eight overlapping targets between two scanning positions. This large number of overlapping targets - three is the strict minimum - ensures a solid registration and minimisation of the target-to-target registration errors based on a least-squares optimisation (< 1 mm registration error). The exact centre of each black-and-white target is recognised by the processing software (Leica Cyclone) and one of these targets is indicated as the so-called 'Master Reference Target', which determines the exact location of the cross-section for the further processing of each measurement.

The control measurements start one week after construction of the monitored tunnel section. By that time, the TBM, which is approximately 100 m long, has fully passed this section. To cover a maximal area of the section surface, only one scanning position is needed: in the centre of the bottom of the tunnel section. The setup and scanning from this one scanning position during a control measurement take about 10 minutes. In this resulting point cloud, areas with no data cannot be avoided, due to the installed pathway, piping installations and a ventilation tube (Figure 3-4).

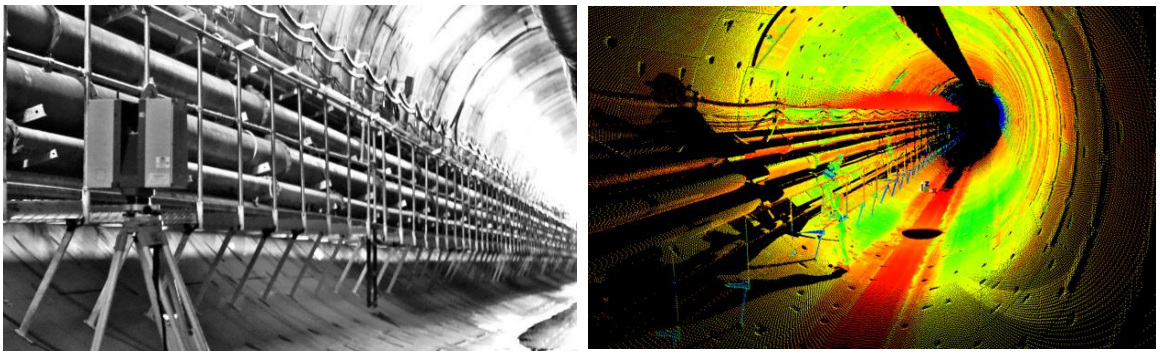

Figure 3-4: Picture (left) and point cloud (right) of a scanning position during a control measurement ('Liefkenshoek Rail Link' project)

From each scanning position, the point cloud covers the whole field of view of the laser scanner (i.e. Leica HDS6100: 360° horizontal – 310° vertical). The density of these point clouds varies, depending on the type of measurement. For a control measurement, the horizontal and vertical angle increment between two consecutive points was set at 0.036°, resulting in a point every 4 mm at the maximum distance of about 6 m on the concrete surface of the monitored tunnel ring. For a reference measurement, the selected angle increment was 0.018°, which resulted in a point every 2 mm at a maximum distance of about 6 m. During the optimised processing of the point clouds from measurements immediately

after placement though, only 1 point out of 4 (1 out of 2 horizontally and 1 out of 2 vertically) was imported in the laser scanning processing software (Leica Cyclone), resulting in a point cloud resolution of about 4 mm or higher. The original scanning resolution for measurements immediately after placement did not significantly contribute to the necessary level of detail or accuracy, so in the future, an angle increment of 0.036° would be sufficient for measurements immediately after placement. Moreover, the overlap of the three scanning positions in this type of measurements increases the point density to a level comparable with the control measurements. This resolution offers enough details to interpret and filter the point clouds and to automatically identify the black-and-white targets by the software (Leica Cyclone). The used laser scanner Leica HDS6100 manufacturer's specifications mention a 5 mm position accuracy of a single measurement and a distance accuracy for a single measurement of ≤2 mm or ≤3 mm up to 25 m for respectively 90% and 18% albedo (1 sigma). The modelled surface precision is 1 mm at 25 m; 2 mm at 50 m for 90% albedo (1 sigma) and 2 mm (at 25 m) or 5 mm (at 50 m) for 18% albedo (1 sigma).

3.4.2. Processing of the point cloud and cross-section

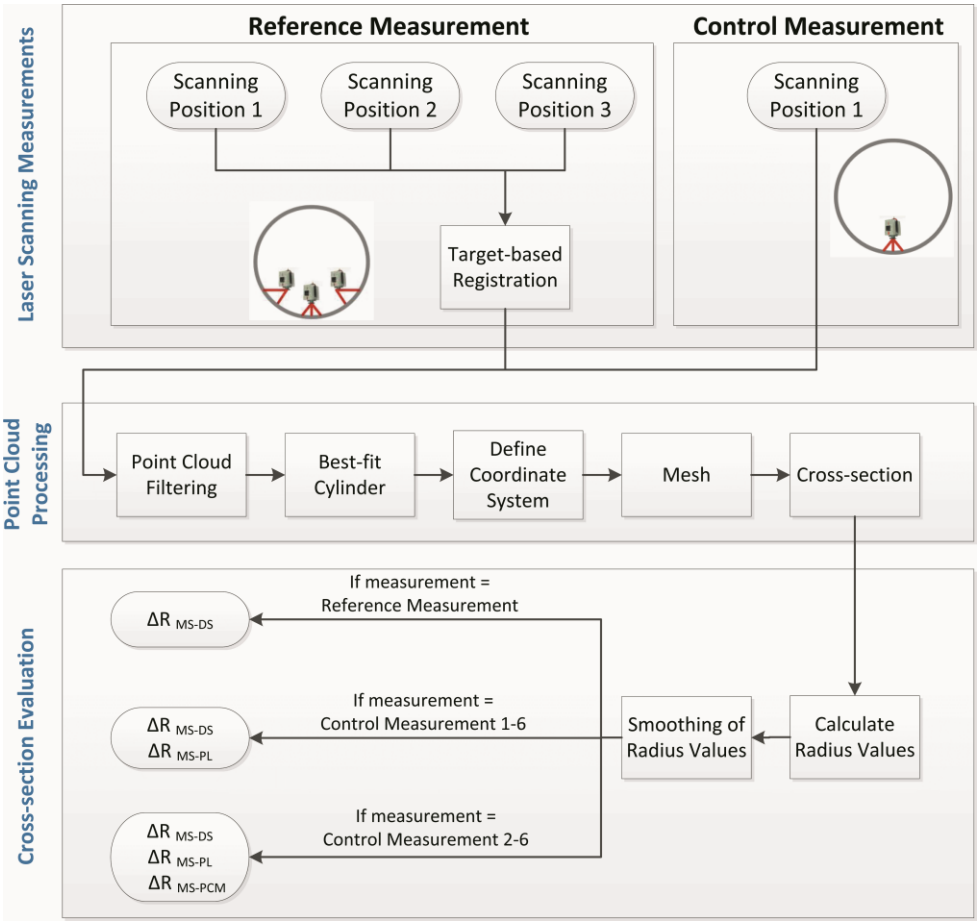

Figure 3-5: Flow diagram of the measurement and processing methodology

Because measurements with a laser scanner are not based on the 'smart selection' of points to measure but on the measurement of all points within the field of view, many spurious points have to be filtered out in the beginning of the point cloud processing (Figure 3-5).

For the reference measurements, a lot of measured points cover the TBM, so they do not contribute to the coverage of the monitored tunnel section. In a control measurement, the point cloud also contains a lot of points of adjacent tunnel sections, pipes, the ventilation equipment and the pathway to the TBM (Figure 3-4). Filtering of the point clouds is performed using the segmentation tools in Leica Cyclone to ensure a thorough quality control, but an automated filtering algorithm delivering equivalent results will be further discussed in chapter 7. It is important to base the following processing steps on a filtered point cloud of the monitored tunnel section, because the changes or removal of obstruction elements (pipes, ventilation equipment, etc.) during the monitoring period do not contribute to the insights on the deformations of the actual concrete tunnel sections. Moreover, for the calculation of a best-fit cylinder on these tunnel sections, filtered point clouds of the consecutive monitoring measurements ensure the most stable determination of the cylinder and tunnel axis and consequently the origin of the evaluated cross-section.

After filtering the point cloud and computing a best-fit cylinder with free diameter on this point cloud, a cross-section through the triangulated surface (mesh) of the tunnel section is determined. According to the design of the tunnel, it can be assumed that each tunnel section approximates a cylindrical shape. Therefore, the longitudinal axis of the best-fit cylinder is considered to represent the axis of the tunnel section. In order to obtain a closed polyline as cross-section instead of a much smaller collection of individual points, a triangulated surface (mesh) of the point cloud of the tunnel section is calculated. The cross-section is defined perpendicular to the tunnel longitudinal axis and its exact intersection on the tunnel section is fixed by the 'Master Reference Target'. The definition of one 'Master Reference Target' for each monitored tunnel section allows a same location of the cross-section between the different consecutive monitoring measurements. The cross-section results in a polyline, representing the triangulated surface of the measured tunnel surface and including all the measured detailed information, ready for further analysis in CAD software.

During data processing, a uniform coordinate system must be defined. The origin of this coordinate system is positioned on the axis of the best-fit cylinder and the coordinate system is further characterised by a horizontal X-axis and an upward Y-axis. The Z-axis is orientated along the longitudinal tunnel axis and in opposite direction of the drilling movement of the TBM (Figure 3-6). This user defined coordinate system for each measurement allows a better comparison between consecutive monitoring measurements of a tunnel section because the original setup point and orientation of the laser scanner is not fixed and thus different for each measurement.

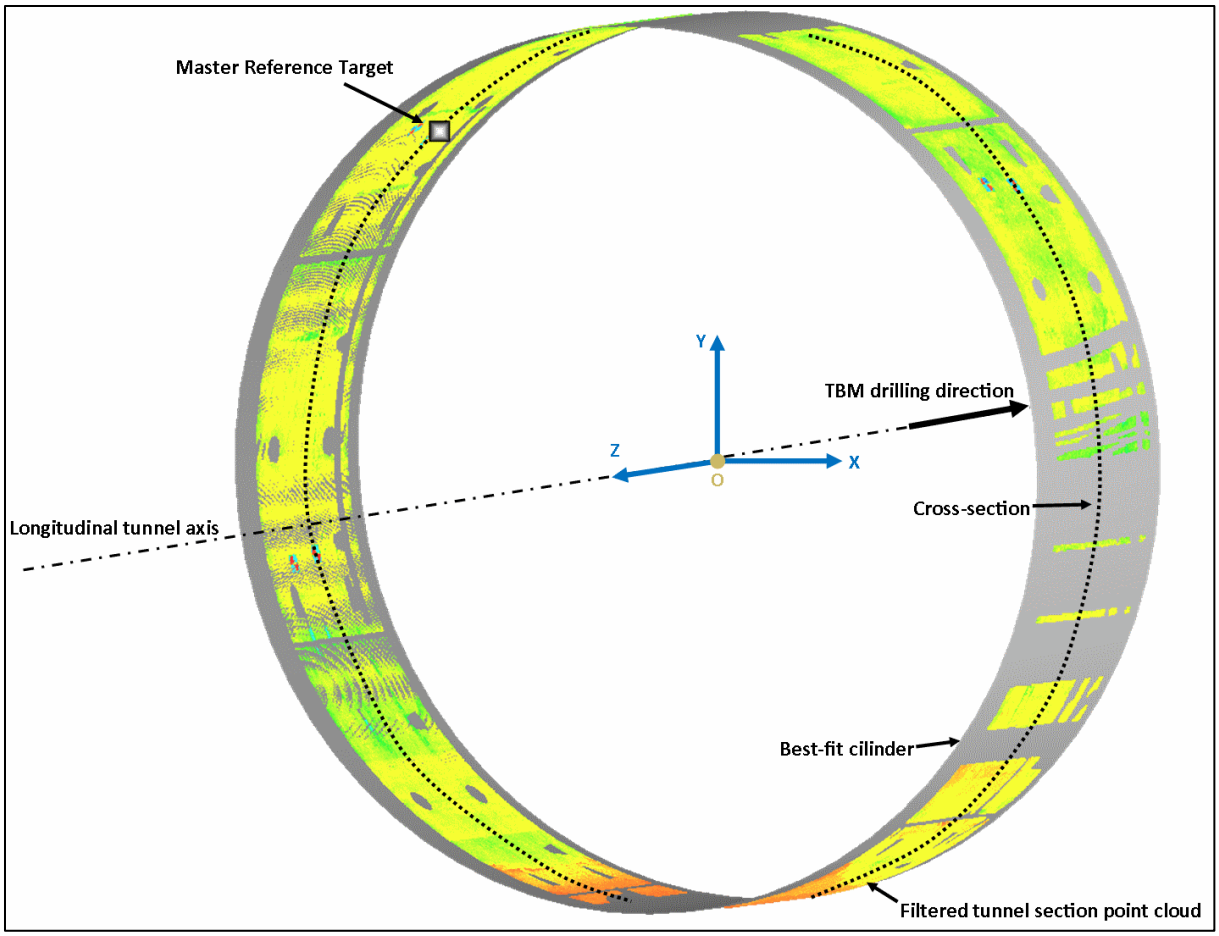

Figure 3-6: Schematic overview of the filtered point cloud, best-fit cylinder, coordinate system and cross-section

Based on the polyline of the cross-section, a radius value from the axis of the best-fit cylinder to the cross-section polyline is determined every 0.1 grad. This 0.1 grad step for each radius value results in a radius value on the tunnel surface every 5.7 mm which is very comparable to the scanning resolution. These 4 000 values are then smoothed by calculating the average of each radius value and an interval of 0.5 grad to the left and to the right of this radius value. Such a 0.5 grad interval corresponds to 2.85 cm on the tunnel surface. When no smoothing is applied on the data, the delivered plots of the comparison between consecutive measurements are not clearly readable or interpretable. Therefore, different smoothing levels were investigated to find the optimum averaging interval. This optimum smoothing level balances between removing the high frequency noise to improve the readability of the plots, keeping sufficient detail to avoid masking excessive measurements and still meeting the accuracy requirements (0.5 mm). Besides the non-smoothed results, the data were processed with smoothing intervals of 0.3 grad, 0.5 grad, 1.0 grad and 2.5 grad left and right of each radius value and an F-test was used to test whether there was a significant difference between the standard deviations for the different smoothing levels for the different tested measurement instruments. For the monitoring projects in this research, a Leica HDS6100 laser scanner was used and measurements taken with this type of

laser scanner resulted in experimentally based standard deviations between 0.34 and 0.58 mm, depending on the applied smoothing level. Taking into account the accuracy requirement of 0.5 mm for this project, the smallest smoothing interval to obtain this accuracy requirement was selected to be implemented, resulting in the applied [x-0.5 grad; x+0.5 grad] smoothing interval on the calculated radius values (Figure 3-7). More details about the comparison of different types of laser scanners and smoothing levels can be read in chapter 4.

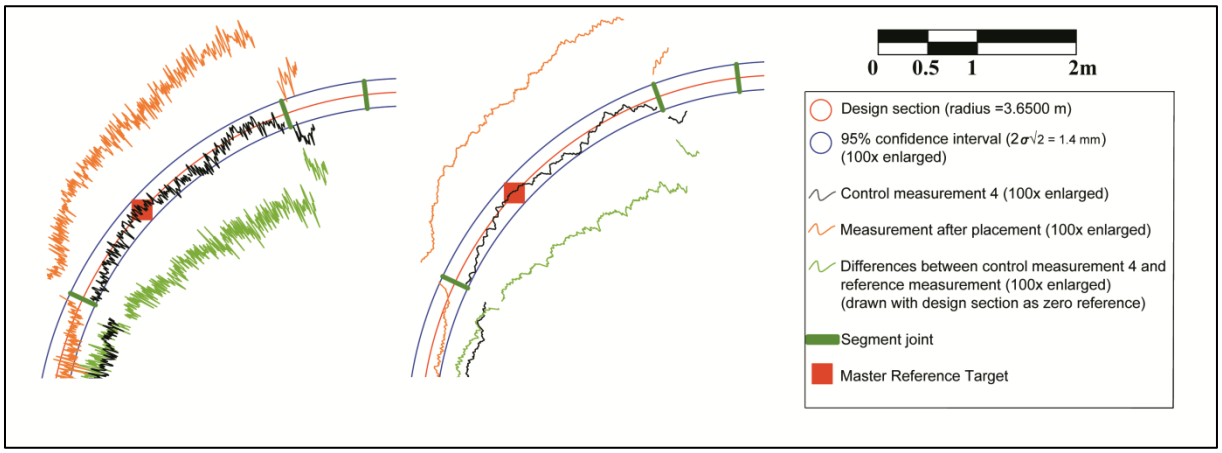

Figure 3-7: Fragment of the plotted result without smoothing (left) and with [x-0.5 grad; x+0.5 grad] grad smoothing interval (right)

Consequently, using smoothed data to interpret cross-sections does not significantly change the conclusions about the deviations from ovalisation of a tunnel section. This smoothing only yields clearer drawings without masking excessive measurements. To check for deviations from ovalisation, the smoothed radius values are compared with the design inner radius of 3.6500 m ($\Delta R_{MS\text{-}DS}$). A control measurement 1 and later control measurements are also compared with the reference measurement (measurement immediately after placement) ($\Delta R_{MS\text{-}PL}$) and from a control measurement 2 or further, these radius values are also compared with the previous control measurement ($\Delta R_{MS\text{-}PCM}$). All calculated deviations from ovalisation are compared with the 95% confidence level, based on the experimental standard deviation (0.4 to 0.5 mm) which has been determined by the authors, to detect any significant changes. The inclusion of the measurement immediately after placement into the monitoring campaign offers the important possibility to assess if the detected deformations are caused by a non-perfect placement of the tunnel ring or if they are indeed caused by the pressure on the tunnel construction over the following months and years.

3.5. Monitoring results

3.5.1. Monitoring during the 'Liefkenshoek Rail Link' project

The summarising table below (Table 3-1) shows the averaged results for all twenty eight monitored sections in the 'Liefkenshoek Rail Link' project. First, for each measurement of the scheduled series the differences between the measured radius (MS) values and the design

radius (DS = 3.6500 m) are calculated. For this comparison, the average of the algebraic deviations ($\Delta R_{MS\text{-}DS}$) is determined (equation (1) and (2)). Additionally, the mean absolute error ($MAE_{MS\text{-}DS}$) (equation (3) and (4)) and the root mean square error ($RMSE_{MS\text{-}DS}$) are calculated (equation (5) and (6)). The mean absolute error represents how close the measurement lies to the design or other reference measurement. The root mean square error is a measure of the residuals between the measured radius values and the reference radius values. By including the square of the errors in the root mean square error however, large errors have a relatively larger influence on the total square error (Willmott & Matsuura, 2005).

Table 3-1: Results of the ovalisation monitoring in the 'Liefkenshoek Rail Link' project

Ovalisation monitoring: averaged results of Tunnel North & Tunnel South									
Meas.	Δ Average Radius - Design (mm)			Δ Average Radius - Placement (mm)			Δ Average Radius - Prev. Control Meas. (mm)		
	$\Delta R_{MS\text{-}DS}$	$MAE_{MS\text{-}DS}$	$RMSE_{MS\text{-}DS}$	$\Delta R_{MS\text{-}PL}$	$MAE_{MS\text{-}PL}$	$RMSE_{MS\text{-}PL}$	$\Delta R_{MS\text{-}PCM}$	$MAE_{MS\text{-}PCM}$	$RMSE_{MS\text{-}PCM}$
0 Pl	1.7	3.0	3.6	---	---	---	---	---	---
1 Wk 1	-1.6	2.9	3.5	-3.3	3.6	4.2	---	---	---
2 Wk 2	-1.5	2.9	3.5	-3.4	3.6	4.3	-0.1	0.5	0.6
3 Wk 3	-1.5	2.9	3.5	-3.2	3.6	4.2	0.0	0.4	0.6
4 Mo 1	-1.5	2.9	3.6	-3.2	3.6	4.2	0.0	0.4	0.5
5 Mo 2	-1.6	3.1	3.7	-3.3	3.7	4.4	-0.1	0.5	0.7
6 Mo 3	-1.7	3.1	3.8	-3.3	3.8	4.4	0.0	0.5	0.7

$$\mathbf{\Delta R_{MS\text{-}DS}} = \frac{1}{m}\sum_{j=1}^{m}\left[\frac{1}{n}\sum_{i=1}^{n}(R_{ij}-3.6500)\right] \quad (3\text{-}1) \quad = \frac{1}{m}\sum_{j=1}^{m}\left[\frac{1}{n}\sum_{i=1}^{n}\Delta R_{MS-DS_{ij}}\right] \quad (3\text{-}2)$$

$$\mathbf{MAE_{MS\text{-}DS}} = \frac{1}{m}\sum_{j=1}^{m}\left[\frac{1}{n}\sum_{i=1}^{n}\left|R_{ij}-3.6500\right|\right] \quad (3\text{-}3) \quad = \frac{1}{m}\sum_{j=1}^{m}\left[\frac{1}{n}\sum_{i=1}^{n}\left|\Delta R_{MS-DS_{ij}}\right|\right] \quad (3\text{-}4)$$

$$\mathbf{RMSE_{MS\text{-}PCM}} = \frac{1}{m}\sum_{j=1}^{m}\sqrt{\frac{1}{n}\sum_{i=1}^{n}(R_{ij}-3.6500)^2} \quad (3\text{-}5) \quad = \frac{1}{m}\sum_{j=1}^{m}\sqrt{\frac{1}{n}\sum_{i=1}^{n}(\Delta R_{MS-DS_{ij}})^2} \quad (3\text{-}6)$$

With R_{ij} = radius value measured at i x 0.1 grad for a measurement of tunnel section
n = number of calculated radius value (every 0.1 grad, n ≤ 4000)
m = number of tunnel section (m ≤ 28)

During the different measurements of a tunnel section, it is not possible to cover the whole section surface due to obstacles on parts of the concrete surface of the tunnel ring. Therefore, not for every 0.1 grad angle a radius value is calculated (n ≤ 4000). In total, 187 scheduled measurements were performed, one reference measurement for each section and six control measurements. A very small number of measurements could not be performed, due to the fact that the TBM had not yet passed the tunnel section at the planned time or due to the construction schedule, according to which it was not possible to enter the tunnel on the scheduled times.

Similar characteristics are calculated for the comparison between each control measurement (control measurement 1 tot 6) and the reference measurement immediately after placement (PL), shown under $\Delta R_{MS\text{-}PL}$, $MAE_{MS\text{-}PL}$ and $RMSE_{MS\text{-}PL}$. For the calculation of these characteristics, the value of 3.6500 in above mentioned equations (3-1), (3-3) and (3-5) has to be replaced with $R_{PL_{ij}}$, and $\Delta R_{MS\text{-}DS_{ij}}$ has to be replaced with $\Delta R_{MS\text{-}PL_{ij}}$ in equations (3-2), (3-4) and (3-6). Also, for the comparison between the control measurements 2 to 6 and their previous control measurement (PCM), the characteristics $\Delta R_{MS\text{-}PCM}$, $MAE_{MS\text{-}PCM}$ and $RMSE_{MS\text{-}PCM}$ are calculated. These characteristics are also based on above mentioned formulas, but by replacing 3.6500 and $\Delta R_{MS\text{-}DS_{ij}}$ with $R_{PCM_{ij}}$ (equation (3-1), (3-3) and (3-5)) and respectively $\Delta R_{MS\text{-}PCM_{ij}}$ (equation (3-2), (3-4) and (3-6)).

Analysing the results of all monitored tunnel sections, it can be concluded that significant changes in ovalisation occur during the first week after construction of the tunnel section. On average, there is a negative change in radius of 3.3 mm during the first week after placement, which corresponds to a change in circumference of about 20.7 mm. These changes may be due to the grouting process (cement injection) shortly after the placement of the tunnel ring, which causes an enormous external pressure on the concrete sections and compresses the ring structure by the closing of the rubber joints between the different segments. After that first week the sections seem to have settled in their final position, because no more significant changes were measured. Compared with the previous control measurement, the changes in radius value vary between 0.0 and -0.1 mm. The 95% confidence levels, based on the experimental standard deviation, can be taken into account as threshold for this determination. For the comparison between a measurement and the design of the section, a 95% confidence level of 1.0 mm is considered, taking into account the achievable standard deviation (0.4 to 0.5 mm) which fulfills the requested accuracy by the client. The 95% confidence level, when comparing two measurements with each other (e.g. control measurement 2 compared to control measurement 1), is $2\sigma*\sqrt{2} = 1.4$ mm. This trend of a convergence towards a stabilised radius can also be seen in Figure 3-8, which shows a graphic representation of the changes in radius values of some of the monitored tunnel sections. The data represented in the graph are the differences for each measurement between the average of the measured radius values of the cross-section and the design shape of the tunnel.

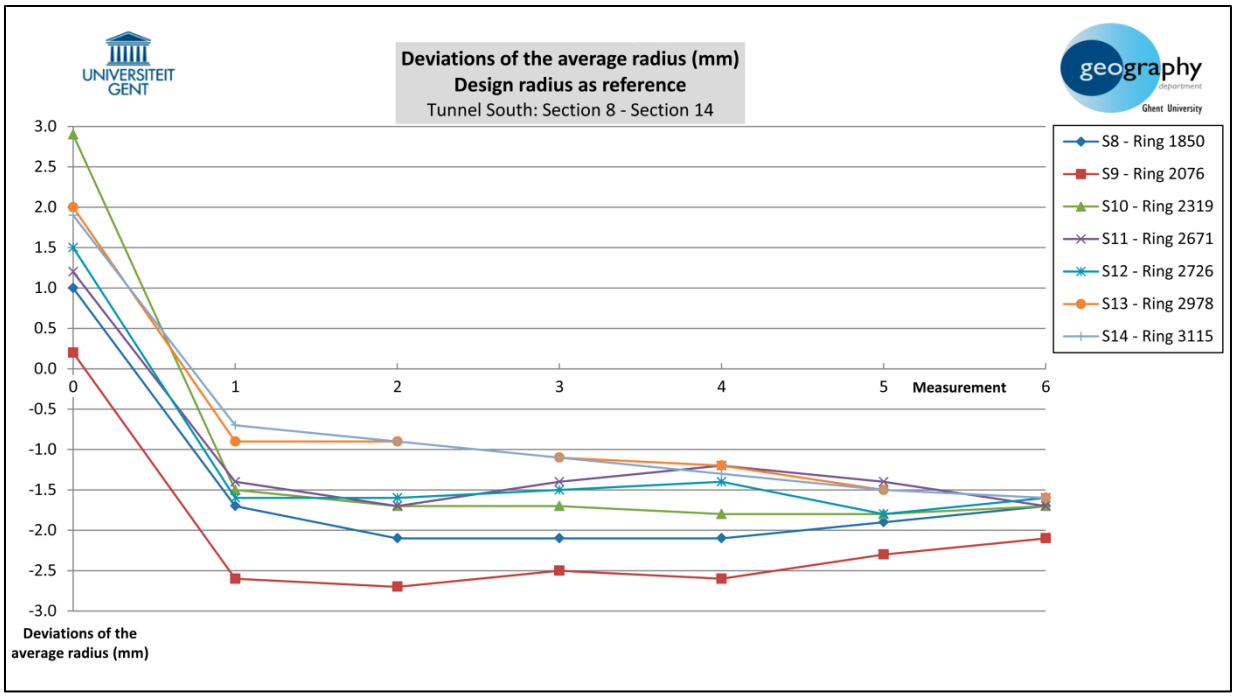

Figure 3-8: Deviations of the average radius – Tunnel South (section 8 to 14)

For each measurement, plots of the cross-sections are elaborated to visually represent the measurement results and deviations. The emphasis is on a 2D representation of these measurements to guarantee an easily interpretable analysis and visualisation. Figure 3-9 shows an example of such a plot. The deviations between a control measurement and the previous control measurement are indicated by the green curve. The coincidence of this green curve with the red design shape of the tunnel section indicates that there is no significant deviation between both measurements. Any deviation between the two blue circles, indicating the 95% confidence interval, is not considered to be significant, based on the achievable standard deviation. This type of 2D cross-section drawing gives a very quick overview of areas of the cross-section where significant deviations occur. To improve the visual interpretation, all deviations in the drawings are enlarged one hundred times. The indicated numerical values however, represent the real (not enlarged) absolute deviations between both measurements.

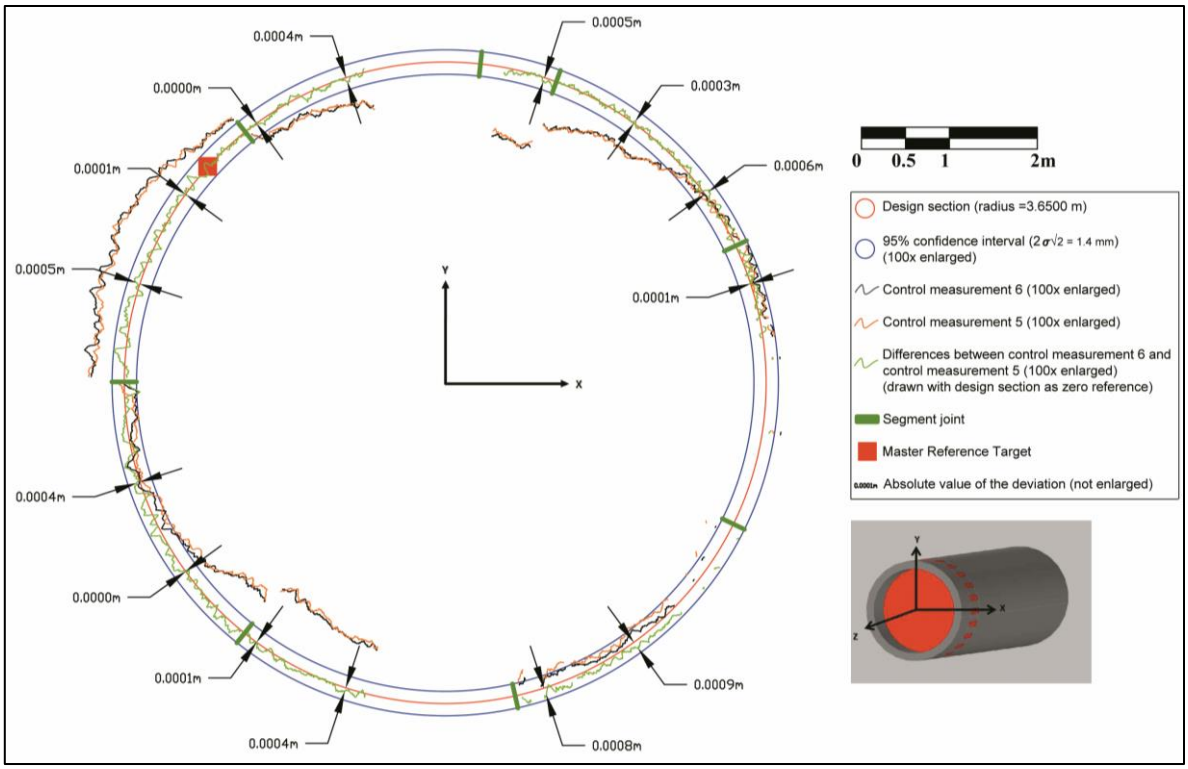

Figure 3-9: Example of a plot of the deviations between 2 control measurements

For the interpretation of the results, it is important to mention that the centre of the cross-section of each measurement is based on the axis of the best-fit cylinder, as described in the developed methodology. As this best-fit cylinder is determined for each measurement, based on the filtered point cloud, small variations may occur in the orientation of this best-fit cylinder and its centre point, even if there are no deformations in the sections shape. Due to the fact that the measurements are not located in an absolute coordinate system, a vertical shift of the whole tunnel structure cannot be detected in the deviations. The influence of the small variations on the best-fit cylinder on the average difference in radius is limited, but may not be negligible when analysing the minimal or maximal differences between two measurements. Therefore, the main conclusions or analyses are performed on the average differences in radius values. Moreover, caution is needed with regard to the absolute value of these averaged values as the measured areas are not equally spread around the tunnel ring. If a realistic or complete average tunnel radius should be computed, the ovalisation axis and the deformation pattern should be taken into account in order to compensate for the non-measured areas. That extended analysis however, lies outside the scope of the research questions of this dissertation.

3.5.2. Impact of the drilling of the adjacent tunnel

Based on the monitoring measurements to assess the impact of the drilling of the adjacent tunnel, the deviations shown by the following measurements indicate no significant changes occurred while drilling was underway. The average deviations vary between 0.0 and -0.3 mm. The mean absolute errors vary between 0.5 and 0.6 mm. Because the same 95%

confidence interval of 1.4 mm can be used to evaluate these results, we can conclude that all changes during the drilling of the adjacent tunnel fall well within this interval.

3.6. Conclusions

In two recent tunnelling projects in Belgium, laser scanning has been applied for the first time to monitor a tunnel's construction from immediately after placement until three months after construction of each monitored tunnel section. The results of such a systematic monitoring program allowed the contractors or engineers involved to validate the deformation models and to compare these models with the actual behaviour of large diameter shield tunnelling in soft soil. This is highly valuable because very few measurements at this early stage of a tunnel construction are available to evaluate the performance and accuracy of such deformation models. The inclusion of a measurement immediately after ring assembly into the monitoring campaign offers the important possibility to assess if the detected deformations are caused by a non-perfect placement of the tunnel ring or if they occurr during the following months or years of the tunnel's life cycle.

For the ovalisation measurements in the 'Liefkenshoek Rail Link' project, the observed differences of the average radius values generally show a decrease in the first week after ring erection, which amounts to an average of -3.3 mm. This corresponds to a change in circumference of about 20.7 mm and is mainly caused by the compression of the ring structure by the closing of the rubber joints between the different segments and the construction and building tolerances. After this first week after ring erection, the observed variations of the average radius generally show little or no variation, with differences that amount to maximum -0.1 mm, averaged over all measured 28 tunnel sections in the project. These variations are well below the 1.4 mm boundary and are therefore attributed to monitoring accuracy.

The successfully developed methodology is mainly focused on achieving a very small standard deviation (<0.5 mm), developing a clear and operator controllable processing workflow and delivering easily interpretable results and drawings to locate areas with significant deviations from ovalisation. This experimental standard deviation means that the 95% confidence interval of the ovalisation measurements is of mm-order. Therefore, to assess the sub-millimetre level deformations of the individual concrete tunnel segments themselves, the research on strain gauge measurements applied simultaneously in the mentioned Belgian tunnelling projects can be employed. Moreover, this research includes not only a clear definition of the tunnel axis based on a best-fit cylinder, but also a meshing step in the workflow to determine the cross-section through a triangulated surface instead of the original point cloud. The highly detailed picture of the cross-sections allows detection of the segment joints and analysis of the individual segments in further research is possible, complying with the need for segmental deformation analysis (see also section 9.2).

3.7. References

Argüelles-Fraga, R., Ordonez, C., Garcia-Cortes, S., & Roca-Pardinas, J. (2013). Measurement planning for circular cross-section tunnels using terrestrial laser scanning. *Automation in Construction, 31*, 1–9. doi:10.1016/j.autcon.2012.11.023

Beraldin, J.-A., Blais, F., Boulanger, P., Cournoyer, L., Domey, J., El-Hakim, S. F., Godin, G., Rioux, M., & Taylor, J. (2000). Real world modelling through high resolution digital 3D imaging of objects and structures. *ISPRS Journal of Photogrammetry & Remote Sensing, 55*, 230–250.

Bizjak, K. F., & Petkovsek, B. (2004). Displacement analysis of tunnel support in soft rock around a shallow highway tunnel at Golovec. *Engineering Geology, 75*(1), 89–106. doi:10.1016/j.enggeo.2004.05.003

Büyüköztürk, O. (1998). Imaging of concrete structures. *NDT&E International, 31*(4), 233–243.

Clarke, T. A. (1996). A review of tunnel profiling methods. Optical Metrology Centre.

Delaloye, D., Hutchinson, J., & Diederichs, M. (2011). Accuracy issues associated with Lidar scanning for tunnel deformation monitoring. In *2011 Pan-Am CGS Geotechnical Conference*. Toronto, Ontario, Canada.

Fekete, S., Diederichs, M., & Lato, M. (2010). Geotechnical and operational applications for 3-dimensional laser scanning in drill and blast tunnels. *Tunnelling and Underground Space Technology, 25*(5), 614–628. doi:10.1016/j.tust.2010.04.008

Gordon, S. J., & Lichti, D. D. (2007). Modeling Terrestrial Laser Scanner Data for Precise Structural Deformation Measurement. *ASCE Journal of Surveying Engineering, May 2007*, 72–80. doi:10.1061/(ASCE)0733-9453(2007)133:2(72)

Han, J.-Y., Guo, J., & Jiang, Y.-S. (2013a). Monitoring tunnel deformations by means of multi-epoch dispersed 3D LiDAR point clouds: An improved approach. *Tunnelling and Underground Space Technology, 38*, 385–389. doi:10.1016/j.tust.2013.07.022

Han, J.-Y., Guo, J., & Jiang, Y.-S. (2013b). Monitoring tunnel profile by means of multi-epoch dispersed 3-D LiDAR point clouds. *Tunnelling and Underground Space Technology, 33*(186-192), 186. doi:10.1016/j.tust.2012.08.008

Hesse, C., & Stramm, H. (2004). Deformation measurements with laser scanners. Possibilities and challenges. In *International Symposium on Modern Technologies, Education and Professional Practice in Geodesy and Related Fields* (pp. 228–240). Sofia, Bulgaria.

Huang, K.-P., Wang, T.-T., Huang, T.-H., & Jeng, F.-S. (2010). Profile deformation of a circular tunnel induced by ambient stress changes. *Tunnelling and Underground Space Technology, 25*(3), 266–278. doi:10.1016/j.tust.2009.12.006

Lindenbergh, R., & Pfeifer, N. (2005). A statistical deformation analysis of two epochs of terrestrial laser data of a lock. In *Optical 3-D Measurement Techniques VII*.

Molins, C., & Arnau, O. (2011). Experimental and analytical study of the structural response of segmental tunnel linings based on an in situ loading test. Part 1: Test configuration and execution. *Tunnelling and Underground Space Technology, 26*(6), 764–777. doi:10.1016/j.tust.2011.05.002

Monserrat, O., & Crosetto, M. (2008). Deformation measurements using terrestrial laser scanning data and least square 3D surface matching. *ISPRS Journal of Photogrammetry & Remote Sensing, 63*, 142–154. doi:10.1016/j.isprsjprs.2007.07.008

Ninkov, T., Bulatovic, V., Susic, Z., & Vasic, D. (2010). Application of Laser Scanning Technology for Civil Engineering Projects in Serbia. In *The XXIV FIG International Congress 2010 "Facing the Challenges - Building the Capacity."* Sydney, Australia: FIG.

Nuttens, T., De Wulf, A., Bral, L., De Wit, B., Carlier, L., De Ryck, M., Stal, C., Constales, D., & De Backer, H. (2010). High Resolution Terrestrial Laser Scanning for Tunnel Deformation Measurements. In *The XXIV FIG International Congress 2010 "Facing the Challenges - Building the Capacity."* Sydney, Australia: FIG.

Roberts, G. W., Brown, C. J., & Ogundipe, O. (2010). Monitoring Bridges by GNSS. In *The XXIV FIG International Congress 2010 "Facing the Challenges - Building the Capacity."* Sydney, Australia: FIG.

Schueremans, L., & Van Genechten, B. (2008). The use of 3D-laser scanning in assessing the safety of masonry vaults - A case study on the church of Saint-Jacobs. *Optics and Lasers in Engineering, 47*, 329–335. doi:10.1016/J;optlaseng.2008.06.009

Stal, C., De Wulf, A., De Coene, K., De Maeyer, P., Nuttens, T., & Ongena, T. (2012). Digital Representation of Historical Globes: Methods to Make 3D and Pseudo-3D Models of Sixteenth Century Mercator Globes. *The Cartographic Journal, 49*(2), 107–117. doi:10.1179/1743277412Y.0000000002

Stiros, S. C., & Psimoulis, P. A. (2012). Response of a historical short-span railway bridge to passing trains: 3-D deflections and dominant frequencies derived from Robotic Total Station (RTS) measurements. *Engineering Structures, 45*, 362–371. doi:10.1016/j.engstruct.2012.06.029

Teachavorasinskun, S., & Chub-uppakarn, T. (2010). Influence of segmental joints on tunnel lining. *Tunnelling and Underground Space Technology, 25*(4), 490–494. doi:10.1016/j.tust.2010.02.003

Teza, G., Galgaro, A., & Moro, F. (2009). Contactless recognition of concrete surface damage from laser scanning and curvature computation. *NDT&E International, 42*(4), 240–249. doi:10.1016/j.ndteint.2008.10.009

TUC Rail. (2010). Antwerp: The tunnel borers for the Liefkenshoek rail tunnel. TUC Rail - Belgian Rail Engineering.

Van Bogaert, P. (2009). Recent and future railway tunnels in Belgium. In *Proc. ITA World Tunnel Conference "Safe Tunnelling for the City and the Environment"* (pp. 689–690). Budapest: Hungarian Tunnelling Association, ISBN 9789630672399.

Van Gosliga, R., Lindenbergh, R., & Pfeifer, N. (2006). Deformation analysis of a bored tunnel by means of terrestrial laser scanning. In H.-G. Maas & D. Schneider (Eds.), *ISPRS Commission V Symposium "Image Engineering and Vision Metrology"* (Vol. Volume XXX). Dresden, Germany: IAPRS Volume XXXVI, Part 5.

Willmott, C. J., & Matsuura, K. (2005). Advantages of the mean absolute error (MAE) over the root mean square error (RMSE) in assessing average model performance. *Climate Research, 30*, 79–82.

Yoon, J.-S., Sagong, M., Lee, J. S., & Lee, K. (2009). Feature extraction of a concrete tunnel liner from 3D laser scanning data. *NDT&E International, 42*, 97–105. doi:10.1016/j.ndteint.2008.10.001

CHAPTER 4
LASER SCANNING FOR OVALISATION MEASUREMENTS: STANDARD DEVIATIONS AND SMOOTHING LEVELS ('DIABOLO' PROJECT, BELGIUM)

4. LASER SCANNING FOR OVALISATION MEASUREMENTS: STANDARD DEVIATIONS AND SMOOTHING LEVELS ('DIABOLO' PROJECT, BELGIUM)

Modified from Nuttens, T., Stal, C., De Backer, H., Deruyter, G., Schotte, K., Van Bogaert, P., & De Wulf, A. Laser scanning for ovalization measurements: standard deviations and smoothing levels (Diabolo project, Belgium). ASCE Journal of Surveying Engineering. (Under review)

4.1. Abstract

Monitoring measurements need to be supported by a thorough knowledge of the achievable accuracy of the measurement equipment and the processing methodology. For ovalisation monitoring with laser scanning in tunnels under construction, the focus lies on the most adapted type of laser scanner based on achievable accuracy and scanning performance. Additionally, to deliver clearly interpretable plots of the results, research on the optimum smoothing level of the data is necessary. The experimentally based standard deviations determined in the 'Diabolo' and the 'Liefkenshoek Rail Link' project indicate that the phase-based laser scanner Leica HDS6100 delivers highly accurate results with standard deviations between 0.34 and 0.58 mm, depending on the applied smoothing level. In this research, this laser scanner was used, together with a [x-0.5 grad; x+0.5 grad] smoothing interval on the calculated radius values to meet the accuracy requirement (0.5 mm), even when using multiple setups. The Leica C10 also delivers standard deviations around this range, but this type has a lower scanning speed and a smaller vertical field of view, making it less adapted for measurements in time restricted tunnel monitoring projects.

4.2. Introduction

Laser scanning has become frequently applied for the acquisition of accurate and dense 3D data sets in civil engineering. The high scanning speed, in combination with a high accuracy, offers significant advantages compared to more traditional techniques (Lindenbergh et al., 2005). Moreover, these advantages enable a measurement solution in high demanding projects to monitor the stability of civil technical structures in difficult field conditions (Fekete et al., 2010; Lague, Brodu, & Leroux, 2013). The performance of deformation monitoring has increased significantly with the highly abundant data offered by laser scanning (Argüelles-Fraga et al., 2013; Yoon et al., 2009). However, the often ad hoc and little automated processing of the laser scanning data remains an important barrier for a practical and straightforward implementation of laser scanning in many projects (Pejić, 2013; Zogg & Ingensand, 2008).

During deformation monitoring such as tunnel monitoring projects, it is important to understand the structure's actual behaviour caused by the *in situ* stresses (Peeters et al.,

2009). Actual behaviour measurements of tunnel constructions with high resolution laser scanning contribute to the improvement of existing mathematical engineering models (Arnau & Molins, 2012; Wang, Wu, Guo, & Ge, 2012). In general, few systematic measurements in the early stage of tunnel construction are available, so this part of the construction phase is often little or not implemented in deformation models. Moreover, the monitoring based on measurements during the construction phase and the following period, together with the detection of damages which can impact the structural durability are essential to evaluate the risk profile of the structure at different points in time (Aydin, 2012; Blom, van der Horst, & Jovanovic, 1999; Fujino & Siringoringo, 2011; Huang et al., 2010). The large data set, collected with laser scanning, also offers the possibility to use the same point set for different applications by various users, such as radial difference maps, checking bolt spacing, identifying moist and dry shotcrete, tunnel lining… (Fekete et al., 2010). Monitoring data and the consequent conclusions about significant deformations need to be supported by a thorough knowledge of the achievable accuracy of the measurement equipment and the processing methodology (Helmerich et al., 2012; Pejić, 2013). In addition, the results have to be presented in such a way that the involved engineers, surveyors or others can unambiguously interpret them, implying a smart data processing.

The tunnel monitoring projects on which this research was based were the first projects in Belgium in which laser scanning was used to systematically monitor the ovalisation of multiple tunnel sections under construction. This ovalisation monitoring included measurements of different tunnel rings from the moment of assembly until at least three months after construction of the tunnel ring. In the first project, called 'Diabolo' (Zaventem-Brussels, Belgium), the use of laser scanning for this type of monitoring was tested and implemented. After that, the developed workflows were optimised and the processing of the data sets was further elaborated in the 'Liefkenshoek Rail Link' project (Antwerp, Belgium). The extensive and systematic monitoring delivered an important contribution to the understanding of the behaviour of the tunnels between assembly and stabilisation of the structure. The measured 3D point cloud of the maximum visible area of the tunnel section not only gives much more detailed information about the deformations and the ovalisation pattern, but also allows us to recognise and localise the segment joints. Research on the attainable accuracy is essential to interpret the results in a well-founded manner. In the framework of these newly developed workflows, this chapter investigates the most adapted type of laser scanner for this type of tunnel monitoring projects, together with a thorough assessment of the achievable accuracy. Besides, to meet the requirements for clearly interpretable plots of the results, the focus also lies on the most optimal smoothing level of the data.

The next section will go into detail on the 'Diabolo' tunnel monitoring project (Belgium), where most of the data sets were collected for the comparison of the different types of scanning instruments. The following section further details the comparison and accuracy assessment of the different scanning instruments, together with the different tested

smoothing levels of the data. The results presented in that section combine the test measurements from both the 'Diabolo' and 'Liefkenshoek Rail Link' project. The results for the experimental standard deviations and the smoothing levels lead to a discussion on the most adapted and most accurate scanning instrument and the most optimal smoothing of the data. All findings are then summarised in the conclusion section.

4.3. Tunnel monitoring project: 'Diabolo' project (Belgium)

4.3.1. Overview of the 'Diabolo' project

The 'Diabolo' project in Belgium (2007-2012) was set up to improve the northern accessibility of Brussels Airport (Zaventem, Belgium) by the beginning of 2012. This new railway connection allows trains to significantly reduce their travelling time between the northern part of Belgium or the Netherlands and the airport railway station. Part of this new connection is a bored tunnel complex with a 1 km long twin tube tunnel, drilled using the mixshield method in which the Tunnel Boring Machine (TBM) pushes against the last built ring to continue boring. The part of the bored tunnels below the airport is critical, because the tunnels cross an airport runway, taxiing areas and several airport buildings and piers at a depth of 16.5 m without shutting down the airport activities (Figure 4-1). Of course, large settlements of the airport infrastructure and neighbouring hangars during the construction of the tunnels have to be avoided. Therefore, close monitoring of the structure during the construction phase was ordered (Van Bogaert, 2009).

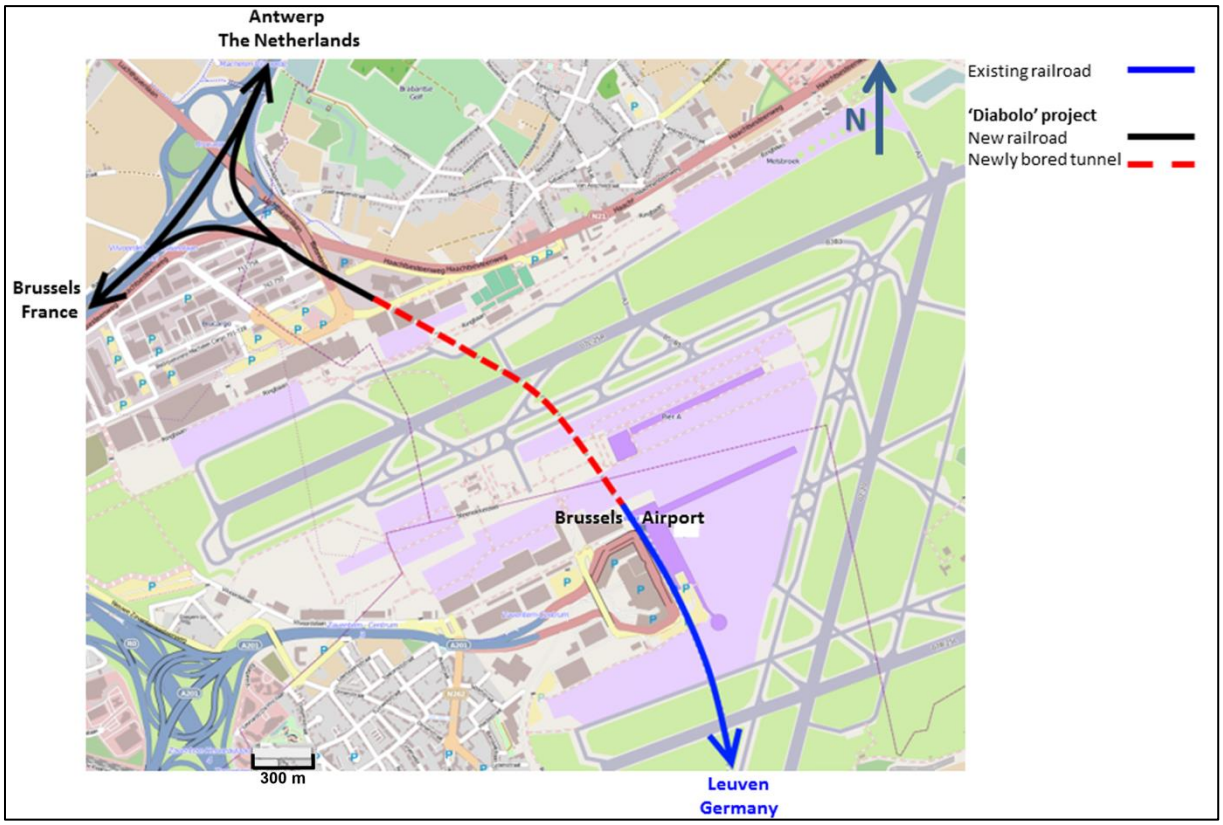

Figure 4-1: 'Diabolo' project: overview of the northern railway connection for Brussels Airport (based on www.openstreetmap.org)

The circular tunnels have an inner diameter of 7.300 m and the tunnel segments have a radial thickness of 0.350 m. Each tunnel ring is 1.500 m wide, measured along the longitudinal axis of the tunnel, and consists of seven concrete segments and one closing key stone. During the construction, six tunnel sections in each tube were closely monitored to detect possible deformations. The monitoring was based on measurements with laser scanning on specific moments in time. Seven moments in time were defined on which the selected tunnel sections had to be measured. The first measurement ('reference measurement') was performed immediately after construction of the tunnel ring. Subsequently, there was a measurement every week during the first month after placement ('control measurement 1 to 4') and a measurement two months and three months after placement ('control measurement 5 and 6'). For each measurement, a cross-section of the tunnel ring, derived from the laser scanning point cloud, was compared to the design shape and, if applicable, also with the reference measurement and the previous control measurement of that tunnel section.

In addition to monitoring with laser scanning, strain gauge measurements were performed on the same sections, in order to measure the strains of the individual concrete segments and also to investigate the link between the strain measurements and the results of the laser scanning measurements (see chapter 5 and 6). The simultaneous data of both laser scanning and strain gauge measurements opens many opportunities to combine the conclusions from both methods and to improve the knowledge of tunnel behaviour in *in situ* conditions.

4.3.2. Methodology for the ovalisation monitoring

To cover the whole tunnel section during a reference measurement, three scanning positions were needed. This was due to the vertical field of view specifications of the used laser scanning instrument and the obstructions caused by the TBM. Two scanning positions were mounted on a metal tunnel bracket attached on the left and right side of the concrete tunnel surface and the third scanning position was located at the centre of the bottom of the tunnel section, where the laser scanner was mounted on a tripod (Figure 4-2). To cover a maximum area of the section's surface during a control measurement, in principle, only one scanning position was needed, located at the centre of the bottom of the tunnel section, because at the moment of a control measurement the TBM had already passed the tunnel section and no other large obstacles were obstructing the tunnel section except for some piping, a pathway and a ventilation tube. But, notwithstanding this almost clear view on the tunnel section, the number of scanning positions needed for a control measurement could exceptionally vary depending on the specific tunnel construction circumstances.

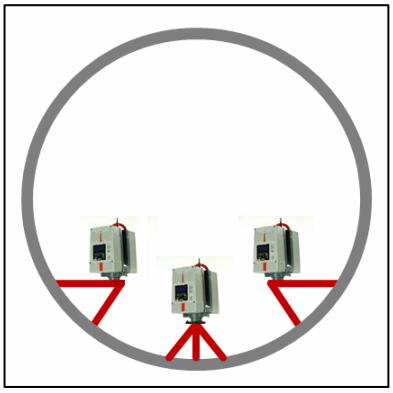

Figure 4-2: Three scanning positions for a reference measurement (left); Third scanning position during a reference measurement in the TBM (right)

The first steps in the processing of the point clouds were removing those points not located on the concrete tunnel surface and the computation of a best-fit cylinder with free diameter on this filtered point cloud. After that, a cross-section through the 3D triangulated surface of the tunnel section was determined. The cross-section was defined perpendicular to the tunnel's longitudinal axis and its exact intersection on the tunnel surface was fixed by the 'Master Reference Target', one of the targets attached to the tunnel surface for registering the different scanning positions of a reference measurement. The cross-section results in a polyline, ready for further analysis in CAD software. During data processing, a uniform coordinate system was defined, in which the Z-axis was orientated along the longitudinal tunnel axis and in opposite direction of the drilling movement of the TBM.

Based on the polyline of the cross-section, a radius value from the axis of the best-fit cylinder to the cross-section polyline was determined every 0.1 grad and subsequently this value was smoothed by calculating the average of each radius value and an interval of 0.5 grad to the left and right of this radius. This specific level of smoothing will be further elaborated in section 4.4.2. To check for deviations caused by ovalisation, the smoothed radius values were compared to the design inner radius of 3.650 m. Every control measurement was also compared to the reference measurement. Control measurements 2, as well as the following control measurements, were also compared to the previous control measurement. All calculated deviations from ovalisation were compared to the 95% confidence level, based on the experimental standard deviation determined by the authors (0.4-0.5 mm, see section 4.4.1 for more details), to detect any significant changes. For these statistical analyses, a normal distribution of the deviations was assumed.

Because of the high resolution of the point cloud, the location of the segment joints and individual segments can be visually identified and in the cross-section of the tunnel rings, this information is included (Figure 4-4).

4.3.3. Monitoring results

By analysing the results of all monitored tunnel sections in the 'Diabolo' project, it can be concluded that significant changes in ovalisation occur during the first week after construction of the tunnel section. On average, there was a decrease in radius of 2.2 mm during the first week after placement, which corresponds to a change in circumference of about 13.9 mm. The largest decrease in radius was -4.6 mm and one section had a change in radius of +0.1 mm. After that first week, the sections seemed to have settled in their final position, because no more significant changes were measured. Compared to the previous control measurement, the changes in radius value varied between -1.4 and 0.9 mm. The 95% confidence levels, based on the experimental standard deviations, were taken into account as a threshold for this determination. Because of the use of different measurement instruments during the 'Diabolo' project, these 95% confidence intervals vary between 1.1 mm and 4.5 mm ($2 * \sqrt{\sigma_1^2 + \sigma_2^2}$) (with σ_i = the experimental standard deviation of the used measurement instrument). An overview of the standard deviations of the different instruments tested during this project is shown in Table 4-2.

This trend of a convergence towards a stabilised radius is illustrated in Figure 4-3, which shows a graphic representation of the changes in radius values of some of the monitored tunnel sections. When a scheduled measurement could not be performed due to the construction works in the tunnel, that part of the graph is left empty (e.g. Figure 4-3– Section 6). The data represented in the graph are the differences for each measurement between the average of the measured radius values of the cross-section and the design shape of the tunnel. This graph clearly shows a significant difference between the radius values immediately after placement (indicated by measurement 0 in Figure 4-3) and the radius values of the measurement one week after construction (measurement 1). For the following measurements, small deviations occur but these deviations cannot be considered as significant, based on the 95% confidence intervals as mentioned above. The graph also indicates that some of the tunnel sections have a stabilised average radius a little larger than the design of 3.6500 m; others have an average radius smaller than the design shape. These trends in the ovalisation results can also be observed in the larger 'Liefkenshoek Rail Link' project (Antwerp, Belgium), based on a similar measurement and processing methodology (see chapter 3).

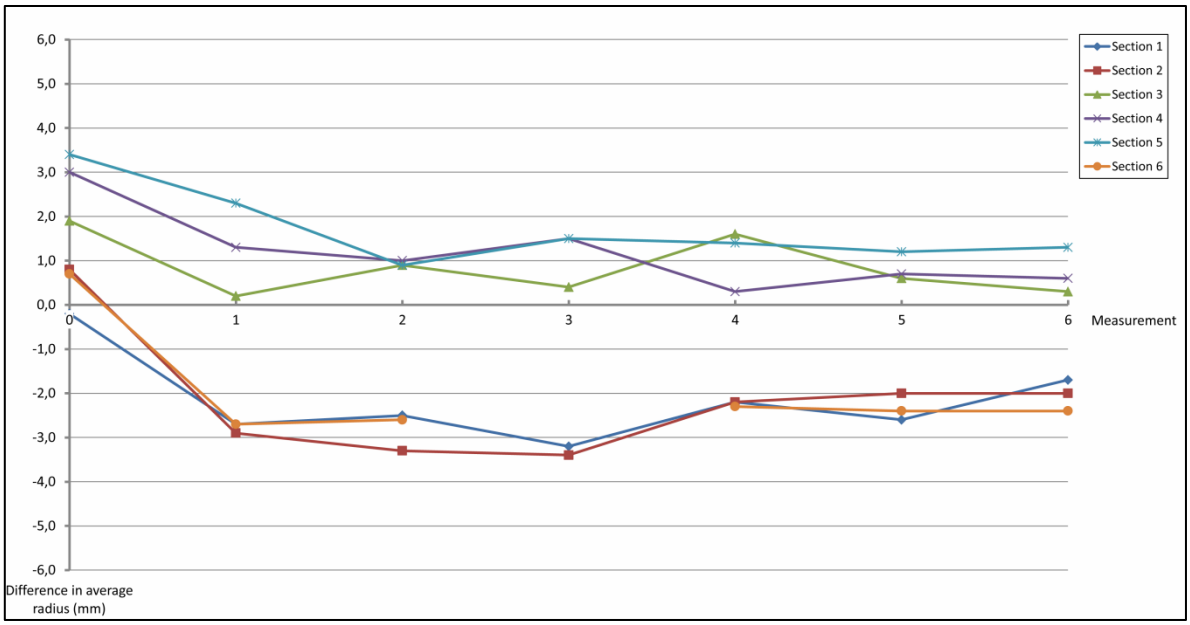

Figure 4-3: Differences (mm) in average radius compared to design shape (3.6500 m) of monitored tunnel sections in the 'Diabolo' project

4.4. Determination of the most optimal scanning instrument and smoothing level

4.4.1. Experimental standard deviations of the tested scanning instruments

The different types of laser scanners, applicable in the field of civil technical constructions, can be categorised in pulse-based and phase-based laser scanners. Triangulation scanners are not included in this research. Pulse-based laser scanners are based on the principle of emitting a laser pulse and capturing the backscatter of that pulse on an object. Half of the time delay between emitting this pulse and receiving its backscatter multiplied with the speed of light results in the distance between the laser scanner and the measured point on the object. This measured distance is then combined with the registered horizontal and vertical angle of the measurement to calculate the 3D coordinates of the measured point (Pfeifer & Briese, 2007b). The scanning speed of this type of laser scanners is mostly up to 50 000 points per second, with a range up to 1 km or more. The measurement principle of phase-based laser scanners consists of emitting a continuous laser beam and the calculation of the phase difference between the emitted and reflected laser beam. The distance between the laser scanner and the object can be calculated from this phase difference. Typically, phase-based laser scanners have a shorter range (up to 120 m), a much higher scanning speed of up to 1 million points per second and a high accuracy at short distances.

At an early stage of the 'Diabolo' project, different laser scanning instruments have been evaluated during *in situ* ovalisation measurements. A further comparison and testing of

more and new instruments was performed in the following tunnel monitoring project ('Liefkenshoek Rail Link', Antwerp, Belgium).

For the pulse-based type of laser scanners, a Leica ScanStation 2 and Leica C10 laser scanner were used. A Leica HDS6100 has been tested for the phase-based type of laser scanners. Next to these two types of laser scanners, a robotic total station (Trimble S6 2" DR300+) with automated measurement function was tested. Table 4-1 gives an overview of the most important specifications of these instruments with regard to the projects demands (measurement speed and field of view). The accuracy of these instruments is not included in this table, but will be further detailed in Table 4-2.

Table 4-1: Specifications of the compared scanning instruments

Instrument	Type	Field of View (H x V)	Max. Scan Rate (pt/s)
Leica ScanStation 2	Pulse-based laser scanner	360° x 270°	50 000
Leica C10	Pulse-based laser scanner	360° x 270°	50 000
Leica HDS6100	Phase-based laser scanner	360° x 310°	500 000
Trimble S6 (2" DR300+)	Robotic Total Station	360° x 310°	2 to 5

The experimental standard deviation of each instrument is based on a series of measurements in which a specific tunnel section was measured four times within a time frame of half an hour to two hours, depending on the scanning speed of the instrument. In this short time frame, it can be assumed that no significant deformation of the tunnel section occurred. Depending on the measurement conditions during tunnel construction, some of these measurements series were performed from multiple scanning positions (e.g. left and right tunnel bracket) or from one central scanning position on a tripod. Experimental standard deviations derived from the data from multiple setups can be expected to be slightly higher, due to the necessary registration of both point clouds at the beginning of the processing workflow. This was also confirmed when comparing the standard deviation of the Leica HDS6100 measurements for one setup with the standard deviation for multiple setups in Table 4-2, independent of the applied smoothing level. Moreover, because the available measurement time on site had to be minimised and the tested instruments have a different measurement speed, the processed point clouds had different point spacing. For a reference measurement, the measurement time was limited to maximum two hours, including the installation of the tunnel brackets and the targets for the registration of the different setups. The obstruction of the tunnel by the tripod for a control measurement was limited to five to

ten minutes. Averaged over the whole surface of a tunnel section, the measurements with the Leica ScanStation2 had a resolution of approximately 1.2 cm and the measurements with the Leica C10 had a resolution of approximately 5 mm. The measurements with the Leica HDS6100 had a point density of approximately 2 mm when using one setup and 3 mm when measured from two setups. For the Trimble S6 robotic total station, the horizontal point density was approximately 40 cm and the vertical point density approximately 17 cm. This point density was much lower because of the much slower measurement speed. The Trimble S6 robotic total station does not strictly belong to the range of scanning instruments, but these measurements give an insight in the achievable accuracy following the developed methodology with a more traditional measurement instrument.

An experimental standard deviation was calculated based on the radius values every 0.1 grad of the four repeated cross-sections for each instrument. Each cross-section contained maximum 4000 radius values for which a standard deviation (s) can be calculated. Due to obstacles on the tunnel surface, the scans did not cover the entire tunnel surface. Hence, the actual number of determined radius values varies between 2502 (Leica C10 measurements) and 3868 (Trimble S6 measurements). Moreover, when applying the different smoothing levels, no smoothed value was calculated when no original radius value was measured. It has to be remarked that only for the 0.1 grad angles for which all four radius values were measured, a standard deviation was calculated (N = 4).

$$s = \sqrt{\frac{1}{N-1}\sum_{i=1}^{N}(x_i - \bar{x})^2}$$ (Moore, McCabe, & Craig, 2009)

With s = experimental standard deviation for each 0.1 grad
N = number of measured radius values for each 0.1 grad (N = 4)
x_i = radius values every 0.1 grad
$\bar{x}$ = mean of the radius values for every 0.1 grad

Also, for each instrument and each applied smoothing interval, an average standard deviation ($\bar{s}$) was calculated based on the calculated standard deviations for each 0.1 grad.

$$\bar{s} = \sqrt{\sum_{j=1}^{M} s_j{}^2 / M}$$ (International Organization for Standardization, 2002)

With $\bar{s}$ = average standard deviation for each instrument and each smoothing level
M = number of radius values for which a standard deviation could be calculated (max (M) = 4000)
s_j = standard deviation for each 0.1 grad

4.4.2. Different levels of smoothing

The newly developed measurement and processing methodology focuses on clearly readable and interpretable deliverables such as plots of the measured cross-sections. On these plots of the cross-sections, the 95% confidence intervals and the differences between two successive measurements are represented with a 100 times enlargement. When no smoothing is applied on the data, these plots are not clearly readable or interpretable (Figure 4-4, upper example). Therefore, different smoothing levels were investigated to find the optimum averaging interval. This optimum smoothing level balances between removing the high frequency noise to improve the readability of the plots and keeping sufficient detail to avoid masking excessive measurements. Besides the non-smoothed results, the data were processed with smoothing intervals of 0.3 grad, 0.5 grad, 1.0 grad and 2.5 grad left and right of each radius value. These smoothing intervals correspond respectively with an average over 7 radius values (or 3.5 cm on the tunnel surface), 11 values (5.7 cm), 21 values (11.5 cm) and 51 values (28.7 cm). The smoothing intervals are not interrupted by the locations of the segment joints. However, the blank areas in the cross-sections at the segment joints are mostly larger than 2.5 grad so the smoothing along the individual segments is not influenced by the adjacent segments.

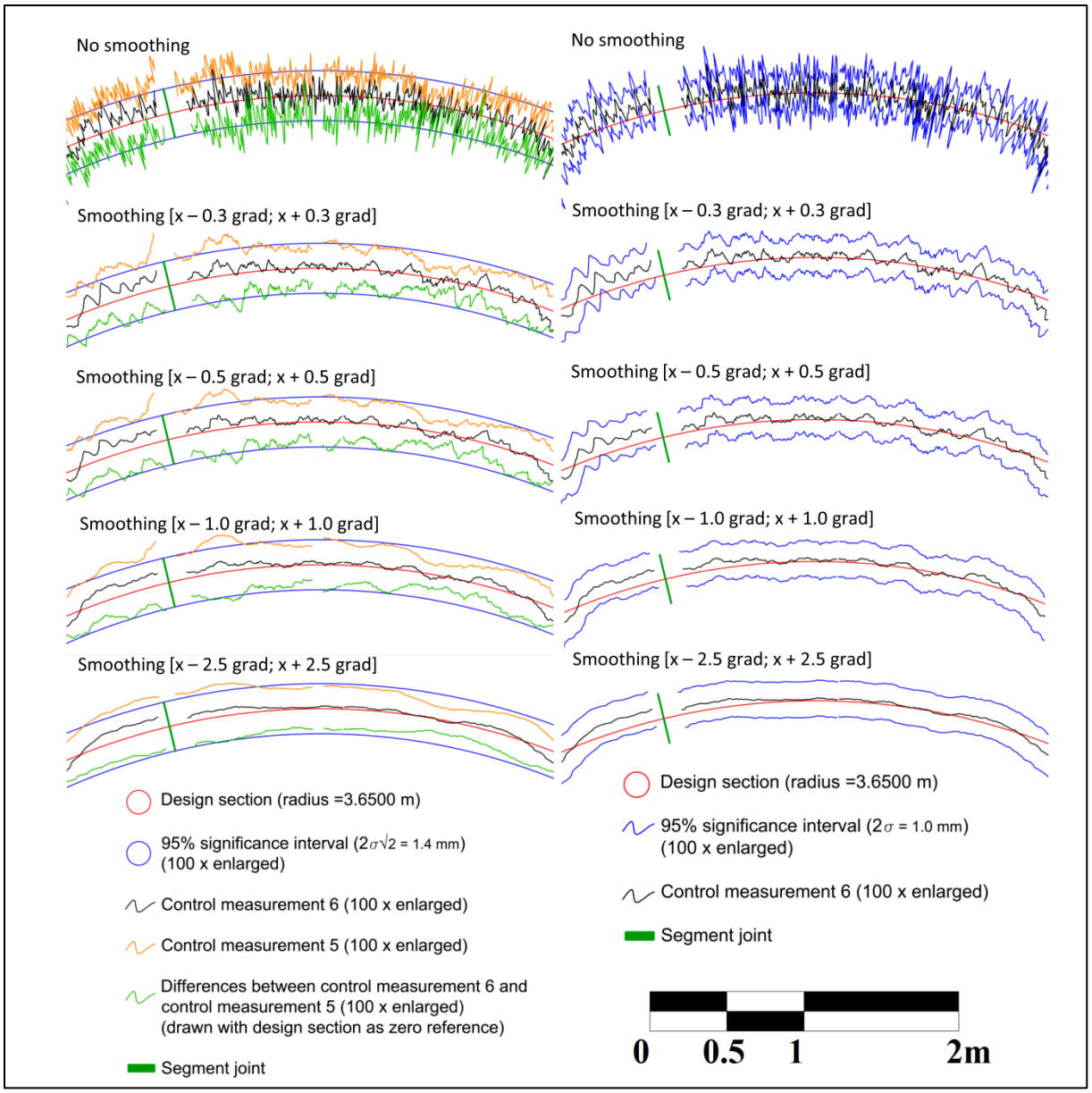

Figure 4-4: Examples of different smoothing levels for the cross-sections: control measurement 5 and 6 and the differences between both control measurements (left); the differences of control measurement 6 with regard to the design and the 95% confidence interval (1.0 mm) (right)

4.4.3. Comparison of the different scanning instruments based on the standard deviations and smoothing levels

Table 4-2: Experimental mean standard deviations of the scanning instruments (mm)

	Experimentally based mean standard deviations (mm) per level of smoothing				
Scanning instrument	**No smoothing**	**[x-0.3 grad; x+0.3 grad]**	**[x-0.5 grad; x+0.5 grad]**	**[x-1.0 grad; x+1.0 grad]**	**[x-2.5 grad; x+2.5 grad]**
Leica ScanStation 2 (multiple setups) (N = 2749*)	1.93	1.75	1.74	1.73	1.72
Leica C10 (1 setup) (N = 2502*)	0.98	0.49	0.43	0.35	0.29
Leica HDS6100 (multiple setups) (N = 2882*)	0.72	0.50	0.48	0.46	0.44
Leica HDS6100 (1 setup) (N = 2740*)	0.58	0.40	0.38	0.36	0.34
Trimble S6 (2" DR300+) (1 setup) (N = 3868*)	1.28	1.27	1.25	1.19	0.99

* N = the number of observations on which the standard deviations are based

The results represented in Table 4-2 clearly indicate a lower standard deviation when a larger smoothing interval is applied for each instrument. Also, the experimentally based standard deviations of both the Leica ScanStation2 and Trimble S6 seem to be much larger than the standard deviations of the Leica HDS6100 and Leica C10.

For the statistical comparison between the different mean standard deviations (Table 4-2), a two-tailed F-test was used to check whether the variances of two independent samples belong to the same statistical population. This F-test was used to test whether there was a significant difference between the standard deviations for the different smoothing levels for each instrument. The F-test was also used to test whether there is a significant difference between the different measurement instruments for each smoothing level. It can be assumed that these observations have a normal distribution, which is a basic assumption for the F-test. The null hypotheses state that the pairwise compared experimental standard deviations (s_1, s_2) are equal.

$$H_0 : s_1^2 = s_2^2$$

$$H_A : s_1^2 \neq s_2^2$$

These null hypotheses are tested on the significance level α = 0.05 by calculating the F-statistic: $F = \frac{s_1^2}{s_2^2}$

The null hypotheses are not rejected if the following condition is fulfilled (International Organization for Standardization, 2002):

$$\frac{1}{F_{1-\alpha/2}(df_1, df_2)} \leq \frac{s_1^2}{s_2^2} \leq F_{1-\alpha/2}(df_1, df_2)$$

With α = 0.05

df = degrees of freedom of the sample

s^2 = variance of the observations

When applying the F-test for the different smoothing levels with a 95% confidence interval (α = 0.05), the results state that the standard deviations for the Trimble S6 robotic total station and the Leica ScanStation2 laser scanner are significantly higher than the other tested instruments. The test measurements of the Leica ScanStation2 are taken from multiple setups, as indicated in Table 4-2. However, considering the small difference between one and multiple setups for the standard deviations of the Leica HDS6100, performing the test measurements for the Leica ScanStation2 from only one scan setup is not expected to result in a significantly better standard deviation or a standard deviation comparable with the other scanning instruments. It has also to be remarked that the point density of the measurements with the Trimble S6 is far less than the density of the laser scanning point clouds, which can have an influence on the calculated standard deviations based on our methodology. Notwithstanding this applied lower point density, the measurements with a total station with scanning function still take a lot more time than the measurements with a laser scanner, which is not in accordance with the time restrictions during construction of the tunnel rings (e.g. 10 minutes for a control measurement). Hence, not only is the achievable standard deviation of the robotic total station not comparable with the standard deviations of the laser scanners, based on the applied point density and methodology, it also does not meet the project requirements.

When no smoothing is applied, the phase-based laser scanner (Leica HDS6100) shows a lower standard deviation than the pulse-based laser scanner (Leica C10), which accords with the general knowledge that phase-based laser scanners deliver more accurate results on short distances. The accuracy results of the Leica C10 and Leica HDS6100 are comparable when a smoothing is applied and the required accuracy of 0.5 mm for these monitoring projects can be obtained. For a further detailed comparison between the Leica C10 and HDS6100, the focus lies on the standard deviations based on one scan setup.

Table 4-3: Statistics of the F-test of the experimental standard deviations Leica C10 and Leica HDS6100 (1 setup). The case where there is no significant difference between both standard deviations is highlighted

Results F-test **Leica HDS6100 (1 setup) - Leica C10 (1 setup)** H_0: $S_1^2 = S_2^2$ H_A: $S_1^2 \neq S_2^2$ ($\alpha = 0.05$) H0 is accepted when $0.926 \leq S_1^2 / S_2^2 \leq 1.080$			
		Leica HDS6100	Leica C10
Leica HDS6100		1	
Leica C10	[No smoothing]	0,350	
	[x-0.3 grad; x+0.3 grad]	0,666	
	[x-0.5 grad; x+0.5 grad]	0,781	1
	[x-1.0 grad; x+1.0 grad]	1,058	
	[x-2.5 grad; x+2.5 grad]	1,375	

Based on the experimentally based standard deviations (Table 4-2) and the F-statistics shown in Table 4-3, it can be concluded that for the case with no smoothing and the cases with the 0.3 and 0.5 smoothing level, the Leica HDS6100 (one setup) delivers the best results with respectively an experimentally based standard deviation of 0.58; 0.40 and 0.38 mm. For the 1.0 grad smoothing level, the standard deviations of both instruments are not significantly different ($s_{HDS6100}$ = 0.36 mm; s_{C10} = 0.35 mm; α = 0.05). When applying the largest smoothing interval (2.5 grad), the measurements with the Leica C10 result in the lowest standard deviation (0.29 mm). These results of the Leica C10 indicate a higher noise on the measurements on short distances. However, this noise is reduced when applying a higher smoothing level, improving the achievable standard deviations to a level comparable with or better than the phase-based laser scanner Leica HDS6100.

The Leica HDS6100 phase-based laser scanner offers important advantages to significantly reduce the measurement time on site, based on its larger vertical field of view and higher scanning speed. Based on the small differences in standard deviations of the Leica HDS6100 and Leica C10, the faster and denser measurements with a phase-based laser scanner can be a decisive factor for ovalisation measurements of a tunnel under construction.

4.5. Conclusions

For tunnel monitoring projects, the measured 3D laser scanning point cloud of the maximum visible area of the tunnel section not only gives much more detailed information about the deformation or ovalisation pattern, it also allows us to recognise and localise the segment joints. The comparison and applicability assessment of the different tested scanning

instruments for tunnel monitoring conditions, as described in this research, are based on multiple key characteristics. Due to the measurement time restrictions during the monitoring of a tunnel under construction, the scanning speed and field of view of the measurement instrument is important. In the 'Diabolo' and 'Liefkenshoek Rail Link' projects, the measurement time for a reference measurement was limited to two hours (installation of the tunnel brackets included) and control measurements were restricted to five to ten minutes. Moreover, the most adapted scanning instruments have to comply with the accuracy restrictions of the client (0.5 mm). Besides, during the processing of the scan data, an appropriate smoothing factor has to be applied to improve the readability and interpretability of the cross-sections on the plots without masking excessive information. The optimum smoothing level finds equilibrium between removing the high frequency noise to improve the readability of the plots and keeping sufficient detail to avoid masking excessive measurements. Apart from the non-smoothed results, the data were processed with smoothing levels of 2.5 grad, 1 grad, 0.5 grad and 0.3 grad left and right of each radius value to find this optimal smoothing level.

The results and experimentally based standard deviations indicate that the phase-based laser scanner Leica HDS6100 delivers very accurate results. Measurements taken from one scan setup result in experimentally based standard deviations between 0.34 and 0.58 mm, depending on the applied smoothing level. For the monitoring projects in this research, this Leica HDS6100 laser scanner was used, together with a [x-0.5 grad; x+0.5 grad] smoothing interval on the calculated radius values. The accuracy requirement for these projects was set at 0.5 mm, even when using multiple setups, so the smallest smoothing interval to obtain this accuracy requirement was applied. The Leica C10 also delivers standard deviations within the 0.5 mm limit, but this type of laser scanner has a lower scanning speed and a smaller vertical field of view. Therefore, it is less adapted for the measurements in time restricted tunnel monitoring projects. However, based on these achievable standard deviations, this type of scanner offers many opportunities in less time restricted applications or for measurements outside the measurement range of the Leica HDS6100.

4.6. References

Argüelles-Fraga, R., Ordonez, C., Garcia-Cortes, S., & Roca-Pardinas, J. (2013). Measurement planning for circular cross-section tunnels using terrestrial laser scanning. *Automation in Construction, 31*, 1–9. doi:10.1016/j.autcon.2012.11.023

Arnau, O., & Molins, C. (2012). Three dimensional structural response of segmental tunnel linings. *Engineering Structures, 44*, 210–221. doi:10.1016/j.engstruct.2012.06.001

Aydin, C. (2012). On the Power of Global Test in Deformation Analysis. *Journal of Surveying Engineering*, (May 2012), 51–56. doi:10.1061/(ASCE)SU.1943-5428.0000064

Blom, C. B. M., van der Horst, E. J., & Jovanovic, P. S. (1999). Three-dimensional Structural Analyses of the Shield-driven "Green Heart" Tunnel of the High-Speed Line South. *Tunnelling and Underground Space Technology, 14*(2), 217–224.

Fekete, S., Diederichs, M., & Lato, M. (2010). Geotechnical and operational applications for 3-dimensional laser scanning in drill and blast tunnels. *Tunnelling and Underground Space Technology, 25*(5), 614–628. doi:10.1016/j.tust.2010.04.008

Fujino, Y., & Siringoringo, D. M. (2011). Bridge monitoring in Japan: the needs and strategies. *Structure and Infrastructure Engineering, 7*(7-8), 597–611. doi:10.1080/15732479.2010.498282

Helmerich, R., Niederleithinger, E., Trela, C., Bien, J., Kamiriski, T., & Bernardini, G. (2012). Multi-tool inspection and numerical analysis of an old masonry arch bridge. *Structure and Infrastructure Engineering, 8*(1), 27–39.

Huang, K.-P., Wang, T.-T., Huang, T.-H., & Jeng, F.-S. (2010). Profile deformation of a circular tunnel induced by ambient stress changes. *Tunnelling and Underground Space Technology, 25*(3), 266–278. doi:10.1016/j.tust.2009.12.006

International Organization for Standardization. (2002). *International Standard ISO 17123-1:2002(E) Optics and optical instruments - Field procedures for testing geodetic and surveying instruments - Part 1: Theory* (p. 14).

Lague, D., Brodu, N., & Leroux, J. (2013). Accurate 3D comparison of complex topography with terrestrial laser scanner: Application to the Rangitikei canyon (N-Z). *ISPRS Journal of Photogrammetry and Remote Sensing, 82*, 10–26. doi:10.1016/j.isprsjprs.2013.04.009

Lindenbergh, R., Pfeifer, N., & Rabbani, T. (2005). Accuracy analysis of the Leica HDS3000 and feasibility of tunnel deformation monitoring. In *ISPRS WG III/3-4, V/3 Workshop "Laser scanning 2005"* (Vol. 36–3/W19, pp. 24–29). Enschede, The Netherlands.

Moore, D. S., McCabe, G. P., & Craig, B. A. (2009). *Introduction to the Practice of Statistics* (Sixth Edit., p. 709). New York: W. H. Freeman and Company, 41 Madison Avenue, New York, NY 10010, Houndmills, Basingstoke RG21 6XS, England.

Peeters, B., Couvreur, G., Razinkov, O., Kündig, C., Van der Auweraer, H., & De Roeck, G. (2009). Continuous monitoring of the Oresund Bridge: system and data analysis. *Structure and Infrastructure Engineering, 5*(5), 395–405. doi:10.1080/15732470701478362

Pejić, M. (2013). Design and optimisation of laser scanning for tunnels geometry inspection. *Tunnelling and Underground Space Technology, 37*, 199–206. doi:10.1016/j.tust.2013.04.004

Pfeifer, N., & Briese, C. (2007b). Laser scanning - Principles and applications. *GeoSiberia 2007*.

Van Bogaert, P. (2009). Recent and future railway tunnels in Belgium. In *Proc. ITA World Tunnel Conference "Safe Tunnelling for the City and the Environment"* (pp. 689–690). Budapest: Hungarian Tunnelling Association, ISBN 9789630672399.

Wang, S., Wu, Z., Guo, M., & Ge, X. (2012). Theoretical solutions of a circular tunnel with the influence of axial in situ stress in elastic-brittle-plastic rock. *Tunnelling and Underground Space Technology, 30*, 155–168. doi:10.1016/j.tust.2012.02.016

Yoon, J.-S., Sagong, M., Lee, J. S., & Lee, K. (2009). Feature extraction of a concrete tunnel liner from 3D laser scanning data. *NDT&E International, 42*, 97–105. doi:10.1016/j.ndteint.2008.10.001

Zogg, H.-M., & Ingensand, H. (2008). Terrestrial laser scanning for deformation monitoring - load tests on the Felsenau Viaduct (CH). In *XXIst ISPRS Congress - Technical Commission V* (Vol. XXXVII–B5). Beijing, China: The International Archives of the Photogrammetry, Remote Sensing and Spatial Information Sciences.

CHAPTER 5
STRAIN GAUGE MEASUREMENTS OF THE PRECAST CONCRETE LINING OF A SHIELD-DRIVEN TUNNEL

5. STRAIN GAUGE MEASUREMENTS OF THE PRECAST CONCRETE LINING OF A SHIELD-DRIVEN TUNNEL

Modified from Schotte, K., De Backer, H., Nuttens, T., De Wulf, A., & Van Bogaert, P. (2013). Strain gauge measurements of the precast concrete lining of a shield-driven tunnel. Insight, Vol. 55, No. 2, p. 88-95, doi: 10.1784/insi.2012.55.2.88 (published)

5.1. Abstract

One of the critical steps in the design process of a shield-driven tunnel is the correct identification of the loads acting on the precast concrete elements of the segmental lining. However, in tunnelling, determination of the loads during ring erection, advance of the tunnel boring machine, building-up of earth pressure and bedding of the articulated ring is difficult and very few monitoring results of actual tunnel behaviour at an early stage are available. Strain gauge measurements can constitute an important contribution in acquiring a better understanding of the real-time behaviour of the tunnel lining under numerous loading conditions, especially during construction. To achieve this, every aspect of the strain gauge installation process should be handled with the utmost care in order to cope with the rough site conditions and deliver accurate measurement results.

This chapter reports on the monitoring program pursued in the Liefkenshoek rail tunnel, located in the Port of Antwerp. It details the practical implementation of the strain gauges and corresponding wireless data acquisitioning system, as well as the ovalisation measurement setup using laser scanning. The collected measurement results serve as a perfect illustration of the achieved reliability and precision of the combined monitoring programme.

5.2. Introduction

Due to increasing urbanisation, the application of mechanised tunnelling techniques is growing worldwide. While new transportation and utility tunnels are created underground, the surface above the tunnel alignment remains mostly undisturbed, apart from the launch and arrival shafts. Although the application depends on specific project parameters, the use of shield tunnels offers several advantages in comparison with the cut-and-cover method regarding noise, vibrations, cost and impact on existing structures. In Belgium, several tunnelling projects have been launched in recent years in order to extend the Belgian railway network. Among them are the Antwerp North-South link tunnel, located along the international high-speed railway lines (Van Bogaert & Vereerstraeten, 2005), an improved connection to Brussels Airport, known as the Diabolo project (Van Bogaert & De Pauw, 2008), and a new freight connection in the Port of Antwerp, called the Liefkenshoek rail link (Van Bogaert, 2008, 2009).

For many years, various deformation models have been used to design bored tunnels. In general, a correct identification of the loads acting on the reinforced concrete segments is an essential step in the design process of the tunnel lining. However, determination of the loads during ring erection, advance of the tunnel boring machine (TBM), building-up of earth pressure and bedding of the articulated ring is quite complex (Gruebl, 2012). As very few measurement results of actual tunnel lining behaviour at an early stage are available, estimating the accuracy of the deformation model output in comparison with the *in situ* material behaviour remains very difficult. Therefore, the start of recent tunnel works has been an excellent opportunity to accompany the boring process with an experimental monitoring programme. After the first experiences with strain gauge measurements and ovalisation measurements in the Diabolo tunnel (Schotte et al., 2010), an improved monitoring programme is pursued in the Liefkenshoek tunnel, which is the main focus of this chapter. The measurement data obtained allow assessment of the real-time behaviour of the concrete segments under numerous loading conditions during construction of the tunnel lining. As a result, the experience with large-diameter shield tunnelling in soft soil may be improved.

5.3. Outline of the 'Liefkenshoek Rail Link' project

The Liefkenshoek rail tunnel aims to directly connect the railway freight transport between the left and right bank of the River Scheldt, in the Port of Antwerp, by 2014. The major part of the 16.2 km long connection, as illustrated in Figure 5-1, is the twin bored tunnel, shield-driven below the River Scheldt and the Port Canal using the mixshield method. The tunnel alignment is mainly located in tertiary sands, with a maximum water pressure above the tunnel floor of about 40 m and a maximum soil overburden along the tunnel route that equals 33.6 m (Boxheimer & Mignon, 2009). Due to the precise control of their support pressure, mixshields are well-adapted to multi-layered, complex geologies and extremely high water pressures. Their principle is based on supporting an unstable tunnel face using a bentonite suspension, a mixture of clay and water that also acts as a conveying medium. In this way, ground with high water permeability, such as sand, can be tunnelled through quickly and safely without causing subsidence or heave above ground. However, in its lower part below the river, the tunnel also passes through tertiary clay, which has a strong tendency to clog the cutting wheel and therefore reduces the speed of advance.

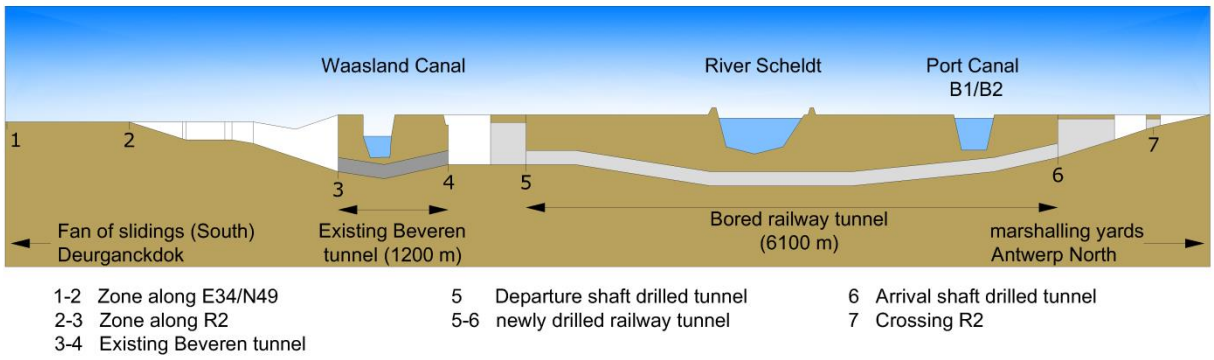

Figure 5-1: Schematic longitudinal profile of the 'Liefkenshoek Rail Link' project (based on CEI – De Meyer nv, 2012)

Two parallel single-track tunnels were excavated, with a length of approximately 6 km and an internal diameter of 7.3 m. Each tunnel ring is 1.8 m wide and consists of seven precast concrete elements and a smaller keystone, all of 0.4 m thickness in C50/60 concrete quality. A photograph of the tunnel interior is shown in Figure 5-2, and Figure 5-3 shows pictures of the working conditions inside the TBM.

Figure 5-2: Inside view of the Liefkenshoek rail tunnel (southern tube)

Figure 5-3: Inside view of the Tunnel Boring Machine: (a) upper side; (b) bottom

5.4. Description of the strain measurement setup

In each tunnel tube, eight particular cross-sections of the tunnel lining were selected for the strain gauge measurements. The distribution of these sections along the tunnel axis allows investigating the effect of several local influences (Schotte, De Backer, Nuttens, et al., 2011; Schotte, De Backer, & Van Bogaert, 2011).

5.4.1. Practical implementation of the strain gauges

Each monitored cross-section consists of a tunnel ring equipped with several strain gauges, distributed across the ring perimeter. Prior to concrete casting in the prefabrication plant, all segments of a measurement ring, except for the smaller keystone, were equipped with two internal strain gauges attached to the inner and outer reinforcement bars in circumferential direction, as shown in Figure 5-4 (a).

The strain gauges used for this embedded application are T rosette strain gauges with two orthogonal measuring grids. This type was chosen to allow for an accurate installation of a Wheatstone half-bridge configuration for each strain gauge. The carrier and protection layer of the strain gauges consists of a thin polyimide layer, while the measuring grid is a constantan foil. The main advantages of this type of strain gauges are their ease of use, sturdiness and flexibility. In addition, the thermal expansion coefficient of 10.8 • 10-6 /K matches the temperature response of the reinforcement steel and surrounding concrete. The size of the strain gauges is 11.5 by 7.3 mm, while the active grids measure only 3 by 3 mm. This size is well adapted to this specific application and allows for a smooth installation of the strain gauges and a correct determination of the strains in the reinforcement bars of 12 mm nominal diameter. The resistance of the internal strain gauges was selected as 350 Ω instead of the more common 120 Ω, which corresponds to less specific heat generation because of the lower measurement current. The soldering islands are chosen to be independent from the carrier in order to facilitate the alignment of the strain gauges along the reinforcement bars and provide strain relief for the strain gauge connections, as shown in Figure 5-4 (b). The solder terminals consist of nickel-plated copper on a polyimide carrier.

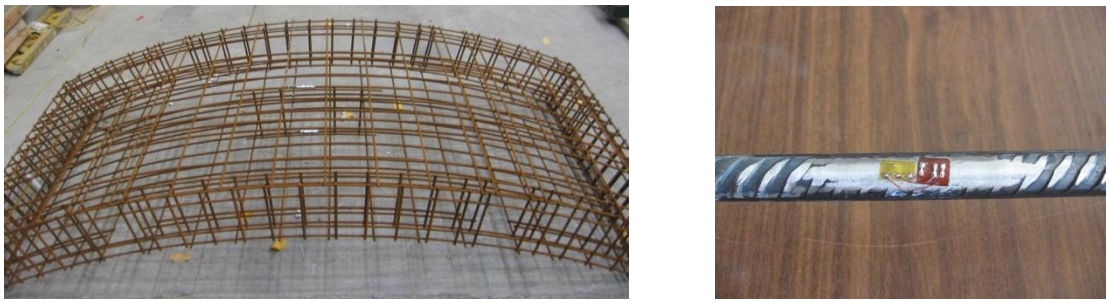

Figure 5-4: (a) Reinforcement cage equipped with strain gauges; (b) Strain gauge installation on reinforcement steel

In order to allow for a full attachment of the strain gauges, the oxidation layer of the reinforcement bars was first locally removed and the bars were smoothed mechanically by removing the ribs. Attention was given that this smoothing was executed without reducing the nominal cross section of the reinforcement steel, as illustrated in Figure 5-4 (b). The contact surface was degreased and pH-neutralised using an effective degreasing solvent and water-based acidic and alkaline surface cleaners. The strain gauges were then glued to the steel surface using a fast-drying, easily applicable and creep free cyanoacrylate glue. This adhesive hardens in one minute, under thumb pressure, followed by a minimum two-minute delay before the cable connections can be soldered. However, the performance of the adhesive can be degraded by humidity conditions or moisture absorption. Hence, all strain gauges were protected from moisture using a covering agent consisting of aluminium foil, coated with a 3 mm thick kneading compound. The cables for data transfer were guided to a small plastic 'waiting box', attached to the reinforcement cage with the exact thickness of the concrete cover, in order to protect the cables during concrete casting and to be able to connect them to the data logger at a later stage. This entire procedure was completed in the prefabrication plant.

The equipped segments were subsequently precast, consolidated in a normal manner and transported to the construction site. Immediately after installation of the segments in the tunnel, each segment was provided with a third strain gauge glued to the inner concrete surface of the tunnel lining. The additional strain gauges were installed at the centre of the concrete segment surface and strains were measured in circumferential direction, corresponding to the internal strain gauges. The installation of these strain gauges could not be done before completion of the ring erection, due to the application of the vacuum segment erector, which creates a vacuum area on the concrete surface to lift and place the segments into position.

The strain gauges used for the surface application are standard, unidirectional strain gauges, yet each time installed as an orthogonal couple to ensure the Wheatstone half-bridge configuration for every measurement location, as shown in Figure 5-5. Identical characteristics for the surface strain gauges apply as for the embedded strain gauges. However the inhomogeneous structure of concrete requires strain gauges with longer

measuring grids for mean value calculation. Therefore, the size of the strain gauges on the concrete surface is 63.6 by 8.2 mm, while the active grid measures 50 by 0.8 mm. This grid length exceeds two times the grain size of the concrete and allows for correct identification and sufficient accuracy of the strains at the concrete surface. Unlike the internal strain gauges, the resistance of the surface strain gauges was chosen as 120 Ω, due to the relative insensitivity to variations in insulation resistance, for example caused by effects of humidity.

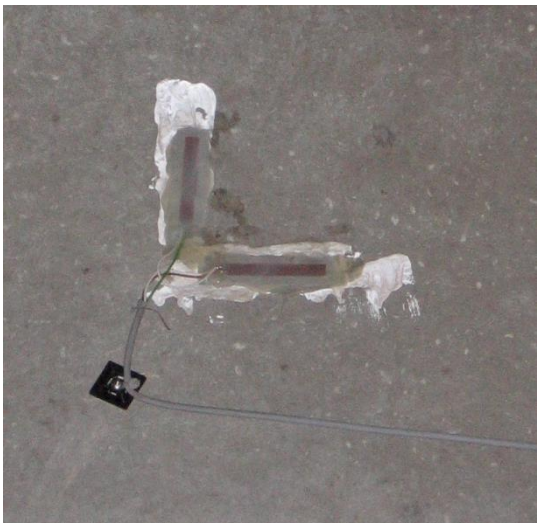

Figure 5-5: Strain gauge installation on the concrete surface

The bonding surface was degreased and the strain gauges were glued to the concrete surface using a methyl methacrylate two-component adhesive paste, which is a strong pore-filling adhesive that bonds reliably even if residual moisture is still present. The strain gauges can be installed using thumb pressure and the adhesive hardens in a few minutes, depending on the temperature. After soldering of the cable connections, all strain gauges were protected from moisture using a thick silicone layer with a neutral pH to minimise interference.

Since the cables leading to the lowest segment would be damaged by the advancing TBM's work train, as can be seen in Figure 5-3 (b), installation of strain gauges in this segment was omitted. Consequently, the process resulted in a total of 18 wired strain gauges, the locations of which are illustrated in Figure 5-6.

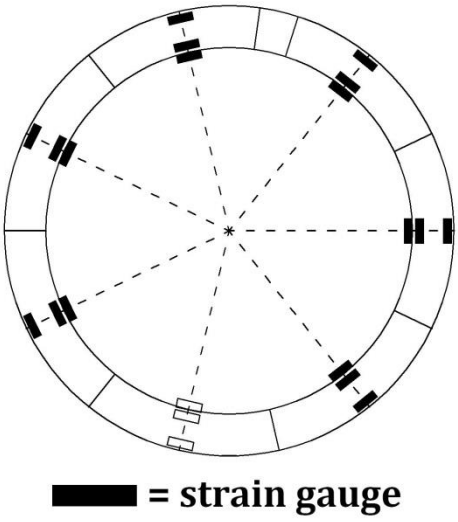

Figure 5-6: Strain gauge locations in the tunnel cross-section

5.4.2. The strain gauge measurement system

Immediately after installation of the precast segments in the tunnel under construction, the waiting boxes were cut open and the cables for data transfer of the embedded strain gauges were connected to the measurement system. Simultaneously, the additional strain gauges on the concrete surface were installed as described and directly connected to the measurement setup. The result of this stage is depicted in Figure 5-7.

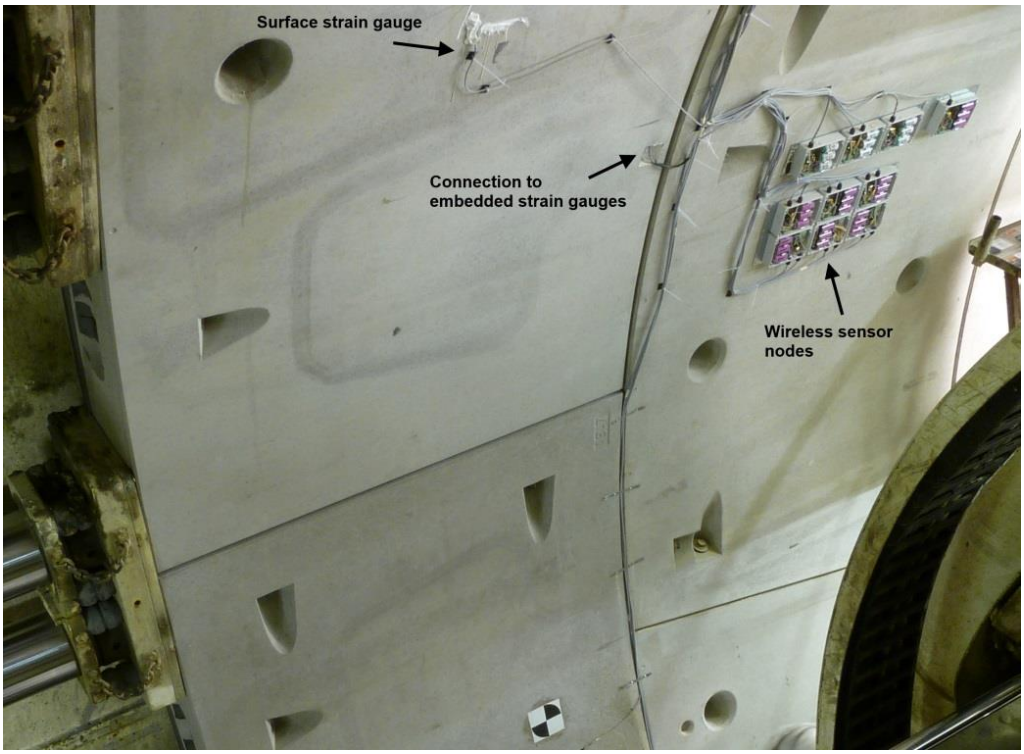

Figure 5-7: Strain measurement setup after ring assembly

The applied measurement system is a commercially available wireless data acquisitioning system, which comprises three main components: wireless sensor nodes, which acquire and transmit strain data; USB base stations, which receive and pass the data to a host (laptop); and a Windows-based software package, which operates the system. Each sensor node provides four differential input channels (strain channels) for 350 Ω strain gauges or, due to issues of power consumption, only two input channels for strain gauges of 120 Ω resistance. This implies that six individual sensor nodes were required to monitor strain data in each measurement ring. The lay-out of a wireless sensor node is depicted in Figure 5-8. Every sensor node employs a 12 bit A/D converter to digitise the voltage on the differential input. The digital data is passed to the on-board microprocessor, processed with the embedded algorithm and saved to the 2 Mb on-board flash memory for later wireless download using the base stations. Furthermore, the integrated circuit of the nodes (Figure 5-8 A) includes Wheatstone bridge completion resistors for each channel and internal resistors for wireless shunt calibration. One entire unit is powered by three lithium-ion D-cell batteries of 3.6 V each (Figure 5-8 C) and the circuitry is built into an IP65 polycarbonate enclosure (Figure 5-8 D) for protection against dirt and moisture. Figure 5-8 so shows the internal on-off switch (B) and cable glands (E).

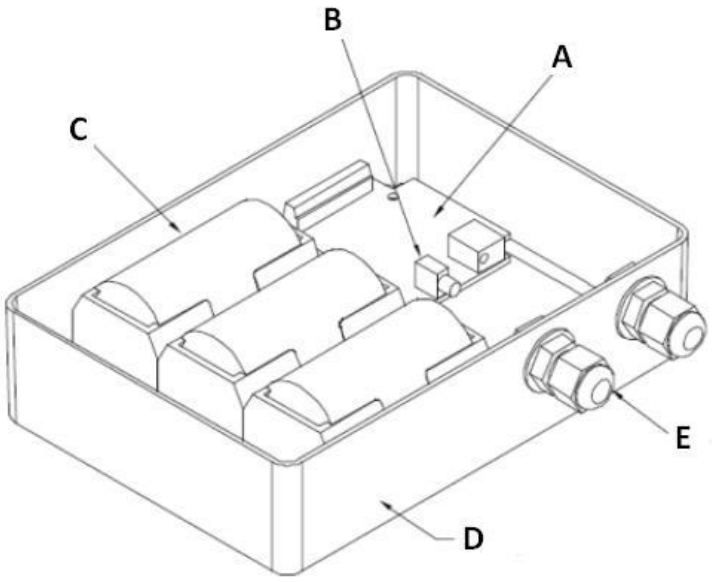

Figure 5-8: Wireless sensor nodes

Host computer software enables downloading and recording of the data to file and erasing the on-board flash memory of the nodes. Furthermore, it allows the user to configure and actuate the system and to perform a wireless shunt calibration of each strain channel. The data acquisitioning system has a measurement resolution of only 1 µS with an accuracy of ±0.1%. The high flexibility of the system combined with the accuracy of the resulting strains makes it the appropriate measurement system for this specific application.

After the first experiences with the measurement setup in the Diabolo tunnel (Schotte et al., 2010), both strengths and weaknesses of the wireless measurement system became clear and some important improvements were completed to the advantage of the monitoring programme in the Liefkenshoek tunnel. In the following paragraphs, some of these issues are discussed.

5.4.2.1. Wheatstone bridge completion

Basically, all strain results should be rectified with a temperature correction, based on calibration graphs supplied by the manufacturer of the strain gauges. These graphs indicate the correction in µS that should be applied for given temperature fluctuations, due to differences in expansion or contraction of the strain gauges compared to the base material. For temperature variations of about 20°C, the correction equals 5 to 10 µS. However, it is not always practical to apply the temperature correction to all strain measurements for several reasons. Most importantly, monitored temperature data concern only the surrounding air inside the tunnel. As the strain gauges attached to the reinforcement are embedded in concrete, the assumption that they adopt the same temperature as the air inside the tunnel would lead to excessive and improper corrections of the monitored strains. The same applies to the strain gauges attached to the concrete surface and covered by a protective layer of silicone.

Hence, the described temperature correction does not appeal for practical application. The alternative is to change the Wheatstone bridge completion. The quarter-bridge system was used in the Diabolo project, whereas in the present measurements the more stable half-bridge configuration is applied. Briefly stated, this involves a change in the electrical circuit of resistors, with a reference gauge built in together with the actual measuring strain gauge in the half-bridge system, as shown in Figure 5-9. In the quarter-bridge configuration, an equivalent reference resistor would be located in the internal electric circuitry of the sensor nodes. One of the main advantages of the half-bridge completion is that the reference resistor is now subject to the same surrounding conditions as the measuring gauge and is consequently subjected to identical temperature changes and ageing. In addition, as each strain gauge is connected to the measuring system by means of three separate cables to complete the half-bridge circuit, in this setup it becomes possible to filter the influence of the leadwires on the resistance. This should result in a nearly complete elimination of deviations due to the aforementioned effects, automatically corrected temperature variations and more stable measurement results in general.

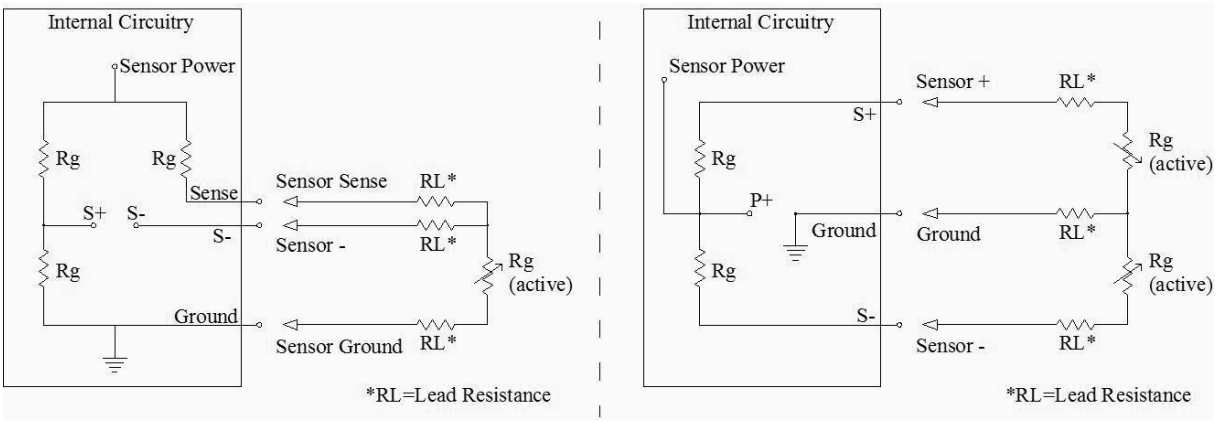

Figure 5-9: Wheatstone bridge completion: quarter-bridge (left); half-bridge (right)

5.4.2.2. Measurement frequency

If the data logging sampling method used in the Diabolo project is applied, the measurement system can be configured to sample data as fast as 2048 Hz on each channel or to decrease the frequency down to 32 Hz. The lowest sampling frequency of 32 Hz already resulted in a very short measurement period of less than five hours and excessively detailed strain data. In this method, downloading of the stored data took about eight minutes for each node and was required before a next data logging session could be initiated. Taking into account the number of sensor nodes used in each measurement ring, wireless transfer of the stored data became a labour-intensive process.

Implementation of a low duty cycle mode (LDC) allowed configuration of sampling frequencies from one sample per hour up to 500 Hz per channel. Activation of this LDC mode in the Liefkenshoek project made it possible to significantly lower the measurement frequency, resulting in a longer monitoring period and fewer download sessions. At a frequency of one sample every 10 seconds, sufficient accuracy of the monitored strains in the first weeks after ring erection was ensured. In addition, wireless transfer of the stored data was reduced to a maximum of one and a half minutes for each sensor node and strain data needed to be downloaded every three weeks only. For long term monitoring, further reduction of the sampling frequency to one sample every two minutes was applied, which needed downloading every three months only.

As a positive side-effect of the lowered frequency, internal heating of the strain gauges at the start of each measurement period was no longer a problem. Strain data in previous applications clearly showed a temperature drift at the start of each monitoring period, due to the sudden initiation of high-frequency measurements and strong electric current through the strain gauges. Since the measurements now run over an extended time lapse and should not normally be interrupted for longer than the duration of a single download, this start-up phenomenon disappeared. Hence, the actual internal heating of strain gauges is

considerably smaller thanks to the reduced measurement frequency and the adequate selection of the strain gauge types.

5.4.2.3. Further issues

In previous paragraphs, several issues were mentioned together with improvement of the measurement method. However, some minor flaws still remain in the data logger setup, which to date could not be solved entirely.

First, the wireless range of the sensor nodes is inadequate for wide application of the measurement system. Theoretically the sensor nodes allow communication up to a range of 70 m line-of-sight. However, on the construction site this is reduced to about 12 m. As the internal diameter of the monitored tunnels equals 7.3 m, this range is sufficient for tunnel measurements. In addition, in the current state of development, downloading data in LDC mode requires manual switching off and reconnection of the sensor nodes to interrupt ongoing measurements. This implies that all sensors have to be installed within reach, which renders the wireless function of the measurement system practically unprofitable.

Secondly, the sensor nodes obviously require a power supply. Due to the installation procedure and passage of the TBM's work train in the first week after assembly, a fixed power cable connection was not practically feasible. To assure the independency of the measurement system and the continuation of the monitoring process in case of power failure, each sensor node is powered by three D-cell batteries. In LDC-mode, the lifetime of these batteries equals approximately five months. As a result, long-term measurements also require accessibility of the sensor nodes to replace batteries when needed.

Finally, the sensor nodes make use of an integrated clock of the RC type to handle time stamping in LDC-mode. The stability of this clock according to product specifications and on-site experience equals ±10%, which is insufficient for accurate use. For example, a single measurement period of three weeks in LDC-mode with one sample every 30 seconds corresponds to a possible deviation of two days. Experience shows that accuracy should be maintained by calculating each time step based on the start and end time of the monitoring period and the total number of enclosed measurement samples.

5.4.3. Strain monitoring programme

Immediately after installation of the ring segments in the tunnel under construction and connection of all data cables to the measurement system, monitoring of the 18 strain gauges in the corresponding measurement section was initiated. At an initial sampling frequency of one sample every 10 seconds on each channel, strains were registered during the various steps in the boring process following the erection of the measurement section. Monitored data include the reaction of the tunnel lining to the tail grout injection, thrust force of the hydraulic shield jacks and transfer of soil and water pressures onto the concrete elements. After this initial stage, the measurement frequency was lowered to one sample per 30 seconds and in a later stage to one sample every two minutes. The saved data were

downloaded on a regular basis for a continuous period of several months to over one year and allow assessment of the real-time behaviour of the tunnel lining under various load states.

5.5. Description of the ovalisation measurement setup

Extensive ovalisation measurements using laser scanning were carried out at fourteen cross-sections in each tunnel tube, eight of which coincide with the strain measurements. Since the laser scanning technique needs no specific lighting conditions and is able to deliver millions of accurate 3D coordinates in a couple of minutes, it proved to be most suitable for detecting deformations of the concrete lining segments in the tunnel under construction (Schäfer, Weber, Kyrinovic, & Zamecnikova, 2004; Zogg & Ingensand, 2008). Test measurements and comparison of different laser scanners during the Diabolo project indicated the phase-based Leica HDS6100 scanner as the most suited laser scanner for this application, based on the high scanning speed (and thus shorter measurement time on site), a larger field of view and the achievable accuracy (Nuttens et al., 2012). An experimental standard deviation of 0.44 mm in actual tunnel conditions was established.

Seven moments in time were defined on which the selected tunnel sections had to be measured: the 'critical' measurement immediately after construction of the tunnel section; a measurement every week during the first month after placement; and measurements two and three months after placement. Due to the limited space in the head of the TBM, three scanning positions were needed to cover the whole tunnel section during a critical measurement. Two scanning positions, one on the left side and one on the right side, were mounted on the tunnel surface using a metal bracket bolted to the concrete segments, as seen in Figure 5-10 (a). For the third scanning position, the laser scanner was mounted on a tripod in the centre of the bottom of the tunnel section. The control measurements required only one scanning position, located in the centre of the tunnel bottom, with the resulting point cloud shown in Figure 5-10 (b).

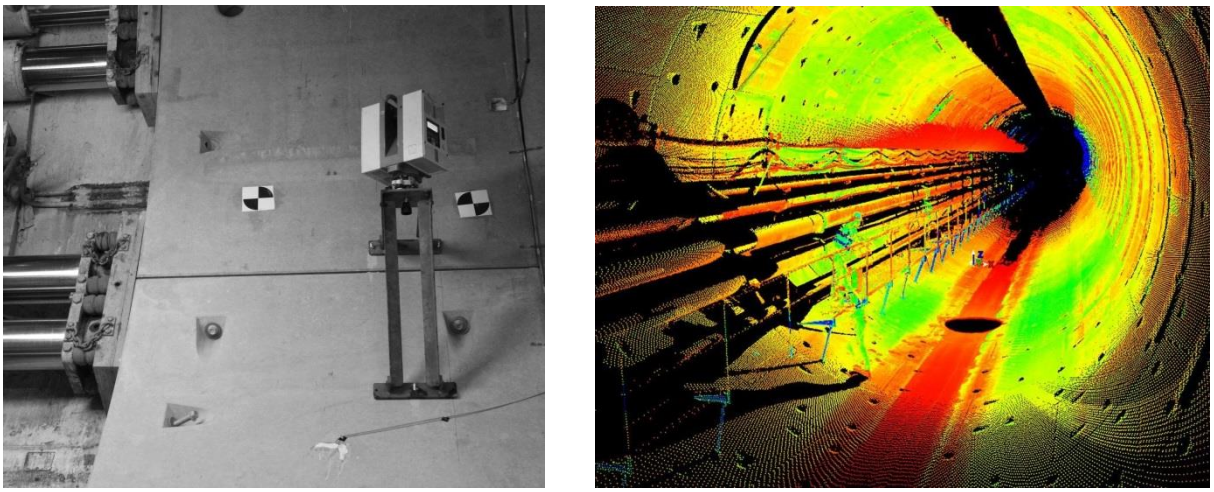

Figure 5-10: (a) Laser scanner mounted on bracket during 'critical' measurement; (b) Point cloud obtained during a control measurement

5.6. Results

5.6.1. Strain gauge measurements

Due to the start-up of the data logging process immediately after assembly of the monitored ring, the strain gauge measurements only relate to changes occurring after ring erection. This implies that the reaction of the tunnel ring due to its dead weight and possible assembly stresses, following the installation of the key segment and temporary bolts, is not visible in the measurement results. Strains were measured in the tangential direction and disregarded the Poisson effect thanks to the applied half-bridge configuration of the Wheatstone bridge circuit. By convention, tensile stresses correspond to positive strains and compressive stresses to negative values. The following paragraphs present some specific results to demonstrate the reliability of the measurement setup and operating procedures.

5.6.1.1. Initial hours after ring assembly

Figure 5-11 shows a preview of the obtained results for a measurement section in the northern tunnel tube (A) during the first hours after ring erection. The various graphs show the various strain gauges installed in this cross-section, each indicated by a coloured code as shown to the right of the chart. For each code, the first number refers to the measurement section, the second one to the segment and the last number indicates the location of the strain gauge: at the outer (3) or inner (2) reinforcement or at the concrete surface (1).

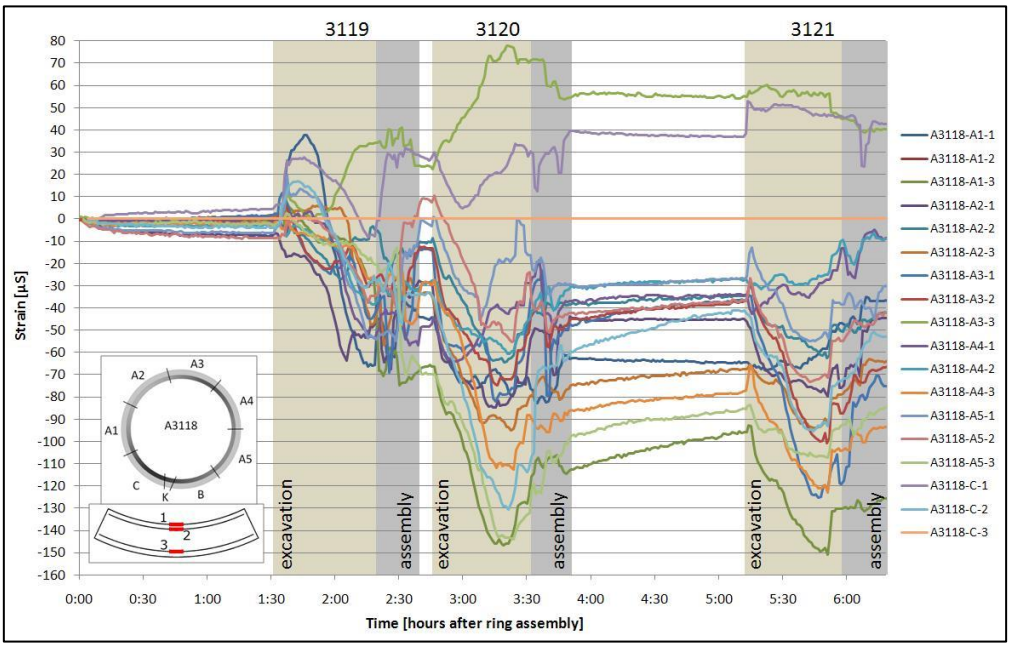

Figure 5-11: Strain results in northern tunnel immediately after ring assembly

Due to the manufacturing and handling of the precast concrete segments and the rough conditions at the actual tunnel site, each measurement section inevitably includes a small fraction of defective strain gauges. This can be caused either by damaged strain gauges, for instance during concrete casting, or by damaged data cables, due to overcrossing by the wheels of the TBM or preparation works for the cross-passages. Apart from those, we can

see that the measurement system gives very good results, enabling the strain conditions to be followed very accurately. The chart shows a clear distinction between the various steps in the boring process following the installation of the measurement ring 3118. It can be seen that drilling works restarted with the excavation of ring 3119 one and a half hours after start-up of the strain monitoring, followed by the assembly of ring 3119. At this time, the measurement ring was already half outside the TBM shield and it had passed the shield tail completely after excavation of ring 3120. Advance was shortly interrupted after the assembly of ring 3120 due to the extension of the slurry feeding pipes and resumed with the excavation and erection of ring 3121. The measurement results of Figure 5-11 allow observation of the gradual development of strains and corresponding stresses in the concrete segments. As the TBM is pushed away from the last ring by the thrust force of the hydraulic jacks, tail grout loading and soil and water pressures are transferred to the tunnel segments. Evaluation of the monitored strains implies an upright ovalisation of the tunnel lining, which is confirmed by the ovalisation measurements using laser scanning for this cross-section and may be explained by the use of excessive tail void grouting pressures compared to soil and water pressures.

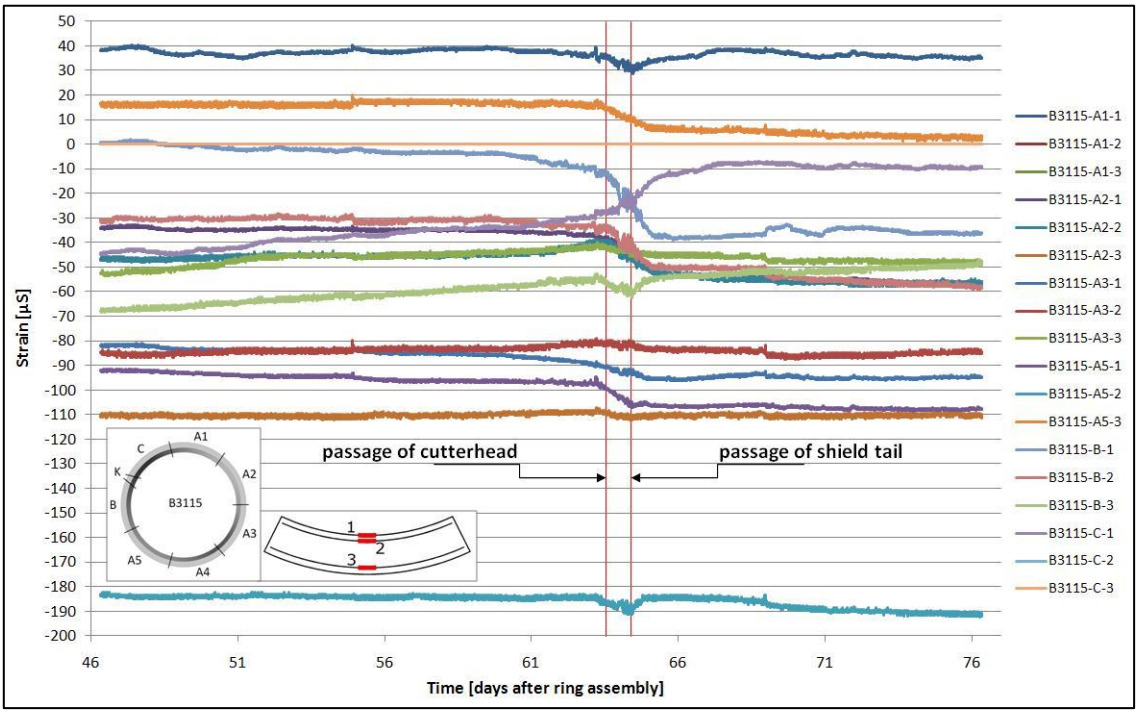

Figure 5-12: Strain results in southern tunnel during passage of northern tunnel drive

5.6.1.2. Passage of the second TBM

After crossing of the River Scheldt, TBM North followed the leading tunnel drive with a delay of approximately two months (Boxheimer & Mignon, 2011). This allowed monitoring of the strains in the lining of the southern tunnel shaft during the passage of the second TBM. Figure 5-12 clearly shows that the passage of the adjacent tunnel drive, at a distance of

approximately 8 m next to the southern tunnel, can be observed distinctly in the stabilised strain results of the latter. The effect already appears before the passage of the cutter head and still continues for a short period after the shield tail has passed the equivalent position of the measurement ring. Evaluation of the strain results shows that the excavation of the adjacent tunnel shaft causes a minor horizontal ovalisation of the segmental lining in the leading tunnel. These observations demonstrate the achieved accuracy of the continuous strain monitoring programme, as the simultaneous ovalisation measurements using laser scanning did not notice significant alterations during this phase.

5.6.1.3. Construction of cross-passages

For safety reasons, 13 cross-passages and 8 evacuation shafts were constructed parallel with the tunnel drive works at a mean distance of 300 m. All cross-passages had to be excavated within a frozen soil body. The intensive works corresponding with the consecutive construction phases are clearly depicted in the strain development of the concrete tunnel segments. Figure 5-13 shows strain results from one of the tunnel rings, which were actually cut during the construction of cross-passage 03. Even the start of the freezing process to create the frozen soil body can be noticed. After completion of the soil freezing, large and sudden jumps can be observed due to the gradual opening of the tunnel shell for the construction of the cross-passage. The variations are particularly pronounced in tunnel segments A1 and A2, which are oriented to the side of the tunnel that is being cut and partly removed.

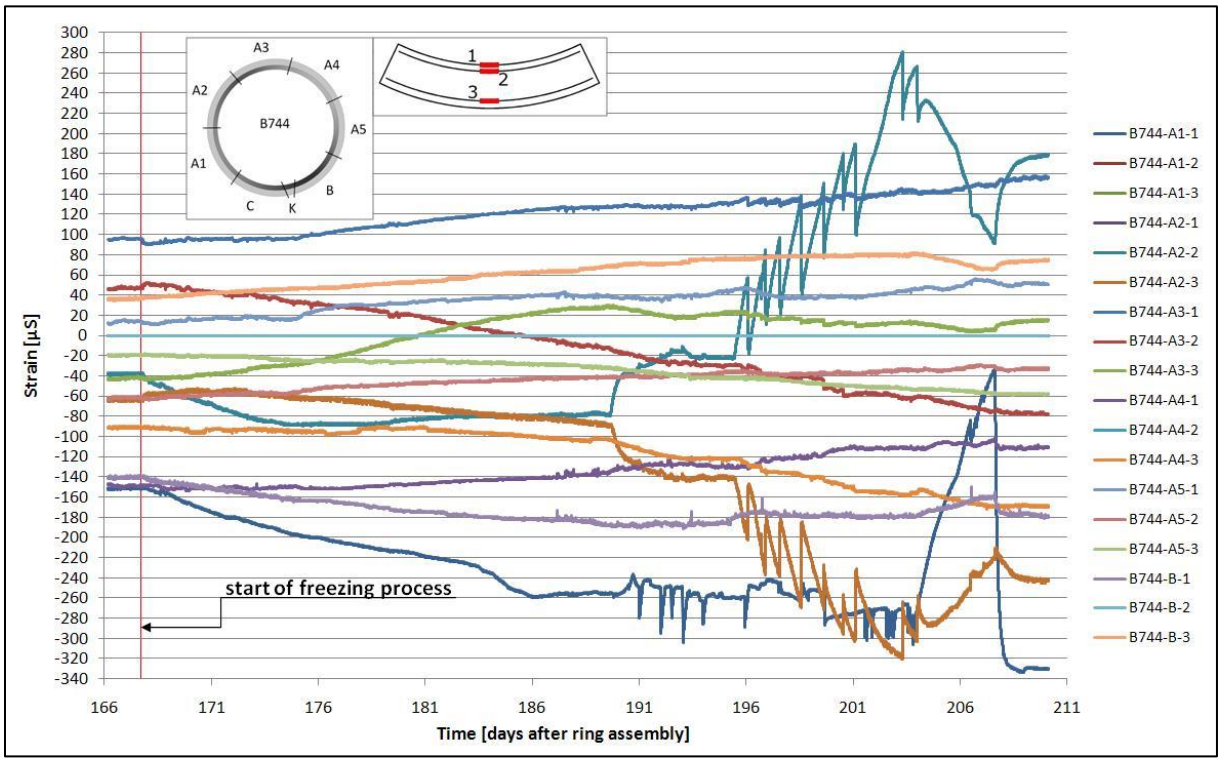

Figure 5-13: Strain results in southern tunnel near cross-passage 03

The connection galleries to the evacuation shafts were mainly built within treated soil by blocks of cement-bentonite with a low strength. During construction of one of these shafts, an incident occurred where the tunnel sealing was breached and a large amount of mud entered the tunnel. With the help of the strain results of the measurement section nearby the faulty area, the safety of the tunnel worksite could be assured. The incident was clearly registered in the strain monitoring results, but did not significantly affect the stress and strain state of the tunnel lining.

5.6.1.4. Below the River Scheldt

During crossing of the River Scheldt, the water level variation of the river, linked to the tides of the North Sea, had to be taken into account. Every twelve hours the level in the River Scheldt varies between the minimum and maximum values of -1.0 m TAW and +6.5 m TAW, with TAW (Tweede Algemene Waterpassing) being the Belgian reference level. This variation has a direct influence on the hydrostatic pressures acting on the tunnel lining.

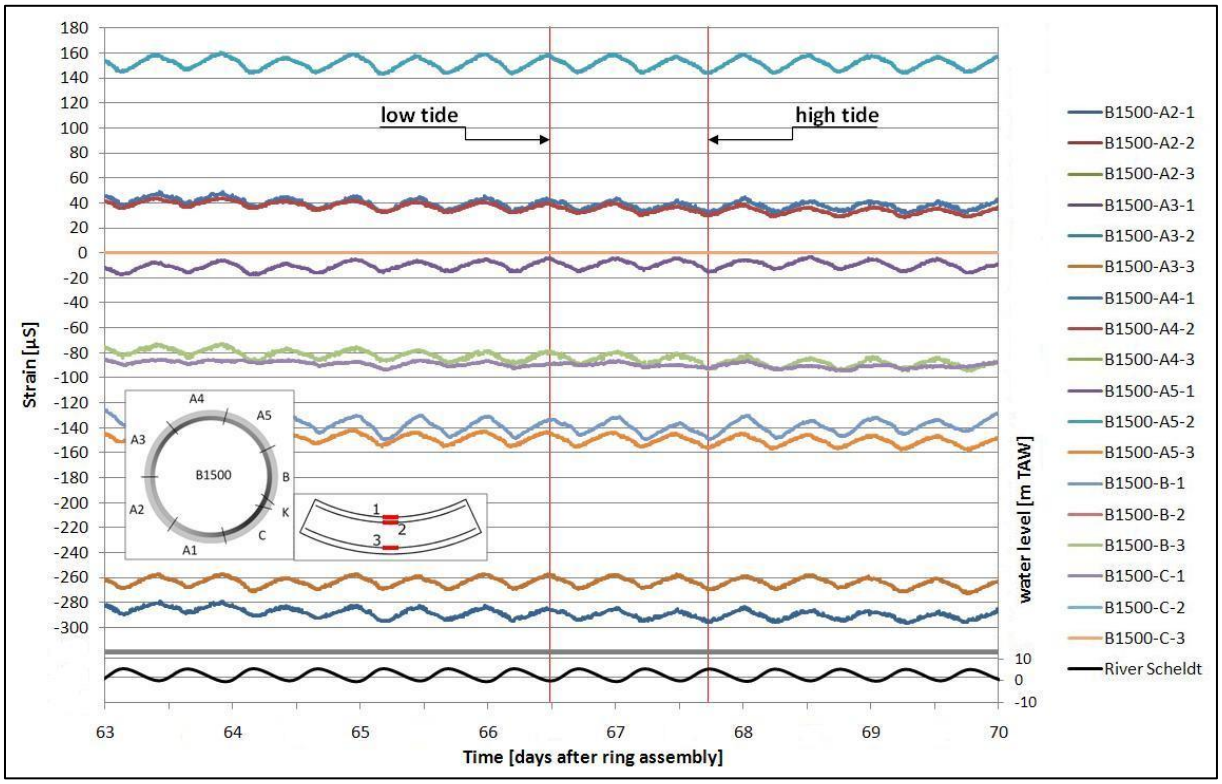

Figure 5-14: Strain results in southern tunnel below the River Scheldt

Figure 5-14 shows the obtained strain results in one of the measurement sections below the river during the tenth week after ring erection. At the bottom, the half-daily fluctuations of the water level of the River Scheldt are plotted. The chart shows that despite strains being almost fully stabilised at this time after ring assembly, the periodic fluctuations of the tidal level are clearly depicted in the strain results. Obviously, high water levels result in a larger uniform compression of the tunnel ring, while compression forces in the tunnel lining decrease at low tide.

5.6.2. Ovalisation measurements

After manual filtering and further processing of the point cloud obtained by laser scanning, the determined cross-section of the tunnel ring was compared to the design shape and, if applicable, to the critical measurement and the previous control measurement of that tunnel section. Figure 5-15 shows the results of the ovalisation measurements of section A3118 in the northern tunnel tube (same tunnel section as in Figure 5-11). Both the control measurement 6 (black) and the previous control measurement (orange) are displayed, taking into account that all deviations are 100 times enlarged. The difference between both measurements is plotted against the nominal cross-section using the green line. The figure shows that deformations of the tunnel lining in this cross-section have an 'egg' shaped ovalisation shape, with the left and right side of the ring showing a larger inward movement than the top and bottom. This complies with the strain gauge results (Figure 5-11) of the tunnel lining deformations of this section under radial soil and hydrostatic loading, showing smaller strains on the left and right side segments, indicating a higher loading state in these areas.

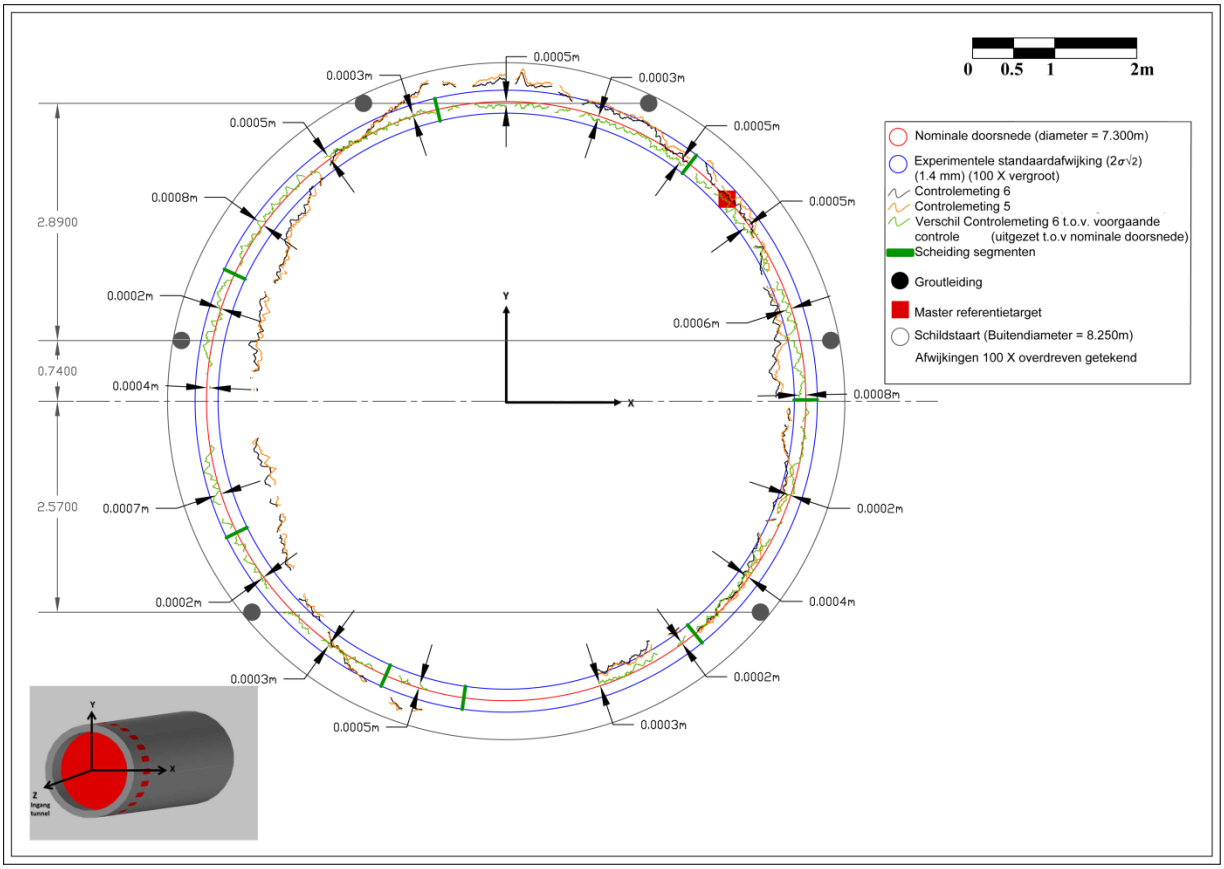

Figure 5-15: Ovalisation measurement results in southern tunnel

Analysing the results of all monitored cross-sections, it can be concluded that significant changes in ring ovalisation always occur during the first week after construction of the monitored tunnel section. After that, no significant changes are observed until the end of

the measurements three months after ring erection. The 2σ significance levels can be taken into account as the threshold for this determination.

5.7. Conclusion

Despite rough site conditions, accurate strain gauge measurements and ovalisation measurements on the precast concrete lining of shield-driven tunnels under construction have become realistic. However, to have successful monitoring every detail of the installation process becomes important in order to cope with practical complications originating from the construction site conditions and product-specific requirements. If this is assured, strain monitoring proves an extremely useful tool to evaluate the *in situ* behaviour of the tunnel lining under numerous loading conditions during and after tunnel drive works. The collected measurement results hereby served as a perfect illustration of the achieved accuracy of the monitoring setup.

5.8. References

Boxheimer, S., & Mignon, J. (2009). Eisenbahntunnel Liefkenshoek in Antwerpen - Liefkenshoek Railway Tunnel in Antwerp. *Tunnel, 7*, 25–31.

Boxheimer, S., & Mignon, J. (2011). Half way of construction of the Liefkenshoek Rail Tunnel. *Tunnel, 03*(March 2011), 41–48.

CEI - De Meyer nv. (2012). Infrabel start met de spooraanleg voor de Liefkenshoekspoorverbinding; strategisch infrastructuurproject in de Antwerpse haven zit op schema. Retrieved from www.bam.nl/pers/persberichten/infrabel-start-met-de-spooraanleg-voor-de-liefkenshoekspoorverbinding-strategisch

Gruebl, F. (2012). Segmental ring design - New challenges with high tunnel diameters. ITA-AITES Muir Wood Lecture 2012.

Nuttens, T., De Wulf, A., Deruyter, G., Stal, C., De Backer, H., & Schotte, K. (2012). Application of laser scanning for deformation measurements : a comparison between different types of scanning instruments . In *FIG Working Week 2012 - Knowing to manage the territory, protect the environment, evaluate the cultural heritage* (pp. 6–10). Rome, Italy: FIG.

Schäfer, T., Weber, T., Kyrinovic, P., & Zamecnikova, M. (2004). Deformation Measurement Using Terrestrial Laser Scanning at the Hydropower Station of Gabcikovo. In *INGEO 2004 - FIG Regional Central and Eastern European Conference on Engineering Surveying*. Bratislava, Slovakia: FIG.

Schotte, K., De Backer, H., Nuttens, T., De Wulf, A., & Van Bogaert, P. (2010). Strain Gauge Measurements during the assembly of the Diabolo Tunnel. In *34th International Symposium on Bridge & Structural Engineering - IABSE Conference* (p. 8). Venice, Italy.

Schotte, K., De Backer, H., Nuttens, T., De Wulf, A., & Van Bogaert, P. (2011). Monitoring strains in the Liefkenshoek railway tunnel. In *Proceedings ITA-AITES World Tunnel Congress 2011* (pp. 254–255).

Schotte, K., De Backer, H., & Van Bogaert, P. (2011). Strain measurements in precast concrete segments of a shield-driven tunnel. In *Proceedings fib Symposium 2011* (pp. 587–590). Prague.

Van Bogaert, P. (2008). Le projet « Liefkenshoek » de liaison ferroviaire sous l ' Escaut. *Tunnels et Ouvrages Souterrains, 205*(janvier / fevrier), 49–55.

Van Bogaert, P. (2009). Recent and future railway tunnels in Belgium. In *Proc. ITA World Tunnel Conference "Safe Tunnelling for the City and the Environment"* (pp. 689–690). Budapest: Hungarian Tunnelling Association, ISBN 9789630672399.

Van Bogaert, P., & De Pauw, B. (2008). New railway connection below Brussels Airport. In *Proceedings IABSE Congress 2008* (pp. 280–281). Chicago.

Van Bogaert, P., & Vereerstraeten, J.-C. (2005). Antwerp North-South railway link for a new urban development tunneling and underground techniques. In *Receuil du Congrès International de l'AFTES* (pp. 279–286).

Zogg, H.-M., & Ingensand, H. (2008). Terrestrial laser scanning for deformation monitoring - load tests on the Felsenau Viaduct (CH). In *XXIst ISPRS Congress - Technical Commission V* (Vol. XXXVII–B5). Beijing, China: The International Archives of the Photogrammetry, Remote Sensing and Spatial Information Sciences.

CHAPTER 6
TERRESTRIAL LASER SCANNING AS KEY ELEMENT IN THE INTEGRATED MONITORING OF THE TIDAL INFLUENCES ON A TWIN TUBE CONCRETE TUNNEL

6. TERRESTRIAL LASER SCANNING AS KEY ELEMENT IN THE INTEGRATED MONITORING OF THE TIDAL INFLUENCES ON A TWIN TUBE CONCRETE TUNNEL

Modified from Nuttens, T., Stal, C., De Backer, H., Schotte, K., Van Bogaert, P., Detry, P., & De Wulf, A. Terrestrial laser scanning as key element in the integrated monitoring of the tidal influences on a twin tube concrete tunnel. The Photogrammetric Record. (Under review)

6.1. Abstract

In 2012, for the first time in Belgium, integrated monitoring was carried out to assess the deformations of a twin tube tunnel below the River Scheldt (Antwerp, Belgium) under influence of river tides. Levelling measurements during a tide cycle showed a variation in height of the levelling bolts of up to 10 mm between low and high tide. Simultaneous strain gauge measurements also showed a significant difference in strains. A deformation of the tunnel section during each twice-daily tide cycle, resulting in an 'egg' or 'pumpkin' shape, could hold large risks for the strength and durability of the tunnel structure. However, the laser scanning results showed that there were no significant deformations of the tunnel section's shape during the tide cycle. The laser scanning measurements resulted in the much needed thorough view on the deformation pattern and improved the long term risk assessment of the tunnel.

6.2. Introduction

A thorough and continuous risk assessment of large infrastructures such as hydro-electrical dams, bridges or concrete beams is indispensable to guarantee the safety of these constructions. Various monitoring instruments and methodologies can be applied, depending on the required accuracy, the type and dimensions of the structure, the field conditions etc. A wide variety of continuous monitoring techniques is available, such as strain measurements or the automated sequential measurement of reference points with total station or GNSS measurements (Fujino & Siringoringo, 2011; Khoo, Tor, & Ong, 2010; Psimoulis & Stiros, 2007). In many projects, discontinuous monitoring measurements are also scheduled during which the entire construction or a limited number of reference points of the structure are measured on specific moments in time. Total station, GNSS, photogrammetry or laser scanning are frequently used for these measurements (Alba et al., 2006; Bertacchini, Boni, Capra, Castagnetti, & Dubbini, 2010; Chounta & Ioannidis, 2012; Needham & Dash, 2012; Peeters et al., 2009; Zogg & Ingensand, 2008). An extensive and systematic monitoring of large projects is not only compulsory during construction, but also during the following years a systematic monitoring can detect possible risks at an early stage. Such a risk assessment has to be based on accurate up-to-date data, clear

information, quick results and conclusions, requiring specific monitoring techniques to meet these demands (Caballero et al., 2007; Lerma Garcia et al., 2008).

During recent years, (terrestrial) laser scanning has been applied as a technique to measure large infrastructures and to meet the specific monitoring demands. The measurement speed, high achievable accuracy and possibility to obtain a detailed and complete 3D image of complex objects are important advantages contributing to the growing use of laser scanning (Han et al., 2013a; Lichti & Chow, 2013; Remondino et al., 2011). While classical surveying measurements with a total station offer higher single point accuracy, they are limited in the number of points that can be measured in a specified time frame (Alba et al., 2006). To cover a denser point grid, stereo photogrammetry can be used as an alternative recording technique. Subsequent 3D models can be used to detect any structural deformations with time. However, additional measurements with a total station or GNSS are often required and the measurement conditions on site usually do not meet the requirements for accurate photogrammetric results, such as sufficient lighting or sufficient contrast on the object's surface. Laser scanning is an active measurement technique and deals as such with many of the afore mentioned restrictions, making accurate measurements of a dense point grid in difficult field conditions and a limited time frame possible, even from a distance up to several hundreds of metres (Lichti et al., 2000; Pfeifer & Briese, 2007b; Rönnholm et al., 2009; Thomas & Isaacs, 2011).

Currently, terrestrial laser scanning is successfully being used for high accuracy deformation measurements of tunnels, either during a long-term monitoring program or during the construction phase (Argüelles-Fraga et al., 2013; Han et al., 2013b; Lam, 2006; Lindenbergh et al., 2005; Pejić, 2013; van Gosliga et al., 2006; Yoon et al., 2009). The research examples clearly indicate the suitability of laser scanning for the accurate and 3D monitoring of large structures. However, as will be discussed in this chapter, a more advanced challenge is to combine this highly accurate laser scanning with other applied monitoring techniques to assess difficult or critical deformation patterns. The combination of simultaneous levelling measurements, strain gauge registrations and laser scanning measurements in the Belgian tunnelling project discussed in this research is an important step forward in the awareness of the relevance of an integrated monitoring strategy for large infrastructural projects and of the relevance to include laser scanning measurements to get a more thorough view on the occurring deformations. Laser scanning not only offers a full 3D view of the tunnel construction, an optimal use of the data also allows detecting other aspects of the tunnel's deformation, resulting in a better judgement of the risks of the deformations.

The following sections will discuss the tunnel monitoring project and the tidal impacts on the tunnel construction in more detail. Subsequently, the levelling and strain gauge measurements will be commented, followed by a more detailed explanation of the laser scanning measurements. The results of the deformation monitoring and the important contribution of the laser scanning measurements to the conclusions about the deformation

pattern are then explained. Further on in this chapter, a discussion about the integration of the various results and the tidal movements of the tunnel structure is given, followed by conclusions concerning the use of laser scanning as an important monitoring technique for this kind of applications.

6.3. 'Liefkenshoek Rail Link' project

The 'Liefkenshoek Rail Link' project (2010-2014) establishes a new railway connection for freight traffic between the left and right bank of the River Scheldt in the Port of Antwerp (Belgium). This new railway connection has a total length of approximately 16 km, of which 6 km consists of two twin tunnels ('Tunnel North' and 'Tunnel South'), constructed in 2010-2011 by two shield driven TBM's using the mixshield method (Van Bogaert, 2009). The first use of this new railway connection is foreseen in the second half of 2014. This newly bored tunnel complex crosses two waterways (River Scheldt and Canal Dock/Port Canal), the soil cover above the tunnel being rather shallow (3 to 10 m) (Figure 6-1).

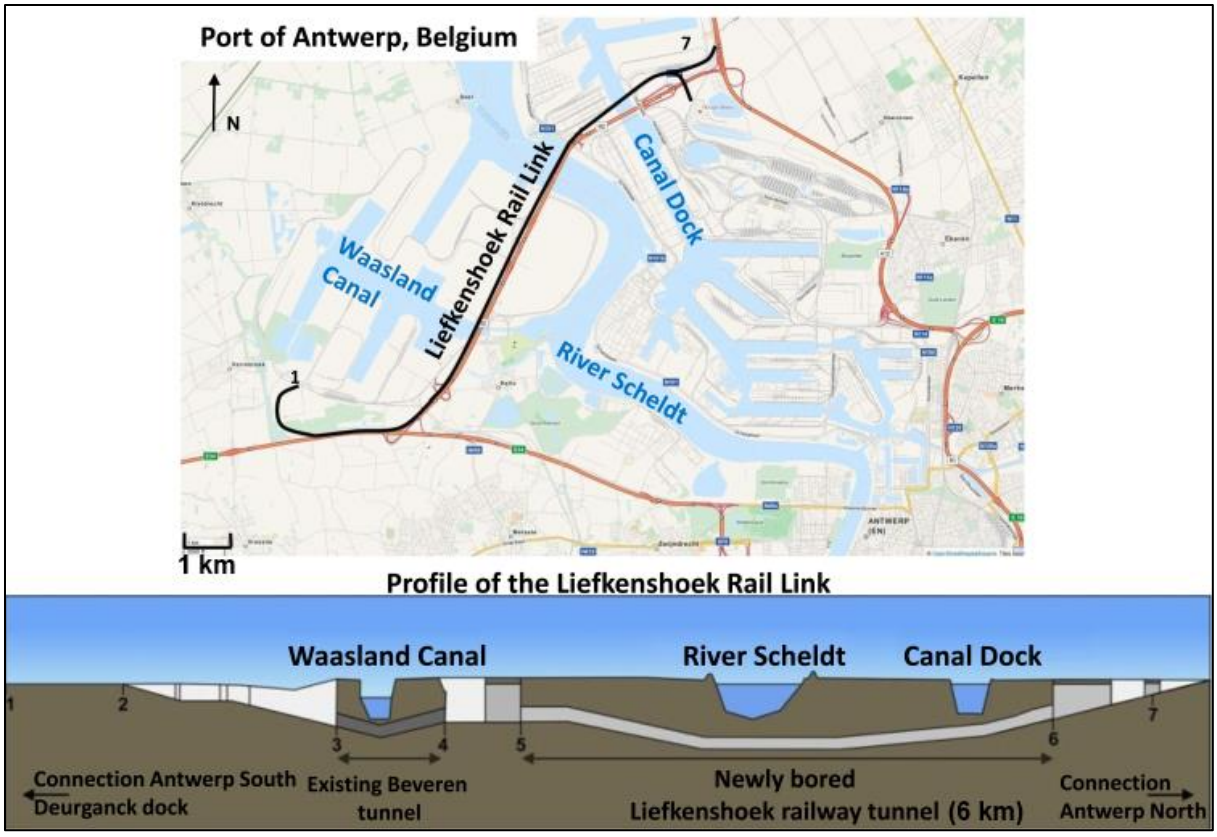

Figure 6-1: Overview of the 'Liefkenshoek Rail Link' project
(based on CEI - De Meyer nv, 2012; openstreetmap.org; maps.google.be, October 2, 2013)

The geological characteristics of the tunnel boring site are of variable nature. The soil stratification has a general downward slope from west to east. The left bank of the River Scheldt (west) consists of sandy layers until a depth of 4 to 6 m. Below these layers, quaternary soft clay, vases and peats are appearing. This clay layer does not occur on the right bank of the river (east). Deeper, one finds a layer of the tertiary era with a maximum

thickness of 6 m, containing silt and a mixture of fine sand and clay. Below this, a 6 m thick tertiary sand stratum, containing silt and clay particles is found, followed by 9 to 14 m thick tertiary fine sands, containing clay as well as glauconite. Both of these sandy layers have a smaller thickness on the left river bank than on the right river bank. At larger depth, the soil consists of Boom clay, which is an over consolidated type of saturated soil, acting as an impermeable layer. The tunnel's trajectory mostly runs through the tertiary sands, but at its deepest point (below the River Scheldt) it also runs partly through the Boom clay.

Figure 6-2: A constructed tunnel ring at the end of one of the tunnel tubes, consisting of seven concrete segments and one smaller key stone

The two newly bored tunnels have an inside diameter of 7.300 m, the concrete tunnel segments having 0.400 m thickness. The longitudinal size of each tunnel ring is 1.800 m, each tunnel ring consisting of seven concrete segments and one smaller key stone (TUC Rail, 2010) (Figure 6-2). During the general monitoring program, in the period from tunnel ring assembly until approximately three months after construction, fourteen tunnel sections in each tunnel tube were selected for monitoring. Seven epochs were defined on which the selected tunnel sections had to be measured with laser scanning: the 'reference measurement' immediately after construction of the tunnel section; a measurement every week during the first month after installation ('control measurement 1 to 4') and measurements two and three months after installation ('control measurement 5 and 6'). The determined cross-sections are compared with the design shape, the reference measurement and the previous control measurement of that tunnel section.

6.4. Tidal influence on the tunnel construction

The River Scheldt has a direct connection with the North Sea and is therefore affected by the tidal water level variation in the North Sea. Twice a day, the River Scheldt reaches its lowest and highest water level, with an average difference in water level of about 5.5 to 6 m. Water level heights are measured in the Belgian height reference system TAW (Figure 6-3). This difference in water level between ebb and flood can increase with an additional 2 m during spring tides. Considering the shallow soil cover above the tunnel at the crossing with the River Scheldt (3 - 10 m ≈ 0.4 to 1.25 D); the continuous variation in water level and water pressure had to be taken into account during the drilling works of both tunnel tubes, as well as for the maintenance of the structure. Moreover, as recent levelling measurements at the final stage of the works have shown, the influence of the variable water pressure still continues.

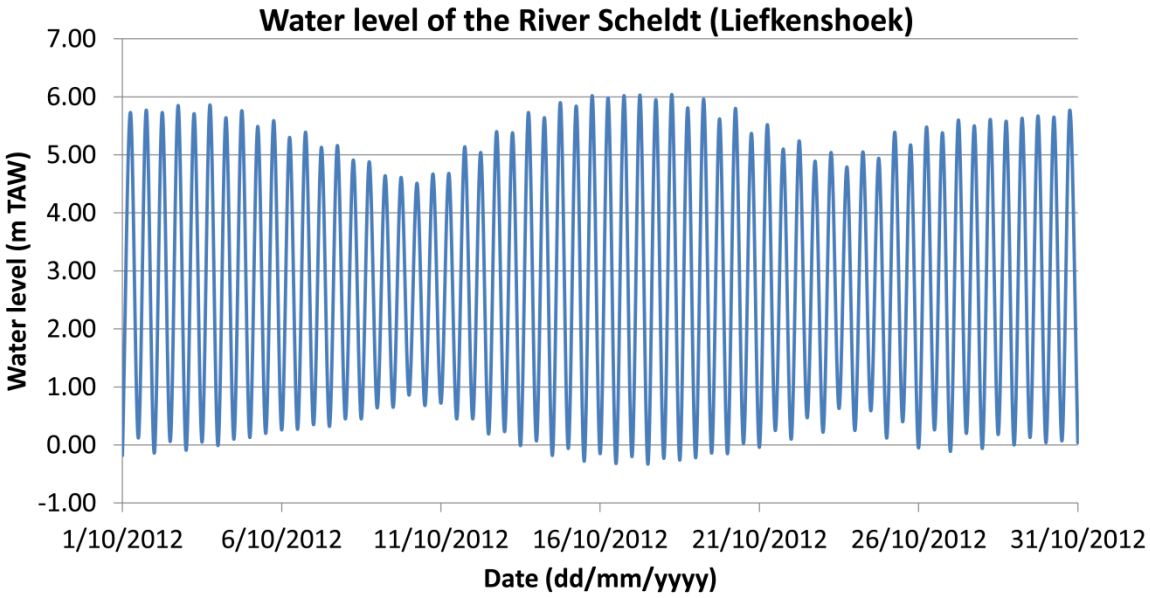

Figure 6-3: Water level of the River Scheldt at Liefkenshoek during October 2012 (Data Source: Hydrological Information Centre (Flanders))

For the levelling measurements during the construction period of the tunnel tubes, specially installed topographical bolts were measured using a Leica DNA10 digital levelling instrument, with a specification of 0.9 mm standard deviation on height measurements per 1 km with the use of an invar staff. Measuring these bolts at different moments in time (starting from a fixed reference height level) showed variations up to 10 mm in height between the various measurement sessions for several bolts below the River Scheldt. After extensive investigation of several levelling measurement series, a relation was found between the change in level of the topographical bolts and the tidal variations of the River Scheldt.

To further investigate this relation between the measured elevations of the topographical bolts, the water level variations and the impact of these water level variations on the whole

surface of the tunnel rings, a combined monitoring program was carried out. The latter combined levelling measurements with the already used strain and laser scanning measurement methodology during the construction phase of the tunnel project. By measuring one specific tunnel ring below the River Scheldt during one day with simultaneous laser scanning measurements, strain registrations and levelling measurements, an extensive image of the impact of the water level variations on the tunnel structure could be obtained. The combinations of these techniques and their respective results can confirm or exclude some deformation patterns and their causes, leading to a thorough knowledge of the deformations of the tunnel rings and their possible long term consequences.

6.5. Integrated monitoring

6.5.1. Levelling measurements

To obtain sufficient data to monitor the influence of the continuously changing water level, the integrated measurements were organised on October 31 2012. Measurements were scheduled between 9:00 and 18:30, encompassing the situation at low (approximately 11:00) and high tide (approximately 16:10) of the River Scheldt.

The first part of the monitoring program consisted of levelling measurements, performed hourly in one of the tunnel tubes ('Tunnel South'). Because of the limited time frame between the successive measurement series, a fixed reference point outside the tidal influence of the river was selected as starting point for the levelling measurements, instead of the beginning or end point of the tunnel tube. From this point (Ring 1100), a two-way measurement was performed. The assumption of Ring 1100 being a stable reference point was confirmed by evaluating the measurement results. The height values of this point remained unchanged during the successive measurement series. Every fifty rings, levelling bolts were measured until the monitored tunnel section in the middle of the River Scheldt in 'Tunnel South' was reached.

During the time frame of the monitoring, eight levelling measurement series could be performed and the results of these measurements are presented in Figure 6-4. The graph in Figure 6-4 is limited between ring number 1250 and 1500 as this area is subject to the largest differences between low and high tide. Including the ring numbers 1100 to 1250 would significantly increase the range needed on the Y-axis, reducing the graph's readability, without contributing to the understanding of the tidal influences on the levelling measurements.

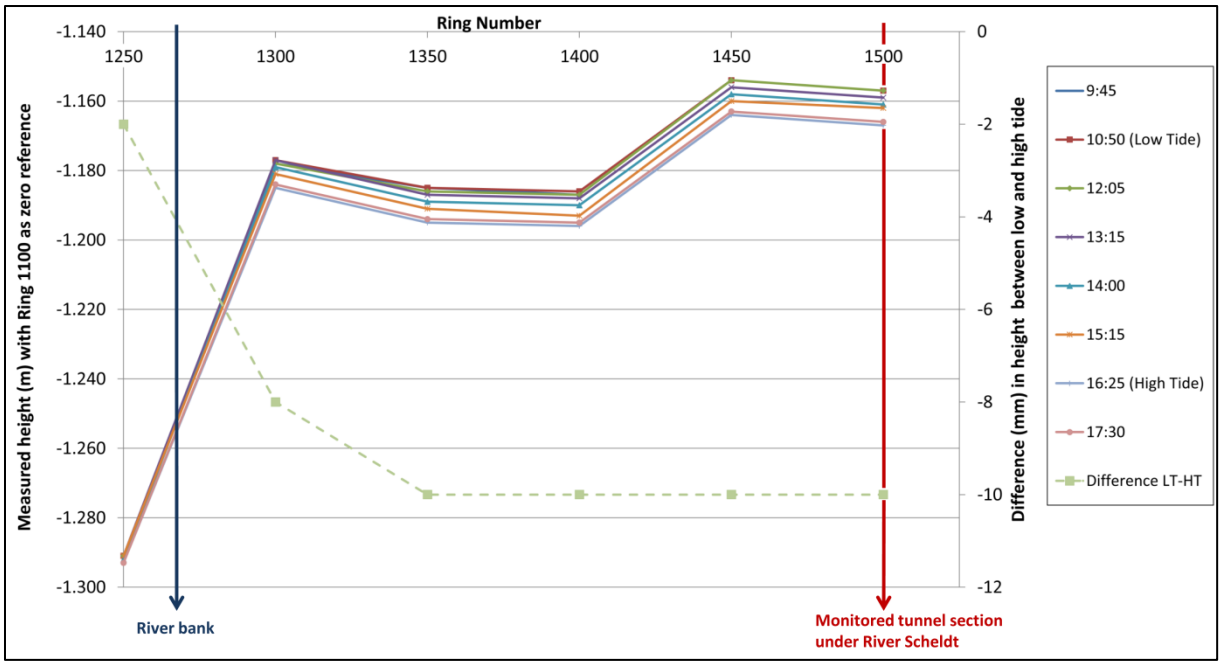

Figure 6-4: Measured heights of the levelling bolts during the different measurement series and the differences between low and high tide (ring number 1250 to 1500)

The graph (Figure 6-4) clearly shows a variation in the height of the bolts below the River Scheldt between the series of measurements and thus between the different tide levels. The variation increases towards the deepest area below the River Scheldt, until the centre of the river is reached (Ring 1500). Moreover, the absolute height values of the monitored bolts wane between low and high tide and increase again after the high tide is passed, indicating the largest pressure on the tunnel structure at high tide. The dotted line in Figure 6-4 and the right vertical axis indicate the difference in height value between low and high tide for every measured levelling bolt. At ring 1250, the difference between low and high tide is maximum 2 mm, where this difference at ring 1300 reaches already 8 mm. After ring 1300 this difference slowly increases to 10 mm difference at ring 1500. This shows that the largest jump in difference between low and high tide can be located between ring number 1250 and 1300, corresponding to the transition between the left river bank and the River Scheldt.

6.5.2. Strain gauge measurements

Simultaneously with the levelling measurements, the integrated monitoring used strain gauge measurements to detect the impacts of the various loading conditions on the concrete segments of the tunnel rings (Figure 6-5). During the tunnel construction phase, eight tunnel sections over the whole length of each tunnel tube were equipped with those strain gauges, including the selected tunnel ring below the River Scheldt. More information about the location of the strain gauges, the installation procedure and results of the monitoring during the construction phase can be found in chapter 5.

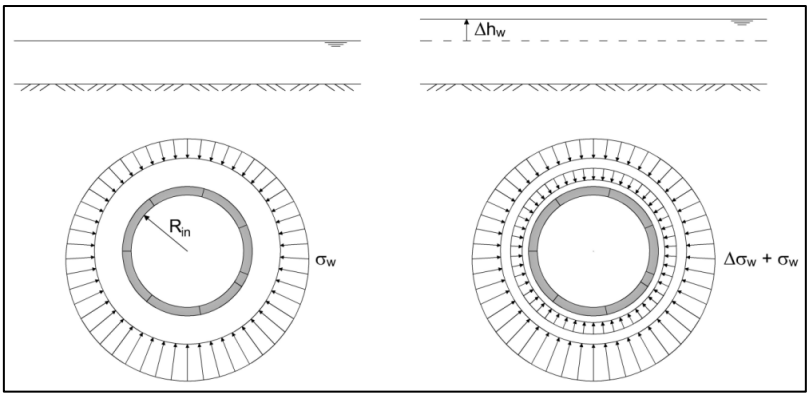

Figure 6-5: Assumptions on radial stress variation of the tunnel structure caused by the tidal changes in water level (Schotte et al., 2013)

The strain measurements during the integrated monitoring show an increase of the strains at low tide, indicating a general decrease of compression of the tunnel rings (Figure 6-6). Between low tide and high tide, the growing water pressure above the tunnel section causes a larger compression of the tunnel rings as shown in the strain recordings. The continuous registration of those strains during the tide cycle also illustrates that there is no delay between the variation of the water level and the strain responses due to the ground cover above the tunnel (Schotte et al., 2013).

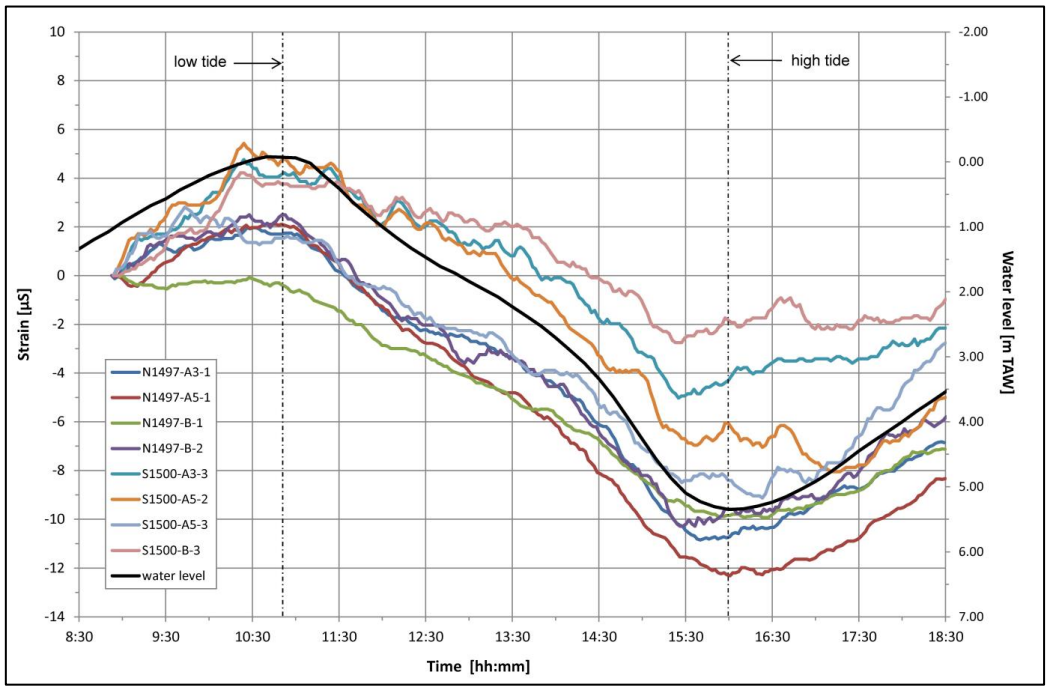

Figure 6-6: Strain recordings in Tunnel North and Tunnel South during the integrated monitoring (Schotte et al., 2013)

6.5.3. Laser scanning measurements

The third part of the monitoring consisted of laser scanning a tunnel section below the River Scheldt in both tunnel tubes every hour and additionally on the specific low and high tide moments. Following the developed measurement methodology as described in chapter 3,

the laser scanner (Leica HDS6100 phase-based laser scanner) is set up on a tripod in the middle of the tunnel section, measuring the tunnel surface with an average point density of 4 mm on 6 m distance. A detailed description of this methodology, which already proved an achievable standard deviation of 0.38 or 0.48 mm when applying a [x-0.5 grad; x+0.5 grad] smoothing interval of the calculated radius values on the cross-section, respectively when using one scanning position or combining multiple laser scanner setups can be found in chapter 4. Between the previous measurements to obtain these standard deviations and the measurements during the monitoring campaign described in this chapter, part of the concrete rail bed was built and the tunnel surface was sprayed with a granular fire protective layer (Figure 6-7). In these measurement conditions, only one laser scanning setup is required to obtain a full coverage of the tunnel section. To measure the impact of these changed tunnel conditions and surface material, new experimental standard deviations were determined for one laser scanning setup. The knowledge on the achievable standard deviations form an essential part in the correct interpretation of detected changes in ovalisation between low and high tide, allowing to conclude whether these changes are due to the measurement error or due to an actual deformation of the tunnel ring.

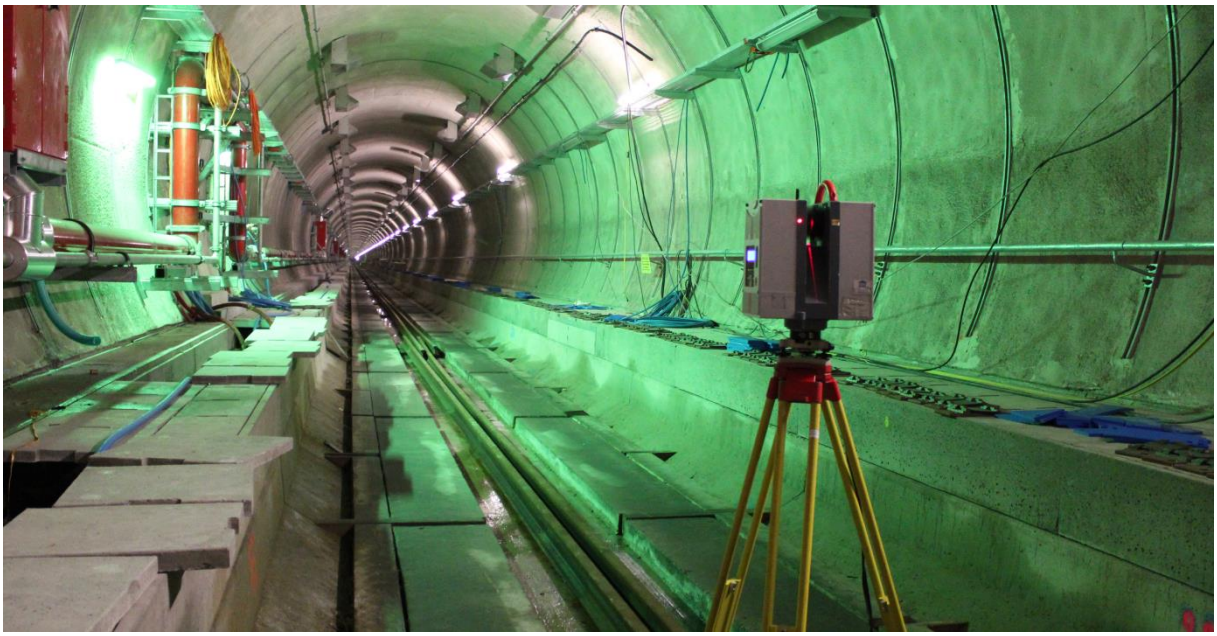

Figure 6-7: Laser scanner setup in the measurement conditions during the integrated monitoring (rail bed and fire protective layer on the tunnel section)

Within a time frame of approximately 20 minutes, one of the tunnel sections was measured multiple times to calculate these new experimental standard deviations, assuming that no significant deformations occurred during this short time span. First, the tunnel section was measured four times from the same scanning position and without any changes on the reference marker. This reference marker is a black-and-white disk that indicates the exact location of the calculated cross-sections. It can be screwed onto a fixed bolt in the tunnel section every time a monitoring measurement has to be performed (Figure 6-8).

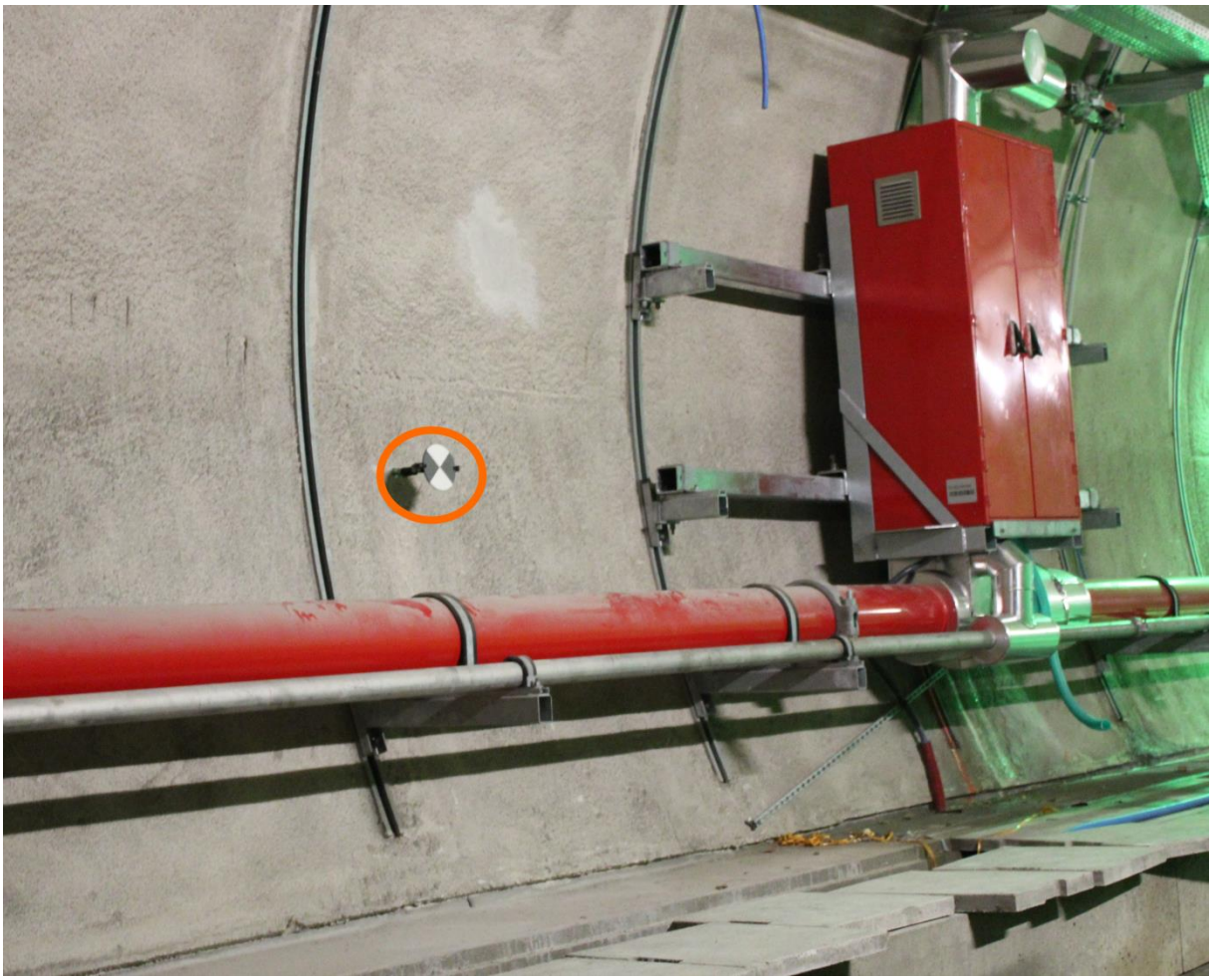

Figure 6-8: Black-and-white reference marker attached to the bolt in the tunnel surface

Another series of four measurements was taken from a different scanning position for each measurement, simulating the measurements of the section on various points in time without any materialised setup point for the laser scanner. In this last series, one reference marker was fixed during all four measurements (comparable to the first series). Another marker was replaced on a second bolt after each measurement, again simulating measurements on different points in time. The processing of these data results in three different standard deviations, indicating the influence of taking into account a fixed or variable scanning position or target position. For the [x-0.5 grad; x+0.5 grad] smoothing interval, the standard deviations are 0.27 mm, 0.42 mm or 0.44 mm, respectively for measurements from the same scanning setup, from different setups without taking off and remounting the reference marker on the fixed bolt and different setups with taking off and remounting the reference marker between each measurement.

If only the upper circular part of the tunnel section is taken into account, the experimentally based standard deviations are slightly higher than the previously determined standard deviations, due to the rough fire protective layer on the concrete segments. However, these values still fall within the 0.5 mm requirements for these tunnel monitoring projects. The lower part of the tunnel section however, consists of a concrete rail bed and this area results

in higher values (0.60 mm; 1.13mm; 1.05 mm). This is mostly due to the extreme incidence angles on the pathway, the bottom part of the field of view of the laser scanner and the loose wooden beams, concrete tiles or mud on the rail bed which can easily have undergone small changes between the different measurements. Because the circular upper part of the tunnel section is the most relevant area of interest to monitor the deformations caused by the water level variations, the analysis will further focus on that part.

To monitor the tidal impacts on the tunnel sections, the laser scanning measurements at low and high tide were processed for each tunnel tube. As detailed below, there was no statistically significant difference between both measurements. To confirm these results, a measurement between low and high tide was also processed ('Middle measurement'). Because this measurement confirmed the previous results, there was no need to process any other measurements within the tidal cycle. Based on the project requirements of 0.5 mm accuracy, which was achieved by the experimental standard deviations, the significance level for the comparison between two measurements is set at $2\sigma\sqrt{2}$ = 1.4 mm. Figure 6-9 shows the difference between the measurement at low tide and the measurement at high tide of 'Tunnel North'. This difference, represented by the black line (100 times exaggerated) and set out to the reference of the design radius, clearly falls within the significance level boundaries (two outside blue circles). Taking only the upper part of the section into account, the arithmetic mean difference (average of the differences) between both measurements is 0.0 mm and the absolute mean difference (the average of the absolute differences) is 0.3 mm. If the part of the rail bed is also taken into account, the values are 0.1 mm and 0.5 mm for respectively the mean difference and the absolute mean difference.

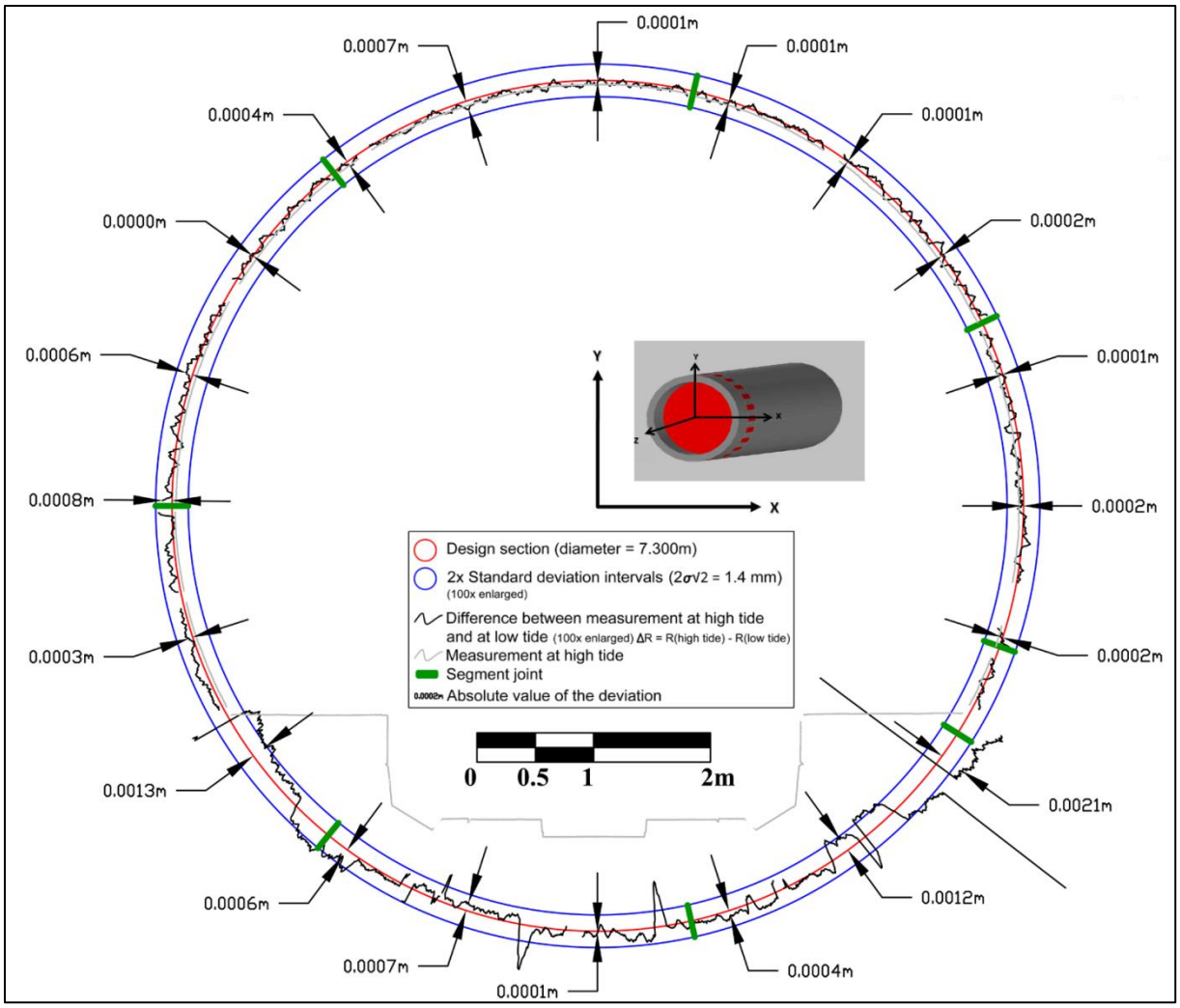

Figure 6-9: Comparison between the measurement at low and high tide ('Tunnel North')

Table 6-1 displays an overview of the mean differences for all processed measurements both in 'Tunnel North' and 'Tunnel South'. Differences between low and high tide, between the middle measurement and low tide and between high tide and the middle measurement fall well within the 95% significance interval. However, only the upper part of the tunnel section is included in these results. The significant differences that occur in the lower area of the tunnel section, as illustrated in Figure 6-9, are caused by, amongst others, the easy displacement of the concrete tiles on the side path and of the wooden beams, the mud layer of the rail bed etc.

Table 6-1: Averaged differences between two measurements of the monitored section in 'Tunnel North' and 'Tunnel South' (only the upper part of the tunnel section)

Differences between two measurements (mm) (only upper part of the tunnel section)				
	Tunnel North		Tunnel South	
	Mean	Absolute Mean	Mean	Absolute Mean
High tide vs. low tide ΔR = R(high tide) - R(low tide)	0.0	0.3	0.1	0.6
Middle measurement vs. low tide ΔR = R(middle) - R(low tide)	0.4	0.5	0.0	0.4
High tide vs. middle measurement ΔR = R(high tide) - R(middle)	-0.4	0.5	0.0	0.7

6.6. Discussion

The levelling measurements during the above described extensive monitoring program confirmed the earlier indications that the tunnel sections below the River Scheldt are impacted by the tidal fluctuations of the water level. The measurements of the levelling bolts indicate a difference in height between low and high tide of up to 10 mm, measured from a fixed reference point outside the influence of the water level variations. The strain gauge measurements during the integrated monitoring show a difference in strains between low and high tide, also confirming that the tunnel structure undergoes a significant impact of the river tide. Based on the 10 mm height difference between low and high tide and the strain gauge results, the question remains whether this height difference is due to a deformation of the tunnel section itself or if the part of the tunnel below the River Scheldt experiences a vertical movement. A deformation of the tunnel section itself during each tide cycle, resulting in an 'egg' or 'pumpkin' shape, could hold large risks for both the strength and durability of the tunnel.

Complementing these levelling and strain gauge results with the highly detailed and accurate 3D laser scanning point clouds, measured at successive stages of the tide cycle, gives new insights on the actual deformation pattern of the tunnel structure. The cross-sections derived from the laser scanning point clouds show with very high accuracy that there is no significant change in ovalisation of the monitored tunnel section during the tide level variations. The combination of the results of the different simultaneous measurement techniques points towards the conclusion that the tunnel structure undergoes a vertical rigid body movement caused by the changing water pressure and no deformation of the shape of the tunnel sections themselves, reducing the critical character of the deformation and actions to undertake.

6.7. Conclusions

Laser scanning is more and more being applied as a measurement technique for large and complex infrastructures. In this chapter, the focus was on the importance of laser scanning as part of an integrated monitoring program in combination with levelling and strain gauge measurements for monitoring a recently built twin tube tunnel complex impacted by river tides.

Due to the water level fluctuations of the River Scheldt, reaching a low and high tide value twice a day, a height difference of up to 10 mm for levelling bolts installed in the tunnels was measured by levelling. Therefore, integrated monitoring was carried out by combining levelling and strain gauge measurements with laser scanning measurements. A tunnel section at the centre of the River Scheldt was measured using laser scanning every hour and on the specific low and high tide moments.

Simultaneous levelling and strain gauge measurements were performed in one of the tunnel tubes ('Tunnel South'), confirming respectively a variation in the height of the bolts below the River Scheldt between the different measurement series and an increase of the strains at low tide, indicating a general decrease of compression of the tunnel rings. Such deformations of the tunnel section itself during each tide cycle, resulting in an 'egg' or 'pumpkin' shape, could hold large risks for both the strength and durability of the tunnel. The laser scanning results, however, clearly show that there is no significant change in ovalisation of the tunnel section during the tidal cycle. The combination of the three different measurement results suggest that the tunnel below the River Scheldt undergoes a vertical movement during each tide cycle, without deformations of the circular shape of the tunnel sections. However, despite the more thorough insights thanks the the combination of the different monitoring techniques, different hypotheses about this vertical movement remain. Possibly, the variable ground composition and local differences in compactness of the grouting around the tunnel structure have an influence on the water pressure around the tunnel tubes. The more thorough view on the deformation pattern, thanks to the integration of laser scanning measurements, significantly improves the risk assessment of the deformations and changes the idea of the possible long term consequences.

6.8. References

Alba, M., Fregonese, L., Prandi, F., Scaioni, M., & Valgoi, P. (2006). Structural monitoring of a large dam by terrestrial laser scanning. In H.-G. Maas & D. Schneider (Eds.), *ISPRS Commission V Symposium "Image Engineering and Vision Metrology"* (Vol. XXXVI–5). Dresden, Germany.

Argüelles-Fraga, R., Ordonez, C., Garcia-Cortes, S., & Roca-Pardinas, J. (2013). Measurement planning for circular cross-section tunnels using terrestrial laser scanning. *Automation in Construction, 31*, 1–9. doi:10.1016/j.autcon.2012.11.023

Bertacchini, E., Boni, E., Capra, A., Castagnetti, C., & Dubbini, M. (2010). Terrestrial Laser Scanner for Surveying and Monitoring Middle Age Towers. In *The XXIV FIG International Congress 2010 "Facing the Challenges - Building the Capacity."* Sydney, Australia: FIG.

Caballero, D., Esteban, J., & Izquierdo, D. B. (2007). ORCHESTRA: a Unified an Open Architecture for Risk Management Applications. *Geophysical Research Abstracts, 9*.

CEI - De Meyer nv. (2012). Infrabel start met de spooraanleg voor de Liefkenshoekspoorverbinding; strategisch infrastructuurproject in de Antwerpse haven zit op schema. Retrieved from www.bam.nl/pers/persberichten/infrabel-start-met-de-spooraanleg-voor-de-liefkenshoekspoorverbinding-strategisch

Chounta, I., & Ioannidis, C. (2012). High Accuracy Deformation Monitoring of a Concrete Beam using Automatic Photogrammetric Techniques. In *FIG Working Week 2012 - Knowing to manage the territory, protect the environment, evaluate the cultural heritage* (p. 16). Rome, Italy: FIG.

Fujino, Y., & Siringoringo, D. M. (2011). Bridge monitoring in Japan: the needs and strategies. *Structure and Infrastructure Engineering, 7*(7-8), 597–611. doi:10.1080/15732479.2010.498282

Han, J.-Y., Guo, J., & Jiang, Y.-S. (2013a). Monitoring tunnel deformations by means of multi-epoch dispersed 3D LiDAR point clouds: An improved approach. *Tunnelling and Underground Space Technology, 38*, 385–389. doi:10.1016/j.tust.2013.07.022

Han, J.-Y., Guo, J., & Jiang, Y.-S. (2013b). Monitoring tunnel profile by means of multi-epoch dispersed 3-D LiDAR point clouds. *Tunnelling and Underground Space Technology, 33*(186-192), 186. doi:10.1016/j.tust.2012.08.008

Khoo, V. H. S., Tor, Y. K., & Ong, G. (2010). Monitoring of High Rise Building using Real-Time Differential GPS. In *The XXIV FIG International Congress 2010 "Facing the Challenges - Building the Capacity."* Sydney, Australia: FIG.

Lam, S. Y. W. (2006). Application of terrestrial laser scanning methodology in geometric tolerances analysis of tunnel structures. *Tunnelling and Underground Space Technology, 21*(3-4), 410. doi:10.1016/j.tust.2005.12.057

Lerma Garcia, J. L., Van Genechten, B., Heine, E., & Santana Quintero, M. (2008). *3D Risk Mapping, Theory and Practice on Terrestrial Laser Scanning. Training Material Based on Practical Applications.* Universidad Politecnica de Valencia, Spain.

Lichti, D. D., & Chow, J. C. K. (2013). Inner Constraints for Planar Features. *The Photogrammetric Record, 28*(141), 74–85. doi:10.1111/j.1477-9730.2012.00700.x

Lichti, D. D., Stewart, M. P., Tsakiri, M., & Snow, A. J. (2000). Calibration and testing of a terrestrial laser scanner. In *International Archives of Photogrammetry and Remote Sensing (Vol. XXXII–B5).* Amsterdam, The Netherlands.

Lindenbergh, R., Pfeifer, N., & Rabbani, T. (2005). Accuracy analysis of the Leica HDS3000 and feasibility of tunnel deformation monitoring. In *ISPRS WG III/3-4, V/3 Workshop "Laser scanning 2005"* (Vol. 36–3/W19, pp. 24–29). Enschede, The Netherlands.

maps.google.be, Oct 2, 2013

Needham, J., & Dash, B. (2012). Dynamic deformation monitoring of a transmission tower undergoing failure test by close range terrestrial photogrammetry. In *FIG Working Week 2012 - Knowing to manage the territory, protect the environment, evaluate the cultural heritage* (p. 15). Rome, Italy: FIG.

www.openstreetmap.org, Oct 2, 2013

Peeters, B., Couvreur, G., Razinkov, O., Kündig, C., Van der Auweraer, H., & De Roeck, G. (2009). Continuous monitoring of the Oresund Bridge: system and data analysis. *Structure and Infrastructure Engineering, 5*(5), 395–405. doi:10.1080/15732470701478362

Pejić, M. (2013). Design and optimisation of laser scanning for tunnels geometry inspection. *Tunnelling and Underground Space Technology, 37*, 199–206. doi:10.1016/j.tust.2013.04.004

Pfeifer, N., & Briese, C. (2007b). Laser scanning - Principles and applications. *GeoSiberia 2007*.

Psimoulis, P. A., & Stiros, S. C. (2007). Measurement of deflections and of oscillation frequencies of engineering structures using Robotic Theodolites (RTS). *Engineering Structures, 29*, 3312–3324. doi:10.1016/j.engstruct.2007.09.006

Remondino, F., Rizzi, A., Barazzetti, L., Scaioni, M., Fassi, F., Brumana, R., & Pelagotti, A. (2011). Review of Geometric and Radiometric Analyses of Paintings. *The Photogrammetric Record, 26*(136), 439–461. doi:10.1111/j.1477-9730.2011.00664.x

Rönnholm, P., Nuikka, M., Suominen, A., Salo, P., Hyyppä, H., Pöntinen, P., Haggrén, H., Vermeer, M., Puttonen, J., Hirsi, H., Kukko, A., Kaartinen, H., Hyyppä, J., & Jaakkola, A. (2009). Comparison of measurement techniques and static theory applied to concrete beam deformation. *The Photogrammetric Record, 24*(128)(December), 351–371.

Schotte, K., De Backer, H., Nuttens, T., De Wulf, A., & Van Bogaert, P. (2013). Influence of tidal level fluctuations of the River Scheldt on the precast concrete lining of the Liefkenshoek Rail Tunnel. *Tunnelling and Underground Space Technology, in preparation*.

Thomas, G., & Isaacs, R. (2011). Basic principles of lasers. *Anaesthesia and Intensive Care Medecine, 12*(12), 574–577.

TUC Rail. (2010). Antwerp: The tunnel borers for the Liefkenshoek rail tunnel. TUC Rail - Belgian Rail Engineering.

Van Bogaert, P. (2009). Recent and future railway tunnels in Belgium. In *Proc. ITA World Tunnel Conference "Safe Tunnelling for the City and the Environment"* (pp. 689–690). Budapest: Hungarian Tunnelling Association, ISBN 9789630672399.

Van Gosliga, R., Lindenbergh, R., & Pfeifer, N. (2006). Deformation analysis of a bored tunnel by means of terrestrial laser scanning. In H.-G. Maas & D. Schneider (Eds.), *ISPRS Commission V Symposium "Image Engineering and Vision Metrology"* (Vol. Volume XXX). Dresden, Germany: IAPRS Volume XXXVI, Part 5.

Yoon, J.-S., Sagong, M., Lee, J. S., & Lee, K. (2009). Feature extraction of a concrete tunnel liner from 3D laser scanning data. *NDT&E International, 42*, 97–105. doi:10.1016/j.ndteint.2008.10.001

Zogg, H.-M., & Ingensand, H. (2008). Terrestrial laser scanning for deformation monitoring - load tests on the Felsenau Viaduct (CH). In *XXIst ISPRS Congress - Technical Commission V* (Vol. XXXVII–B5). Beijing, China: The International Archives of the Photogrammetry, Remote Sensing and Spatial Information Sciences.

CHAPTER 7
AUTOMATED POINT CLOUD FILTERING AND LEVENBERG-MARQUARDT BASED CYLINDER FITTING OF LASER SCANNING DATA OF CYLINDRICAL TUNNELS

7. AUTOMATED POINT CLOUD FILTERING AND LEVENBERG-MARQUARDT BASED CYLINDER FITTING OF LASER SCANNING DATA OF CYLINDRICAL TUNNELS

Modified from Nuttens, T., Stal, C.*, Constales, D., De Backer, H., Schotte, K., & De Wulf, A. Automated point cloud filtering and Levenberg-Marquardt based cylinder fitting of laser scanning data of cylindrical tunnels. Computer-Aided Civil and Infrastructure Engineering. (Under review)*

** Timothy Nuttens and Cornelis Stal equally contributed to this article and are listed alphabetically.*

7.1. Abstract

The filtering of 3D point clouds requires specific filtering parameters, depending on the type of point cloud or application. To enhance the use of laser scanning in tunnel monitoring projects, an innovative automated filtering procedure for cylindrical tunnel point clouds based on a Levenberg-Marquardt cylinder fitting algorithm was developed. This algorithm is implemented in a Java application, together with a cross-section generating function. The application has successfully been tested on monitoring measurements in the Belgian 'Liefkenshoek Rail Link' project.

The convergence of the algorithm for all tested measurements confirms the applicability of the proposed algorithm for cylindrical point cloud filtering. Moreover, the repeatability of the described automated procedure is characterised by an experimentally based standard deviation of 0.27 to 0.31 mm, depending on the applied smoothing level. So this automated filtering procedure not only significantly reduces the processing time, the achievable standard deviations also allow detecting smaller deformations of the circular tunnel structure than with a previously developed manual filtering procedure.

7.2. Introduction

Terrestrial laser scanning is a well-known 3D data acquisition technique for various applications, where acquisition speed and high point accuracy are indispensable. More and more, this measurement technique is applied in the field of civil engineering, e.g. for the monitoring of tunnel profiles (Delaloye et al., 2011; Han et al., 2013b; He, Wu, Kojima, & Asakura, 2009; Park, Lee, Adeli, & Lee, 2007; van Gosliga et al., 2006; Yoon et al., 2009). The use of TLS is an innovative measurement technique to meet the growing need for 3D data to perform a thorough risk assessment (Barpi & Peila, 2012; Bizjak & Petkovsek, 2004; Büyüköztürk, 1998; Lindenbergh & Pfeifer, 2005; Soyoz & Feng, 2009; Špačková & Straub, 2013). A terrestrial laser scanner is able to measure millions of points in a very limited timeframe and by combining the measured distance between the instrument and a reflection point on the object with the corresponding horizontal and vertical angles, accurate

3D coordinates are determined. The distances can be calculated by registering the travelling time between the emission of an electromagnetic pulse and its echo or by registering the phase delay between the emitted and reflected laser beam. The performance of pulse-based and phase-based laser scanners and the achievable accuracies in tunnel projects are extensively discussed in chapter 2 (Delaloye et al., 2011; Gonzalez-Jorge, Solla, Armesto, & Arias, 2012; Lague et al., 2013; Lindenbergh et al., 2005).

This terrestrial laser scanning measurement technique improves the performance of monitoring measurements in comparison with conventional techniques, like a total station (Gómez-García-Bermejo, Zalama, & Feliz, 2013; Lee & Park, 2011). However, the processing of the large amounts of points is still a challenge, but various new methodologies and algorithms to handle large points sets or to automate the processing of point clouds are being developed (González et al., 2012; Han et al., 2013a; Iyer et al., 2005; Rabbani, Dijkman, van den Heuvel, & Vosselman, 2007; Rabbani & van den Heuvel, 2005; Rahayem et al., 2012; Teza et al., 2009; Walsh et al., 2013). The recently developed algorithms to automate the processing of the point clouds mostly focus on specific types of data sets or specific applications. For example, terrestrial laser scanning applications for tunnels require a full 3D approach, whereas a 2.5D approach is often sufficient for airborne laser scanning applications. This makes the filtering procedures of terrestrial laser scanning data more complex, due to the increased dimensional complexity. Moreover, the 'smart filtering' of point clouds by deleting only the points that are irrelevant and keeping the high detail in the relevant parts of the point cloud requires specific filtering parameters.

To further enhance the use of laser scanning in tunnel projects, an innovative automated filtering procedure for cylindrical tunnel point clouds, combined with a cylinder fitting algorithm based on the Levenberg-Marquardt algorithm was implemented. The automated procedure described in this chapter enhances the earlier developed methodology (see chapter 3) for processing point clouds from newly constructed tunnel sections, which contains a manual filtering step. The filtering procedure is implemented in a Java application, together with a cross-section generating function, so that the deliverables are immediately usable for comparison with the design shape of the tunnel or with previous measurements of the same tunnel section.

The following sections detail this automated procedure and assesses its performance. The assessment is based on monitoring measurements from the most recent railway tunnelling project in Belgium ('Liefkenshoek Rail Link' project) and a comparison of manually processed results of the same measurements. The next section gives an introduction on the 'Liefkenshoek Rail Link' project and the measurement conditions. After that, the Levenberg-Marquardt algorithm is explained, including the implementation of this algorithm in the newly developed point cloud filtering procedure for cylindrical tunnels. The following section discusses the processing results and the comparison with the same but manually processed point clouds. At the end of this chapter, conclusions are summarised.

7.3. Monitoring measurements in the 'Liefkenshoek Rail Link' project

The 'Liefkenshoek Rail Link' project establishes a new railway connection for freight traffic between the left and right bank of the River Scheldt in the Port of Antwerp. This new railway connection has a total length of approximately 16 km, of which 6 km was constructed with two new side-by-side tunnels by two shield-driven TBM's using the mixshield method (Van Bogaert, 2009) (Figure 7-1).

The two newly drilled tunnels have an inside diameter of 7.300 m, consisting of concrete tunnel segments with a thickness of 0.400 m. The longitudinal size of each tunnel section is 1.800 m and each tunnel section is made of seven concrete segments and one smaller closing stone (TUC Rail, 2010). In each tunnel tube ('Tunnel North' and 'Tunnel South'), fourteen tunnel sections were selected to be monitored using terrestrial laser scanning.

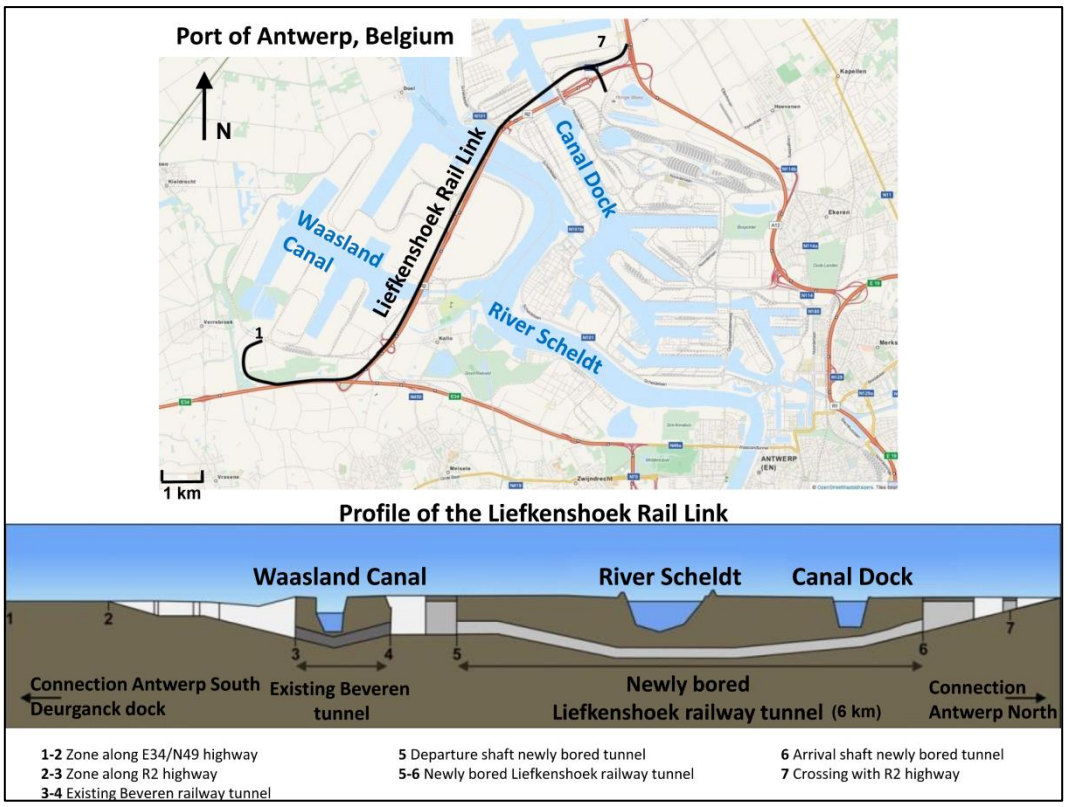

Figure 7-1: Overview and profile of the 'Liefkenshoek Rail Link' project, Antwerp, Belgium (based on CEI - De Meyer nv, 2012; openstreetmap.org; maps.google.be, October 2, 2013)

In this tunnel project, seven moments in time were defined on which the selected tunnel sections had to be measured: the 'reference measurement' immediately after construction of the tunnel section; a measurement every week during the first month after placement ('control measurement 1 to 4') and measurements two and three months after placement ('control measurement 5 and 6'). From each measurement, a cross-section through a fixed point on the tunnel surface was determined. The position of this fixed point was materialised with a circular black-and-white reference marker, easily identifiable in the point cloud by the high local intensity differences and by recognition of the shape of the target

(Pfeifer & Briese, 2007a). The cross-sections were compared with the design shape and, if applicable, also with the reference measurement and the previous control measurement of that tunnel section.

All point clouds, used for ovalisation measurements of the different sections in this project, were measured using a phase based *Leica HDS6100* laser scanner. Based on previous research in similar projects, this laser scanner, with an experimental standard deviation of 0.4 to 0.5 mm for very short distances (< 6 m), appeared very suitable for deformation measurements of tunnel sections. The raw point clouds measured with the *Leica HDS6100* laser scanner were stored as a .zfs file. This is the native binary file format for *Leica* and *Zoller&Fröhlich* laser scanners and is a closed data format for the compression of point clouds.

The previously developed manual processing methodology, as described in chapter 3, was based on the *Leica Cyclone* point processing software for the processing of the point clouds. For each measurement, this software package was used for importing the .zfs file, the manual filtering of the laser scanning data, the calculation of a best-fit cylinder on the cleaned point cloud and the generation of a cross-section. The cross-section was then further processed in a Computer Assisted Design (CAD) software package and a spreadsheet package. During the filtering process, all obstructions and points not belonging to the concrete surface of the monitored tunnel section were manually deleted, e.g. electric cables, pipes, adjacent tunnel sections, the ventilation tube, holes for the bolts in the section segments,… (Figure 7-2)

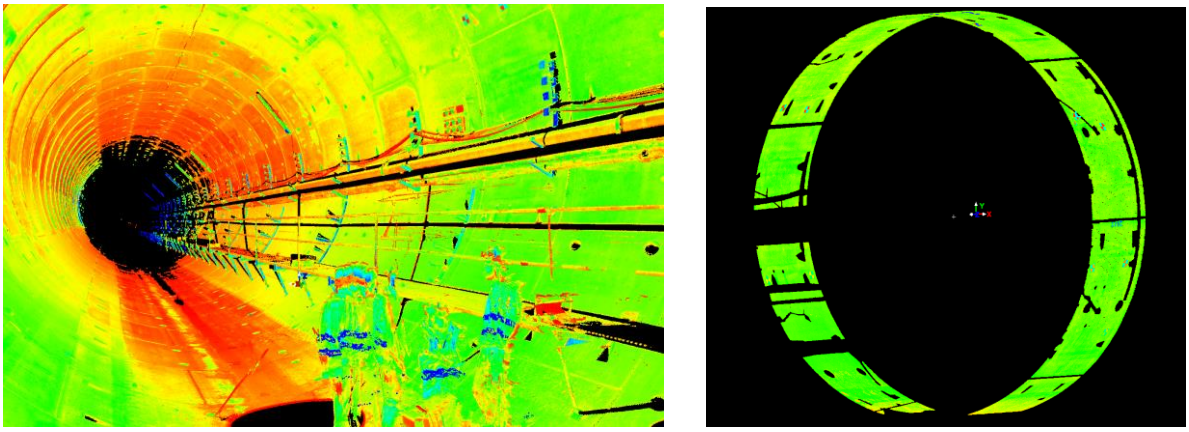

Figure 7-2: Raw point cloud (left) and manually filtered point cloud (right) ready for further processing

Although this manual procedure assures a detailed operator controlled and a high quality result, the time consuming aspect was the motivation to develop an Levenberg-Marquardt algorithm based procedure to perform an automated point filtering, cylinder fitting and cross-section generation (Stal, Nuttens, et al., 2012). The following sections describe this advanced automated filtering procedure in detail, together with a thorough assessment of the achievable results compared to the manual filtering methodology.

7.4. Automated point cloud filtering and cylinder fitting

In this research topic, the problem of filtering tunnel data can be simplified by the assumption that each tunnel section has a cylindrical shape. Even in complex 3D scenes, it is possible to automatically detect and fit these geometrical primitives and describe them by a limited number of parameters (Rusu, Marton, Blodow, & Beets, 2008). Since a cylinder is the only object that needs to be detected and modelled, the presented algorithm is based on the Levenberg-Marquardt algorithm (LMA). The parameters of the best fitting cylinder (origin, rotation matrix and cylinder radius) can be found using this algorithm, which will be implemented in an iterative way. After each iteration, the cylinder parameters are used to filter the tunnel surface and non-surface points in a 3D space. Points belonging to the surface of the cylinder will be used to estimate a new cylinder, until the threshold criterion is fulfilled.

The calculation of a cross-section through the determined centre of the reference marker and perpendicular to the longitudinal axis of the tunnel requires a correct orientation of the point cloud, as well as the calculation of the parameters of a best-fit cylinder. A solid solution was found in the use of the LMA (Marquardt, 1963), as implemented in the Apache Commons Java library (Apache Commons, 2011).

7.4.1. The Levenberg-Marquardt algorithm (LMA)

In general, the LMA is used as an optimiser for least squares problems with nonlinear multivariate functions (Lourakis, 2005). The algorithm is known to give good results for parameter estimation of a cylinder based on point clouds in a non-linear way (Rusu et al., 2008). LMA is a combination of the Gauss-Newton method (or Taylor-series method) and the steepest descent method (or gradient method). On the one hand, the Gauss-Newton method iteratively estimates the optimal cylinder parameters under the assumption of global non-linearity but local linearity by the construction of a Taylor-series. On the other hand, the steepest descent method searches for a local minimum of the cylinder parameters by iterating as a function of the negative gradient around a data point. Both methods have their disadvantages, namely the possible failure of convergence for the Gauss-Newton method and the very slow convergence for the steepest descent method (Marquardt, 1963). Their advantages, namely the speed (Gauss-Newton) and guarantee of success (steepest descent method), however, are combined in the Levenberg-Marquardt algorithm (Lourakis, 2005). The Levenberg-Marquardt algorithm is clearly explained in pseudo-code by (Shakarji, 1998).

For a given point cloud **X** with ($x_i \in R^3$), the estimation of parameter vector p of a cylinder results in a set of parameters (P = {O, A, R}). Here, O is the origin of the cylinder (O = {x_0, y_0, z_0}) , the rotation matrix A contains the direction angles (A = {θ, φ, ω}) of the cylinder and R is the cylinder radius in metre (Lourakis, 2005). The parameter vector p can be found by minimising the squared sum of distances between each point in the point set and the cylinder, which is represented by a Jacobian matrix J. This matrix also defines the objective

function, which is found by a combination of an initial parameter vector p_0 and the derivatives of each parameter. Under optimal conditions, i.e. with errorless laser scanning measurements and with a tunnel section perfectly fitting the design, the translation parameters (O) and rotation parameters (A) should be equal to zero.

Before starting the implementation of the LMA, some important assumptions and a priori conditions have to be defined, as summarised hereunder:

It has already been mentioned that the tunnel section is approximated by a cylinder. Beyond a certain difference between the design radius and the best fitting cylinder, this assumption fails and the algorithm will diverge. This is mainly caused by the imperfect construction of the tunnel. Therefore, a point cloud sequence covering more than one tunnel section in longitudinal direction cannot be approximated by one best-fit cylinder, since the tunnel itself follows a non-linear longitudinal design, which can easily be seen in the tunnel profile in Figure 7-1;

The cross-section through the master target has to be perpendicular to the longitudinal axis of the tunnel. Because the tunnel follows a non-linear longitudinal design, this cross-section is not necessarily vertical. Retaining the vertical axis as a constraint may cause elliptical shaped cross-sections;

For each local tunnel section, the X-axis is defined coinciding with the longitudinal axis of the best-fit cylinder in this automated algorithm. Translations (x_0) and rotations (ω) around this axis are not assumed and will be corrected using the master target.

7.4.2. Implementation of LMA for point cloud filtering of cylindrical tunnels

For the automated point cloud processing procedure, the original data file (.zfs) first needs to be imported in the *Leica Cyclone* processing software because of the closed data format. The *Leica Cyclone* software is used to localise the black-and-white reference marker in the point cloud and to remove a large number of points, not belonging to the 1.8 m long tunnel section. This reduces the data set from approximately 40 million points for one single scan to around 15 million points, significantly decreasing the processing time of the automated processing algorithm. It also allows accepting the above mentioned assumption about the local cylindrical shape of the point cloud for a single section, by only including the concerned tunnel section and a small area of the adjacent tunnel sections. The remaining point cloud is then exported as an ASCII file, in which each line contains the X, Y and Z coordinate of a point, as well as the intensity value of the reflected laser beam.

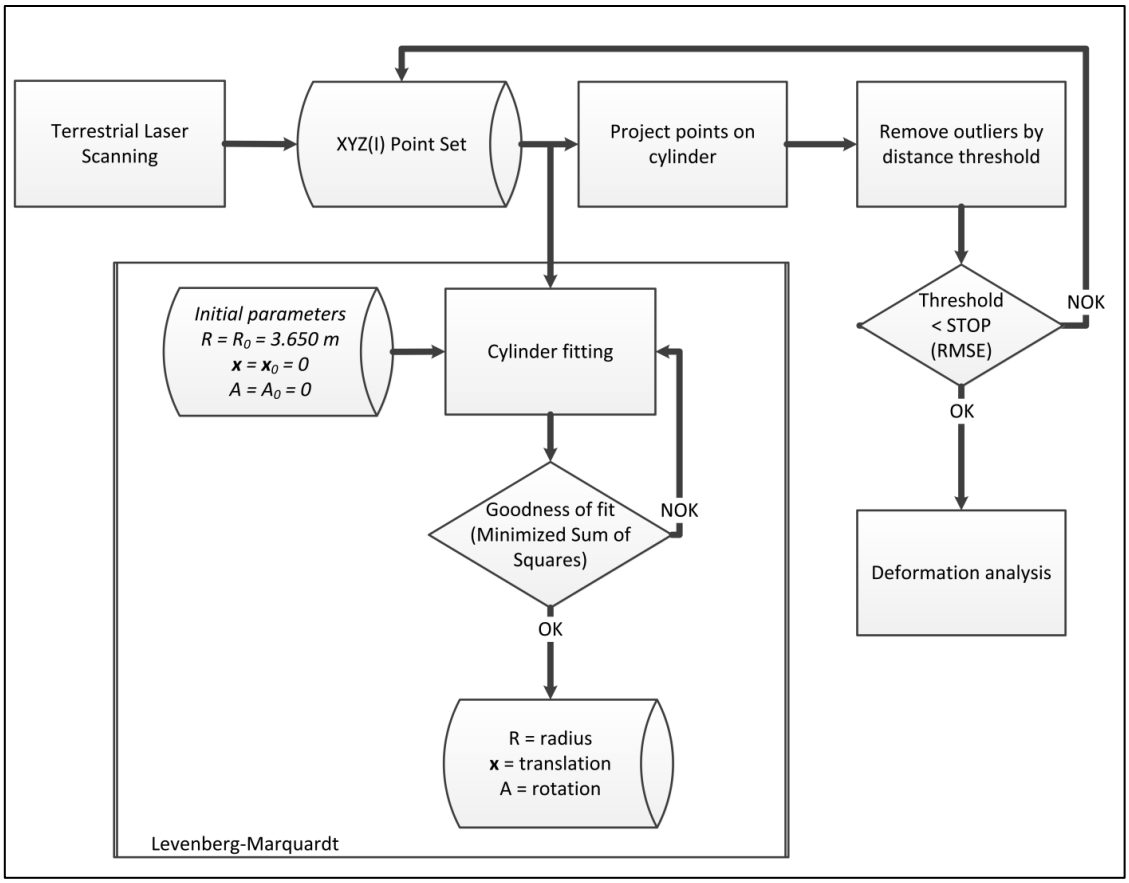

Figure 7-3: Schematic overview of the processing algorithm

This ASCII file can be imported in the Java application (Figure 7-3) in which the LMA is implemented, using the Apache Commons library (http://commons.apache.org). During each iteration, a cylinder is fitted on the point cloud and a distance based criterion is used to evaluate which points belong to the fitted cylinder. The Root Mean Square Error (RMSE) of this cylinder fitting is calculated by the root of the arithmetic mean of the square of all weighted residuals and is also used as a threshold to stop the algorithm. The residuals are the differences between the observed and the model values and they are calculated for each element of the vector-valued function.

A number of initial parameters have to be defined by the operator in the user interface:

The file name (ASCII) which contains the series of points X with $x_i = \mathbf{p_i} = \mathbf{\{x_i, y_i, z_i\}}$;

Threshold for the RMSE: the default value is experimentally set to 0.0020 m but this value can be adjusted by the operator (see further);

First guess for the radius of the fitted cylinder, in this case R = 3.6500 m (design of the tunnel);

Boolean operator to not only filter the point cloud but also to calculate a cross-section. If the cross-section has to be calculated, then the coordinates of the reference marker **M** have to be filled in (**$\mathbf{M = \{x_m, y_m, z_m\}}$**).

All points in the point cloud are loaded as separate features. The initialisation phase is finished by putting all point features in an indexed list. Even after removing points outside the tunnel section, the unfiltered tunnel section contains several million points, still making the estimation of the best fitting cylinder a relatively time consuming task. Therefore, it is opted to estimate the cylinder parameters by taking a random sample of points, containing a statistically significant number of points. This random point cloud and the parameter vector of a perfect cylinder (p_0 = {O,A,R} = {{0, 0, 0}, {0, 0, 0}, 3.65}) are used as initial parameters for the actual cylinder estimation, in order to find adjusted cylinder parameters p_{new} and to define criteria for the point removal phase.

The estimation of the best-fit cylinder algorithm itself is performed in two steps. The first step is the initialisation phase, in which the sampled point cloud and the initial parameters are assigned to a Java class where the abstract estimator object is managed. Thereafter, the best-fit cylinder is calculated by performing the Levenberg-Marquardt optimiser. In the Math module of the Apache Commons library, this optimiser is based on a differential multivariate vectorial function, using Jacobian values of the objective function. The values of this matrix are derived by numerical differentiation of the values of parameter vector p. An optimal solution for a new parameter vector p_{new} is found by minimising the values of this matrix. Further technical details about this optimiser are given by (Lourakis, 2005; Marquardt, 1963; Shakarji, 1998).

This parameter estimator will return an adjusted parameter vector p_{new}, where the translation parameters O and rotation parameters R are most likely unequal to zero. Before removing points, the entire point cloud is translated and rotated using the estimated parameter vector because it is more efficient to calculate the distance between each point and the best-fit cylinder if the axis of the cylinder is orientated along one of the axes of the coordinate system. Instead of using a sample set of the point cloud, the rotation and translation is performed on the entire point cloud. The adjusted coordinates are now centered on the origin of the new coordinate system and oriented along the longitudinal axis of the estimated cylinder. For each point, the distance to the longitudinal axis of the cylinder can be calculated. If the calculated distance deviates more than a given metrical threshold from the initial guess R = 3.65 m, this point is considered to belong to the cylinder. Otherwise, the point is removed from the point cloud. The root of the squared sum of these retained distance values results in the previously mentioned RMSE as threshold to stop the algorithm. After this removal step, the metrical threshold is reduced and the process restarts with the construction of a random point sample from the retained points and the estimation of a new best fitting cylinder, using this sample and once again parameter vector with p_0 = {O,A,R} = {{0, 0, 0}, {0, 0, 0}, 3.65}. The process iterates until the RMSE of the best fitting cylinder is lower than the predefined threshold. This value has to be found experimentally and is limited by the accuracy of the laser scanner and the correspondence of the newly built structure with the design. If the RMSE threshold is too high, the cylinder parameters, and

thus the cross-section, are based on points not belonging to the surface of the cylinder. If the RMSE threshold is too strict, the algorithm will diverge or remove too many points.

The filtered point cloud can be used for further tunnel deformation analysis, with respect to the calculated cylinder axis and design value for the tunnel radius. In order to perform this analysis, the filtered points are inserted in a kD-Tree for neighbourhood analysis. During the initialisation of the filtering process, the original coordinates of the black-and-white reference marker are inserted for the definition of the cross-section's location. As with all other points in the point cloud, these coordinates of the master target are also rotated and translated into every new coordinate system. It must be remembered that no rotations along the X-axis ($\omega = 0$) are allowed. Finally, the coordinates of the reference marker are orthogonally projected on the axis of the cylinder, resulting in the base point of the cross-section. From this base point, perpendicular to the axis of the cylinder and with a zenithal increment of 0.1 grad, 4000 hypothetical points are calculated, at a distance of 3.65 m from the base point. These points represent the local tunnel surface, according to the design. For each of those 4000 points, the five nearest points from the filtered point cloud are determined. A nearest angular distance larger than 0.5 grad on the surface of the cylinder indicates a 'no data zone' or blank area. This threshold corresponds with a Euclidean length of 28.7 mm. The mean of those 5 points results in the radius value of the measured cross-section for that 0.1 grad zenithal angle. As a result, in contrary to the manual procedure, no meshing is performed in this algorithm. The measured distance per zenithal angle is then adjusted by taking the mean of this distance and five distances left and right from this angular value (=$[R_i - 0.5$ grad; $R_i + 0.5$ grad$]$). Based on the manual processing as described in chapter 3, this smoothing level appeared to be advisable to reduce high frequency noise.

7.5. Results

7.5.1. Performance of the filtering and cylinder fitting algorithm

The automated point filtering and cylinder fitting algorithm was applied on different test data sets from a number of monitored tunnel sections. First, three consecutive control measurements of three different tunnel sections were used as test sets (A1, A2, A3; B1, B2, B3 and C1, C2, C3). Each set of three consecutive measurements has a one week or one month interval between the different measurements, according to the monitoring project schedule. Moreover, four measurements of the same tunnel section were also used as test set. These four measurements were all performed within a 15 minute time frame, during which no deformations are expected (D1, D2, D3, D4). As demonstrated in Figure 7-4 and Figure 7-5, the cylinder fitting algorithm converges to a solution after a limited number of iterations (24 to 29 iterations). The algorithm automatically stops when the RMSE of the best-fit cylinder reaches the default threshold of 2.0 mm. This threshold value has to be increased when the algorithm tends to diverge (too many points are removed) or decreased when the filtered point cloud still contains a large number of non-surface points. In the test cases, the final RMSE values vary between 1.8 mm and 2.7 mm. After the final iteration step,

the error on the calculated radius for each best-fit cylinder varies between 0.06 and 0.09 mm. The processing time for the automated filtering, cylinder fitting and cross-section generation procedure varies between 53 and 70 seconds on a powerful desktop PC (Intel® Core™ i7-3930R CPU, 3.20 GHz clock rate, 32GB RAM). The manual processing takes about 1 to 2 hours, depending on the amount of obstructions in the point cloud and the performance of the processing desktop computer. This means that the automated procedure results in a 98.1% to 99.3% time reduction.

The significant reduction of processing time is an important advantage compared to the manual processing workflow. The convergence of the algorithm for all tested measurements lets us conclude that the assumption of a cylindrical shape of the tunnel section was allowed.

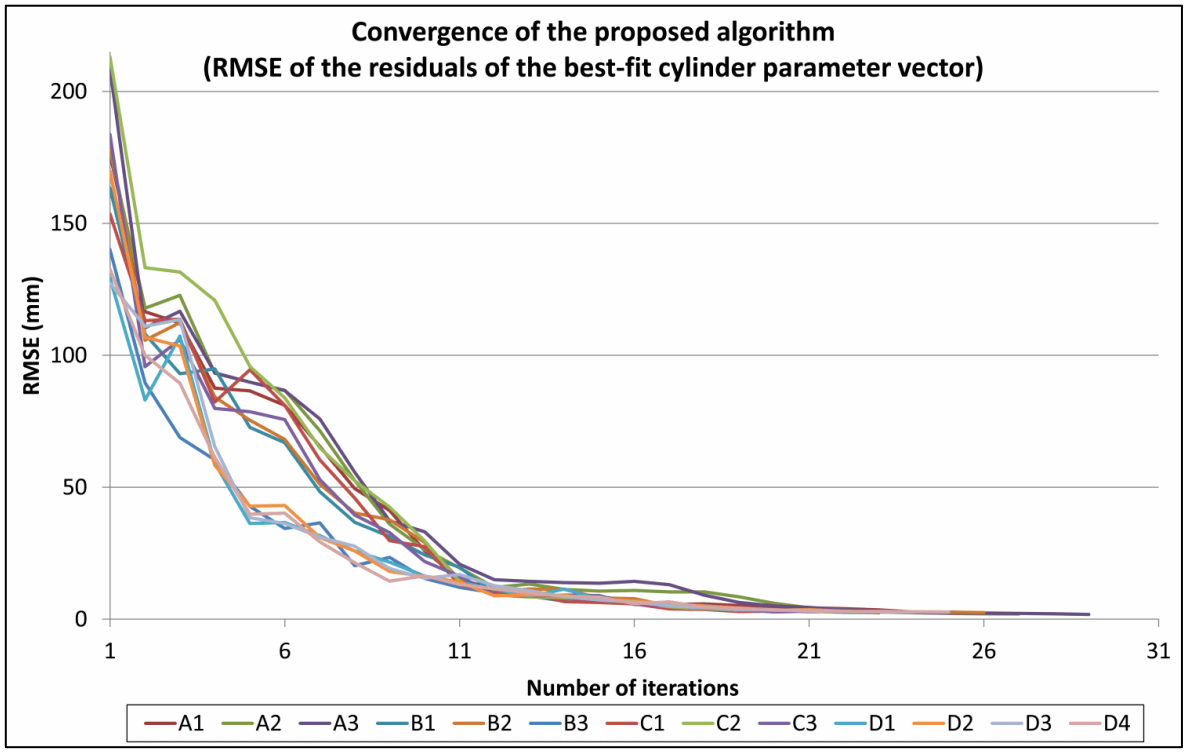

Figure 7-4: Graph of the RMSE (mm) of the best-fit cylinder parameter vector residuals

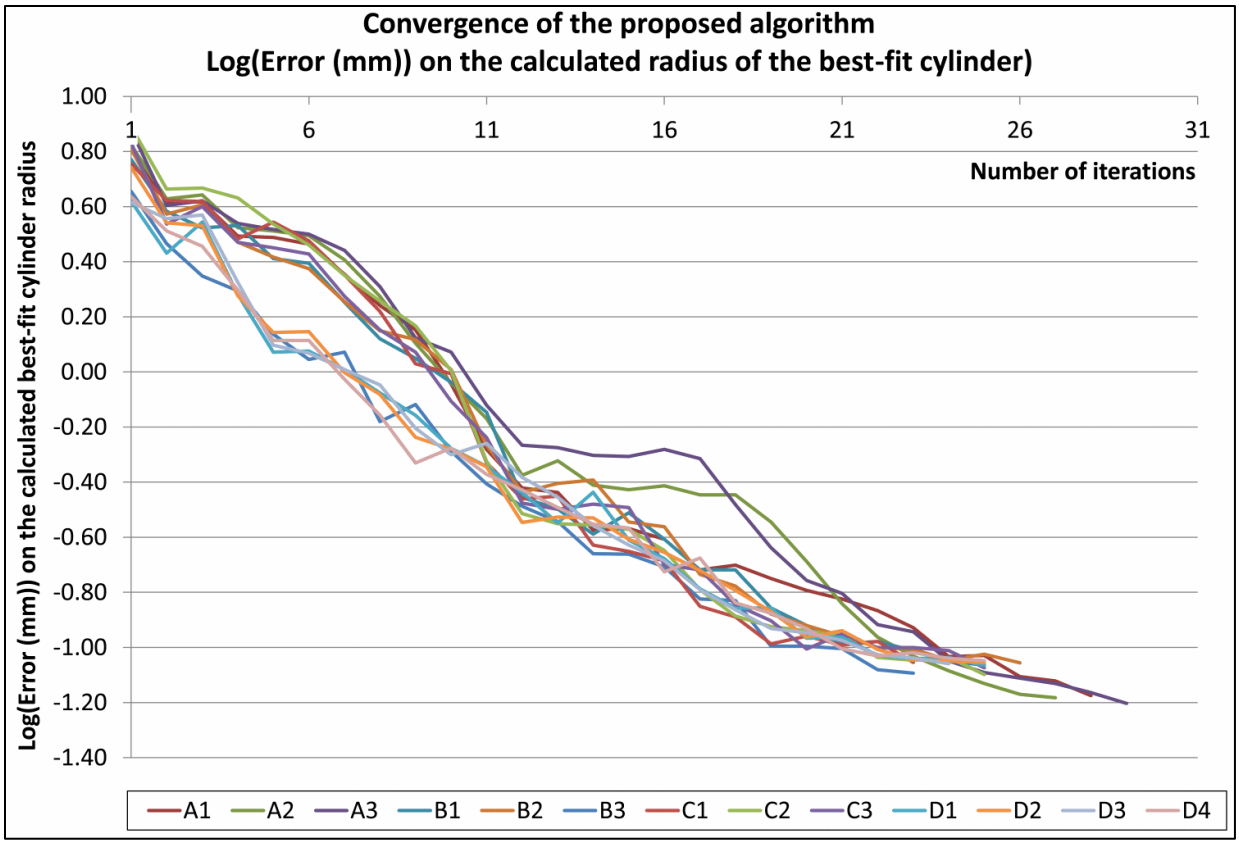

Figure 7-5: Graph of the errors (mm) on the calculated best-fit cylinder radius after each iteration step

For a comparison between the number of remaining points after filtering, the data sets resulting from the manual and automated processing of Section D can be compared. Based on those four measurements of the same section, a standard deviation of the number of remaining points after filtering can be calculated. The actual number of points is difficult to compare between both procedures, because the manually filtered point cloud is not necessarily more correct and the automatically filtered point cloud still contains points of adjacent tunnel sections in this phase. During the manual filtering, it is common for an operator to delete more points than strictly necessary to avoid any erroneous point in the filtered point cloud. For the manual procedure, the average number of remaining points after filtering is 9 755 671, with a standard deviation of 109 001 points (1.12 %). The automated procedure results in an average number of remaining points of 14 059 060, with a standard deviation of 235 313 points (1.67 %) (Figure 7-6).

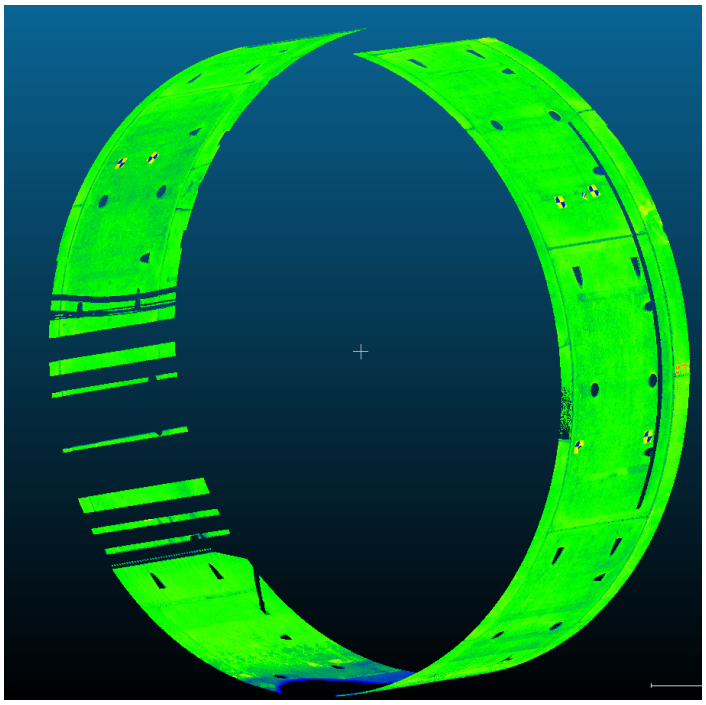

Figure 7-6: Screenshot of an automatically filtered point cloud

These filtering results give a first impression of the performance of the developed automated filtering and cylinder fitting procedure, but the following cross-section evaluations, focusing on the repeatability (experimental standard deviation) and comparison of the radius values, give a more profound assessment of the results.

7.5.2. Cross-section evaluation

As mentioned above, the filtered point cloud is used to generate a cross-section perpendicular to the axis of the cylinder and through the master target. The difference between the measured radius of the tunnel and the design is calculated for each 0.1 grad along this cross-section. These values are also compared with previously generated cross-sections of the same measurement, obtained by following the manual processing workflow. For each 0.1 grad locations where a radius value was calculated in both workflows (sample size n), the difference can be calculated. The results of this comparative study are presented in Table 7-1. Based on this table, it becomes clear that the results of the manual and automated filtering seem to be comparable, with differences below 1 mm for most tested sections. The MAE (Mean Absolute Error) is defined as:

$$\frac{1}{n}\sum_{i=1}^{n}\left|d_i - \bar{d}\right| \qquad (1)$$

and the RMSE (Root Mean Square Error) is defined as:

$$\sqrt{\frac{1}{n}\sum_{i=1}^{n}\left(d_i - \bar{d}\right)^2} \qquad (2)$$

with d_i as the difference d between the manually and automatically processed cross-section radius at a given angular index i and $\bar{d}$ as the mean difference over the entire cross-section.

The MAE is defined by the deviations from the mean difference, where the direction of the deviation is eliminated.

Table 7-1: Overview of the cross-section radius differences between manual and automated procedure (mm)

Comparison cross-sections manual vs. automated procedure				
	Mean (mm)	MAE (mm)	RMSE (mm)	Sample size n
SectionA_M1	0.31	0.55	0.76	2945
SectionA_M2	0.33	0.60	0.77	2693
SectionA_M3	0.35	0.59	0.76	2760
SectionB_M1	0.13	0.76	0.94	2798
SectionB_M2	0.25	0.96	1.15	2667
SectionB_M3	0.08	0.66	0.84	3373
SectionC_M1	-0.07	0.83	1.01	2907
SectionC_M2	-0.03	0.64	0.80	2830
SectionC_M3	-0.01	0.62	0.77	2956

In order to statistically evaluate these results, the significance of the difference between the automatically and manually filtered data sets is tested by performing a two-sided t-test (Moore et al., 2009) for all measurements. The null hypothesis (H_0) and alternative hypothesis (H_A) are set up to assess if the differences significantly differ from 0.

$$H_0: \bar{d} = 0 \qquad H_A: \bar{d} \neq 0$$

In words, the null hypothesis states that the average difference between the automatically and manually filtered cross-sections is equal to zero, in contrast to the alternative hypothesis, which states that the average difference between the two data sets is unequal to zero, based on a α = 0.05 significance level. The following statistic reformulates the null hypothesis:

$$H_0: \; t_{\left(v,\frac{\alpha}{2}\right)} \leq \frac{\bar{d}-0}{s_{\bar{d}}}\sqrt{n} \leq t_{\left(v,1-\frac{\alpha}{2}\right)} \qquad (3)$$

With v = degrees of freedom (= n-1)

α = significance level of 0.05

$\bar{d}$ = average difference (mean)

$s_{\bar{d}}$ = standard deviation of the differences (= RMSE if expected average difference is equal to zero and standard deviation is normally distributed)

n = sample size

The results of the t-test state that only for Section C2 and Section C3, the null hypothesis is not rejected at α = 0.05. So it cannot be generally concluded that there is no significant difference between the cross-sections derived from the manual and automated procedure.

Because both procedures contain a certain margin of error, none of them can be considered as the ground truth so the real shape of the tunnel section and the real radius values every 0.1 grad are not exactly known. However, there is no absolute reference to determine which method most accurately represents the true radius values of the tunnel section. Therefore, for a further evaluation of the developed automated filtering procedure, we focus on the repeatability based on the experimentally determined standard deviation and the inferred conclusions about the deformations or stability of the tunnel construction.

The calculation of an experimental standard deviation is based on the four measurements of Section D. These four measurements were performed in a very short time frame, so no deformations of this section are assumed between the four measurements. The measurements are processed according to the proposed automated procedure, so four cross-sections are generated and four radius values for every 0.1 grad are calculated. The different smoothing intervals applied for the manual procedure are also applied for this automated procedure and for all smoothing intervals, an average experimentally based standard deviation is calculated, according to the following formula.

$$\bar{s} = \sqrt{\sum_{i=1}^{N} s_i^2 / N}$$ (International Organization for Standardization, 2002) (4)

With $\bar{s}$ = average standard deviation for each instrument and each smoothing level

N = number of radius values for which a standard deviation could be calculated (max (N) = 4000)

s_i = standard deviation for each 0.1 grad, based on the four measurement of that tunnel section

The results are summarised in Table 7-2 and Table 7-3. Table 7-2 shows the experimentally determined standard deviation for both the manual and automated procedure without any further smoothing of the radius values. Table 7-3 gives an overview of the experimental standard deviations for the automated procedure over all tested smoothing levels. More detailed information about the calculation of these standard deviations and the comparison of the different smoothing levels can be found in chapter 4.

Table 7-2: Overview of the experimentally based standard deviations (mm) for the Leica HDS6100 laser scanner (1 setup) – automated vs. manual procedure with no smoothing

Experimentally based standard deviations (mm) per level of smoothing	
Laser scanner *Leica HDS6100*	**No smoothing**
Automated procedure (1 setup) (N = 3999)	0.31
Manual procedure (1 setup) (N = 2740)	0.58

* The number of observations (N) on which the standard deviations are based, are mentioned between brackets

Table 7-3: Overview of the experimentally based standard deviations (mm) for the Leica HDS6100 laser scanner (1 setup) – automated procedure for different smoothing levels

	Experimentally based standard deviations (mm) per level of smoothing				
Laser scanner *Leica HDS6100*	**No smoothing**	**[x-0.3 grad; x+0.3 grad]**	**[x-0.5 grad; x+0.5 grad]**	**[x-1.0 grad; x+1.0 grad]**	**[x-2.5 grad; x+2.5 grad]**
Automated procedure (1 setup) (N = 3999)	0.31	0.30	0.30	0.29	0.27

* The number of observations (N) on which the standard deviations are based, are mentioned between brackets

To compare the different standard deviations, a two-sided F-test is used:

$H_0: s_1^2 = s_2^2 \qquad H_A: s_1^2 \neq s_2^2$

$$\frac{1}{F_{1-\frac{\alpha}{2}}(df_1, df_2)} \leq \frac{s_1^2}{s_2^2} \leq F_{1-\frac{\alpha}{2}}(df_1, df_2) \qquad (5)$$

With α = 0.05
df = degrees of freedom of the sample (N-1)
s^2 = variance of the observations of the sample

The result of the F-test applied on the standard deviations for the manual and automated procedure without smoothing (Table 7-2) states that both standard deviations are significantly different from each other (α = 0.05). The achievable standard deviation with the automated processing of the point clouds is much lower than the standard deviation with

the manual procedure, without applying any smoothing on the radius values. This makes it possible to detect even smaller deviations during the monitoring measurements when the compared measurements are processed with the automated procedure.

When comparing the standard deviations for the different smoothing levels of the automated procedure, only the standard deviations for the [x-0.3 grad; x+0.3 grad] and [x-0.5 grad; x+0.5 grad] statistically belong to the same population (α = 0.05). However the standard deviations for the other smoothing levels appear to be significantly different from each other, the differences are relatively small (0.27 vs. 0.31 mm). This comparison leads to conclude that when using the automated procedure, applying a smoothing level on the radius values is not really indispensable because only a very small improvement in accuracy can be achieved. Moreover, as Figure 7-7 illustrates, the results without extra smoothing of the radius values of the automated procedure deliver a much smoother cross-section than the non-smoothed manual procedure or even the [x-0.5 grad; x+0.5 grad] smoothed manually processed result. So, also from the visual interpretation's point of view, no supplementary smoothing of the automated procedure results is necessary.

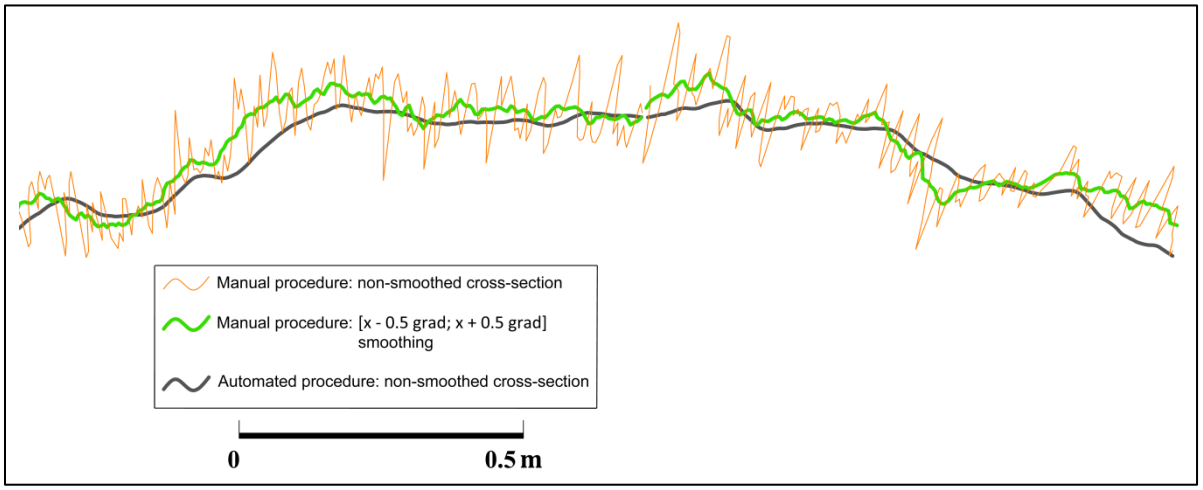

Figure 7-7: Sample of cross-sections from manual procedure (non-smoothed and [x – 0.5 grad; x + 0.5 grad] smoothing) and automated procedure (non-smoothed)

The automated procedure with the significantly lower achievable standard deviations can then, when implemented in the JAVA application, be used to assess the deformations between a series of consecutive measurements. Figure 7-8 shows an example of the deformation assessment between measurement A1 and A2, taking into account a smoothing of the calculated radius values for each cross-section over the same interval as implemented in the manual procedure ([x-0.5 grad; x+0.5 grad]). Comparing these two consecutive control measurements and considering the $2\sigma_{automated}\sqrt{2}$ = 0.85 mm criterion (95% confidence interval) lets us conclude that the structure has stabilised. In Figure 7-8, this comparison between measurement A1 and A2 is indicated with a green line (difference between the two consecutive measurements), which is located well within the 95% confidence interval (indicated by the two blue circles around the design shape of R = 3.65 m). The only small

locations where the difference exceeds the limits of the 95% confidence interval are the areas where no data points where available, such as the bottom and upper part of the tunnel section and some smaller areas at the left side where the pipes on the tunnel surface where located. On the areas where the concrete surface of the tunnel section was measured, no areas with significant deformations are detectable. Similar results are obtained when comparing the other tested consecutive measurements.

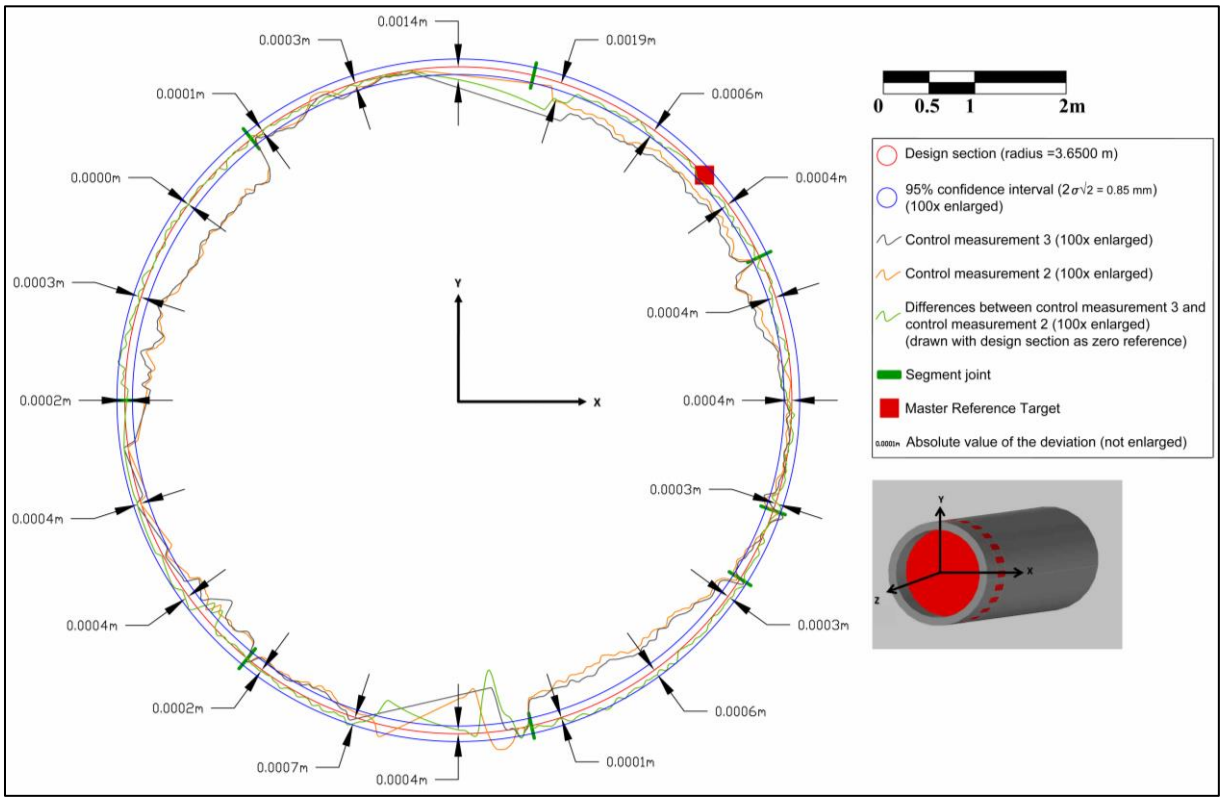

Figure 7-8: Comparison of the cross-sections of the consecutive measurements A1 and A2

7.6. Conclusions

The 'smart filtering' of 3D point clouds means that only the irrelevant points are deleted and that the highly detailed information in the relevant areas is kept. However, this requires specific filtering parameters, depending on the type of point cloud or application. To further enhance the use of laser scanning in tunnel monitoring projects, the authors developed an automated filtering procedure for cylindrical tunnel point clouds to replace a manual filtering procedure. This procedure is based on a cylinder fitting algorithm (Levenberg-Marquardt algorithm) and is implemented in a Java application, together with a cross-section generating function, so that the deliverables can immediately be compared with the design shape of the tunnel and earlier manually processed measurements. This application has been tested on monitoring measurements in the Belgian 'Liefkenshoek Rail Link' project and delivers very good results, which improve both the processing time and the achievable accuracy of the monitoring methodology.

The assessment of the usability and performance of the newly developed cylinder fitting and point cloud filtering procedure is based on different factors. The procedure significantly reduces the processing time by 98.1% to 99.3%. The convergence of the algorithm for all tested measurements confirms the applicability of the proposed algorithm for cylindrical point cloud filtering. But more importantly, the repeatability of the automated procedure is characterised by a smaller experimentally based standard deviation (0.31 mm) than the standard deviation determined for the manual procedure (0.58 mm) when applying no supplementary smoothing of the radius values. This makes it possible to detect even smaller deviations during the monitoring measurements when the compared measurements are processed with the automated procedure. Moreover, when using the automated procedure, applying a smoothing level on the radius values only results in a very small improvement of the achievable accuracy.

The successful results of the implementation of this automated procedure as part of an existing tunnel monitoring methodology significantly enhance the use of laser scanning for monitoring applications. Not only is the total processing time reduced with 98.1% to 99.3%, the automated procedure also improves the achievable standard deviation with almost 50% and, as a consequence, allows detecting smaller deformations of the circular tunnel structures.

7.7. References

Apache Commons. (2011). Commons-Math: The Apache Commons mathematics library. Retrieved January 27, 2012, from http://commons.apache.org/math/

Barpi, F., & Peila, D. (2012). Influence of the Tunnel Shape on Shotcrete Lining Stresses. *Computer-Aided Civil and Infrastructure Engineering, 27*(4), 260–275. doi:10.1111/j.1467-8667.2011.00728.x

Bizjak, K. F., & Petkovsek, B. (2004). Displacement analysis of tunnel support in soft rock around a shallow highway tunnel at Golovec. *Engineering Geology, 75*(1), 89–106. doi:10.1016/j.enggeo.2004.05.003

Büyüköztürk, O. (1998). Imaging of concrete structures. *NDT&E International, 31*(4), 233–243.

CEI - De Meyer nv. (2012). Infrabel start met de spooraanleg voor de Liefkenshoekspoorverbinding; strategisch infrastructuurproject in de Antwerpse haven zit op schema. Retrieved from www.bam.nl/pers/persberichten/infrabel-start-met-de-spooraanleg-voor-de-liefkenshoekspoorverbinding-strategisch

Delaloye, D., Hutchinson, J., & Diederichs, M. (2011). Accuracy issues associated with Lidar scanning for tunnel deformation monitoring. In *2011 Pan-Am CGS Geotechnical Conference*. Toronto, Ontario, Canada.

Gómez-García-Bermejo, J., Zalama, E., & Feliz, R. (2013). Automated Registration of 3D Scans Using Geometric Features and Normalized Color Data. *Computer-Aided Civil and Infrastructure Engineering, 28*(2), 98–111. doi:10.1111/j.1467-8667.2012.00785.x

González, M. J., Lucena, M., Fuertes, J. M., Rueda, A. J., & Segura, R. (2012). Automatic detection of unstructured elements in 3D scanned scenes. *Automation in Construction, 26*, 11–20. doi:10.1016/j.autcon.2012.05.005

Gonzalez-Jorge, H., Solla, M., Armesto, J., & Arias, P. (2012). Novel method to determine laser scanner accuracy for applications in civil engineering. *Optica Applicata, XLII*(1), 43–53. doi:10.5277/oa120104

Han, J.-Y., Guo, J., & Jiang, Y.-S. (2013a). Monitoring tunnel deformations by means of multi-epoch dispersed 3D LiDAR point clouds: An improved approach. *Tunnelling and Underground Space Technology, 38*, 385–389. doi:10.1016/j.tust.2013.07.022

Han, J.-Y., Guo, J., & Jiang, Y.-S. (2013b). Monitoring tunnel profile by means of multi-epoch dispersed 3-D LiDAR point clouds. *Tunnelling and Underground Space Technology, 33*(186-192), 186. doi:10.1016/j.tust.2012.08.008

He, W., Wu, Z., Kojima, Y., & Asakura, T. (2009). Failure Mechanism of Deformed Concrete Tunnels Subject to Diagonally Concentrated Loads. *Computer-Aided Civil and Infrastructure Engineering, 24*(6), 416–431. doi:10.1111/j.1467-8667.2009.00600.x

International Organization for Standardization. (2002). *International Standard ISO 17123-1:2002(E) Optics and optical instruments - Field procedures for testing geodetic and surveying instruments - Part 1: Theory* (p. 14).

Iyer, N., Jayanti, S., Lou, K., Kalyanaraman, Y., & Ramani, K. (2005). Three-dimensional shape searching: state-of-the-art review and future trends. *Computer-Aided Design, 37*, 509–530. doi:10.1016/j.cad.2004.07.002

Lague, D., Brodu, N., & Leroux, J. (2013). Accurate 3D comparison of complex topography with terrestrial laser scanner: Application to the Rangitikei canyon (N-Z). *ISPRS Journal of Photogrammetry and Remote Sensing, 82*, 10–26. doi:10.1016/j.isprsjprs.2013.04.009

Lee, H. M., & Park, H. S. (2011). Gage-Free Stress Estimation of a Beam-like Structure Based on Terrestrial Laser Scanning. *Computer-Aided Civil and Infrastructure Engineering, 26*(8), 647–658. doi:10.1111/j.1467-8667.2011.00723.x

Lindenbergh, R., & Pfeifer, N. (2005). A statistical deformation analysis of two epochs of terrestrial laser data of a lock. In *Optical 3-D Measurement Techniques VII*.

Lindenbergh, R., Pfeifer, N., & Rabbani, T. (2005). Accuracy analysis of the Leica HDS3000 and feasibility of tunnel deformation monitoring. In *ISPRS WG III/3-4, V/3 Workshop "Laser scanning 2005"* (Vol. 36–3/W19, pp. 24–29). Enschede, The Netherlands.

Lourakis, M. (2005). A Brief Description of the Levenberg-Marquardt Algorithm Implemented by Levmar. *Foundation of Research & Technology, Hellas*(Greece), 1–6.

maps.google.be, Oct 2, 2013

Marquardt, D. (1963). An Algorithm for Least-Square Estimation of Nonlinear Parameters. *Journal of the Society for Industrial and Applied Mathematics, 11*(2), 431–441.

Moore, D. S., McCabe, G. P., & Craig, B. A. (2009). *Introduction to the Practice of Statistics* (Sixth Edit., p. 709). New York: W. H. Freeman and Company, 41 Madison Avenue, New York, NY 10010, Houndmills, Basingstoke RG21 6XS, England.

www.openstreetmap.org, Oct 2, 2013

Park, H. S., Lee, H. M., Adeli, H., & Lee, I. (2007). A New Approach for Health Monitoring of Structures: Terrestrial Laser Scanning. *Computer-Aided Civil and Infrastructure Engineering, 22*(1), 19–30. doi:10.1111/j.1467-8667.2006.00466.x

Pfeifer, N., & Briese, C. (2007a). Geometrical Aspects of Airborne Laser Scanning and Terrestrial Laser Scanning. *International Archives of Photogrammetry and Remote Sensing, 36*(3), 311–319.

Rabbani, T., Dijkman, S., van den Heuvel, F., & Vosselman, G. (2007). An integrated approach for modelling and global registration of point clouds. *ISPRS Journal of Photogrammetry and Remote Sensing, 61*(6), 355–370. doi:10.1016/j.isprsjprs.2006.09.006

Rabbani, T., & van den Heuvel, F. (2005). Efficient Hough transform for automatic detection of cylinders in point clouds. In *ISPRS WG III/3 III/4 V/3 Workshop "Laser scanning 2005."* Enschede, The Netherlands.

Rahayem, M., Werghi, N., & Kjellander, J. (2012). Best ellipse and cylinder parameters estimation from laser profile scan sections. *Optics and Lasers in Engineering, 50*(9), 1242–1259. doi:10.1016/j.optlaseng.2012.03.014

Rusu, R., Marton, Z., Blodow, N., & Beets, M. (2008). Learning Informative Point Classes from Acquisition of Object Model Maps. In *Proceedings of the 10th International Conference on Control, Automation, Robotics and Vision (ICARCV)* (p. 6). Hanoi, Vietnam.

Shakarji, C. (1998). Least-Squares Fitting Algorithms of the NIST Algorithm Testing System. *Journal of Research of the National Institute of Standards and Technology, 103*(6), 633–641.

Soyoz, S., & Feng, M. Q. (2009). Long-Term Monitoring and Identification of Bridge Structural Parameters. *Computer-Aided Civil and Infrastructure Engineering, 24*(2), 82–92. doi:10.1111/j.1467-8667.2008.00572.x

Špačková, O., & Straub, D. (2013). Dynamic Bayesian Network for Probabilistic Modeling of Tunnel Excavation Processes. *Computer-Aided Civil and Infrastructure Engineering, 28*(1), 1–21. doi:10.1111/j.1467-8667.2012.00759.x

Stal, C., Nuttens, T., Constales, D., Schotte, K., De Backer, H., & De Wulf, A. (2012). Automatic Filtering of Terrestrial Laser Scanner Data from Cylindrical Tunnels. In FIG (Ed.), *FIG Working Week 2012 - Knowing to manage the territory, protect the environment, evaluate the cultural heritage*. Rome, Italy: FIG.

Teza, G., Galgaro, A., & Moro, F. (2009). Contactless recognition of concrete surface damage from laser scanning and curvature computation. *NDT&E International, 42*(4), 240–249. doi:10.1016/j.ndteint.2008.10.009

TUC Rail. (2010). Antwerp: The tunnel borers for the Liefkenshoek rail tunnel. TUC Rail - Belgian Rail Engineering.

Van Bogaert, P. (2009). Recent and future railway tunnels in Belgium. In *Proc. ITA World Tunnel Conference "Safe Tunnelling for the City and the Environment"* (pp. 689–690). Budapest: Hungarian Tunnelling Association, ISBN 9789630672399.

Van Gosliga, R., Lindenbergh, R., & Pfeifer, N. (2006). Deformation analysis of a bored tunnel by means of terrestrial laser scanning. In H.-G. Maas & D. Schneider (Eds.), *ISPRS Commission V Symposium "Image Engineering and Vision Metrology"* (Vol. Volume XXX). Dresden, Germany: IAPRS Volume XXXVI, Part 5.

Walsh, S. B., Borello, D. J., Guldur, B., & Hajjar, J. F. (2013). Data Processing of Point Clouds for Object Detection for Structural Engineering Applications. *Computer-Aided Civil and Infrastructure Engineering, 28*(7), 495–508. doi:10.1111/mice.12016

Yoon, J.-S., Sagong, M., Lee, J. S., & Lee, K. (2009). Feature extraction of a concrete tunnel liner from 3D laser scanning data. *NDT&E International, 42*, 97–105. doi:10.1016/j.ndteint.2008.10.001

CHAPTER 8
DISCUSSION

8. DISCUSSION

8.1. Research results

This research covered the application of static laser scanning for deformation monitoring of newly built concrete circular tunnels, from the moment of construction until several months after construction. A new methodology has been developed, tested, implemented and further optimised in two Belgian tunnel monitoring projects. Moreover, experimental standard deviations of different types of laser scanners and different smoothing levels of cross-sections have been assessed, based on the developed methodology. Another important result is the combination of laser scanning monitoring with the monitoring results from strain gauge and levelling measurements, applied in the 'Liefkenshoek Rail Link' project, to improve the knowledge about the deformation pattern of a circular tunnel structure under tidal influences. Finally, the developed methodology was further automated to reduce the processing time, resulting in an even higher achievable accuracy.

The developed methodology deliveres very good results for the deformation monitoring of circular tunnels. This methodology, containing the measurements on site, the processing of the laser scanning point clouds and the visualisation of the results, focuses on a clear and operator controlled processing workflow and unambiguously interpretable results. As mentioned in the description of the methodology, the largest part of the measurements has been processed with Leica Cyclone software although Trimble Realworks (Advanced-Modeler) software was also used, especially during the 'Diabolo' project. For the tunnel monitoring projects performed in this research, several specific criteria have influenced the choice between the wide range of available point cloud processing software packages. Besides general characteristics such as processing speed for large point clouds and "user friendliness" of the software packages, specific functionalities such as data compatibility, registration functions, meshing functions and export possibilities to a CAD compatible format are indispensable for the point cloud processing in this research. Third party software packages often lack registration and meshing functions or they are specifically designed for complex 3D modelling of objects or scenes which made them less usable for these projects' needs. Manufacturer dependent software packages, such as Trimble Realworks and Leica Cyclone, do have the required functionalities for the processing of point clouds according to the developed methodology. However, a further choice between those packages was highly dependent on the type of laser scanner being used. An incompatibility between laser scanner and software package often requires a detour via a general (ASCII) point cloud data format. This detour not only increases the processing time, in practice both software packages (the software package compatible with the laser scanner and the other one which is to be used for the further processing of the data) are needed. If both elements (laser scanner and software) do not originate from the same manufacturer, a direct import of the laser scanning data in the software is often not possible. The detour via a more general data

format, implies a first import of the original scan data in the compatible software, an export to a general data format and a (second) import of that general data format into the desired software package. Therefore, in the final configuration with the Leica HDS6100 laser scanner, it was opted to use the Leica Cyclone software for the processing of the data because of the direct compatibility between the laser scanner data format and the software and because of the fact that a comparison of the processing results with both software packages generally showed no significant results. However, if further developments in the field of laser scanning lead to the use of another type of laser scanner, the developed processing methodology can easily be implemented in other software packages.

For all monitored tunnel sections in the 'Liefkenshoek Rail Link' project, similar conclusions can be drawn. During the first week after ring assembly, when taking into account all 28 monitored sections, an average decrease in radius value of 3.3 mm is observed, resulting in an ovalised shape of the tunnel sections. This decrease can mainly be attributed to the closing of the rubber joints between the ring segments due to the large pressure of the grouting process shortly after ring assembly. After this first week after construction, little or no variation in the radius values can be observed, based on the 95% confidence interval of 1.4 mm. These results are very similar to the results of the monitoring program during the construction of the 'Diabolo' project. During the construction of the 'Diabolo' tunnel, an average decrease in radius of 2.2 mm during the first week after construction was measured, based on the twelve monitored sections. After the first week after construction of a monitored tunnel section, no more significant deformations were measured.

For a correct interpretation of these results, it is important to remark that the centre of the cross-section of each measurement is based on the centre of the best-fit cylinder, as described in the methodology. As this best-fit cylinder is determined on the filtered point cloud for each measurement, small variations may occur in its orientation, the calculated radius and its centre point. The influence of these variations on the average difference in radius is very limited but may be not neglected when considering the minimal or maximal differences. Moreover, a remark is needed considering the interpretation of the calculated average value of the tunnel radius, derived from a measured cross-section. Because the measured areas often do not cover the complete tunnel surface and because they are often not equally spread over the tunnel ring, the average radius does not necessarily represent the 'real' average radius value of the tunnel ring. If a realistic "average tunnel radius" should be computed, the ovalisation axis and the deformation pattern should be taken into account in order to compensate for the non-measured areas.

The significant deviations are determined with a 95% confidence interval based on the experimental standard deviations that were achieved with the developed methodology in combination with a specific type of laser scanner and a specific smoothing level of the cross-sections. In the 'Liefkenshoek Rail Link' project, the methodology has been applied with a Leica HDS6100 phase-based laser scanner and a cross-section smoothing level of [x-0.5 grad;

x+0.5grad], resulting in an achievable standard deviation of 0.48 mm. When comparing a measurement of a tunnel section with its design shape (a circle with a radius of 3.65 m) the 95% confidence interval is 0.96 mm. When comparing two measurements, a 95% confidence interval of 1.36 mm can be used to detect significant deformations between both epochs. The 95% confidence intervals during the 'Diabolo' project were variable because several types of laser scanners were used for these monitoring measurements, each type of laser scanner having a specific experimental standard deviation and thus another 95% confidence interval for the comparison with either the design shape or with another cross-section.

The achievable standard deviations are, especially from a surveyor's point of view, a main criterion in the choice for the most suited type of laser scanner for tunnel deformation monitoring, besides other factors such as available measurement time on site, required range of the laser scanner and field of view of the laser scanner. For the tunnel monitoring projects in this research, several characteristics and requirements had to be taken into account, leading to a choice of the best suited type of laser scanner. Because the measurements were performed in a tunnel under construction, the measurement time needed to be minimised. For a reference measurement in the front of the TBM, no vibrations were allowed, so the TBM had to be temporarily shut down. However, this downtime had to be reduced to a minimum. For the following control measurements, the laser scanner was set up in the middle of a tunnel section, blocking the work traffic from and to the TBM. Therefore, the measurement methodology foresees a measurement time of 2 hours for a reference measurement (3 scanning setups; placing of the black-and-white targets and installation and removal of the tunnel brackets included) and a measurement time of 5 to 10 minutes for a control measurement. These time limits are based on a comparison of several types of laser scanners during the monitoring projects, in which the phase-based laser scanner Leica HDS6100 delivered the best results, both with the highest scanning speed and largest field of view. The distance range of a type of laser scanner was a less critical factor in these tunnel monitoring projects, because the diameter of the tunnels is 7.3 m, falling well within the achievable range of every type of laser scanner.

Moreover, the accuracy requirement during these tunnel monitoring projects was 0.5 mm. To compare the achievable accuracy of the different tested laser scanners in the real measurement conditions, their experimental standard deviations were calculated based on *in situ* tunnel measurements. Besides the measurement accuracy of the instrument itself, the smoothing level during the processing of the cross-sections is a factor which can be optimised to improve the achievable results. This is done by finding a balance between removing high frequency noise in the data to improve the readability of the cross-section plans and keeping sufficient detail so no excessive measurements are hidden. The smoothing levels that have been tested are [x-2.5 grad; x+2.5 grad], [x-1 grad; x+1 grad], [x-0.5 grad; x+0.5 grad], [x-0.3 grad; x+0.3 grad] and no smoothing.

The choice for the Leica HDS6100 phase-based laser scanner for these tunnel monitoring projects is, besides the scanning speed and field of view of this type of laser scanner, also based on the very accurate achievable measurement results. The achievable standard deviations for this laser scanner lie between 0.34 and 0.58 mm for respectively a [x-2.5 grad; x+2.5 grad] smoothing interval and no applied smoothing, when using only 1 scanning setup (control measurements). When using multiple setups for a reference measurement in the TBM, the achievable standard deviations vary between 0.44 and 0.72 mm for respectively a [x-2.5 grad; x+2.5 grad] smoothing interval and no applied smoothing (Table 8-1). To meet the required accuracy level of 0.5 mm -even with multiple scanning positions- and to minimise the applied smoothing, it was opted to use the [x-0.5 grad; x+0.5 grad] smoothing level on the cross-section of every measurement, with matches with a smoothing over 5.7 cm on the concrete tunnel surface. The higher errors on the measurements from multiple setups can be assigned to the registration errors when combining the different point clouds and the small mismatches between the different point clouds that occur due to these registration steps in the processing.

Table 8-1: Overview of the experimentally based standard deviations for the tested scanning instruments

	Experimentally based mean standard deviations (mm) per level of smoothing				
Scanning instrument	**No smoothing**	**[x-0.3 grad; x+0.3 grad]**	**[x-0.5 grad; x+0.5 grad]**	**[x-1.0 grad; x+1.0 grad]**	**[x-2.5 grad; x+2.5 grad]**
With manual processing procedure					
Trimble S6 (2" DR300+) (1 setup) (N = 3868*)	1.28	1.27	1.25	1.19	0.99
Leica ScanStation 2 (multiple setups) (N = 2749*)	1.93	1.75	1.74	1.73	1.72
Leica C10 (1 setup) (N = 2502*)	**0.98**	**0.49**	**0.43**	**0.35**	**0.29**
Leica HDS6100 (multiple setups) (N = 2882*)	**0.72**	**0.50**	**0.48**	**0.46**	**0.44**
Leica HDS6100 (1 setup) (N = 2740*)	**0.58**	**0.40**	**0.38**	**0.36**	**0.34**
With automated filtering procedure					
Leica HDS6100 (1 setup) (N = 3999*)	**0.31**	**0.30**	**0.30**	**0.29**	**0.27**

* N = the number of observations on which the standard deviations are based

Besides the phase-based Leica HDS6100, also the pulse-based Leica C10 achieves a standard deviation of at least 0.5 mm with one scanning setup, depending on the smoothing level. When no smoothing is applied, the achievable standard deviation is 0.98 m. For the other smoothing levels, the standard deviation varies between 0.29 and 0.49 mm, for respectively [x-2.5 grad; x+2.5 grad] and [x-0.3 grad; x+0.3 grad] smoothing (Table 8-1). This instrument has not been tested for multiple scanning positions in the TBM. Notwithstanding the high

accuracy, the ten times slower scanning speed is an important disadvantage to apply this instrument for the time restricted tunnel monitoring measurements.

The developments in the field of laser scanning and measurement instruments result in a continuous release of new laser scanner models, often with a larger range or a larger scanning speed (up to 1 million points per second). As earlier stated, based on the specification sheets of surveying instruments, it is difficult to predict how these instruments will perform in *in situ* tunnel monitoring measurements compared to the other tested instruments. As for other laser scanning projects, the real performance of a scanning instrument can only be assessed after a series of field tests in real measurement conditions. However, the ranging errors on the specification sheets of the recently released laser scanners do not appear to significantly enhance the achievable accuracies (distance accuracies between 2 to 3 mm). It is also doubtful whether the higher scanning speed will significantly improve the measurement procedures for tunnel monitoring measurements, because the largest part of the measurement workflow, specifically for the reference measurements in the TBM, is the setup and removal of the tunnel brackets, the attaching of the black-and-white targets and the setups of the instrument. Reducing the actual measurement time would only have a small influence of up to 10 minutes on the total time needed for a reference measurement. For a control measurement, the time reduction would only be around 1 or 2 minutes.

In the processing of the point clouds however, further optimisation is still possible. An important enhancement to the methodology has been suggested in chapter 7. The automated processing of the data not only further improves the achievable accuracy but decimates the processing time needed thanks to the automated filtering of the point clouds. The developed automated filtering procedure for cylindrical tunnel point clouds, based on the Levenberg-Marquardt cylinder fitting algorithm, allows eliminating the manual filtering procedure in the methodology. This algorithm is implemented in a Java application and combined with a cross-section generating function, so that the deliverables can immediately be compared to the design tunnel shape or to previous measurements. The results including the implementation of this automated point cloud filtering and cylinder fitting algorithm show that the processing time for filtering the point cloud and generating the desired cross-section can be reduced by up to 99.3%, thus decimating the processing time from 1 or 2 hours to around 1 minute. This automated procedure has been tested with scanning data from the Leica HDS6100, according to the control measurement methodology by scanning a cross-section from one scanning setup in approximately the middle of the section. The experimentally based standard deviations for this instrument with the automated filtering procedure lie between 0.27 and 0.31 mm, for respectively [x-2.5 grad; x+2.5 grad] and no smoothing applied, while these values are respectively 0.34 and 0.58 mm for the manual procedure (Table 8-1). The successful development of this Levenberg-Marquardt based algorithm not only allows detecting even smaller deformation in the tunnel shape, but also defines a mathematical procedure for the filtering of the tunnel section point cloud.

Moreover, as the range of experimentally based standard deviations for the different smoothing levels shows, extra smoothing of the radius values only has a minimal effect on the achievable standard deviation, indicating the strong performance of the algorithm.

The laser scanning methodology as developed in this research, makes it possible to measure and monitor millimetre level deformations of the tunnel shape and, if further investigated, the changes in 3D position of the individual segments and of the intermediate joints. To measure the sub-millimetre deformations of the concrete segments themselves, however, laser scanning is not suited. Therefore, strain gauge measurements formed the ideal monitoring technique during the 'Diabolo' and 'Liefkenshoek Rail Link' project to be combined with laser scanning measurements.

The strain gauge measurement methodology explained in chapter 5 consists of the practical implementation of the strain gauge measurements on the concrete segments, including the selection of the most suited type of strain gauges, the placement of the strain gauges during manufacturing of the segments and during assembly of the tunnel ring and the data transfer and acquisition system. As with the laser scanning measurements, the strain recording starts immediately after the ring assembly. Because of the continuous strain recording, the results also allow clearly identifying the different loading stages of the concrete segments during the different steps in the boring process of the next rings, such as boring of the next ring, installing the ring segments, grouting, thrust forcing of the hydraulic jacks to move the TBM forward, passing of the TBM trailers over the installed ring, etc. This information is not available in the laser scanning measurements, due to the TBM trailers blocking the tunnel ring during the first hours or days after assembly. The interpretation of the strain results shows an upright ovalisation ('egg' shape) or laying ovalised shape ('pumpkin' shape) of the tunnel ring, depending on the monitored tunnel section. Especially during the 'Diabolo' project, a cylinder with the large axis parallel to the vertical axis ('egg' shape) is generally observed, which is in contrast to the expected deformation pattern. Notwithstanding the fact that the strain gauge measurements monitor the deformations on a different scale than the laser scanning measurements, the interpretations of the strain results and conclusions about the appearing ovalisation shape are corresponding to the laser scanning results for each tunnel section. Measuring the same deformation shape with the two independent measurement techniques allows concluding that the deformation models have to be modified.

The results of strain gauge and laser scanning measurements were also combined with simultaneous levelling measurements in the 'Liefkenshoek Rail Link' project to monitor the variation in height of the tunnel tubes caused by tidal variations of the River Scheldt. Each separate monitoring technique could not unambiguously evaluate the occurring twice-daily deformation pattern and could therefore not deliver an accurate risk assessment. The conclusion that the tunnel structure itself is probably moving vertically during the variation in water level of the River Scheldt is based on a combination of the stress results from the

strain gauges, with the height differences detected with levelling and the laser scanning results which clearly showed that there was no deformation in shape of the tunnel section. Although this conclusion reduces the acute risk for the durability of the tunnel structure, further measurements are necessary to locate the points around both river banks where the tunnel structure changes from the situation where it is not influenced by the tidal water level variations to the state where the twice-daily variations do occur.

The research in this dissertation contributes to the surveying engineering research, in which monitoring the stability of large infrastructural projects has been a topic for several decades. During recent years, the need for fast, high resolution and accurate 3D measurements has grown, together with the need for methods to quickly and unambiguously visualise and interpret the results. Because the application of the most suited measurement equipment and processing methodology is largely dependent on the scale and type of structure, the measurement conditions and the required accuracy, there is no uniform solution to perform deformation monitoring in the wide variety of possible applications.

For the first time in Belgium, laser scanning has been applied in the 'Diabolo' and 'Liefkenshoek Rail Link' project to monitor the tunnel constructions from the moment of assembly of the tunnel rings until several months after construction of the measured tunnel rings. Because very few systematic monitoring measurements are available during such an early stage of tunnel constructions, these data sets allow validating the mathematical engineering deformation models and comparing the actual tunnel lining behaviour with these model predictions, specifically for large diameter mixshield tunnelling in soft soil circumstances. Moreover, by including laser scanning measurements immediately after assembly of the tunnel rings, this cross-section information can be used to better interpret the deformation measurements during the following months or years of the construction's life cycle. Detected deformations in these following months or years can be assessed with regard to the shape of the tunnel section after ring assembly to evaluate if the deformations are caused by changes in stress on the tunnel construction or whether these deviations from the circular shape were already caused by a non-perfect placement of the tunnel ring segments. Besides, the highly detailed 3D image of the tunnel section -and even a larger part of the tunnel construction- allows accurately and visually determining the position of the individual segments and their intermediate joints. Based on this information, the deformations between different epochs of the individual segments can be assessed in further research, meeting the need for segmental deformation analysis (see section 9.2). The importance of a high resolution 3D recording of a larger part of the tunnel structure has also been confirmed during the 'Liefkenshoek Rail Link' project where the excavation of one of the cross-passages was recorded. An excavated cross-passage between both tunnel tubes was ready to be equipped with a pre-fabricated steel reinforcement construction when it was noticed that the steel construction did not fit the excavated cross-passage. The fast and accurate 3D recording with laser scanning proved to be indispensable to deliver a detailed

3D model of the cross-passage, instead of using a limited number of individual measured points with a total station.

The described measurement methodology in this research combines different previous research results, for example concerning the most optimal measurement positions as mentioned in (Argüelles-Fraga et al., 2013). The importance of placing the measurement instrument as close as possible to the centre of the tunnel is implemented in the measurement procedure for the control measurements. As the incidence angles increase when the instrument is placed further away from the tunnel's centre, the accuracy of the measurement is optimised when using a scanning setup as close as possible to the centre. For a reference measurement, three scanning positions are implemented, not only to cover the entire tunnel surface, but also to cover this tunnel surface with limited incidence angles. Also in the processing of the data, previous research results have been implemented to obtain the best possible results. Considering the research of (Delaloye et al., 2011), it has been opted to calculate a surface from the point cloud data to determine the deformations instead of using the individual points of the point cloud. In the automated procedure such a surface is not used, but this is compensated by calculating an average of neighbouring points around the cross-section.

Compared to other methods, the developed methodology offers a clear definition of the tunnel axis which is used to define the radius values and forthcoming deformations between different epochs. The tunnel axis is based on a best-fit cylinder on the filtered point cloud of the monitored tunnel section, either by manual filtering and cylinder fitting in point cloud processing software (i.c. Leica Cyclone) or by applying the automated filtering and Levenberg-Marquardt based cylinder fitting procedure. The methodology applied in the 'Diabolo' and 'Liefkenshoek Rail Link' projects also includes the determination of a cross-section through the triangulated surface of the point cloud of the tunnel section, instead of a cross-section based on the individual points of the point cloud.

Besides the added-value of the highly accurate results with the presented methodology, an important aspect is also the important role laser scanning results can play for the assessment of difficult or critical deformation patterns. The successful integration of results from different monitoring techniques (i.c. levelling, laser scanning and strain gauges) and the different measurement scale of these techniques during the 'Liefkenshoek Rail Link' project is an important step forward in the awareness of the relevance of an integrated monitoring strategy for large infrastructural projects and in the awareness of the valuable contributions of laser scanning point clouds.

8.2. References

Argüelles-Fraga, R., Ordonez, C., Garcia-Cortes, S., & Roca-Pardinas, J. (2013). Measurement planning for circular cross-section tunnels using terrestrial laser scanning. *Automation in Construction, 31*, 1–9. doi:10.1016/j.autcon.2012.11.023

Delaloye, D., Hutchinson, J., & Diederichs, M. (2011). Accuracy issues associated with Lidar scanning for tunnel deformation monitoring. In *2011 Pan-Am CGS Geotechnical Conference*. Toronto, Ontario, Canada.

CHAPTER 9
RESEARCH PROSPECTS

9. RESEARCH PROSPECTS

A proven key role for laser scanning in deformation assessment and an optimised and highly accurate methodology are important contributions of this research to the field of deformation monitoring, especially for tunnels. Besides these contributions, the valuable data set that has been collected during the 'Diabolo' and 'Liefkenshoek Rail Link' projects opens several further research options. As part of the rounding phase of this research, a preview on two further research topics is given below.

9.1. User self-calibration

Medium range laser scanners (1-150 m), the type of laser scanners mostly applied for monitoring in civil engineering, have a typical single point accuracy of 3 to 9 mm, a distance range error of 1 to 4 mm and an angular error of 8" to 12" (Leica Geosystems, 2009a, 2011, 2013b; Lerma Garcia et al., 2008; Trimble, n.d., 2012, 2013). Based on these already very small values, significant reductions of the instrumental errors are not very likely to be expected in the near future. However, this does not mean that we have reached the accuracy limits for monitoring or other civil engineering applications. Improvements of the achievable accuracies can still be reached by limiting environmental influences or, more importantly, by thoroughly and repeatedly calibrating the used measurement instruments.

Over the last years, the development of calibration methods and modelling the calculated systematic errors became more and more focused on test measurements in real measurement conditions and on methodologies that can be applied by the end user of the instrument (Kersten et al., 2008; Lichti et al., 2000). Through self-calibration the remaining systematic errors after the manufacturer's calibration can be reduced, possibly improving the geometric accuracy to sub-millimetre level (Chow, Teskey, & Jovse, 2011).

(Chow et al., 2012) describe two user self-calibration methods for terrestrial laser scanners. One method is a point-based self-calibration method, the other one is a geometric feature-based method. The point-based method, when for example applied in a standard room, is based on a large amount of reference markers evenly spread over all walls, floor and ceiling, measured from different scanning positions. The markers are then used to register the different point clouds, using a 3D rigid body transformation, a parametric least-squares adjustment and additional parameters to correct for axes misalignments, biases etc. Alternatively, geometric features such as planes or cylinders instead of individual points can be used for the calibration. For example, when using a plane-based calibration method, the four plane parameters are estimated while minimising the sum of squares of the residuals, instead of minimising the residuals of the tie points as in the point-based calibration method. Test results show an improvement in the geometric accuracy when one of the above mentioned calibration methods is applied, with larger advantages at longer ranges.

Further optimisation of such self-calibration methodologies still seems possible, especially for measurements near the zenith, which is important for tunnel monitoring measurements.

The point-based self-calibration, as described by (Chow et al., 2012) has been applied for Leica C10 (pulse-based) and Leica HDS6100 (phase-based) laser scanners which were used during the 'Liefkenshoek Rail Link' project. Test measurements with both types of laser scanners were performed, in collaboration with Jacky Chow (University of Calgary, Canada), from three different scanning positions in a standard office room (5 x 5 x 3 m), with 139 black-and-white targets spread over all the walls, ceiling and floor (Figure 9-1).

Figure 9-1: Setup of a laser scanner Leica C10 for a user self-calibration measurement

The computation was based on the determination of the X, Y and Z coordinates of each target for every scanning position, after which the incidence angles for each target and for each scanning position were calculated. From the coordinates, the range, the horizontal and vertical angle were computed. By applying a bundle adjustment, the three point clouds for every laser scanner setup were transformed in one common coordinate system and the residuals on the angles and on the range were calculated. Also, the incidence angles were taken into account to apply a weighting factor for the adjustment. The determined residuals can be used to apply a set of correction parameters on the measured coordinates with the tested measurement instrument to eliminate or minimise systematic errors.

These first test measurements indicate a small systematic angular error in the vertical direction for the tested Leica HDS6100, although the measured target coordinates were still more accurate than with the tested Leica C10. This is mostly due to the short distances that were measured in the relatively small office test room. An indication of a vertical angle error

can be seen in Figure 9-2, showing the vertical angles in function of the horizontal angles, with in the left example the result without correction parameters and in the right example the results after correction for the vertical angle error. Moreover, a comparison of these results with earlier tested Leica HDS6100 laser scanners by J. Chow confirms that even within a certain type of laser scanner differences occur between individual instruments of a same type.

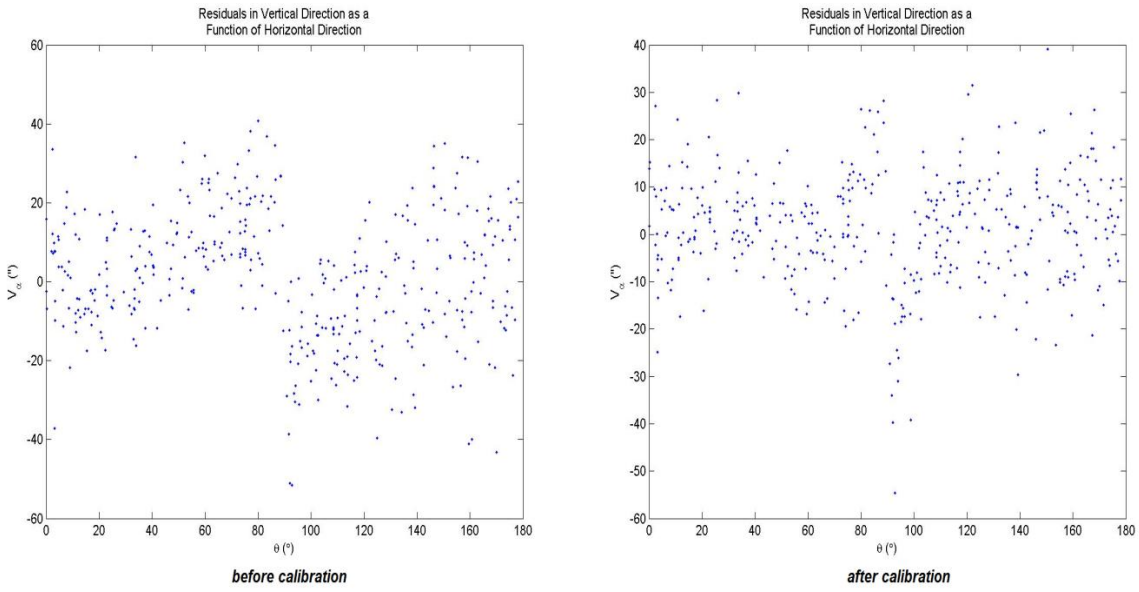

Figure 9-2: Sample of self-calibration results for the tested Leica HDS6100 laser scanner

These calibration research results strengthen the earlier formulated statement that *in situ* test measurements are indispensable to assess the achievable accuracies with individual used laser scanners. The manufacturer's specification sheets do not provide enough detailed information to assess the achievable accuracy and moreover, individual differences between fabricated instruments occur.

Further collaboration with the University of Calgary can focus on improving the applicability of the user self-calibration for tunnel measurements with reference markers on site and including adjustments for measurements near the zenith.

9.2. Monitoring of individual tunnel segments

The highly detailed and very accurate laser scanning monitoring of tunnel sections in the 'Diabolo' project and in the 'Liefkenshoek Rail Link' project resulted in a valuable and systematic data set for the monitoring of tunnel structures under real loading conditions. Moreover, because the data set covers a time span from the moment of ring assembly until several months after construction and because the laser scanning point clouds can be combined with simultaneous strain gauge measurements, new or better insights in the real deformation pattern of tunnel linings can be extracted. The methodology based on 2D cross-sections and with very low achievable standard deviations developed in this research,

already holds important steps forward in the ovalisation monitoring of tunnel structures. Notwithstanding this research progress, the measured data sets offer a lot of opportunities for further extending the knowledge on the occurring deformation patterns. Not only from a civil engineering point of view but also from a surveying point of view, fully using the information in the measured point clouds as accurately as possible opens a lot of new insights. Because very few systematic monitoring measurements are available during the early stage of tunnel constructions, the data sets that are available from this research allow validating the mathematical engineering deformation models and comparing the actual tunnel lining behaviour with these model predictions, specifically for large diameter mixshield tunnelling in soft soil circumstances. Not only do these data sets include laser scanning measurements immediately after assembly of the tunnel rings, they also include an hourly monitoring of a tunnel section under the River Scheldt (Antwerp, Belgium) during a tidal cycle, giving profound insights in tunnel ovalisation under influence of continuous water level variations.

One of the main advantages of laser scanning measurements is the almost complete and very detailed 3D recording of a large part of the tunnel structure, without limiting the measurements to specific points or dimensions of the structure. The upper and lower edges of the segments (adjacent to the other segments on the tunnel ring) are, for example, clearly visual in the point cloud. The detailed information of the tunnel rings measured with laser scanning also allows extracting information of the individual segments of a tunnel ring and how their positions change due to the different loading stages. Preliminary research results on the rotations of the individual concrete tunnel segments in the cross-section plane are already available. The research until now mainly consisted of indicating the different segments on the plans together with the locations of the segment joints and representing the best-fit segments on the plans that compare the measured cross-section with the design shape. This step in the research also investigated different mathematical functions to calculate best-fit circular segments on the determined cross-sections, resulting in a currently used slope and interception function $y=ax+b$ to determine the best-fit segments. Based on these best-fit segments on different points in time, 2D changes in position of the segments were determined (Figure 9-3 and Figure 9-4). The monitoring of the translations and rotations of the individual segments is tested, but such a systematic monitoring is currently not yet implemented in the methodology. However, the intermediate results until now show that it is certainly possible based on the developed monitoring and data processing methodology.

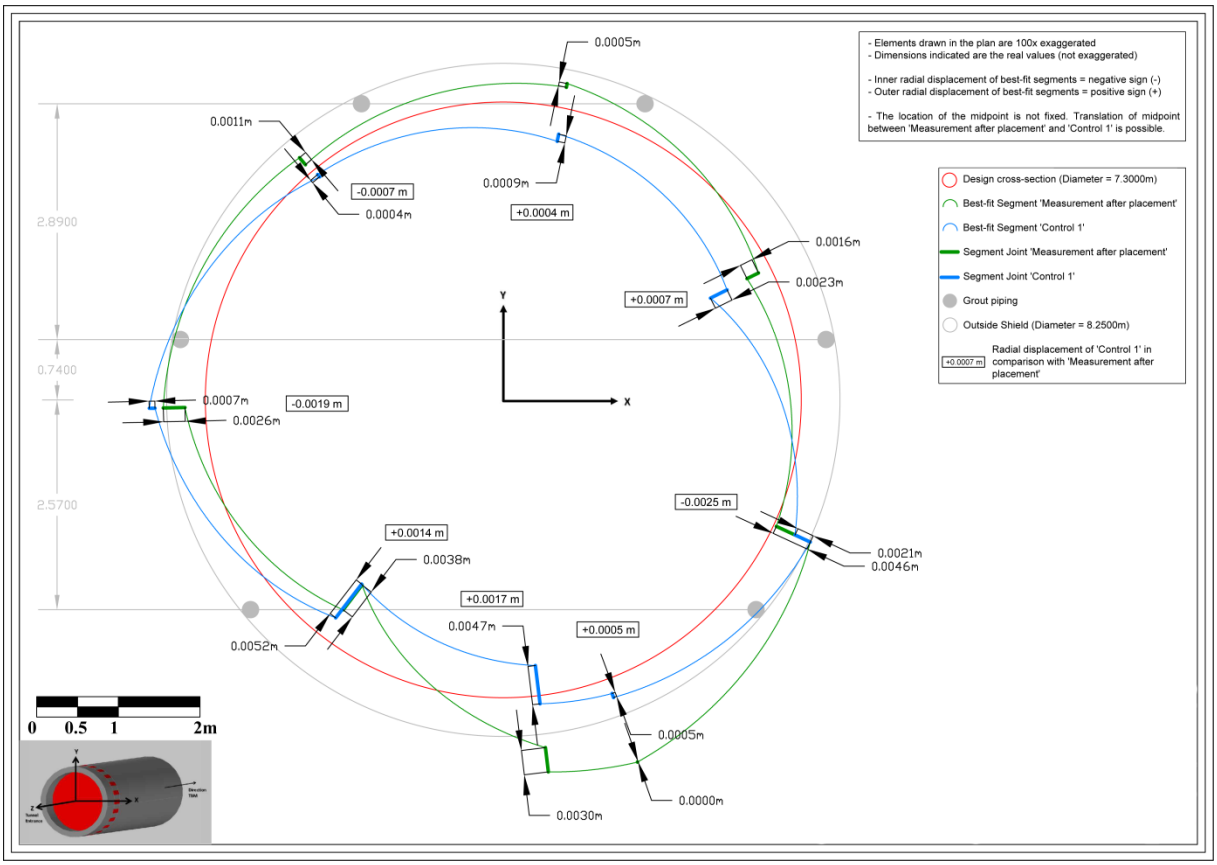

Figure 9-3: Example of segmental monitoring - differences in joints between two epochs

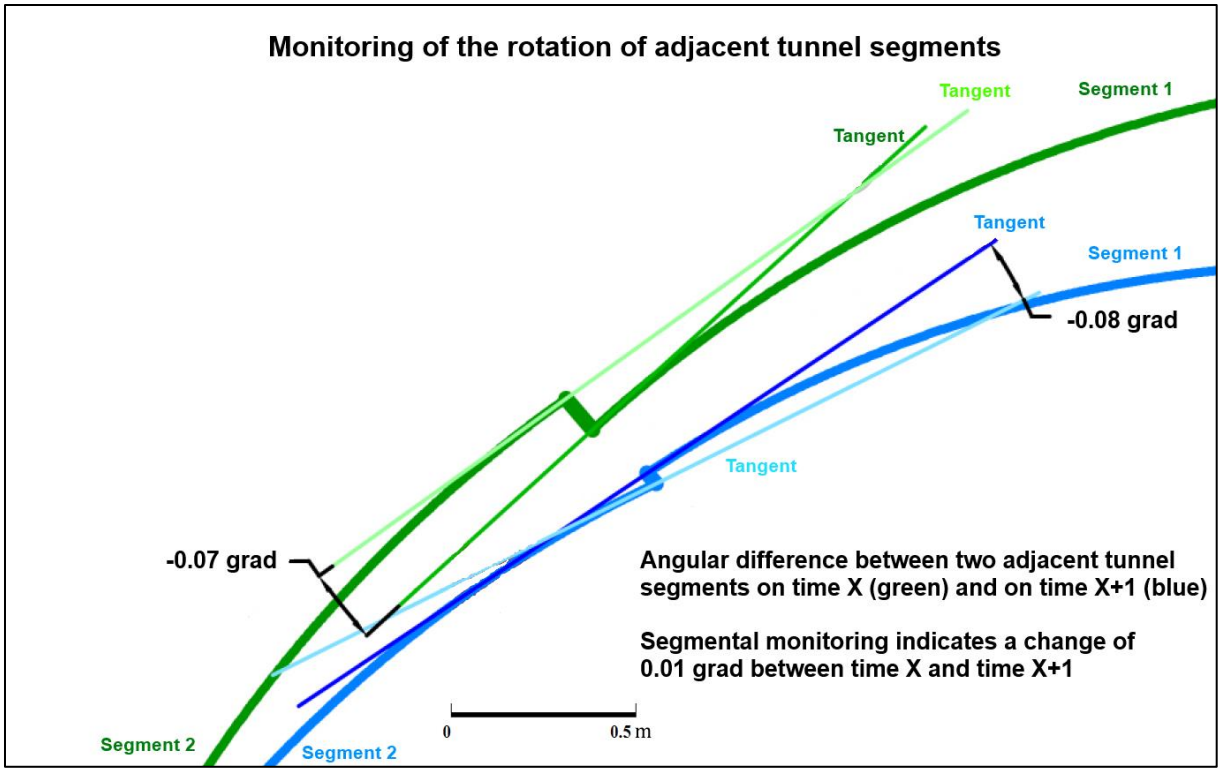

Figure 9-4: Example of the monitoring of the 2D rotation of segments between two epochs

This 2D segmental monitoring research further enhances the knowledge of real tunnel lining behaviour, because an essential part of the deformation monitoring of circular tunnels is how the segments of the tunnel rings respond to the different loading stages, especially during the construction phase when the tunnels are being drilled with a Tunnel Boring Machine (TBM) (Caratelli, Meda, Rinaldi, & Romualdi, 2011; Molins & Arnau, 2011; Teachavorasinskun & Chub-uppakarn, 2010). Further new developments in this research topic are still necessary and possible with the available 3D data sets. How the individual concrete segments react on the different loading stages can partly be measured with for example strain gauges, measuring the tensions in the concrete segments. However, to obtain the much needed detailed insights in the configuration pattern of these segments, a full 3D recording of the tunnel structure during the construction phase and of the performance of the segments in real loading conditions is indispensable. Current research in literature confirms that a 2D monitoring of tunnel segments of a specific tunnel ring (e.g. based on a single cross-section) needs to be expanded to a 3D monitoring approach, for instance due to the interaction between adjacent rings, especially in soft soil conditions (Arnau & Molins, 2012; Blom, 2002). Future research can focus on the development of a methodology for the detection, the quantification and the visualisation of the 3D displacements of the segments of the tunnel rings. Furthermore, also the movements of the segments of adjacent tunnel rings and their influence on each other can be measured based on the point cloud data. Besides the deformations in ovalisation of the tunnel rings, also the changes in segmental configuration in longitudinal direction (making the tunnel lining narrower or wider) can be determined. The results and conclusions from a 3D segmental deformation monitoring can then be evaluated and compared with the mathematical models of the expected deformation patterns and with the simultaneously performed strain gauge measurements.

9.3. References

Arnau, O., & Molins, C. (2012). Three dimensional structural response of segmental tunnel linings. *Engineering Structures, 44*, 210–221. doi:10.1016/j.engstruct.2012.06.001

Blom, C. B. M. (2002). *Design philosophy of concrete linings for tunnels in soft soils*. TU Delft.

Caratelli, A., Meda, A., Rinaldi, Z., & Romualdi, P. (2011). Structural behaviour of precast tunnel segments in fiber reinforced concrete. *Tunnelling and Underground Space Technology, 26*, 284–291. doi:10.1016/j.tust.2010.10.003

Chow, J., Lichti, D., & Teskey, W. (2012). Accuracy assessment of the FARO Focus3D and Leica HDS6100 panoramic-type terrestrial laser scanners through point-based and plane-based user self-calibration. In *FIG Working Week 2012 - Knowing to manage the territory, protect the environment, evaluate the cultural heritage* (p. 15). Rome, Italy.

Chow, J., Teskey, W., & Jovse, J. (2011). In-situ self-calibration of terrestrial laser scanners and deformation analysis using both signalized targets and intersection planes for indoor applications. In *Joint International Symposium on Deformation Monitoring*. Hong Kong, China.

Kersten, T. P., Mechelke, K., Lindstaedt, M., & Sternberg, H. (2008). Geometric Accuracy Investigations of the Latest Terrestrial Laser Scanning Systems. In *Integrating Generations - FIG Working Week 2008*. Stockholm, Sweden: FIG.

Leica Geosystems. (2009a). Leica HDS6100 Datasheet. Heerbrugg, Switzerland: Leica Geosystems AG. Retrieved from www.leica-geosystems.com/hds

Leica Geosystems. (2011). Leica ScanStation C10 Datasheet. Heerbrugg, Switzerland: Leica Geosystems AG. Retrieved from www.leica-geosystems.com/hds

Leica Geosystems. (2013b). Leica ScanStation P20 Datasheet. Heerbrugg, Switzerland: Leica Geosystems AG. Retrieved from www.leica-geosystems.com/hds

Lerma Garcia, J. L., Van Genechten, B., Heine, E., & Santana Quintero, M. (2008). *3D Risk Mapping, Theory and Practice on Terrestrial Laser Scanning. Training Material Based on Practical Applications*. Universidad Poltiecnica de Valencia, Spain.

Lichti, D. D., Stewart, M. P., Tsakiri, M., & Snow, A. J. (2000). Calibration and testing of a terrestrial laser scanner. In *International Archives of Photogrammetry and Remote Sensing (Vol. XXXII–B5).* Amsterdam, The Netherlands.

Molins, C., & Arnau, O. (2011). Experimental and analytical study of the structural response of segmental tunnel linings based on an in situ loading test. Part 1: Test configuration and execution. *Tunnelling and Underground Space Technology, 26*(6), 764–777. doi:10.1016/j.tust.2011.05.002

Teachavorasinskun, S., & Chub-uppakarn, T. (2010). Influence of segmental joints on tunnel lining. *Tunnelling and Underground Space Technology, 25*(4), 490–494. doi:10.1016/j.tust.2010.02.003

Trimble. (n.d.). Trimble FX scanner Datasheet. Trimble Navigation Limited.

Trimble. (2012). Trimble TX5 scanner Datasheet. Trimble Navigation Limited. Retrieved from www.trimble.com

Trimble. (2013). Trimble TX8 Laser scanner Datasheet. Trimble Navigation Limited. Retrieved from www.trimble.com

CHAPTER 10
CONCLUSIONS

10. CONCLUSIONS

This last chapter summarises the research that has been described in detail in the previous parts. The research questions on which this dissertation was based and the proposed answers to these questions will be recapitulated in the following paragraphs.

The starting point for this research was the question how the use of the still growing innovative 3D measurement techniques can contribute to tunnel ovalisation monitoring. This question arose from the knowledge that a thorough risk assessment of large infrastructures is very important and that the complex nature of these structures asks for a new approach to meet the need for accurate and detailed 3D information. The necessary measurements for this research were performed during the construction of twin tube tunnel complexes, both in the 'Diabolo' project (Zaventem, Belgium) and the 'Liefkenshoek Rail Link' project (Antwerp, Belgium). In order to provide a scientific contribution to the stated research problem, several more detailed research questions were formulated, each focussing on the use of laser scanning for tunnel ovalisation monitoring. The combination of the different chapters in this dissertation offers a thorough answer on each of these specific questions.

The first research question dealt with the development of a methodology to apply laser scanning for the monitoring of circular tunnels, starting from the moment of construction of a tunnel ring in the Tunnel Boring Machine (TBM) until several months after ring assembly. Based on the projects' restrictions, the methodology needed to provide an answer to the following requirements: an accuracy of 0.5 mm or higher; reference markers on every monitored tunnel section because a measurement immediately after ring assembly (reference measurement) and control measurements during the following weeks and months had to be performed; a maximal coverage of the tunnel section; limited downtime of the TBM during a reference measurement and a minimum obstruction of the site's traffic passage during control measurements. The implementation of the developed methodology, first during the 'Diabolo' project and further optimised during the 'Liefkenshoek Rail Link' project, proved that the measurement procedure, the data processing procedure and the results meet these requirements. By using three scanning positions during a reference measurement and one scanning position during a control measurement, a maximal coverage of the tunnel section is obtained and the methodology is based on several black-and-white reference markers spread over the tunnel surface. Moreover, the methodology is based on the filtering of the point cloud until only the concrete surface of the monitored tunnel section remains, a best-fit cylinder on this filtered point cloud, the meshing of the tunnel section and the generation of a cross-section of the tunnel ring through the 'Master Reference Target'. The comparison of cross-sections from subsequent moments in time for the monitoring of the ovalisation results in clearly interpretable reports and plots.

To evaluate the achievable accuracy of the developed methodology, different types of laser scanners and different smoothing levels of the cross-sections were assessed. Based on the assessment of different types of laser scanners, a phase-based laser scanner Leica HDS6100 was chosen as the most suited type of laser scanner for this monitoring application, because of the achievable experimental standard deviations of 0.34 to 0.72 mm in combination with the large field of view (360° horizontal and 310° vertical) and the high scanning speed (up to 500 000 points per second). The search for a balance between removing the high frequency noise in the data and keeping a sufficiently detailed cross-section resulted in the choice for a [x-0.5 grad; x+0.5 grad] smoothing level (a smoothing over 5.7 cm on the tunnel's cross-section), which corresponds with a standard deviation lower than 0.5 mm. The originally developed methodology contains a manual filtering step to clean up the measured point cloud. In a final phase of the research, however, this manual filtering step could be replaced by an automated point cloud filtering and cylinder fitting procedure, directly resulting in the desired cross-section for the ovalisation monitoring. This automation of the processing procedure, based on the Levenberg-Marquardt algorithm, did not only result in a significant reduction of the needed processing time but also increased the achievable standard deviations up to 0.27 mm.

The importance of the ovalisation monitoring during the 'Diabolo' and 'Liefkenshoek Rail Link' projects lies not only in the systematic measurement of several tunnel rings from the moment of assembly in the TBM until several months after construction, but also in the combination of the laser scanning measurements with simultaneous strain gauge measurements. Both measurement techniques record the impact of the different loading conditions on the tunnel structure, but on a different scale level. The strain gauge measurements allow to acquire a thorough understanding of the real-time loads acting on the individual precast concrete segments of the tunnel rings. Laser scanning mainly measures the changes in position of the segments and the influence of these changes on the ovalised shape of the tunnel ring. As for the laser scanning methodology, a methodology for the strain gauge measurements and the processing of the data was developed (by the Department of Civil Engineering - UGent), taking into account every aspect of the strain gauge installation process and the data processing.

Based on the laser scanning measurements and the strain gauge measurements, it can be concluded that significant deformations of the tunnel structure occur during the first week after ring assembly, resulting in a 'egg' or 'pumpkin' shaped tunnel ring. These deformations are mainly due to the grouting process shortly after the installation of a tunnel ring. For the laser scanning measurements, this conclusion is based on the comparison between the measured cross-section of the reference measurement and the control measurement one week after construction. Because of the continuous data logging of the strain gauges, these data give an even more detailed view on the real-time tunnel lining behaviour, including the impact of drilling the consecutive tunnel rings, pushing away of the TBM with the hydraulic jacks or installing the next tunnel ring. After the second week after construction, the laser

scanning measurements show no more significant deformations in the ovalised shape of the tunnel ring. The strain gauge measurements, however, record small changes in stress when the second TBM is passing in the adjacent tunnel ('Liefkenshoek Rail Link' project, Tunnel North) or when the cross-passages are being constructed ('Liefkenshoek Rail Link' project, Tunnel South near cross-passage 3).

As mentioned above, both the laser scanning and strain gauge measurements lead to the same general conclusion about the tunnel ovalisation. Moreover, the integration of both types of results offers new insights in complex deformation patterns. This is proven in the case study of the monitoring of a tunnel section under the River Scheldt during a tide cycle. The joint results and conclusions from the laser scanning measurements at low and high tide, the strain gauge measurements and the additional levelling measurements have led to the conclusion that the tunnel structure undergoes a vertical movement during each twice-daily tide cycle without any significant deformation of the tunnel shape itself.

Further improvements on the developed methodology have already been performed by applying the automated filtering procedure. Obtaining higher accuracies with the proposed methodology is not immediately to be expected from new measurement instruments, but can be achieved by applying a measurement instrument calibration and the resulting calibration parameters on the measurements. The developed methodology can also be used for a segment wise 2D monitoring between different epochs, based on the already derived cross-sections. But more importantly, the segment wise monitoring research can be extended to a full 3D approach by using the highly accurate and detailed point cloud information to the fullest. A further optimisation of the proposed methodology also takes into account investigating the still growing possibilities of using 3D photo modelling for accurate high resolution 3D measurements. Detecting individual segments of a tunnel structure in 3D models from different epochs could result in an alternative methodology for 3D ovalisation monitoring. Moreover, these 3D models based on high resolution images offer the possibility to monitor visually water leakages, segments joint or other parts of the tunnel.

The 'Diabolo' and 'Liefkenshoek Rail Link' project were the first large infrastructural projects in Belgium during which ovalisation monitoring with laser scanning was incorporated from the moment of construction. This opportunity was used to develop a measurement and data processing methodology which surpasses the currently described methodologies in literature, not only in the achievable accuracy and processing speed but also, for example, in the definition of the tunnel axis. Moreover, the added-value of highly accurate laser scanning data for monitoring applications has been investigated by demonstrating how the laser scanning monitoring, besides more established monitoring techniques, can offer new insights in complex deformation patterns. Moreover, the detailed and accurate 3D point clouds can be used for an even more advanced segment wise monitoring. So this research provides an answer to the question how laser scanning, as a typical example of innovative

3D measurement techniques, can be used to contribute to tunnel ovalisation monitoring. Based on the described advances in deformation monitoring with laser scanning, this research hopefully supports important steps forward in an accurate and up-to-date risk assessment of not only tunnel structures, but large infrastructural projects in general.

REFERENCES

Abellán, A., Vilaplana, J. M., Calvet, J., García-Sellés, D., & Asensio, E. (2011). Rockfall monitoring by Terrestrial Laser Scanning – case study of the basaltic rock face at Castellfollit de la Roca (Catalonia, Spain). *Natural Hazards and Earth System Science*, *11*(3), 829–841. doi:10.5194/nhess-11-829-2011

Alba, M., Fregonese, L., Prandi, F., Scaioni, M., & Valgoi, P. (2006). Structural monitoring of a large dam by terrestrial laser scanning. In H.-G. Maas & D. Schneider (Eds.), *ISPRS Commission V Symposium "Image Engineering and Vision Metrology"* (Vol. XXXVI–5). Dresden, Germany.

Alba, M., Roncoroni, F., & Scaioni, M. (2008). Investigations about the accuracy of target measurement for deformation monitoring. In *XXIst ISPRS Congress - Technical Commission V* (Vol. XXXVII–B5, pp. 1053–1060). Beijing, China: The International Archives of the Photogrammetry, Remote Sensing and Spatial Information Sciences.

Amiri Parian, J., & Grün, A. (2005). Integrated laser scanner and intensity image calibration and accuracy assessment. *The International Archives of the Photogrammetry, Remote Sensing and Spatial Information Sciences*, *XXXVI*(Part 3/W19), 18–23.

Apache Commons. (2011). Commons-Math: The Apache Commons mathematics library. Retrieved January 27, 2012, from http://commons.apache.org/math/

Argüelles-Fraga, R., Ordonez, C., Garcia-Cortes, S., & Roca-Pardinas, J. (2013). Measurement planning for circular cross-section tunnels using terrestrial laser scanning. *Automation in Construction*, *31*, 1–9. doi:10.1016/j.autcon.2012.11.023

Arnau, O., & Molins, C. (2012). Three dimensional structural response of segmental tunnel linings. *Engineering Structures*, *44*, 210–221. doi:10.1016/j.engstruct.2012.06.001

Aydin, C. (2012). On the Power of Global Test in Deformation Analysis. *Journal of Surveying Engineering*, (May 2012), 51–56. doi:10.1061/(ASCE)SU.1943-5428.0000064

Bakker, K. J., de Boer, F., Admiraal, J. B. M., & van Jaarsveld, E. P. (1999). Monitoring Pilot Projects Using Bored Tunnelling: the Second Heinenoord Tunnel and the Botlek Rail Tunnel. *Tunnelling and Underground Space Technology*, *14*(2), 121–129.

Baltsavias, E. P. (1999). A comparison between photogrammetry and laser scanning. *ISPRS Journal of Photogrammetry & Remote Sensing*, *54*, 83–94.

Barber, D., Mills, J., & Bryan, P. (2003). Towards a standard specification for terrestrial laser scanning of cultural heritage. In *CIPA International Archives for Documentation of Cultural Heritage*.

Barpi, F., & Peila, D. (2012). Influence of the Tunnel Shape on Shotcrete Lining Stresses. *Computer-Aided Civil and Infrastructure Engineering*, *27*(4), 260–275. doi:10.1111/j.1467-8667.2011.00728.x

Beraldin, J.-A., Blais, F., Boulanger, P., Cournoyer, L., Domey, J., El-Hakim, S. F., Godin, G., Rioux, M., & Taylor, J. (2000). Real world modelling through high resolution digital 3D imaging of objects and structures. *ISPRS Journal of Photogrammetry & Remote Sensing*, *55*, 230–250.

Bertacchini, E., Boni, E., Capra, A., Castagnetti, C., & Dubbini, M. (2010). Terrestrial Laser Scanner for Surveying and Monitoring Middle Age Towers. In *The XXIV FIG International Congress 2010 "Facing the Challenges - Building the Capacity."* Sydney, Australia: FIG.

Biosca, J. M., & Lerma, J. L. (2008). Unsupervised robust planar segmentation of terrestrial laser scanner point clouds based on fuzzy clustering methods. *ISPRS Journal of Photogrammetry & Remote Sensing*, *63*, 84–98. doi:10.1016/j.isprsjprs.2007.07.010

Bizjak, K. F., & Petkovsek, B. (2004). Displacement analysis of tunnel support in soft rock around a shallow highway tunnel at Golovec. *Engineering Geology*, *75*(1), 89–106. doi:10.1016/j.enggeo.2004.05.003

Blom, C. B. M. (2002). *Design philosophy of concrete linings for tunnels in soft soils*. TU Delft.

Blom, C. B. M., van der Horst, E. J., & Jovanovic, P. S. (1999). Three-dimensional Structural Analyses of the Shield-driven "Green Heart" Tunnel of the High-Speed Line South. *Tunnelling and Underground Space Technology*, *14*(2), 217–224.

Boehler, W., & Marbs, A. (2003). *Investigating Laser Scanner Accuracy*. i3Mainz, Institute for Spatial Information and Surveying Technology, FH Mainz, University of Applied Sciences, Mainz, Germany.

Boxheimer, S., & Mignon, J. (2009). Eisenbahntunnel Liefkenshoek in Antwerpen - Liefkenshoek Railway Tunnel in Antwerp. *Tunnel*, *7*, 25–31.

Boxheimer, S., & Mignon, J. (2011). Half way of construction of the Liefkenshoek Rail Tunnel. *Tunnel*, *03*(March 2011), 41–48.

Büyüköztürk, O. (1998). Imaging of concrete structures. *NDT&E International*, *31*(4), 233–243.

Caballero, D., Esteban, J., & Izquierdo, D. B. (2007). ORCHESTRA: a Unified an Open Architecture for Risk Management Applications. *Geophysical Research Abstracts*, *9*.

Caratelli, A., Meda, A., Rinaldi, Z., & Romualdi, P. (2011). Structural behaviour of precast tunnel segments in fiber reinforced concrete. *Tunnelling and Underground Space Technology*, *26*, 284–291. doi:10.1016/j.tust.2010.10.003

CEI - De Meyer nv. (2012). Infrabel start met de spooraanleg voor de Liefkenshoekspoorverbinding; strategisch infrastructuurproject in de Antwerpse haven zit op schema. Retrieved from www.bam.nl/pers/persberichten/infrabel-start-met-de-spooraanleg-voor-de-liefkenshoekspoorverbinding-strategisch

Chounta, I., & Ioannidis, C. (2012). High Accuracy Deformation Monitoring of a Concrete Beam using Automatic Photogrammetric Techniques. In *FIG Working Week 2012 - Knowing to manage the territory, protect the environment, evaluate the cultural heritage* (p. 16). Rome, Italy: FIG.

Chow, J. C. K., Lichti, D. D., & Teskey, W. (2012). Accuracy assessment of the FARO Focus3D and Leica HDS6100 panoramic-type terrestrial laser scanners through point-based and plane-based user self-calibration. In *FIG Working Week 2012 - Knowing to manage the territory, protect the environment, evaluate the cultural heritage* (p. 15). Rome, Italy.

Chow, J. C. K., Teskey, W., & Jovse, J. (2011). In-situ self-calibration of terrestrial laser scanners and deformation analysis using both signalized targets and intersection planes for indoor applications. In *Joint International Symposium on Deformation Monitoring*. Hong Kong, China.

Clarke, T. A. (1996). A review of tunnel profiling methods. Optical Metrology Centre.

Damask, J. N. (2005). *Polarization Optics in Telecommunications*. Springer Science+Business Media.

Delaloye, D., Hutchinson, J., & Diederichs, M. (2011). Accuracy issues associated with Lidar scanning for tunnel deformation monitoring. In *2011 Pan-Am CGS Geotechnical Conference*. Toronto, Ontario, Canada.

Favalli, M., Fornaciai, A., Isola, I., Tarquini, S., & Nannipieri, L. (2012). Multiview 3D reconstruction in geosciences. *Computers & Geosciences*, *44*, 168–176. doi:10.1016/j.cageo.2011.09.012

Fekete, S., Diederichs, M., & Lato, M. (2010). Geotechnical and operational applications for 3-dimensional laser scanning in drill and blast tunnels. *Tunnelling and Underground Space Technology*, *25*(5), 614–628. doi:10.1016/j.tust.2010.04.008

Fujino, Y., & Siringoringo, D. M. (2011). Bridge monitoring in Japan: the needs and strategies. *Structure and Infrastructure Engineering*, *7*(7-8), 597–611. doi:10.1080/15732479.2010.498282

Gielsdorf, F., Rietdorf, A., & Gruendig, L. (2004). A Concept for the calibration of terrestrial laser scanners. In FIG (Ed.), *Proceedings of the FIG Working Week 2004*. Athens, Greece.

Girardeau-Montaut, D., Roux, M., Marc, R., & Thibault, G. (2005). Change detection on point cloud data acquired with a ground laser scanner. In *ISPRS WG III/3-4, V/3 Workshop "Laser scanning 2005"* (Vol. 36–3/W19, pp. 30–35). Enschede, The Netherlands.

Gómez-García-Bermejo, J., Zalama, E., & Feliz, R. (2013). Automated Registration of 3D Scans Using Geometric Features and Normalized Color Data. *Computer-Aided Civil and Infrastructure Engineering*, *28*(2), 98–111. doi:10.1111/j.1467-8667.2012.00785.x

González, M. J., Lucena, M., Fuertes, J. M., Rueda, A. J., & Segura, R. (2012). Automatic detection of unstructured elements in 3D scanned scenes. *Automation in Construction*, *26*, 11–20. doi:10.1016/j.autcon.2012.05.005

Gonzalez-Jorge, H., Solla, M., Armesto, J., & Arias, P. (2012). Novel method to determine laser scanner accuracy for applications in civil engineering. *Optica Applicata*, *XLII*(1), 43–53. doi:10.5277/oa120104

Gordon, S. J., & Lichti, D. D. (2007). Modeling Terrestrial Laser Scanner Data for Precise Structural Deformation Measurement. *ASCE Journal of Surveying Engineering*, *May 2007*, 72–80. doi:10.1061/(ASCE)0733-9453(2007)133:2(72)

Gruebl, F. (2012). Segmental ring design - New challenges with high tunnel diameters. ITA-AITES Muir Wood Lecture 2012.

Grün, A., & Akca, D. (2005). Least squares 3D surface and curve matching. *ISPRS Journal of Photogrammetry & Remote Sensing*, *59*, 151–174. doi:10.1016/j.isprsjprs.2005.02.006

Haala, N., & Alshawabkeh, Y. (2006). Combining Laser scanning and Photogrammetry - A Hybrid Approach for Heritage Documentation. In *CIPA 2006*. Cyprus.

Han, J.-Y., Guo, J., & Jiang, Y.-S. (2013a). Monitoring tunnel deformations by means of multi-epoch dispersed 3D LiDAR point clouds: An improved approach. *Tunnelling and Underground Space Technology*, *38*, 385–389. doi:10.1016/j.tust.2013.07.022

Han, J.-Y., Guo, J., & Jiang, Y.-S. (2013b). Monitoring tunnel profile by means of multi-epoch dispersed 3-D LiDAR point clouds. *Tunnelling and Underground Space Technology*, *33*(186-192), 186. doi:10.1016/j.tust.2012.08.008

He, W., Wu, Z., Kojima, Y., & Asakura, T. (2009). Failure Mechanism of Deformed Concrete Tunnels Subject to Diagonally Concentrated Loads. *Computer-Aided Civil and Infrastructure Engineering*, *24*(6), 416–431. doi:10.1111/j.1467-8667.2009.00600.x

Helmerich, R., Niederleithinger, E., Trela, C., Bien, J., Kamiriski, T., & Bernardini, G. (2012). Multi-tool inspection and numerical analysis of an old masonry arch bridge. *Structure and Infrastructure Engineering*, *8*(1), 27–39.

Henriques, M. J., & Casaca, J. (2006). Uncertainty in tacheometric measurement of convergences in tunnels. In *3rd IAG / 12th FIG Symposium*. Baden, Switzerland: FIG.

Hesse, C., & Stramm, H. (2004). Deformation measurements with laser scanners. Possibilities and challenges. In *International Symposium on Modern Technologies, Education and Professional Practice in Geodesy and Related Fields* (pp. 228–240). Sofia, Bulgaria.

http://www.globalspec.com. (2013). Electromagnetic spectrum.

Huang, K.-P., Wang, T.-T., Huang, T.-H., & Jeng, F.-S. (2010). Profile deformation of a circular tunnel induced by ambient stress changes. *Tunnelling and Underground Space Technology*, *25*(3), 266–278. doi:10.1016/j.tust.2009.12.006

Infrabel. (n.d.). The Diabolo Project. Retrieved December 27, 2013, from http://www.infrabel.be/en/about-infrabel/mobility-projects/airport-railway-projects?display=normal

Infrabel. (2009). Langsdoorsnede Diabolo. *Diabolo-boorschild graaft 13 meter per dag. Danté boort eerste tunnelkoker onder start- en landingsbaan luchthaven.*

International Organization for Standardization. (2002). *International Standard ISO 17123-1:2002(E) Optics and optical instruments - Field procedures for testing geodetic and surveying instruments - Part 1: Theory* (p. 14).

Iyer, N., Jayanti, S., Lou, K., Kalyanaraman, Y., & Ramani, K. (2005). Three-dimensional shape searching: state-of-the-art review and future trends. *Computer-Aided Design*, *37*, 509–530. doi:10.1016/j.cad.2004.07.002

Jacobs, G. (2004). High Definition Surveying - 3D Laser Scanning: Understanding the "Useful Range" of Laser Scanners. *Professional Surveyor*, *24*(11).

Jacobs, G. (2005). High Definition Surveying - 3D Laser Scanning: Understanding Laser Scanning Terminology. *Professional Surveyor*, *25*(2).

Jacobs, G. (2006). 3DScanning. Understanding Spot Size for Laser Scanning. *Professional Surveyor Magazine*.

Kavvadas, M. J. (2003). Monitoring and modelling ground deformations during tunnelling. In *11th FIG Symposium on Deformation Measurements*. Santorini, Greece: FIG.

Kersten, T. P., Mechelke, K., Lindstaedt, M., & Sternberg, H. (2008). Geometric Accuracy Investigations of the Latest Terrestrial Laser Scanning Systems. In *Integrating Generations - FIG Working Week 2008*. Stockholm, Sweden: FIG.

Khoo, V. H. S., Tor, Y. K., & Ong, G. (2010). Monitoring of High Rise Building using Real-Time Differential GPS. In *The XXIV FIG International Congress 2010 "Facing the Challenges - Building the Capacity."* Sydney, Australia: FIG.

Kontogianni, V. A., & Stiros, S. C. (2005). Induced deformation during tunnel excavation: Evidence from geodetic monitoring. *Engineering Geology*, *79*(1-2), 115–126. doi:10.1016/j.enggeo.2004.10.012

Lague, D., Brodu, N., & Leroux, J. (2013). Accurate 3D comparison of complex topography with terrestrial laser scanner: Application to the Rangitikei canyon (N-Z). *ISPRS Journal of Photogrammetry and Remote Sensing*, *82*, 10–26. doi:10.1016/j.isprsjprs.2013.04.009

Lam, S. Y. W. (2006). Application of terrestrial laser scanning methodology in geometric tolerances analysis of tunnel structures. *Tunnelling and Underground Space Technology*, *21*(3-4), 410. doi:10.1016/j.tust.2005.12.057

Lee, H. M., & Park, H. S. (2011). Gage-Free Stress Estimation of a Beam-like Structure Based on Terrestrial Laser Scanning. *Computer-Aided Civil and Infrastructure Engineering*, *26*(8), 647–658. doi:10.1111/j.1467-8667.2011.00723.x

Leica Geosystems. (n.d.). Leica C10 Field of View. Leica Geosystems AG.

Leica Geosystems. (2009a). Leica HDS6100 Datasheet. Heerbrugg, Switzerland: Leica Geosystems AG. Retrieved from www.leica-geosystems.com/hds

Leica Geosystems. (2009b). Leica HDS6100 User Manual Version 2.0 English. Heerbrugg, Switzerland: Leica Geosystems AG. Retrieved from www.leica-geosystems.com

Leica Geosystems. (2011). Leica ScanStation C10 Datasheet. Heerbrugg, Switzerland: Leica Geosystems AG. Retrieved from www.leica-geosystems.com/hds

Leica Geosystems. (2013a). Leica HDS8810 Datasheet. Heerbrugg, Switzerland: Leica Geosystems AG. Retrieved from www.leica-geosystems.com

Leica Geosystems. (2013b). Leica ScanStation P20 Datasheet. Heerbrugg, Switzerland: Leica Geosystems AG. Retrieved from www.leica-geosystems.com/hds

Lerma Garcia, J. L., Van Genechten, B., Heine, E., & Santana Quintero, M. (2008). *3D Risk Mapping, Theory and Practice on Terrestrial Laser Scanning. Training Material Based on Practical Applications*. Universidad Politecnica de Valencia, Spain.

Lichti, D. D., & Chow, J. C. K. (2013). Inner Constraints for Planar Features. *The Photogrammetric Record*, *28*(141), 74–85. doi:10.1111/j.1477-9730.2012.00700.x

Lichti, D. D., Gordon, S. J., Stewart, M. P., Franke, J., & Tsakiri, M. (2002). Comparison of Digital Photogrammetry and Laser Scanning. In *Proceedings of the CIPA WG6 International Workshop on scanning for cultural heritage recording*.

Lichti, D. D., Gordon, S. J., & Tipdecho, T. (2005). Error Models and Propagation in Directly Georeferenced Terrestrial Laser Scanner Networks. *ASCE Journal of Surveying Engineering*, *November*, 135–142. doi:10.1061/(ASCE)0733-9453(2005)131:4(135)

Lichti, D. D., Stewart, M. P., Tsakiri, M., & Snow, A. J. (2000). Calibration and testing of a terrestrial laser scanner. In *International Archives of Photogrammetry and Remote Sensing* (Vol. XXXII–B5). Amsterdam, The Netherlands.

Lindenbergh, R., & Pfeifer, N. (2005). A statistical deformation analysis of two epochs of terrestrial laser data of a lock. In *Optical 3-D Measurement Techniques VII*.

Lindenbergh, R., Pfeifer, N., & Rabbani, T. (2005). Accuracy analysis of the Leica HDS3000 and feasibility of tunnel deformation monitoring. In *ISPRS WG III/3-4, V/3 Workshop "Laser scanning 2005"* (Vol. 36–3/W19, pp. 24–29). Enschede, The Netherlands.

Livieratos, E. (1992). Empiric, topographic or photogrammetric recording? Answers to properly phrased questions. In *Proceedings of "Terrestrial Photogrammetry and Geogrpahic Information Systems for the Documentation of the National Cultural Heritage."* Thessaloniki, Greece.

Lourakis, M. (2005). A Brief Description of the Levenberg-Marquardt Algorithm Implemented by Levmar. *Foundation of Research & Technology*, *Hellas*(Greece), 1–6.

Mahdevari, S., & Torabi, S. R. (2012). Prediction of tunnel convergence using Artificial Neural Networks. *Tunnelling and Underground Space Technology*, *28*, 218–228. doi:10.1016/j.tust.2011.11.002

maps.google.be, Oct 2, 2013

Marquardt, D. (1963). An Algorithm for Least-Square Estimation of Nonlinear Parameters. *Journal of the Society for Industrial and Applied Mathematics*, *11*(2), 431–441.

Mayer, R. (1999). *Scientific Canadian : invention and innovation from Canada's National Research Council*. Vancouver, Canada: Raincoast Books.

Mizoguchi, T., Koda, Y., Iwaki, I., Wakabayashi, H., Kobayashi, Y., Shirai, K., … Lee, H.-S. (2013). Quantitative scaling evaluation of concrete structures based on terrestrial laser scanning. *Automation in Construction*, *35*, 263–274. doi:10.1016/j.autcon.2013.05.022

Molins, C., & Arnau, O. (2011). Experimental and analytical study of the structural response of segmental tunnel linings based on an in situ loading test. Part 1: Test configuration and execution. *Tunnelling and Underground Space Technology*, *26*(6), 764–777. doi:10.1016/j.tust.2011.05.002

Monserrat, O., & Crosetto, M. (2008). Deformation measurements using terrestrial laser scanning data and least square 3D surface matching. *ISPRS Journal of Photogrammetry & Remote Sensing*, *63*, 142–154. doi:10.1016/j.isprsjprs.2007.07.008

Moore, D. S., McCabe, G. P., & Craig, B. A. (2009). *Introduction to the Practice of Statistics* (Sixth Edit., p. 709). New York: W. H. Freeman and Company, 41 Madison Avenue, New York, NY 10010, Houndmills, Basingstoke RG21 6XS, England.

Moosavi, M., & Khazaei, S. (2003). Absolute deformation profile measurement in tunnels using relative convergence measurements. In *Proceedings 11th FIG Symposium on Deformation Measurements*. Santorini, Greece.

Needham, J., & Dash, B. (2012). Dynamic deformation monitoring of a transmission tower undergoing failure test by close range terrestrial photogrammetry. In *FIG Working Week 2012 - Knowing to manage the territory, protect the environment, evaluate the cultural heritage* (p. 15). Rome, Italy: FIG.

Ninkov, T., Bulatovic, V., Susic, Z., & Vasic, D. (2010). Application of Laser Scanning Technology for Civil Engineering Projects in Serbia. In *The XXIV FIG International Congress 2010 "Facing the Challenges - Building the Capacity."* Sydney, Australia: FIG.

Nuttens, T., De Wulf, A., Bral, L., De Wit, B., Carlier, L., De Ryck, M., Stal, C., Constales, D., & De Backer, H. (2010). High Resolution Terrestrial Laser Scanning for Tunnel Deformation Measurements. In *The XXIV FIG International Congress 2010 "Facing the Challenges - Building the Capacity."* Sydney, Australia: FIG.

Nuttens, T., De Wulf, A., Deruyter, G., Stal, C., De Backer, H., & Schotte, K. (2012). Application of laser scanning for deformation measurements : a comparison between different types of scanning instruments . In *FIG Working Week 2012 - Knowing to manage the territory, protect the environment, evaluate the cultural heritage* (pp. 6–10). Rome, Italy: FIG.

www.openstreetmap.org, Oct 2, 2013

Park, H. S., Lee, H. M., Adeli, H., & Lee, I. (2007). A New Approach for Health Monitoring of Structures: Terrestrial Laser Scanning. *Computer-Aided Civil and Infrastructure Engineering*, *22*(1), 19–30. doi:10.1111/j.1467-8667.2006.00466.x

Peeters, B., Couvreur, G., Razinkov, O., Kündig, C., Van der Auweraer, H., & De Roeck, G. (2009). Continuous monitoring of the Oresund Bridge: system and data analysis. *Structure and Infrastructure Engineering*, *5*(5), 395–405. doi:10.1080/15732470701478362

Pejić, M. (2013). Design and optimisation of laser scanning for tunnels geometry inspection. *Tunnelling and Underground Space Technology*, *37*, 199–206. doi:10.1016/j.tust.2013.04.004

Pfeifer, N., & Briese, C. (2007a). Geometrical Aspects of Airborne Laser Scanning and Terrestrial Laser Scanning. *International Archives of Photogrammetry and Remote Sensing*, *36*(3), 311–319.

Pfeifer, N., & Briese, C. (2007b). Laser scanning - Principles and applications. *GeoSiberia 2007*.

Psimoulis, P. A., & Stiros, S. C. (2007). Measurement of deflections and of oscillation frequencies of engineering structures using Robotic Theodolites (RTS). *Engineering Structures*, *29*, 3312–3324. doi:10.1016/j.engstruct.2007.09.006

Qingwu, H., & Wanlin, Y. (2012). Tempo-space Deformation Detection of Subway Tunnel based on Sequence Temporal 3D Point Cloud. *Disaster Advances*, *5*(4).

Rabbani, T., Dijkman, S., van den Heuvel, F., & Vosselman, G. (2007). An integrated approach for modelling and global registration of point clouds. *ISPRS Journal of Photogrammetry and Remote Sensing*, *61*(6), 355–370. doi:10.1016/j.isprsjprs.2006.09.006

Rabbani, T., & van den Heuvel, F. (2005). Efficient Hough transform for automatic detection of cylinders in point clouds. In *ISPRS WG III/3 III/4 V/3 Workshop "Laser scanning 2005."* Enschede, The Netherlands.

Rahayem, M., Werghi, N., & Kjellander, J. (2012). Best ellipse and cylinder parameters estimation from laser profile scan sections. *Optics and Lasers in Engineering*, *50*(9), 1242–1259. doi:10.1016/j.optlaseng.2012.03.014

Remondino, F., Rizzi, A., Barazzetti, L., Scaioni, M., Fassi, F., Brumana, R., & Pelagotti, A. (2011). Review of Geometric and Radiometric Analyses of Paintings. *The Photogrammetric Record*, *26*(136), 439–461. doi:10.1111/j.1477-9730.2011.00664.x

Rioux, M. (1994). Digital 3-D imaging: theory and applications. In *SPIE Proceedings, Videometrics III, International Symposium on Photonic and Sensors for Controls for Commercial Applications* (pp. 2–15). Boston, USA.

Roberts, G. W., Brown, C. J., & Ogundipe, O. (2010). Monitoring Bridges by GNSS. In *The XXIV FIG International Congress 2010 "Facing the Challenges - Building the Capacity."* Sydney, Australia: FIG.

Rönnholm, P., Honkavaara, E., Litkey, P., Hyyppä, H., & Hyyppä, J. (2007). Integration of laser scanning and photogrammetry. In *ISPRS WG III/3 III/4 V/3 VIII/11 "Laser Scanning 2007 and SilviLaser 2007"* (Internatio.). Espoo, Finland: IAPRS Volume XXXVI, Part 3/W52.

Rönnholm, P., Nuikka, M., Suominen, A., Salo, P., Hyyppä, H., Pöntinen, P., Haggrén, H., Vermeer, M., Puttonen, J., Hirsi, H., Kukko, A., Kaartinen, H., Hyyppä, J., & Jaakkola, A. (2009). Comparison of measurement techniques and static theory applied to concrete beam deformation. *The Photogrammetric Record*, *24(128)*(December), 351–371.

Rusu, R., Marton, Z., Blodow, N., & Beets, M. (2008). Learning Informative Point Classes from Acquisition of Object Model Maps. In *Proceedings of the 10th International Conference on Control, Automation, Robotics and Vision (ICARCV)* (p. 6). Hanoi, Vietnam.

Rüther, H., Chazan, M., Schroeder, R., Neeser, R., Held, C., Walker, S. J., Matmon, A., & Horwitz, L. K. (2009). Laser scanning for conservation and research of African cultural heritage sites: the case study of Wonderwerk Cave, South Africa. *Journal of Archaeological Science*, *36*, 1847–1856. doi:10.1016/j.jas.2009.04.012

Schäfer, T., Weber, T., Kyrinovic, P., & Zamecnikova, M. (2004). Deformation Measurement Using Terrestrial Laser Scanning at the Hydropower Station of Gabcikovo. In *INGEO 2004 - FIG Regional Central and Eastern European Conference on Engineering Surveying*. Bratislava, Slovakia: FIG.

Schotte, K., De Backer, H., Nuttens, T., De Wulf, A., & Van Bogaert, P. (2010). Strain Gauge Measurements during the assembly of the Diabolo Tunnel. In *34th International Symposium on Bridge & Structural Engineering - IABSE Conference* (p. 8). Venice, Italy.

Schotte, K., De Backer, H., Nuttens, T., De Wulf, A., & Van Bogaert, P. (2011). Monitoring strains in the Liefkenshoek railway tunnel. In *Proceedings ITA-AITES World Tunnel Congress 2011* (pp. 254–255).

Schotte, K., De Backer, H., Nuttens, T., De Wulf, A., & Van Bogaert, P. (2013). Influence of tidal level fluctuations of the River Scheldt on the precast concrete lining of the Liefkenshoek Rail Tunnel. *Tunnelling and Underground Space Technology*, *in preparation*.

Schotte, K., De Backer, H., & Van Bogaert, P. (2011). Strain measurements in precast concrete segments of a shield-driven tunnel. In *Proceedings fib Symposium 2011* (pp. 587–590). Prague.

Schueremans, L., & Van Genechten, B. (2008). The use of 3D-laser scanning in assessing the safety of masonry vaults - A case study on the church of Saint-Jacobs. *Optics and Lasers in Engineering*, *47*, 329–335. doi:10.1016/J;optlaseng.2008.06.009

Shakarji, C. (1998). Least-Squares Fitting Algorithms of the NIST Algorithm Testing System. *Journal of Research of the National Institute of Standards and Technology*, *103*(6), 633–641.

Shan, J., & Toth, C. K. (Eds.). (2009). *Topographic Laser Ranging and Scanning*. CRC Press, Taylor & Francis Group.

Soyoz, S., & Feng, M. Q. (2009). Long-Term Monitoring and Identification of Bridge Structural Parameters. *Computer-Aided Civil and Infrastructure Engineering*, *24*(2), 82–92. doi:10.1111/j.1467-8667.2008.00572.x

Špačková, O., Šejnoha, J., & Straub, D. (2013). Probabilistic assessment of tunnel construction performance based on data. *Tunnelling and Underground Space Technology*, *37*, 62–78. doi:10.1016/j.tust.2013.02.006

Špačková, O., & Straub, D. (2013). Dynamic Bayesian Network for Probabilistic Modeling of Tunnel Excavation Processes. *Computer-Aided Civil and Infrastructure Engineering*, *28*(1), 1–21. doi:10.1111/j.1467-8667.2012.00759.x

Stal, C., De Wulf, A., De Coene, K., De Maeyer, P., Nuttens, T., & Ongena, T. (2012). Digital Representation of Historical Globes: Methods to Make 3D and Pseudo-3D Models of Sixteenth Century Mercator Globes. *The Cartographic Journal*, *49*(2), 107–117. doi:10.1179/1743277412Y.0000000002

Stal, C., Nuttens, T., Constales, D., Schotte, K., De Backer, H., & De Wulf, A. (2012). Automatic Filtering of Terrestrial Laser Scanner Data from Cylindrical Tunnels. In FIG (Ed.), *FIG Working Week 2012 - Knowing to manage the territory, protect the environment, evaluate the cultural heritage*. Rome, Italy: FIG.

Stal, C., Tack, F., De Maeyer, P., De Wulf, A., & Goossens, R. (2013). Airborne photogrammetry and LIDAR for DSM extraction and 3D change detection over an urban area: a comparative study. *International Journal of Remote Sensing*, *34*(4), 1087–1110.

Sternberg, H., & Kersten, T. P. (2007). Comparison of terrestrial laser scanning systems in industrial as-built-documentation applications. In Gruen & Kahmen (Eds.), *Optical 3-D Measurement Techniques VIII* (Vol. Vol. I, pp. 389–397). Zurich, Switzerland: Vol I.

Stiros, S. C., & Psimoulis, P. A. (2012). Response of a historical short-span railway bridge to passing trains: 3-D deflections and dominant frequencies derived from Robotic Total Station (RTS) measurements. *Engineering Structures*, *45*, 362–371. doi:10.1016/j.engstruct.2012.06.029

Tao, C. V., Chapman, M. A., & Chaplin, B. A. (2001). Automated processing of mobile mapping image sequences. *ISPRS Journal of Photogrammetry & Remote Sensing*, *55*, 330–346.

Teachavorasinskun, S., & Chub-uppakarn, T. (2010). Influence of segmental joints on tunnel lining. *Tunnelling and Underground Space Technology*, *25*(4), 490–494. doi:10.1016/j.tust.2010.02.003

Teza, G., Galgaro, A., & Moro, F. (2009). Contactless recognition of concrete surface damage from laser scanning and curvature computation. *NDT&E International*, *42*(4), 240–249. doi:10.1016/j.ndteint.2008.10.009

Thomas, G., & Isaacs, R. (2011). Basic principles of lasers. *Anaesthesia and Intensive Care Medecine*, *12*(12), 574–577.

Trimble. (n.d.). Trimble FX scanner Datasheet. Trimble Navigation Limited.

Trimble. (2012). Trimble TX5 scanner Datasheet. Trimble Navigation Limited. Retrieved from www.trimble.com

Trimble. (2013). Trimble TX8 Laser scanner Datasheet. Trimble Navigation Limited. Retrieved from www.trimble.com

TUC Rail. (2010). Antwerp: The tunnel borers for the Liefkenshoek rail tunnel. TUC Rail - Belgian Rail Engineering.

Van Bogaert, P. (2008). Le projet « Liefkenshoek » de liaison ferroviaire sous l ' Escaut. *Tunnels et Ouvrages Souterrains*, *205*(janvier / fevrier), 49–55.

Van Bogaert, P. (2009). Recent and future railway tunnels in Belgium. In *Proc. ITA World Tunnel Conference "Safe Tunnelling for the City and the Environment"* (pp. 689–690). Budapest: Hungarian Tunnelling Association, ISBN 9789630672399.

Van Bogaert, P., & De Pauw, B. (2008). New railway connection below Brussels Airport. In *Proceedings IABSE Congress 2008* (pp. 280–281). Chicago.

Van Bogaert, P., & Vereerstraeten, J.-C. (2005). Antwerp North-South railway link for a new urban development tunneling and underground techniques. In *Receuil du Congrès International de l'AFTES* (pp. 279–286).

Van Gosliga, R., Lindenbergh, R., & Pfeifer, N. (2006). Deformation analysis of a bored tunnel by means of terrestrial laser scanning. In H.-G. Maas & D. Schneider (Eds.), *ISPRS Commission V Symposium "Image Engineering and Vision Metrology"* (Vol. Volume XXX). Dresden, Germany: IAPRS Volume XXXVI, Part 5.

Walsh, S. B., Borello, D. J., Guldur, B., & Hajjar, J. F. (2013). Data Processing of Point Clouds for Object Detection for Structural Engineering Applications. *Computer-Aided Civil and Infrastructure Engineering*, *28*(7), 495–508. doi:10.1111/mice.12016

Wang, S., Wu, Z., Guo, M., & Ge, X. (2012). Theoretical solutions of a circular tunnel with the influence of axial in situ stress in elastic-brittle-plastic rock. *Tunnelling and Underground Space Technology*, *30*, 155–168. doi:10.1016/j.tust.2012.02.016

Wehr, A., & Lohr, U. (1999). Airborne laser scanning—an introduction and overview. *ISPRS Journal of Photogrammetry and Remote Sensing*, *54*(2-3), 68–82. doi:10.1016/S0924-2716(99)00011-8

Willmott, C. J., & Matsuura, K. (2005). Advantages of the mean absolute error (MAE) over the root mean square error (RMSE) in assessing average model performance. *Climate Research*, *30*, 79–82.

Yastikli, N. (2007). Documentation of cultural heritage using digital photogrammetry and laser scanning. *Journal of Cultural Heritage*, *8*, 423–427. doi:10.1016/J.culher.2007.06.003

Yoon, J.-S., Sagong, M., Lee, J. S., & Lee, K. (2009). Feature extraction of a concrete tunnel liner from 3D laser scanning data. *NDT&E International*, *42*, 97–105. doi:10.1016/j.ndteint.2008.10.001

Zeibak, R., & Filin, S. (2007). Change detection via terrestrial laser scanning. In *ISPRS WG III/3 III/4 V/3 VIII/11 "Laser Scanning 2007 and SilviLaser 2007"* (Internatio.). Espoo, Finland: IAPRS Volume XXXVI, Part 3/W52.

Zogg, H.-M., & Ingensand, H. (2008). Terrestrial laser scanning for deformation monitoring - load tests on the Felsenau Viaduct (CH). In *XXIst ISPRS Congress - Technical Commission V* (Vol. XXXVII–B5). Beijing, China: The International Archives of the Photogrammetry, Remote Sensing and Spatial Information Sciences.

CURRICULUM VITAE

Timothy Nuttens (°1985, Deinze) received his Master's degree in Geography - option Surveying in 2007 at the Department of Geography, Faculty of Sciences, Ghent University. After graduating, he started working as a surveyor in a private firm. From January 2008 until December 2013, he worked as an academic assistant staff member at the Department of Geography at Ghent University (3D Data Acquisition research group). During this time he combined his teaching activities with his PhD research dealing with laser scanning. Since January 2014, he continues his research work as a member of the research staff at the same department.

His PhD research focused on the use of high accuracy terrestrial laser scanning for deformation measurements, more specifically for the monitoring of newly built concrete circular tunnels. Timothy conducted research in different Belgian tunnelling projects to monitor the deformations of concrete elements of newly built tunnels by aims of laser scanning ('Diabolo' project, Zaventem-Brussels; 'Liefkenshoek Rail Link' project, Antwerp). Besides these research activities closely related to his PhD research, Timothy also cooperated in other projects such as topographical field campaigns on archaeological sites and photogrammetric restitution or 3D photo modelling of archaeological remnants (Titani, Greece; Malta; Urumqi, China). He presented his research on various national and international conferences and he is the (co-)author of more than 60 publications and conference proceedings on laser scanning, photogrammetry and surveying education.

LIST OF PUBLICATIONS

(A1) Articles in scientific journals included in one of the ISI Web of Science databases 'Science Citation Index', 'Social Science Citation Index' or 'Arts and Humanities Citation Index' and limited to publications of the type of: article, review, letter, note or proceedings paper

Published

Stal, C., De Wulf, A., De Coene, K., De Maeyer, P., **Nuttens, T.,** Ongena, T., (2012). Digital Representation of Historical Globes: Methods to Make 3D and Pseudo-3D Models of Sixteenth Century Mercator Globes. *The Cartographic Journal*, *Vol. 49, No. 2*, pp. 107-117, doi: 10.1179/1743277412Y.0000000002.

Schotte, K., De Backer, H., **Nuttens, T.**, De Wulf, A., Van Bogaert, P. (2013). Strain gauge measurements of the precast concrete lining of a shield-driven tunnel. *Insight, Vol. 55, No. 2*, pp. 88-95, doi: 10.1784/insi.2012.55.2.88.

Nuttens, T., Stal, C., De Backer, H., Schotte, K., Van Bogaert, P., De Wulf, A. (2014). Methodology for the ovalization monitoring of newly built circular train tunnels based on laser scanning: Liefkenshoek Rail Link (Belgium). *Automation in Construction, Vol. 43,* pp. 1-9, doi: 10.1016/j.autcon.2014.02.017.

Stal, C., Briese, C., De Maeyer, P., Dorninger P., **Nuttens, T.**, Pfeifer, N., De Wulf, A. (2014). Classification of airborne laser scanning point clouds based on binomial logistic regression analysis. *International Journal of Remote Sensing, Vol. 35, No. 9*, pp. 3219-3236, doi: 10.1080/01431161.2014.904973.

Stal, C., Van Liefferinge, K., De Reu, J., Docter, R., Dierkens, G., De Maeyer, P., Mortier, S., **Nuttens, T.**, Pieters, T., van den Eijnde, F., van de Put, W., De Wulf, A., (2014). Integrating geomatics in archaeological research at the site of Thorikos (Greece). Journal of Archaeological Science, Vol. 45, pp.112-125, doi: 10.1016/j.jas.2014.02.018.

Submitted – Under review

Nuttens, T., Stal, C., De Backer, H., Deruyter, G., Schotte, K., Van Bogaert, P., De Wulf, A. Laser scanning for ovalization measurements: standard deviations and smoothing levels (Diabolo project, Belgium). *ASCE Journal of Surveying Engineering.*

Stal, C., De Maeyer, P., De Meyer, R., Pauwels, P., **Nuttens, T.**, Verstraeten, R., & De Wulf, A. 3D city mapping and data management using interconnected GI-software and Python. *International Journal of Digital Earth*.

Nuttens, T.*, Stal, C.*, Constales, D., De Backer, H., Schotte, K., De Wulf, A. Automated point cloud filtering and Levenberg-Marquardt based cylinder fitting of laser scanning data of cylindrical tunnels. *Computer-Aided Civil and Infrastructure Engineering.*

** Joint first authorship.*

Nuttens, T., Stal, C., De Backer, H., Schotte, K., Van Bogaert, P., Detry, P., De Wulf, A. Laser scanning as the key element to assess the tidal influences on a twin tube concrete tunnel in Belgium. *The Photogrammetric Record.*

Ooms, K., De Maeyer, P., De Wit, B., Maddens, R., **Nuttens, T.**, Van de Weghe, N., Vervust, S., Zwartjes, L. The User Centred Design of Weblectures. *Journal of Geography in Higher Education*.

Stal, C., De Maeyer, P., De Meyer, R., Pauwels, P., **Nuttens, T.**, Verstraeten, R., De Wulf, A. 3D city mapping and data management using interconnected GI-software and Python. *International Journal of Digital Earth.*

Stal, C., Briese, C., De Maeyer, P., Goossens, R., Hendrickx, M., **Nuttens, T.**, Pfeifer, N., De Wulf, A. Comparison of airborne laser scanning and image based modelling techniques. *The Photogrammetric Record.*

(P1) Conference proceedings included in one of the ISI Web of Science databases 'Conference Proceedings Citation Index – Science' or 'Conference Proceedings Citation Index – Social Science and Humanities' and limited to publications of the type of: article, review, letter, note, proceedings paper, except for publications already included in category A1

Nuttens, T., De Wulf, A., Stal, C., Constales, D., De Backer, H., Schotte, K. (2011). Ovalisation measurements of newly built concrete tunnels by means of terrestrial laser scanning. *11th International Multidisciplinary Scientific GeoConference SGEM 2011, www.sgem.org, SGEM2011 Conference Proceedings, Vol. 2,* pp. 287-294, June 20-25 2011, ISSN 1314-2704, doi: 10.5593/SGEM2011/s07.112

De Wulf, A., **Nuttens, T.**, Stal, C., De Maeyer, P. (2011). Evaluation and reformation (2011) of the geomatics education programs at Belgium academic universities. In: Chova, L.G., Torres, I.C., Martinez, A.L. (Eds.) *INTED 2011: 5th International Technology, Education and Development Conference,* International Association of Technology, Education and Development (IATED), Valencia, Spain, pp. 3183-3192, ISBN 978-84-614-7423-3.

Nuttens, T., De Wulf, A., Deruyter, G., Stal, C., De Backer, H., Schotte, K. (2012). Deformation monitoring with terrestrial laser scanning: measurement and processing optimization through experience. *12th International Multidisciplinary Scientific GeoConference SGEM 2012, www.sgem.org, SGEM2012 Conference Proceedings, Vol. 2*, pp. 707-714, June 17-23 2012, ISSN 1314-2704, doi: 10.5593/SGEM2012/S07.V2006

Stal, C., De Wulf, A., De Maeyer, P., Goossens, R., **Nuttens, T.,** Tack F. (2012). Statistical comparison of urban 3D models from photo modeling and airborne laser scanning. *12th International Multidisciplinary Scientific GeoConference SGEM 2012, www.sgem.org, SGEM 2012 Conference Proceedings, Vol. 2*, pp. 901-908, June 17-23 2012, ISSN 1314-2704, doi: 10.5593/SGEM2012/S08.V2008

Stal, C., De Wulf, A., De Maeyer, P., Deruyter, G., Goossens, R., Hendrickx, M., **Nuttens, T.** (2013). Change detection on cultural heritage by radiometric comparison of terrestrial photos and terrestrial laser scanning. *13th International Multidisciplinary Scientific GeoConference SGEM 2013, www.sgem.org, SGEM 2013 Informatics, Geoinformatics and Remote Sensing Conference Proceedings, Vol. II*, pp. 587-594, June 16-22 2013, ISBN 978-619-710-01-8, ISSN 1314-2704, doi: 10.5593/SGEM2013/BB2.V2/S10.006

Deruyter, G., Van Quickelberghe, A., **Nuttens, T.,** Stal, C., De Wulf, A. (2013). Risk assessment: a comparison between the use of laser scanners and total stations in a situation where time is the critical factor. *13th International Multidisciplinary Scientific GeoConference SGEM 2013, www.sgem.org, SGEM 2013 Informatics, Geoinformatics and Remote Sensing Conference Proceedings, Vol. II*, pp. 687-694, June 16-22 2013, ISBN 978-619-710-01-8, ISSN 1314-2704, doi: 10.5593/SGEM2013/BB2.V2/S10.019

De Wulf, A., De Maeyer, P., De Ryck, M., **Nuttens, T.,** Stal, C., Libert, M., Annaert, A. (2013). Higher hydrography education in Belgium. *13th International Multidisciplinary Scientific GeoConference SGEM 2013, www.sgem.org, SGEM 2013 Ecology, Economics, Education and Legislation Conference Proceedings, Vol. II,* pp. 429-436, June 16-22 2013, ISBN 978-619-7105-05-6, ISSN 1314-2704, doi: 10.5593/SGEM2013/BE5.V2/S22.011

De Wulf, A., **Nuttens, T.,** Stal, C., Deruyter, G. (2013). Renewed (2013) geomatics Bachelor, Master and PhD programs at Belgian academic universities. *13th International Multidisciplinary Scientific GeoConference SGEM 2013, www.sgem.org, SGEM 2013 Ecology, Economics, Education and Legislation Conference Proceedings, Vol. II*, pp. 497-504, June 16-22 2013,ISBN 978-619-7105-05-6, ISSN 1314-2704, doi: 10.5593/SGEM2013/BE5.V2/S22.020

Deruyter, G., Vandedrinck, F., **Nuttens, T.,** Stal, C., De Wulf, A. (2013). The evolution of education in land surveying in Flanders, Belgium: a work in progress. *13th International Multidisciplinary Scientific GeoConference SGEM 2013, www.sgem.org, SGEM 2013 Ecology, Economics, Education and Legislation Conference Proceedings, Vol. II*, pp. 557-564, June 16-22 2013, ISBN 978-619-7105-05-6, ISSN 1314-2704, doi: 10.5593/SGEM2013/ BE5.V2/S22.028

(VABB) Articles in scientific journals included in the VABB-SHW list and limited to publications of the type of: article, review, letter, note

Nuttens, T., Goossens, R., Tytgat, C., De Wulf, A., Van Damme, D., Hennau, M., Devriendt, D. (2007). The Virtual Reconstruction of the "Titane" Archaeological Site (Greece) by aims of Photogrammetry. *Proceedings of the XXI International CIPA Symposium, Athens, Greece (FP108). International Archives of the Photogrammetry, Remote Sensing and Spatial Information Sciences, Vol. 34, Part XXX,* p. 1-4, ISSN 1682-1750; 1682-1777.

Stal, C., De Maeyer, P., De Wulf, A., **Nuttens, T.,** Vanclooster, A., Van de Weghe, N. (2010). An optimized workflow for processing airborne laserscan data in a GIS-based environment. 5th International Conference on 3D GeoInformation, 2010, Berlin, Germany, Commission IV, WG IV/8, *International Archives of the Photogrammetry, Remote Sensing and Spatial Information Sciences*, *Vol. XXXVIII-4/W15*, p. 163-167, ISSN 1682-1750.

Stal, C., **Nuttens, T.,** Bourgeois, J., Carlier, L., De Maeyer, P., De Wulf, A. (2011). Accuracy assessment of a LIDAR digital terrain model by using RTK GPS and total station. *EARSeL eProceedings, Vol. 10, No. 8*, pp. 1-8, ISSN 1729-3782.

Bourgeois, J., Bourgeois, I., De Reu, J., **Nuttens, T.,** De Mulder, G. (2011). Een bronstijdgrafheuvel in Brecht (prov. Antwerpen, België): veldprospecties 2010. *Lunula, Archeologia Protohistorica, Vol. 19*, pp. 15-19, ISSN 1373-8623.

(A2) Articles in widely spread international scientific journals which rely on international experts for peer review and are not included in category A1

Docter, R., Vella, N., Cutajar, N., Bonanno, A., Pace, A., Anastasi, M., Bechtold, B., De Dapper, M., De Wulf, A., Dierkens, G., Garsallah, S., Goossens, R., Telmini, B. M., Nacef, J., **Nuttens, T.,** Ruiz I Cano, X., Spiteri, M., Stal, C., van de Put, W., Vella, C., Verdonck, L., Wood, J., Zerafa, R. (2012). Rural Malta: first results of the joint Belgo-Maltese survey project. *BABESCH, Bulletin Antieke Beschaving, Vol. 87*, pg. 1-47, ISSN 0165-9367.

(A3) Articles in national scientific journals with peer review which are not included in category A1 and A2

/

(A4) Articles in journals not included in category A1, A2 and A3

Nuttens, T., De Wulf, A., Bral, L., De Wit, B., Carlier, L., De Ryck, M., Stal, C., Constales, D., De Backer, H. (2012). Terrestrial laser scanning for tunnel deformation measurements. *PositionIT, April/May 2012,* pp. 24-32, ISSN 1818-2097.

Stal, C., De Wulf, A., **Nuttens, T.** (2012). Tunnel Measurements and Point Filtering: Automated point set filtering of cylindrical tunnel point sets. *GIM International, August 2012*, *Vol. 26, Nr. 8*, pp. 30-35.

(B2) Author or co-author of chapter(s) of books

Tytgat, C., De Wulf, A., Goossens, R., Hennau, M., **Nuttens, T.**, Van Damme D. (2013). Titane: The survey 2004-2006 by the Belgian School at Athens. In: Kissas, K., Niemeier, W.-D. (Eds.) *Athenaia 4, The Corinthia and the Northeast Peloponnese, Topography and History from Prehistoric Times until the End of Antiquity, Proceedings of the International Conference Organized by the Directorate of Prehistoric and Classical Antiquities and the German Archaeological Institute*, Loutraki, Athens, March 26-29, 2009, ISBN: 978-3-7774-2122-3, pp. 525-529.

(C1) Full articles in scientific conference proceedings not included in category A1, A2, A3 and P1

Nuttens, T., De Wulf, A., Goossens, R., Tytgat, C., Van Damme, D., Devriendt, D. (2008). Digital photogrammetric restitution and virtual reconstruction of the 'Titane' archaeological site (Greece). *Proceedings of the IX TOP-CART International Congress on Geomatics and Surveying Engineering*, Valencia, Conference CD nr. 201.

De Wulf, A., Goossens, R., De Rouck, J., Van Damme, L., Hanssens, P., Van Damme, D., Hennau, M., **Nuttens, T.** (2008). Monitoring of Harbour Breakwaters using Digital Close Range Photogrammetry. *Proceedings of the IX TOP-CART International Congress on Geomatics and Surveying Engineering*, Valencia, Conference CD nr. 1010.

De Wulf, A., Deruyter, G., De Maeyer, P., Goossens, R., Van de Weghe, N., **Nuttens, T.** (2008). Ph.D. Studies in Geomatics and Surveying in Belgium. *Proceedings of the IX TOP-CART International Congress on Geomatics and Surveying Engineering*, Valencia, Conference CD nr. 193.

Nuttens, T., De Wulf, A., Goossens, R., Tytgat, C., Van Damme, D., Devriendt, D. (2008). Using digital photogrammetric restitution for the virtual reconstruction of the walls around the 'Titani' acropolis (Greece). *1st International EARSeL Workshop "Advances on Remote Sensing for Archaeology and Cultural Heritage Management"*, Rome, Italië, pp. 253-256.

Nuttens, T., De Wulf, A., Goossens, R., De Maeyer, P., Matthys, M. (2009). Comparison of terrestrial laser scanning and digital photogrammetry for cultural heritage. *Proceedings of the 4th International Workshop on 3D Geo-Information*, Ghent, Belgium, DCL Print&Sign, pp. 159-166, ISBN: 978-90-9024820-2.

Nuttens, T., De Wulf, A., Bral, L., De Wit, B., Carlier, L., De Ryck, M., De Backer, H. (2009). Tunnel deformation measurements with high resolution laser scanning. *Proceedings of the 4th International Workshop on 3D Geo-Information*, Ghent, Belgium, DCL Print&Sign, pp. 167-181, ISBN: 978-90-9024820-2.

Nuttens, T., De Wulf, A., Goossens, R., Tytgat, C., Van Damme, D., Devriendt, D. (2010). Digital photogrammetry used for the 3D reconstruction of the walls around the acropolis of Titani (Greece). *Proceedings of the XXIV FIG International Congress 2010*, International Federation of Surveyors (FIG), Sydney, Australia.

Nuttens, T., De Wulf, A., Bral, L., De Wit, B., Carlier, L., De Ryck, M., Stal, C., Constales, D., De Backer, H. (2010). High resolution terrestrial laser scanning for tunnel deformation measurements. *Proceedings of the XXIV FIG International Congress 2010*, International Federation of Surveyors (FIG), Sydney, Australia.

Schotte, K., De Backer, H., **Nuttens, T.**, De Wulf, A., Van Bogaert, P. (2010). Strain gauge measurements during the assembly of the Diabolo Tunnel. *Proceedings of the 34th IABSE Symposium*, International Association for Bridge and Structural Engineering, IABSE-AIPC-IVBH.

Stal, C., Bourgeois, J., De Maeyer, P., De Mulder, G., De Wulf, A., Goossens, R., **Nuttens, T.**, Stichelbaut, B. (2010). Kemmelberg (Belgium) case study: comparison of DTM analysis methods for the detection of relicts from the First World War. *Proceedings of the 30th EARSeL Symposium 2010, Remote Sensing for Science, Education and Natural and Cultural Heritage*, Paris, France, European Association of Remote Sensing Laboratories (EARSeL), pp. 65-72.

De Wulf, A., **Nuttens, T.**, Stal, C., De Maeyer, P. (2011). Geomatics education in Belgium: 2011 program reformation at Belgian universities. *Proceedings of the FIG Working Week 2011 and 6th national congress of ONIGT*, International Federation of Surveyors (FIG), Marrakesh, Morocco.

De Wulf, A., Constales, D., Meskens, J., **Nuttens, T.**, Stal, C. (2011). Procedure for analyzing geometrical characteristics of an EDM calibration bench. *Proceedings of the FIG Working Week 2011 and 6th national congress of ONIGT*, International Federation of Surveyors (FIG), Marrakesh, Morocco.

Nuttens, T., De Maeyer, P., De Wulf, A., Goossens, R., Stal, C. (2011). Terrestrial laser scanning and digital photogrammetry for cultural heritage: an accuracy assessment. *Proceedings of the FIG Working Week 2011 and 6th national congress of ONIGT*, International Federation of Surveyors (FIG), Marrakesh, Morocco.

Stal, C., De Maeyer, P., De Ryck, M., De Wulf, A., Goossens, R., **Nuttens, T.** (2011). Comparison of geometric and radiometric information from photogrammetry and color-enriched laser scanning. *Proceedings of the FIG Working Week 2011 and 6th national congress of ONIGT*, International Federation of Surveyors (FIG), Marrakesh, Morocco.

Schotte, K., De Backer, H., **Nuttens, T.**, De Wulf, A., Van Bogaert, P. (2011). Monitoring strains in the Liefkenshoek railway tunnel. *Proceedings of the ITA-AITES World Tunnel Congress 2011*, Helsinki, Finland, May 21-26, ISSN 0356-9403, ISBN 978-951-758-531-6.

De Wulf, A., Docter, R., Stal, C., Goossens, R., **Nuttens, T.**, Vella, N. (2011). Integrated 3D Geomatics for Archaeology: Case Study Malta. *Proceedings of the 31st EARSeL Symposium 2011*, Prague, Czech Republic, May 30 – June 2, pp. 604-612.

Nuttens, T., De Maeyer, P., De Wulf, A., Goossens, R., Stal, C. (2011). Comparison of 3D accuracy of terrestrial laser scanning and digital photogrammetry: an archaeological case study. *Proceedings of the 31st EARSeL Symposium 2011*, Prague, Czech Republic, May 30 – June 2, pp. 66-74.

Stal, C., De Wulf, A., **Nuttens, T.**, De Maeyer, P., Goossens, R. (2011). Reconstruction of a Medieval Wall: Photogrammetric Mapping and Quality Analysis by Terrestrial Laser Scanning. *Proceedings of the 31st EARSeL Symposium 2011*, Prague, Czech Republic, May 30 – June 2, pp. 54-65.

Nuttens, T., De Wulf, A., Deruyter, G., Stal, C., De Backer, H., Schotte, K. (2012). Application of laser scanning for deformation measurements: a comparison between different types of scanning instruments. *Proceedings of the FIG Working Week 2012*, International Federation of Surveyors (FIG), Rome, Italy, ISBN 97887-90907-98-3.

Stal, C., **Nuttens, T.**, Constales, D., Schotte, K., De Backer, H., De Wulf, A. (2012). Automatic Filtering of Terrestrial Laser Scanner Data from Cylindrical Tunnels. *Proceedings of the FIG Working Week 2012*, International Federation of Surveyors (FIG), Rome, Italy, ISBN 97887-90907-98-3.

De Wulf, A., **Nuttens, T.**, Stal, C., De Wit, B., Seube, N., Boder, V. (2012). Erasmus Intensive Program (2011-2013) in Hydrography and Geomatics. *Proceedings of the FIG Working Week 2012*, International Federation of Surveyors (FIG), Rome, Italy, ISBN 97887-90907-98-3.

De Wulf, A., Constales, D., Stal, C., **Nuttens, T.** (2012). Accuracy Aspects of Processing and Filtering of Multibeam Data: Grid Modeling versus TIN Based Modeling. *Proceedings of the FIG Working Week 2012*, International Federation of Surveyors (FIG), Rome, Italy, ISBN 97887-90907-98-3.

Stal, C., Bourgeois, J., De Maeyer, P., De Mulder, G., De Wulf, A., Goossens, R., Hendrickx, M., **Nuttens, T.**, Stichelbaut, B. (2012). Test case on the quality analysis of structure from motion in airborne applications. *Proceedings of the 32nd EARSeL Symposium: 'Advances in Geosciences'*, Mykonos, Greece, May 21-24, p.11 (CD-ROM).

Stal, C., De Maeyer, P., De Wulf, A., Goossens, R., Maddens, R., **Nuttens, T.** (2012). Virtual Reconstruction of a Maya Temple Using Total Station and Photo Modelling. *Proceedings of the CAA Conference*, Southampton, United Kingdom, March 26-30, p. 12 (CD-ROM).

De Wulf, A., Constales, D., **Nuttens, T.**, Stal, C. (2012). Grid models versus TIN: geometric accuracy of multibeam data processing. *Proceedings of Hydro2012 conference 'Taking care of the sea'*, Rotterdam, The Netherlands, November 13-15, p. 6 (CD-ROM).

Seube, N., De Wulf, A., Böder, V., Touzé, T., Debese, N., Moitié, R., Probst, I., Morin, M. A., **Nuttens, T.**, Stal, C. (2012). International cooporation in education: the Vassivière Erasmus Intensive Training Program (2011-2013) on hydrography and geomatics. *Proceedings of Hydro2012 conference 'Taking care of the sea'*, Rotterdam, The Netherlands, November 13-15, p. 8 (CD-ROM).

Nuttens, T., Vandendriessche, B., Tytgat, C., De Wulf, A., Stal, C., Van Damme, D., Goossens, R. (2012). Photogrammetric restitution of a presumed ancient Asclepius temple in Titani, Peloponnesos, Greece. *Proceedings of the 3th International EARSeL Workshop on the advances in Remote Sensing for Archaeology and Cultural Heritage Management*, Gent, Belgium, September 19-22, p. 9 (CD-ROM).

Stal, C., De Wulf, A., De Maeyer, P., Goossens, R., **Nuttens, T.** (2012). Evaluation of the accuracy of 3D data acquisition techniques for the documentation of cultural heritage. *Proceedings of the 3th International EARSeL Workshop on the advances in Remote Sensing for Archaeology and Cultural Heritage Management*, Gent, Belgium, September 19-22, p. 8 (CD-ROM).

Stal, C., De Roo, B., De Maeyer, P., **Nuttens**, **T.**, De Wulf, A. (2013). Considerations on the fusion of multi-sensor spatial data for cultural heritage. *Proceedings of the 16th AGILE Conference on Geographic Information Science*, Leuven, Belgium, May 14-17, p. 3.

Stal, C., Goossens, R., Carlier, L., Debie, J., Haoudy, K., Nuttens, T., De Wulf, A. (2013). Cultural heritage documentation and integrated geomatics techniques in an educational context: case Bois-Du-Luc (Belgium). In: Grussenmeyer, P. (Ed.), XXIV International CIPA Symposium, Strasbourg, France, September 2-6, *International Archives of the Photogrammetry, Remote Sensing and Spatial Information Sciences, Vol. XL-5/W2*, pp. 611-615, doi: 10.5194/isprsarchives-XL-5-W2-611-2013.

Incoul, A., **Nuttens, T.**, De Maeyer, P., Seube, N., Stal, C., Touzé, T., De Wulf, A. (2014). Mobile laser scanning of intertidal zones of beaches using an amphibious vehicle. In: Kopacik, A., Kyrinovic, P., Stroner, M. (Eds.), *Proceedings of the 6th International Conference on Engineering Surveying INGEO2014,* Prague, Czech Republic, April 03-04, 2041, p. 6.

Nuttens, T., Stal, C., De Backer, H., Schotte, K., Van Bogaert, P., De Wulf, A. (2014). Assessment of the tidal influences on tunnels based on different monitoring techniques: laser scanning, levelling and strain gauges. In: Kopacik, A., Kyrinovic, P., Stroner, M. (Eds.), *Proceedings of the 6th International Conference on Engineering Surveying INGEO2014,* Prague, Czech Republic, April 03-04, 2041, p. 6.

(C3) Conference meeting abstracts

Schotte, K., De Backer, H., **Nuttens, T.**, De Wulf, A., Van Bogaert, P. (2010). Strain gauge measurements during the assembly of the Diabolo Tunnel. *IABSE Venice Symposium Report, 34th IABSE Symposium: International Association for Bridge and Structural Engineering*, IABSE-AIPC-IVBH, pp.626-627.

Schotte, K., De Backer, H., **Nuttens, T.**, De Wulf, A., Van Bogaert, P. (2011). Monitoring strains in the Liefkenshoek railway tunnel. *Proceedings of the ITA-AITES World Tunnel Congress 2011*, Helsinki, Finland, May 21-26, pp. 254-255, ISSN 0356-9403, ISBN 978-951-758-531-6.

Stal, C., De Wulf, A., De Coene, K., De Maeyer, P., **Nuttens, T.**, Ongena, T. (2012). Digital Representation of Historical Globes: Methods to Make 3D and Pseudo-3D Models of 16th Century Mercator Globes. In: Vervust, S., Ooghe, B., De Maeyer, P. (Eds.) *Proceedings of 'Mercator revisited: Cartography in the age of discovery' Conference*, Sint-Niklaas, Belgium, April 25-28, pp. 117.

Vandendriessche, B., Tytgat, C., De Wulf, A., **Nuttens, T.**, Van Damme, D., Goossens, R. (2012). Photogrammetric restitution of a presumed ancient Asclepius temple in Titani, Peloponnesos, Greece. *Book of abstracts of the 3th International EARSeL Workshop on the advances in Remote Sensing for Archaeology and Cultural Heritage Management*, Gent, Belgium, September 19-22, pp. 83-84 (CD-ROM).

Stal, C., De Wulf, A., De Maeyer, P., Goossens, R., **Nuttens, T.** (2012). Evaluation of the accuracy of 3D data acquisition techniques for the documentation of cultural heritage. *Book of abstracts of the 3th International EARSeL Workshop on the advances in Remote Sensing for Archaeology and Cultural Heritage Management*, Gent, Belgium, September 19-22, pp. 24-25 (CD-ROM).

Docter, R., Verdonck, L., Dierkens, G., Van De Put, W., Vella, N. C., Bonanno, A., Anastasi, M., Cutajar, N., Pace, A., Spiteri, M., Zerafa, R., De Dapper, M., De Wulf, A., Goossens, R., **Nuttens, T.**, Stal, C., Bechtold, B., Telmini, B. M. (2013). Rural sites in Northwest Malta: Results of the Belgo-Maltese Survey Project. In: Vermeulen, F., Corsi, C. (Eds.) *Book of abstracts of the Radio-Past Colloquium 'Non-destructive approaches to complex archaeological sites in Europe: A round-up'*, Ghent, Belgium, January 15-17, pp. 40.

Nuttens, T., De Wulf, A., Goossens, R., De Maeyer, P., Van de Weghe, N., Nyssen, J., De Dapper, M., Van Eetvelde, V., Antrop, M. (2013). Archeometry at the Department of Geography. In: Vermeulen, F., Corsi, C. (Eds.) *Book of abstracts of the Radio-Past Colloquium 'Non-destructive approaches to complex archaeological sites in Europe: A round-up'*, Ghent, Belgium, January 15-17, pp. 56.